UNIVERSITÀ DEGLI STUDI DI MILANO
DIPARTIMENTO DI BIOSCIENZE

PhD School in Molecular and Cellular Biology
XXXIII Cycle

Bioscience Department

Characterization of *REM* genes involved in the reproductive development of *Arabidopsis thaliana*

BIO/18 - BIO/01

Francesca CASELLI

Scientific Supervisor: Martin M. KATER
Tutor: Veronica GREGIS

A.A.
2019/2020

INDEX

RIASSUNTO

Il lavoro svolto durante la mia tesi di dottorato si è focalizzato principalmente sulla caratterizzazione di tre fattori di trascrizione, *REM34, REM35* e *REM36*, approfondendo in particolare il loro ruolo durante la fase riproduttiva dell'organismo modello *Arabidopsis thaliana. REM34, REM35* e *REM36* appartengono alla famiglia di geni *REM,* caratterizzata dalla presenza del dominio B3 di legame al DNA, e sono localizzati in un cluster sul genoma di Arabidopsis. Questi geni sono omologhi e condividono lo stesso pattern di espressione, per tanto è probabile che siano ridondanti tra di loro.

Per studiare la funzione di questi geni, il mio lavoro di dottorato è stato diviso in tre parti principali: per prima cosa, diverse tecniche di biologia molecolare sono state sfruttate per perturbare il livello di espressione di *REM34, REM35* e *REM36* o per creare mutanti stabili di questi geni, in secondo luogo è stato analizzato in dettaglio il ruolo che questi geni hanno durante lo sviluppo del gametofito maschile e femminile ed, in fine, è stato approfondito il ruolo che *REM34, REM35* e *REM36* svolgono nella modulazione del signaling dell'ormone auxina, durante lo sviluppo riproduttivo.

Queste analisi hanno dimostrato che *REM34, REM35* e *REM36* svolgono diversi ruoli fondamentali durante lo sviluppo riproduttivo di Arabidopsis: sono infatti necessari per il corretto sviluppo dei gametofiti femminili e maschili e sono coinvolti nello stabilire la corretta architettura dell'infiorescenza. Inoltre, durante il mio lavoro di tesi, è stato anche dimostrato che *REM34, REM35* e *REM36* svolgono questa funzione modulando il network genetico di risposta all'auxina, interagendo in particolare con ARF19.

In conclusione, questo lavoro ha permesso di chiarire la funzione e il meccanismo di azione di *REM34, REM35* e *REM36* durante lo sviluppo dell'infiorescenza di Arabidopsis, fornendo nuove evidenze del loro coinvolgimento nel signaling dell'auxina.

ABSTRACT

Role of *REM34, REM35* and *REM36* in gametophytes development

The *REproductive Meristem* (*REM*) gene family encodes for transcription factors belonging to the B3 DNA binding domain superfamily. In *Arabidopsis thaliana*, this family is composed of 45 members, preferentially expressed during flower, ovule, and seed developments. Only a few members of this family have been functionally characterized: *VERNALIZATION1* (*VRN1*) and, most recently, *TARGET OF FLC AND SVP1* (*TFS1*), which are involved in the regulation of flowering time and *VERDANDI* (*VDD*) which, together with *VALKYRIE* (*VAL*) controls the death of the synergid cell in the female gametophyte. We investigated the role of *REM34*, *REM35*, and *REM36*, three closely related and linked on chromosome 4 genes with similar expression profiles during the reproductive development of Arabidopsis.

The functional characterization of *REM34, REM35* and *REM36* presented several challenges, as these genes are in linkage in the genome and redundant. We thus developed two different approaches, the first based on a multiplexed RNA interference (RNAi) technology and the second on the fusion of REM34 with the EAR repressive domain, to modify their expression and identifying their role during inflorescence development.

Plants generated with both methods were characterized by a partial sterility. An *in situ* hybridization analysis showed that *REM34, REM35* and *REM36* share the same expression pattern throughout reproductive organs development. As these genes were found to be expressed both in female and male reproductive tissues, the developmental steps of both gametes were followed in both the *REM_RNAi* and *35S:REM34-EAR* lines; these analyses clearly showed that the partial sterility of these lines is caused by a postmeiotic block in both female and male gametophytes. Furthermore, protein interaction assays revealed that REM34 and REM35 interact, which suggests that they work together during the first stages of gametogenesis.

ABSTRACT

Role of *REM34, REM35* and *REM36* in inflorescence architecture determination

REM34, REM35 and *REM35* were shown to be expressed from the earliest stages of the reproductive development of Arabidopsis, in the inflorescence meristem and in the flower meristems; however, their role in these tissues is still unclear.

With the aim of functionally characterize these genes, *REM_RNAi* lines, in which the three genes of interest were downregulated, as well as *35S:REM34-EAR* dominant repressor lines were generated. At the same time, single (*rem34, rem35* and *rem36*) mutants and multiple mutant combinations (*rem34 rem35, rem34 rem36* and *rem35 rem36* were generated by using the CRISPR/Cas9 genome editing technology.

Wild type Arabidopsis plants are characterized by a spiral phyllotaxy, in which successive siliques arise at an angle of 137.5°, the single and multiple knock-out mutants, as well as the *REM_RNAi* and *35S:REM34-EAR* lines, instead displayed an altered phyllotactic pattern, with the divergence angles distributed around three main values: 90°, 140° and 180°. At the inflorescence meristem level, the establishment of the phyllotactic pattern is tightly regulated by two hormones, auxin and cytokinin, that regulate the timing and spacing between new organs formation.

The analysis of several marker lines and the effect of exogenous auxin applications clearly showed that auxin was correctly produced and distributed in the inflorescence meristem but the perception of this hormone was perturbed in the *REM_RNAi* and knock-out mutants.

We also showed that REM35 was able to interact with REM34 as well as with the Auxin Responsive Factor 19 (ARF19), which loss-of-function mutant is also characterized by a defective phyllotactic pattern. Furthermore, *LBD18,* which is a direct target of ARF19 and whose expression is auxin-dependent, was upregulated in the *rem* knock out mutant.

Taken together, these findings suggest that *REM34, REM35* and *REM36* are involved in the negative control of auxin response, in the inflorescence, and that they carry out this function working in complex with ARF19.

AIM OF THE THESIS

Plants have the ability to continuously producing new organs, throughout their life cycle, from pools of stem cells organized in niches, called meristems. During embryogenesis, two main meristems are specified: the root apical meristem (RAM), which is in charge of producing the root apparatus of the plant, and the shoot apical meristem (SAM), from which most of the areal organs of the plant are generated. During the transition to the reproductive phase of the plant life cycle, the SAM acquires the identity of inflorescence meristem (IM), that gives rise to the inflorescence, the reproductive structure of the plant which bears flowers, fruits and seeds. Plants are characterized by a striking variety of inflorescence architectures, which differ mainly as a consequence of their different branching abilities. Furthermore, the organization of lateral organs around the main stem of the inflorescence, which is called phyllotaxis, follows strict geometrical constraints. The spiral phyllotactic pattern is the most diffused in nature and is characterized by organs arising at constant divergences angles from one another, often following the Fibonacci sequence.

Modulation of traits beneficial for cultivation and yield is one of the main goals of crop improvement and one of the targets for enhancing productivity is changing the architecture of inflorescences, since in many species it determines fruit and seed yield. Inflorescence shape and organization is genetically established during the early stages of reproductive development and depends on the number, arrangement, activities, and duration of meristems during the reproductive phase of the plant life cycle.

The genetic network that controls the inflorescence meristem activity and thus inflorescence architecture have been partially unraveled, however the precise mechanism that controls the timing and spacing between new organs initiation at the meristem level is still unknown.

Whit the aim of identifying new players involved in this mechanism, the main focus of my thesis was to functionally characterize three members of the poorly characterized *REM (Reproductive Meristem)* genes family in the model species *Arabidopsis thaliana.*

There are 45 *REM* genes in the Arabidopsis genome, all characterized by the presence of multiple B3 DNA binding domains, most of which are organized in clusters and are preferentially expressed during the reproductive phase of the Arabidopsis' life cycle. We chose to focus on *REM34,* and on its homologues *REM35* and *REM36* as an extensive analysis of this family showed that these genes are expressed in the inflorescence and

flower meristems. Furthermore, *REM34* was found to be co-expressed with several floral meristem identity genes, which are involved in flower meristem specification, suggesting that this transcription factor is likely to be involved in the same biological process.

REM34, REM35 and *REM36* are homologous and share the same expression pattern and are thus likely to be redundant between each other. They are located in linkage on the genome, in a 7.5 kb region of the fourth chromosome. The first aim of this thesis was to develop and test different methodologies to functional characterize these genes, overcoming the difficulties derived from working with redundant and in linkage genes.

To do so *REM_RNAi, 35S:REM34-EAR* constructs and single and double CRISPR knock-out mutant combinations for the genes of interest were produced.

These lines were characterized by partial sterility, which was further investigated with molecular biology and microscopy techniques, due to a post-meiotic block in both female and male gametophytes development. Additionally, these lines were also displaying a mutated phyllotactic pattern, which was found to be caused by permutations in the hormone auxin signaling pathway.

Taken together, these evidences suggest that *REM34, REM35* and *REM36* play different key roles during inflorescence development, from primordia initiation to gametes development, and that they do so by modulating auxin response in the inflorescence meristem.

I. INTRODUCTION

I.I Reproductive development in plants

Plant development is characterized by the continuous formation of lateral organs from pools of stem cells, which are maintained throughout the entire life cycle of the plant, localized in niches called meristems. During the earliest stages of plant development, the two main meristems, the root and shoot apical meristems, are determined; the first one is responsible for root growth while the Shoot Apical Meristem (SAM) gives rise to most of the aerial organs of the plant (Busch *et al.*, 2010).

The life cycle of flowering plants can be divided into a vegetative phase and a reproductive phase. During the vegetative phase, the SAM is responsible for the production of leaves; the change to the reproductive phase is called floral transition and causes a reprogramming of the SAM that starts to produce the inflorescence, the reproductive structure of Angiosperms. The floral transition is triggered by exogenous signals, such as photoperiod, light quality and temperature, and endogenous inputs, which include hormonal biosynthesis and signaling, and, during this phase, the SAM acquires the identity of Inflorescence Meristem (IM) (Andrés and Coupland, 2012).

Inflorescence development is a key process in the life of the plant, as it ensures offspring establishment, and is of great agronomical value, because it determines the number of fruits/seeds that the plant will produce. Angiosperms are characterized by a striking variety of inflorescence types, whose shape is determined by the fine-tuning of the proliferation of the stem cells of the Indeterminate Meristems (IMe), and their ability to differentiate into Determinate Meristems (DMe), giving rise to the different organs of the inflorescence (Prusinkiewicz *et al.*, 2007).

In the dicot model species *Arabidopsis thaliana*, the indeterminate inflorescence meristem (IM) produces a number of determinate flower meristems (FMs), whose destiny unequivocally leads to flower formation and the depletion of meristematic cells. Other dicotyledons, such as Solanaceae, are characterized by a Cymose inflorescence in which IM differentiate into a flower meristem and, at the same time, it also produces a new IM on the side which reiterates the same developmental pattern.

In monocots, like grasses, the IM produces different meristem types which ultimately differentiate into a spikelet meristem (SM), producing florets that can be directly attached to the main inflorescence axis, as in spikes, or developing on flower-bearing branch meristems (BMs), as in panicles (Figure I-1).

There is an increasing interest in understanding the regulatory mechanisms which determine inflorescence architecture, since in many species this process is strictly correlated with fruit and seed yield. Furthermore, regularly-organized reiterative patterns are commonly found in morphogenic processes of different complex organisms (Shyer *et al.*, 2013; Corson *et al.*, 2017; Marcon and Sharpe, 2012) and phyllotaxis has been employed several time as a model to understand the mechanisms behind this regularity (Guédon *et al.*, 2013; Refahi *et al.*, 2016).

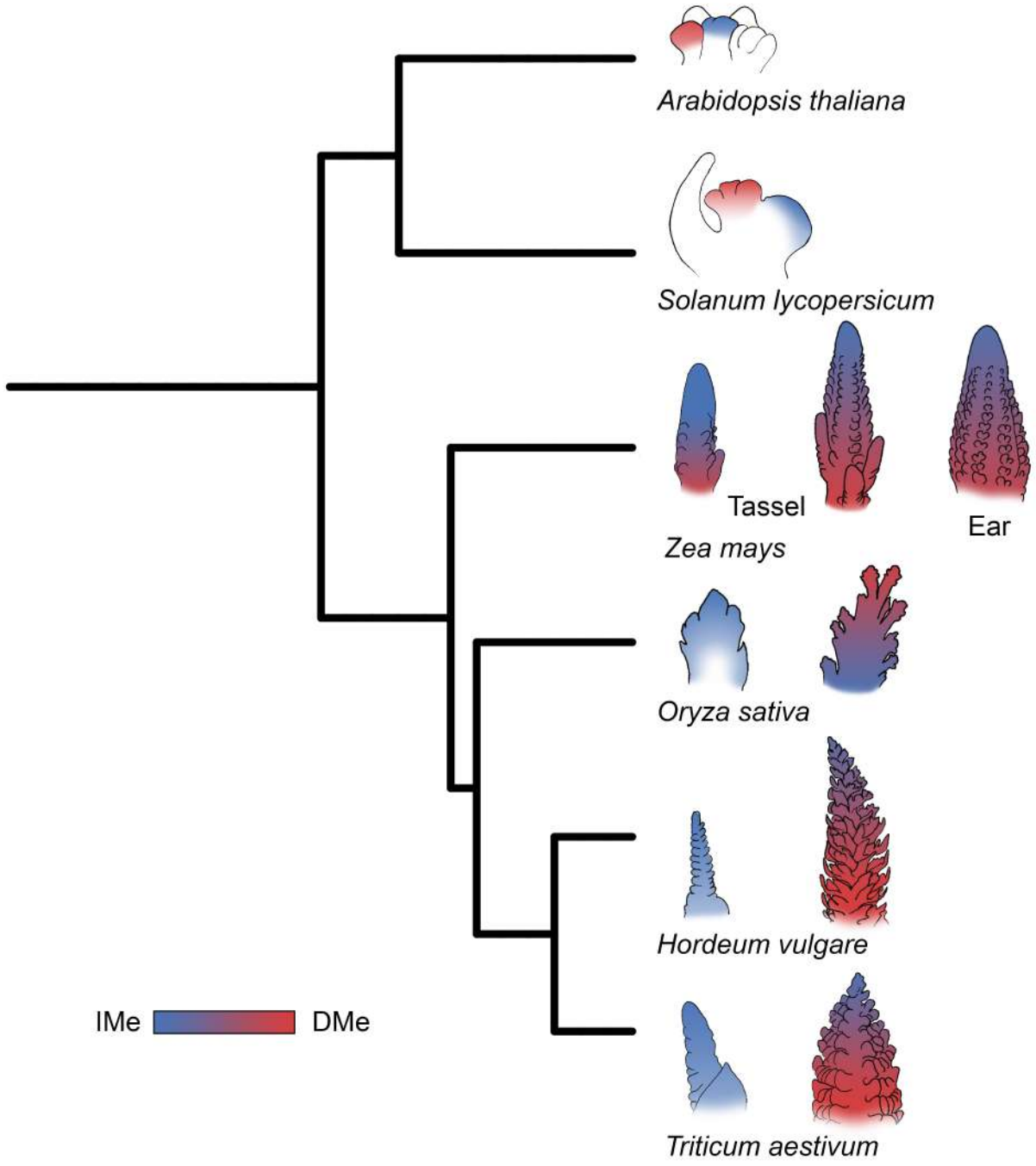

Figure I-1 Schematic representation of reproductive meristems in different plant species

In the dicot Arabidopsis the indeterminate Inflorescence Meristem continuously produces new determinate flower meristems on its flank, throughout the entire reproductive development of the plant. *Solanum lycopersicum* is characterized by a cymose inflorescence, in which the inflorescence meristem, called sympodial inflorescence meristem SIM, differentiate into a determinate flower meristem and into a new SIM, the firs will produce the flower while the second ensures the growth of the inflorescence.
Oryza sativa (rice) and the male inflorescence (tassel) of *Zea mays* (maize) are characterized by the production of a branched inflorescence called panicle. In these inflorescences, the indeterminate reproductive meristem differentiates into branch meristems, which will then produce a determinate number of spikelet meristems (SM), from which flowers originate.
In *Hordeum vulgare* (barley), *Triticum aestivum* (Wheat) and in the female inflorescence of maize (ear), the reproductive structure is an unbranched inflorescence called spike. In this case the indeterminate inflorescence meristem differentiates directly into SM, which will develop a specific number of flower meristems.
For each specie, a scheme of the reproductive meristem is represented, with the Indeterminate Meristems (Ime) highlighted in blue and the Determinate Meristems (DMe) in red.
The figure is adapted from Caselli *et al.,* 2020.

I.II *Arabidopsis thaliana* reproductive development

Arabidopsis thaliana as a model organism in plant biology and genetics

Arabidopsis thaliana is a small flowering plant, belonging to the Brassicaceae family. Despite its lack of agronomical value, Arabidopsis quickly imposed itself as one of the major model organism in plant biology. This plant is indeed characterized by a short life cycle, small dimension and it is easily grown in restricted spaces. It is also a self-pollinating plant, able to produce a large number of offspring. Furthermore, its small genome (12.5 Mb) was the first plant genome to be completely sequenced (The Arabidopsis Genome Initiative, 2000) and it can be easily manipulated with different genome engineering techniques.

The Arabidopsis genome encloses several duplicated chromosomal segments derived from one or more rounds of genome duplication followed by gene loss and divergence. Many gene families are organized in tandem arrays, which supports the hypothesis of the evolution of the genome through events of gene duplication and specialization. Whole genome duplication events caused the presence of multiple gene copies in the Arabidopsis genome, leading to functional redundancy between highly homologous genes, which has to be taken into account when approaching genomics studies in this organism (Bevan and Walsh, 2005).

Importantly, despite of the difference in gene numbers between *Arabidopsis thaliana* and crop species, there are no gene classes in crop species that are not present in Arabidopsis. Therefore, by establishing orthologous relationships between Arabidopsis and crop genes it is possible to exploit the knowledge obtained from the functional characterization of Arabidopsis genes to identify genes with similar roles in crops.

Inflorescence architecture determination

Arabidopsis has an indeterminate inflorescence in which the inflorescence meristem continuously produces floral meristems on its flank with a precise pattern. Floral and inflorescence meristem identity is controlled by a complex gene regulatory network in which IM genes ensure the conservation of the population of stem cells while the FM identity genes (FMI) specify for the floral meristem fate.

Organogenesis at the inflorescence level is a very complex process that requires a high spatiotemporal regulation and gives rise to a precise geometrical pattern, called phyllotaxis, in which successive primordia are positioned along the main axis in a Fibonacci spiral with a divergence angle of 137.5° (Galvan-Ampudia et al., 2016) (Figure I-2A).

It has long been proposed that phyllotaxis establishment, at the IM level, is a self-organizing process resulting from the combinatory effects of inhibitory fields, generated by the emerging primordia, that prevent organogenesis in the proximity of existing organs (Douady and Couder, 1996). As the stem elongates and newly formed primordia move away from the apex, their inhibitory effect decreases allowing the formation of a new primordium where the sum of the inhibitory fields is lowest. The inhibitory effect on new primordium initiation by the already formed lateral organs was demonstrated by surgical dissection and laser ablation of

preexisting primordia, that causes a permutation of the position where the new organ arises (Snow and Snow, 1932; Reinhardt *et al.*, 2004).

At the IM level, the spatial information for new primordia initiation is mainly given by the phytohormone auxin: this molecule is transported directionally toward the area in which a new primordium has to arise, where its accumulation is able to trigger a complex transcriptional response that controls the specification of the developing primordium. Auxin depletion around the new primordium, which acts as a sink for auxin accumulation, generates the inhibitory fields that set the spacing between successive organ initiations (Heisler *et al.*, 2005; Benková *et al.*, 2003; Vernoux *et al.*, 2000) (Figure I-2B).

The polar transport of auxin in the meristem is mainly controlled by the efflux carrier PIN proteins, which are polarly localized on the cell membranes. The disruption of the auxin efflux in the Arabidopsis IM causes the formation of pin-like inflorescences, that are no longer able to produce lateral organs (Okada *et al.*, 1991). Local auxin micro-application on the IM flanks are able to rescue flower formation in the *pin1* mutant, indicating that this hormone is necessary and sufficient to trigger organogenesis (Reinhardt *et al.*, 2000).

In the inflorescence meristem, auxin accumulates only in the epidermal cell (L1) layer, where organ initiation takes place. In this cell layer PIN1 is polarized toward the incipient primordia and it has been shown that the correct polarization of this efflux carrier in the cell membrane of the L1 layer of the meristem is fundamental to specify a correct phyllotactic pattern (Kierzkowski *et al.*, 2013; Jönsson *et al.*, 2006; Smith *et al.*, 2006).

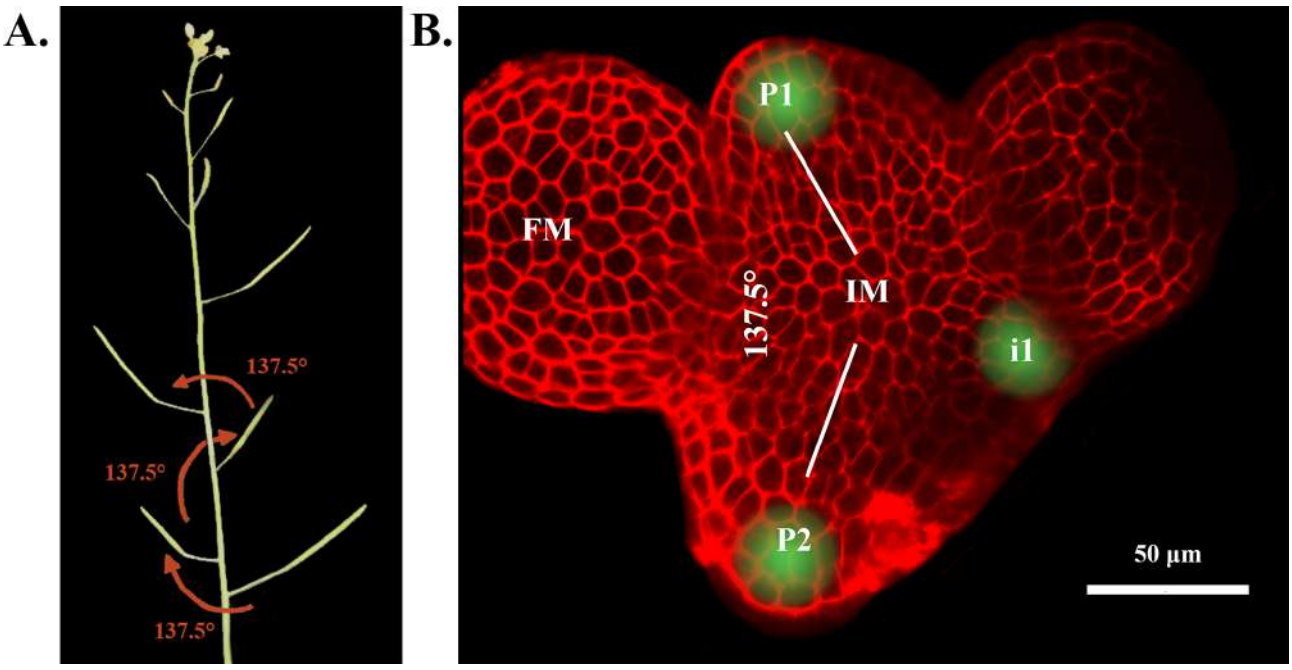

Figure I-2 Arabidopsis thaliana inflorescence architecture

A. Arabidopsis primary inflorescence, successive siliques arise from the stem at a divergence angle of 137.5° as indicated by the arrows. B. Arabidopsis inflorescence meristem, the IM generates new primordia on its flanks with a divergence angle of 137.5°. Auxin maxima, indicated in green, indicate the position where the new primordia will arise. FM: Floral Meristem; IM: Inflorescence Meristem; P1/P1: Primordium 1/2; i1: initiation site of the new primordium.

Auxin is both polarly transported from other plant tissues and directly produced in the IM itself, as demonstrated by the fact that different enzymes involved in its biosynthesis, such as *YUCCA1* (*YUC1*), *YUC2*, *YUC4*, *YUC6* and *TRYPTOPHAN AMINOTRANSFERASE OF ARABIDOPSIS* (*TAA1*), are expressed in this tissue (Cheng *et al.*, 2006b). *Yucca* mutants display different developmental defects, including short inflorescences and sterility. It has been shown that these defects cannot be rescued by exogenous auxin application but the expression of the bacterial auxin biosynthetic gene iaaM, under the control of the *YUCCA6* promoter, in the *yucca* background leads to the formation of wild type-like plant.

These evidences indicate not only that auxin produced in the meristematic tissues is fundamental to ensure the correct reproductive development of the plant but also that its biosynthesis needs to be strictly regulated to ensure a correct inflorescence development (Cheng *et al.*, 2006a).

The production of auxin in the meristem is partially controlled by *PLETHORA* transcription factors, which positively regulate the expression of *YUC1* and *YUC4,* and when these genes are mutated, plants lose the ability to ensure new organ formation at the correct position showing an alterated phyllotactic pattern, in which the predominant divergence angle is 180° (Pinon *et al.*, 2013; Prasad *et al.*, 2011). A similar role was shown for the *INDETERMINATE DOMAIN (IDD)14, IDD15* and *IDD16* transcription factors, which regulate both auxin biosynthesis and transport at the meristem level. Mutants in these genes show alteration in their inflorescence architecture and a partial sterility and, also in these mutants, these defects could be partially rescued by reestablishing auxin biosynthesis (Cui *et al.*, 2013).

Different tools have been developed to allow the visualization of auxin dynamics *in vivo* (Liao *et al.*, 2015; Mir *et al.*, 2017), which have recently been employed as a tool to study the correlation between the rhythmic organ patterning at the IM level and the tight spatiotemporal regulation of auxin distribution in this tissue (Galvan-Ampudia *et al.*, 2020).

The regularity of the spatial distribution of auxin in the inflorescence meristem, and the consequent spiral phyllotactic pattern, depends, among other factors, also on the function of the VIP subunit of the RNA polymerase II-associated factor 1 complex (Paf1c). When these proteins are mutated, the divergence angles between successive organs show an increased variance compared to the wild type and non-canonical regions of auxin maxima in the meristem (Fal *et al.*, 2017).

Although auxin is considered to be sufficient to promote organogenesis at the meristem level, a second hormone, cytokinin, was found to be necessary for the precise regulation of phyllotaxis. Auxin and cytokinin play opposite roles in the IM, where the first is involved in organogenesis and cell proliferation while the second is important for the maintenance of the indeterminate meristem (Leibfried *et al.*, 2005; Su *et al.*, 2011). A negative signaling pathway involving the precise expression in the emerging primordia of the *ARABIDOPSIS HISTIDINE PHOSPHOTRANSFER PROTEIN 6* (*AHP6*) phosphatase, a phosphotransfer protein involved in cytokinin signaling, regulates the timing of new organ formation ensuring the establishment of the correct phyllotactic pattern (Besnard, Rozier, *et al.*, 2014; Besnard, Refahi, *et al.*, 2014b).

A similar role was found for the *DORNRÖSCHEN-LIKE* (*DRNL*) transcription factor, which shares the same expression pattern as *AHP6* in the founding cells of the primordia: its correct expression is important to maintain the spiral phyllotactic pattern of organ formation in the IM (Chandler *et al.*, 2011; Comelli *et al.*, 2020; Comelli *et al.*, 2016).

Cytokinin signaling, in the reproductive meristem, is partially mediated by the *ERECTA* receptor kinases and mutants show severe defects in meristem maintenance and final architecture of the plant (Uchida *et al.*, 2013; Mandel *et al.*, 2014).

Although the spatiotemporal pattern of new organ initiation is mainly established at the IM level, the final architecture of the plant and the phyllotactic pattern is also influenced by post-meristematic elongation of the stem. For instance, mutants in the boundary genes *CUP-SHAPED COTILEDON* (*CUC*) *2* and *3* show a regular organ initiation in the apical meristem but an altered phyllotaxis due to defects in growth and cell division during the stem elongation (Burian *et al.*, 2015; Peaucelle *et al.*, 2007).

Finally, the formation of new organs is also dependent on changes in the cell wall composition, that needs to be loosen in order to allow cell elongation and division, that lead to primordia outgrowth (Peaucelle *et al.*, 2011; Peaucelle *et al.*, 2008).

Besides from these molecular cues, also changes in the meristem size can affect the phyllotactic pattern: plants with larger meristems show a higher rate of permutation events at the level of the phyllotaxis while smaller meristems display a more robust phyllotactic pattern (Landrein *et al.*, 2015a).

The spiral phyllotactic pattern, where consecutive organs emerge from the central axis with a divergence angle of 137°, is very robust and the most represented one among plant species. This prevalence in nature might be linked to advantages in light capture as well as the consequence of developmental constrains (Strauss *et al.*, 2020) and, since this trait strongly correlates with the overall plant biomass and with fruits production, understanding the mechanisms behind it could be beneficial for yield improvement. For instance, Arabidopsis plants in which the divergence angle between successive siliques is narrower (e.g. of 90°) are potentially able to produce more siliques without increasing the total height of the plant. Plants with an opposite phyllotactic pattern, in which consecutive organs arise from the stem at the same time at a divergence angle of 180°, can produce more flowers/fruits in the same amount of time than species characterized by a spiral phyllotaxis.

Finally, the advancements in understanding the mechanisms behind the spatiotemporal specification of new primordia during inflorescence development in Arabidopsis can be applied to improve the yield of agronomically important plants, which are usually characterized by more complex and branched inflorescences.

Gametophytes development

The life cycle of plants is characterized by the alternation between the diploid sporophytic generation and the haploid gametophytic generations, which in Angiosperms develop within the flower in the female and male reproductive organs.

As soon as the reproductive phase is triggered by day-length, temperature and internal factors, the SAM change its identity becoming an IM and the pool of genes devoted to its

maintenance, among which *TERMINAL FLOWER 1*, start to be expressed (Parcy *et al.*, 2002). At the same time, the transcription factors *LEAFY* (*LFY*) and *APETALA 1*(*AP1*), start to be expressed in the cells that will give rise to the flower meristem (FM), which arises initially as a spherical protrusion on the flank of the IM.

SHORT VEGETATIVE PHASE (*SVP*) and *AGAMOUS LIKE 24* (*AGL24*) are also required in this process, first for the floral transition and later for the specification of the FM. In particular, these genes, together with *AP1*, initially act repressing floral organ identity genes and are thus important for the specification of the floral primordium. Once the FM is established, genes involved in floral organ differentiation start to be expressed and, together with AP1, they repress *AGL24* and *SVP* (Gregis *et al.*, 2008). Flower organogenesis is orchestrated by the ABC(D)E homeotic genes, whose expression leads to the formation of the different floral organ primordia. The different floral organs are organized in four concentric whorls: sepals, petals, stamens (male reproductive organs) and carpels (female reproductive organs) (Coen and Meyerowitz, 1991; Rijpkema *et al.*, 2010).

Flower development, from primordium initiation until fertilization, takes about two weeks and can be divided in 12 stages based on morphogenesis, growth rate and structure of the floral tissues (Smyth et al., 1990). As mentioned above, flower development is tightly correlated with gametes production which, after fertilization, will give rise to mature seeds.

Arabidopsis is a heterosporous plant, characterized by the production of two unisexual gametophytes, the female megagametophyte (embryo sac), and the male microgametophyte (pollen). Developments of both female and male gametophytes can be divided into two main steps: sporogenesis, during which meiosis occurs giving rise to haploid spores, and gametogenesis, which leads to the formation of the gametes (Berger and Twell, 2011).

The Arabidopsis female gametophyte develops inside the gynoecium, which is the innermost whorl of the flower and its composed by two fused carpels. The first step of megasporogenesis consists in the formation of the ovule primordia, which initially arise as a finger-like protrusion of the placenta. One of the cells enclosed by this protrusion differentiates into the megaspore mother cell (MMC) or megasporocyte, which goes thorough meiosis, giving rise to four haploid megaspores. Three of these spores degenerate and only one, the functional megaspore, continues its development and after three mitotic divisions forms a mature embryo sac composed of eight nuclei and seven cells: three antipodal cells, two medial polar nuclei, and one egg cell surrounded by two synergids (Mansfield and Briarty, 1991) (Figure I-3A).

In the anthers, with a similar process, the microspore mother cell gives rise, through meiosis, to four microspores, which all develop into mature pollen grains, containing two sperm cells surrounded by the vegetative cell (Hafidh *et al.*, 2016) (Figure I-3B).

The transition from sporogenesis to gametogenesis is directly correlated with the cell cycle transition from mitosis to meiosis and back to mitosis. During gametogenesis, the number of mitotic divisions (two for the male and three for the female gametophyte) has to be tightly regulated and coordinated with cytokinesis.

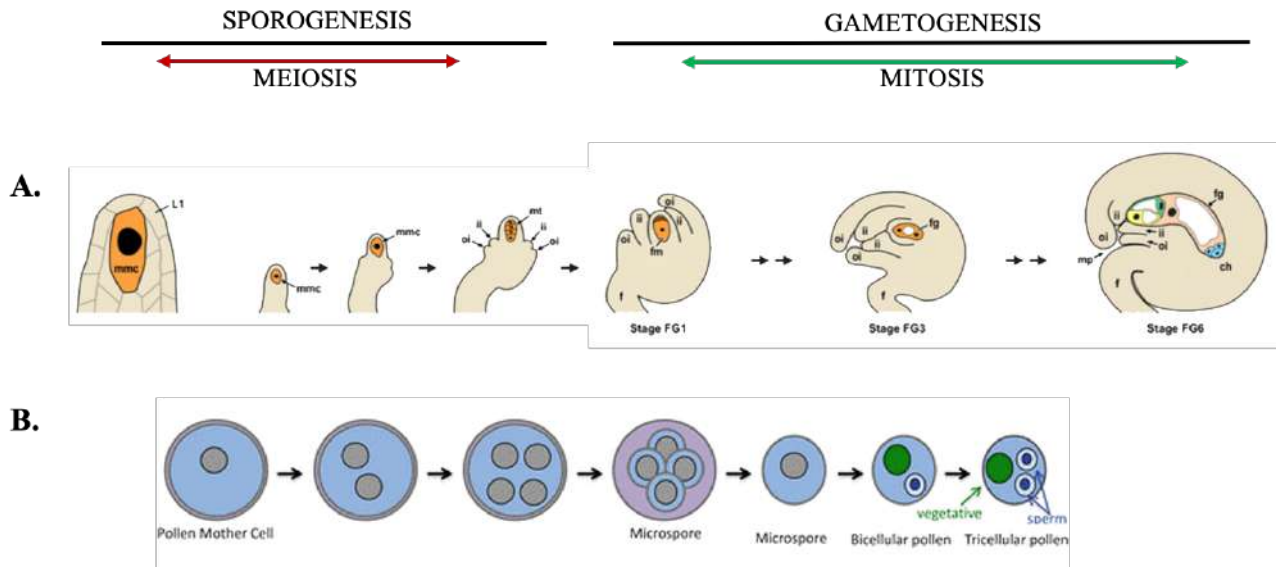

Figure I-3 Female and Male Gametophyte Development

A. Ovule (Female gametophyte) development takes places in the nucella and is divided in megasporogenesis and megagametogenesis. Megasporogenesis consist of three major events: the megaspore mother cell (MMC) formation, meiosis to produce haploid megaspores, and megaspore selection. Three of the megaspores degenerate and one survives, originating the embryo sac. During megagametogenesis the embryo sac undergoes three rounds of mitosis without cytokinesis, resulting in a seven-celled structure consisting of three antipodal cells (localized at the chalazal pole), one central cell (which contains the two polar nuclei), two synergid cells (localized at the micropylar pole), and one egg cell. DM: degenerating megaspores; FM: functional megaspore; II: inner integument; L1: L1 epidermal layer of the ovule primordium; MMC: megaspore mother cell; MT: meiotic tetrad; OI: outer integument; AC: antipodal cells; CC: central cell; CCN: central cell nucleus; CH: chalazal region of the ovule; EC: egg cell; F: funiculus; FG: female gametophyte; MP: micropyle; PN: polar nuclei; SC: synergid cells. Adapted from Drews & Koltunow, 2011.B. Pollen (Male gametophyte) development takes place in anther loculi where the pollen mother cells, are localized. The formation of the male gametophyte consists of two distinct processes: microsporogenesis, the formation of the haploid immature pollen grain, inside the microsporangia; and microgametogenesis, the development of the microgametophyte though two mitotic rounds, which lead to the formation of a mature pollen grain, containing a vegetative cell and two sperm nuclei. Adapted from Rutley & Twell, 2015.

This cell division process is complex and requires the integration of different pathways such as those involved in cell cycle progression (Ebel *et al.*, 2004; Ingouff *et al.*, 2006; Johnston *et al.*, 2008; Zhao *et al.*, 2017; Liu *et al.*, 2008), and chromatin modifications (Huanca-Mamani *et al.*, 2005; Latrasse *et al.*, 2008). Moreover, mitotic progression during gametogenesis is also affected when interfering with basic biological processes such as organelle and ribosome biogenesis (Shi *et al.*, 2005; Li *et al.*, 2009; Wang *et al.*, 2012). The perturbation of these pathways often results in an arrest of the cell divisions at earliest stages of both female and male gametophytes development.

The hormone auxin, which acts as a morphogen in different developmental processes, was found to have a crucial role in the correct development and patterning of both gametophytes.

Auxin is both imported from the sphoropytic placenta and directly synthesized in the mycropilar pole of the female gametophyte and it is distributed in the gametophyte forming a gradient, which gives to the developing cells of the embryo sac the positional information for their differentiation (Pagnussat *et al.*, 2009; Panoli *et al.*, 2015). Indeed, when auxin transportation is perturbed, megagametogenesis progression is impaired (Ceccato *et al.*, 2013).

Auxin biosynthesis and transportation in the male gametophyte was also proven essential for the transition from microsporogenesis to microgametogenesis (Yao *et al.*, 2018; Ding *et al.*, 2012). An auxin maximum was proposed to play a key role in late stamen development and essential for correct and coordinated pollen maturation, anther dehiscence and filament elongation (Cecchetti *et al.*, 2017).

Finally, auxin function in the female gametophyte is coordinated in a stamen-dependent manner, and auxin synthetized in the stamen is thought to play an important role in the synchronization of the maturation of the female and male reproductive organs, to ensure a successful fertilization (Larsson *et al.*, 2017).

Auxin production in the gynoecium is at least partially controlled by the cytokinin signaling pathway and the cross-talk between these two hormones is important to ensure the correct specification of the female reproductive organs primordia (Müller *et al.*, 2017).

Cytokinins appear to play an important role also in providing positional information to the developing ovule. Cytokinin signaling originates from the chalaza and is essential for the production of a functional megaspore (Cheng *et al.*, 2013).

Genetic studies have identified a large number of loci that control gametophyte development. Molecular cloning and characterization of some of them have revealed insights in sporocyte formation, meiosis/mitosis, and gametophyte development. Detailed phenotypic and molecular characterization of mutants remains a big challenge also because of the complication to work with such mutants, which often are partially sterile or even lethal (Muralla et al., 2011).

I.III Auxin homeostasis in the inflorescence meristem

Auxin biosynthesis and transport

As mentioned above, in plants auxin plays a crucial role in almost all the developmental processes, from embryogenesis to root and shoot/flower growth and development. The main auxin in plant is Indole-3-acetic acid (IAA), which can be *de novo* synthetized starting from tryptophan or released from inactive conjugated forms.

The main IAA biosynthetic pathway is composed of two steps: the first step is catalyzed by the TRYPTOPHAN AMINOTRANSFERASE OF ARABIDOPSIS (TAA) and consists in the conversion of Trp in Indole-3-pyruvate (IPA), which is then decarboxylated into IAA by the YUCCA (YUC) monooxygenases enzymes (Won *et al.*, 2011; Mashiguchi *et al.*, 2011).

TAA and its homologues *TAA RELATED* (*TAR*) belong to a small family, composed of five genes in total. Multiple mutants are characterized by several developmental defects, including a severe reduction of areal tissue production, flower development and partial or complete sterility. Their expression is restricted to specific groups of cells in all the different sectors of the plant, suggesting that a precise spatial regulation of auxin biosynthesis is required throughout plant development (Stepanova *et al.*, 2008; Tao *et al.*, 2008).

In Arabidopsis, the *YUCCA* family has 11 members four or which, YUC1 YUC2 YUC4 and YUC6, were found to play a crucial role in inflorescence meristem development. The analysis of the quadruple mutant, which is impaired in auxin synthesis at the meristem level,

is complemented by expressing a bacterial IAA synthesis gene under the *YUC1* promoter, but its phenotype cannot be rescued by exogenous auxin applications, clearly demonstrating that the spatiotemporal regulation of the expression of these enzymes is crucial for correct flower development (Cheng *et al.*, 2006b). Recently, it has been suggested that, in the shoot apical meristem, auxin is mainly produced in older primordia and subsequentially transported towards the meristem and incipient primordia, and that this flux is regulating phyllotaxis and meristem size (Shi *et al.*, 2018; Galvan-Ampudia *et al.*, 2020).

IAA can naturally enter the plasma membrane from the apoplast, thanks to the fact that the low pH of the cell wall causes this molecule to become protonated. Once IAA reaches the cytosol, the higher pH of the environment leads to the deprotonation of this molecule and to the loss of its ability to freely cross the plasma membrane. As a consequence, auxin efflux from the cells can only be achieved by active transport. As mentioned above, the main effectors of this active efflux are the member of the PINFORMED carrier family.

The dynamic and polar distribution of PIN efflux carrier proteins on the plasma membrane of the cells, in the shoot apical meristem, reflects the asymmetric distribution of auxin maxima and minima in the shoot apical meristem which, in turn, regulates organogenesis in these region (Vernoux *et al.*, 2000; Galvan-Ampudia *et al.*, 2020; Reinhardt *et al.*, 2003).

Despite the fact that auxin can autonomously enter the cell, a family of transporters associated with auxin uptake from the apoplast, the AUX/LAX influx carrier, were found to be expressed across the L1 layer of the apical meristem. Unlike the PIN efflux carriers, these proteins are evenly distributed on the plasma membrane. It is thus unlikely that these proteins are involved in controlling the asymmetric auxin flux, but they rather facilitate the uptake of auxin from lower cell layers to the meristem surface, where PINs are expressed and in charge of the polar redistribution of this hormone.

The characterization of multiple AUX/LAX and PIN mutants showed that these influx carriers play a precise role in the regulation of the phyllotactic pattern and organ boundaries establishment in the meristem (Bainbridge *et al.*, 2008; Reinhardt *et al.*, 2003).

It is finally important to underline that a precise integration of the processes of auxin production and transport, at the meristem level, is fundamental for the correct spatiotemporal and dynamic distribution of this molecule, which is crucial to ensure the reiteration of a precise organogenic pattern. A feedback loop that coordinates auxin biosynthesis and transport was individuated both during root and shoot development (Ljung *et al.*, 2001; Cheng *et al.*, 2006b; Cheng *et al.*, 2007) and is a good example of the complex mechanisms behind the robustness and stability of phyllotaxis.

Auxin signaling

Auxin accumulation triggers a short signaling cascade that leads to major changes in genes expression which, in the inflorescence meristem, guide primordia formation and organogenesis.

This signaling pathway relies on three components: Auxin Response transcription Factors (ARFs), which can either function as activators or repressors, Aux/IAA repressors and the $SCF^{TIR1/AFB}$ ubiquitin ligase complex. In the classical model, in low auxin conditions ARFs are bound to the Auxin Responsive Elements (AuxREs) in the promoter of their target genes. Their activity as transcriptional activators is however inhibited by their interaction with the Aux/IAA repressors, which, acting in a complex with TOPLESS, are able to recruit histone deacetylases that keep the chromatin of ARFs targets in a repressive state (Szemenyei *et al.*, 2008; Wang *et al.*, 2013; Long *et al.*, 2006).

Auxin can directly bind to the $SCF^{TIR1/AFB}$ complex and it acts as a molecular glue, enhancing its affinity to the Aux/IAA repressors, which are then targeted and degraded by the 26S proteasome (Gray *et al.*, 2001). The degradation of the Aux/IAA activates the ARF transcription factors, which can regulate the expression of genes downstream of auxin response (Figure I-4).

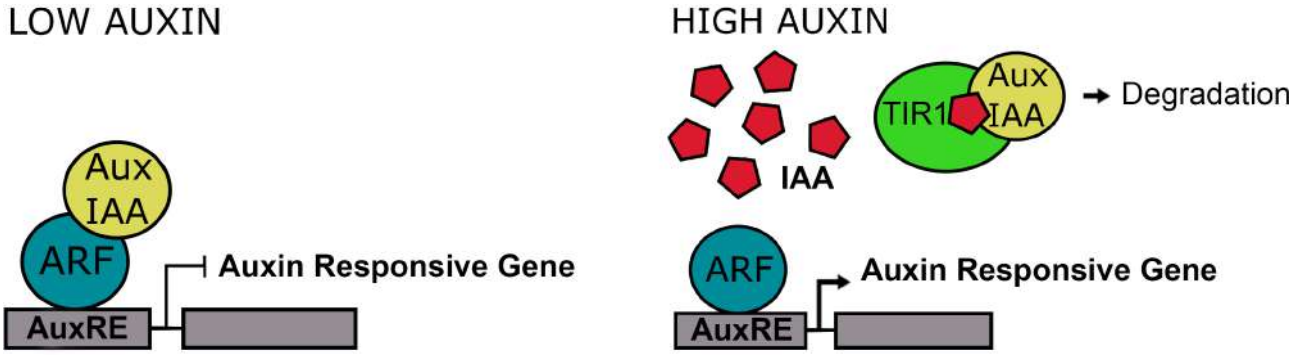

Figure I-4 Regulation of Auxin Mediated Gene Expression

In low auxin conditions the ARF transcription factors are bound to the AuxRE sequences in the Auxin Responsive genes promoters but their activity as transcriptional activator is inhibited by their interaction with the Aux/IAA repressors. When auxin enters the cell, it can bind the $SCF^{TIR1/AFB}$ complex, which is then able to bind the Aux/IAA, causing their degradation and allowing the transcription of Auxin Induced Genes.

The modularity of the auxin response cascade is, at least partially, explained by the spatiotemporal expression of the different members of the ARFs and Aux/IAAs and by the specific combinations of the ARF-Aux/IAA protein-protein interactions (Vernoux *et al.*, 2011). Furthermore, the interaction between the $SCF^{TIR1/AFB}$ complex and the different Aux/IAA repressors was found to change in an auxin-dependent manner: different $SCF^{TIR1/AFB}$-Aux/IAA pairs can indeed form at different auxin concentration (Calderón Villalobos *et al.*, 2012).

Finally, despite the fact that the *TIR1* and *AFBs* subunits of the SFC complex are ubiquitously expressed in the different tissues of the plant, their expression is restricted post-transcriptionally mainly by the action of small RNAs (Chen *et al.*, 2011; Si-Ammour *et al.*, 2011).

Several auxin-responsive gene families have been individuated through transcriptomic analysis of auxin-treated tissues. Among these families, there are genes involved in the regulation of auxin homeostasis, such as the *GRETCHEN HAGEN 3* (*GH3*) auxin amido-conjugases, which conjugate auxin in an inactive form the Aux/IAA repressors and the carrier involved in auxin redistribution (PINs and AUX/LAXs).

The GH3 and Aux/IAA are both important, as they are involved in a feedback mechanism that controls auxin concentration and activity within the cell. Other auxin-responsive families, such as the *LATERAL ORGAN BOUNDARY DOMAIN (LOBs)* transcription factors and the small auxin up-regulated RNA (SAUR), are involved in the control of the developmental pathways downstream of auxin induction (Paponov *et al.*, 2008). It is worth underlining that some of these factors are induced in all the different parts of the plant, while for others the induction seems to be tissue-specific, indicating that auxin can elicit different transcriptional responses throughout the plant.

The $SCF^{TIR1/AFB}$-Aux/IAA-ARF interaction model has been well characterized, however, it only partially explains the complexity of auxin signaling. For instance, this mechanism is only applicable to the activating ARFs, while there is little evidence of interaction between the Aux/IAAs and the repressive ARFs (Vernoux *et al.*, 2011). It is thus possible to speculate that, at least the ARFs that act as repressors, work in an auxin-independent way.

The visualization of auxin dynamics at the inflorescence meristem level, showed that this molecule is present at high concentrations both in the newly emerging primordia and in the dome of the IM. However, auxin is only able to trigger organ differentiation in the cells of primordia but not in the meristem dome, suggesting that the auxin signaling model should include a niche of cells, though which auxin flows, which are auxin insensitive (Ma *et al.*, 2019; Galvan-Ampudia *et al.*, 2020; Vernoux *et al.*, 2011)

I.IV The B3 superfamily

The B3 binding domain superfamily is composed of transcription factors, all characterized by the presence of one or more ~110 aa long DNA binding domain, called the B3 binding domain. The B3 binding domain was first discovered in maize in the *VIVIPAROUS1* gene (McCarty *et al.*, 1991) and it is a plant-specific domain widespread in different species.

This superfamily can be divided in five different families: Auxin Response Factor (ARF), Abscisic Acid-Insensitive3 (ABI3), High Level Expression of Sugar Inducible (HSI), Related to ABI3/VP1 (RAV) and REproductive Meristem (REM).

Among these, the ARF family is the better characterized one, while the others are yet to be exhaustively characterized. From the evidences available, it appears that proteins containing this domain might be involved in hormonal regulation: in fact, as described above, the *ARFs* are the main effectors of auxin signaling, the *RAV* family are connected to the regulation of the response to brassinosteroids and the HSI family seems to respond to abscisic acid (Swaminathan *et al.*, 2008).

The B3 DNA binding domain is composed of seven β strands that are folded into an open β barrel (Waltner *et al.*, 2005) and, while the tertiary folding is maintained, the loops connecting the β strands show some differences between families, suggesting that the folding is responsible for the interaction with the DNA while the loops might be determinant for the sequence specificity of the different proteins carrying this domain (Romanel *et al.*, 2009).

ARF gene family

In *Arabidopsis thaliana* the ARF gene family is composed of 23 transcription factors, which share the same modular structure (Figure I-5). These factors are indeed characterized by the presence of three major domains: the N-terminal DNA binding domain, a middle domain, whose aminoacidic composition differs between activators and repressors, and a C-terminal PB1 protein interaction domain, which mediates the ARF-ARF and ARF-Aux/IAA binding.

Among the Arabidopsis's ARFs, five are predicted to be activators (ARF5, ARF6, ARF7, ARF8 and ARF19), 14 are repressors and four are truncated and lack the PB1 domain (Guilfoyle and Hagen, 2007).

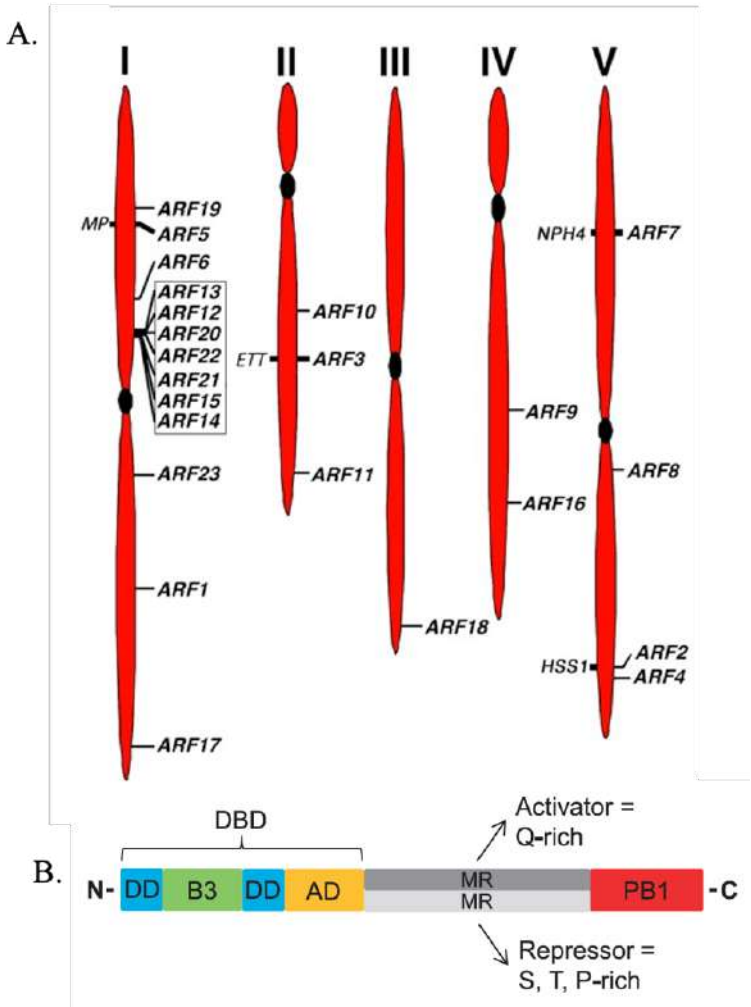

Figure I-5 ARF Transcription Factor Family

A. Location of the 23 *ARF* genes on Arabidopsis chromosome (Okushima et al., 2005). B. Schematic representation of the AFR transcription factors structure. DD: dimerization domain; B3: DNA-binding domain; AD: ancillary region, MR: middle region; PB1: Phox and Bem1 domain (Chandler, 2006).

Single and multiple mutants characterization studies showed high redundancy between members of this family, as single mutants often do not show any visible phenotype (Okushima *et al.*, 2005).

ARFs are able to bind DNA, through the B3 binding domain, in a sequence specific way to the so called AuxRE sequences. This TGTCTC consensus sequence was originally identified in the promoter sequence of the soybean GH3 gene (Liu Zhan Bin *et al.*, 1994), and was later demonstrated to be bound by different ARF proteins. Exploiting this sequence, an auxin responsive promoter, called DR5 promoter, containing several repeats of the AuxRE motif, was developed and broadly employed as an auxin sensor in plants (Ulmasov *et al.*, 1997).

In recent years, advances have been made in understanding the DNA binding mechanism of these proteins that led to the idea that the ARFs are able to bind with high affinity other sequences besides from the classical TGTCTC (O'Malley *et al.*, 2016; Lieberman-Lazarovich *et al.*, 2019; Sassi *et al.*, 2014; Liao *et al.*, 2015).

High-throughput yeast-2-hybrid interaction assays showed that many ARFs are able to homo- and heterodimerize and this interaction is thought to modulate the cell sensitivity to auxin and to increase the different cell-specific effects that auxin triggers in different tissues (Muto *et al.*, 2006; Hardtke *et al.*, 2004; Farcot *et al.*, 2015). This interaction is thought to be mediated both by the P1 dimerization domain and by a second protein-protein dimerization domain, localized near the DNA binding domain (Boer *et al.*, 2014).

Besides from ARF-ARF interactions, evidences show that these proteins are able to heterodimerize with proteins belonging to other families, which act as *cis*-regulatory factors modulating auxin response (Cherenkov *et al.*, 2018). For instance, it is known that the interaction between MYB77 and ARF7 is fundamental for the correct regulation of lateral root growth (Shin *et al.*, 2007).

Due to the redundancy among genes belonging to the ARF family, it has been difficult to understand the functions that the different members of this family play during plant development. Among the different ARFs expressed during the reproductive phase of Arabidopsis life cycle, a clear role has been assigned only to *ARF3, ARF4, ARF5, ARF6* and *ARF8.*

ARF3 or *ETTIN* plays a crucial role in the determination of the floral meristem identity, integrating the function of the floral meristem identity genes *AGAMOUS* and *APETALA2* (Liu *et al.*, 2014). ARF3 in the inflorescence meristem is also involved in the direct regulations of three uncharacterized genes, *TARGETS UNDER ETTIN CONTROL* (*TEC*) 1, 2 and 3, which are involved in the establishment of a correct phyllotactic pattern (Simonini *et al.*, 2017). *ARF5* or *MONOPTEROS* is also involved, together with *ARF3* and *ARF4,* in the transcriptional regulation of several genes involved with the flower development initiation process (Yamaguchi *et al.*, 2013; Wu *et al.*, 2015; Chung *et al.*, 2019). Finally, *ARF6* and *ARF8* control fertilization and fruit maturation (Finet *et al.*, 2010).

Up to today however, the function of other members of this family which are expressed in the inflorescence meristem, such as *ARF7* and *ARF19,* is still unclear.

REM gene family

In *Arabidopsis thaliana* the *REM* gene family is composed of 45 genes, most of which are located in clusters on the genome, and because of the high functional redundancy between members of this family and their clustered position in the genome, up to now not much is known about their function (Figure I-6A).

All the REM transcription factors are characterized by the presence of multiple copies of the B3 DNA binding domain. The fact that the DNA binding domain is often present in multiple copies suggests that it is unlikely that the members of this family can bind DNA in a specific manner, further more from the analysis of the structure of the B3 binding domain of REM genes it appears that members of this family can bind DNA in a less sequence

specific way, compared to other transcription factor carrying the same domain (Waltner *et al.*, 2005). Over the years, some hypothetical consensus sequences for some of the components of this family have been individuated. Through DAP-seq analysis it was shown, for instance, that REM5 and REM19, involved in the cold-induced flowering process (Berke and Snel, 2015), preferentially bind to a long poly-A motif (O'Malley *et al.*, 2016).

An protein-binding microarray *in vitro* approach allowed also the identification of a binding DNA sequence for REM34, but this sequence has yet to be confirmed *in planta* (Franco-Zorrilla *et al.*, 2014).

Only a few members of this family have been functionally characterized: *VERDANDI* (*VDD* or *REM20*) and *VALKYRIE* (*VAL* or *REM11*), which have a function in gametophyte development (Matias-Hernandez *et al.*, 2010; Mendes *et al.*, 2016). *VERNALIZATION1* (*VRN1* or *REM5*), *REM19* and *TARGET OF FLC AND SVP1* (*TFS1* or *REM17*) were shown to be involved in the control of flowering time (Richter *et al.*, 2019; Levy, 2002; Sung and Amasino, 2004).

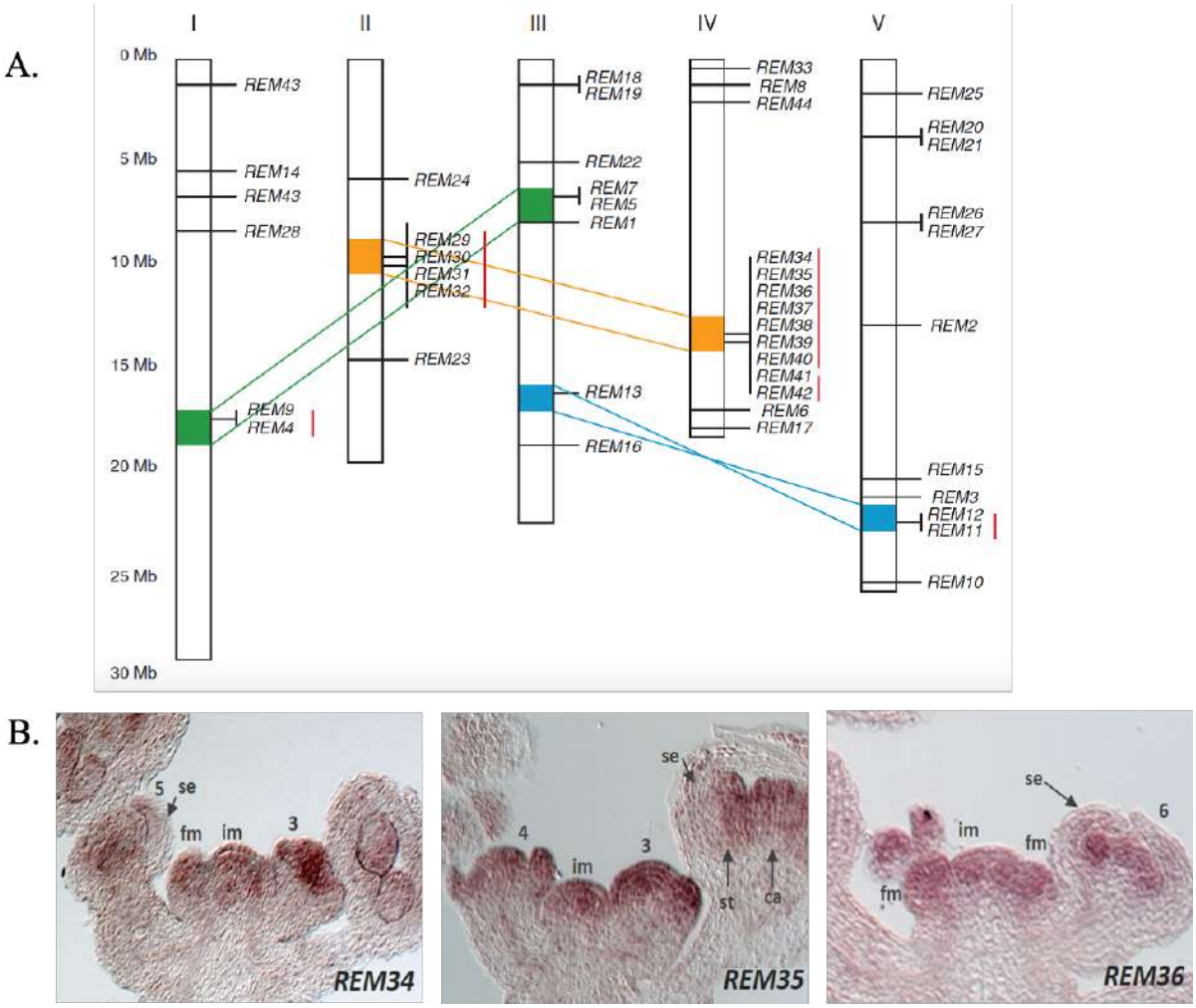

Figure I-6 *REM* Transcription Factor Family

A. *REM* genes on Arabidopsis' chromosomes, with colors indicating the different phylotegenetic relationships. The largest cluster is located on a 30 kb region on the fourth chromosome and it contains nine genes in total. From Mantegazza et al., 2014. B. *REM34*, *REM35* and *REM36* expression pattern, the numbers indicate the developmental stage of the flowers; im: inflorescence meristem; fm: floral meristem; se: sepals; From Mantegazza et al., 2014.

More recently, *REM16* was associated with the regulation of the flowering pathway through the direct regulation of *SOC1* and *FT* (Yu *et al.*, 2020). Finally, *rem33* was identify as an ovule defective mutant in a high-throughput screening but a complete functional characterization of this gene is still lacking (Pagnussat *et al.*, 2005).

To better understand the possible role of the *REM* genes during Arabidopsis development a deep characterization of this family was performed by Mantegazza *et al.,* (2014). The expression pattern of the *REM* genes was investigated by both analyzing the available microarray data and by qPCR which showed that the majority of the members of this family are preferentially expressed during flower and seed development. This analysis resulted in the identification of a set of genes, *REM34 REM35* and *REM36*, which seem to be involved in the earliest stages of flower development. *REM34, REM35* and *REM36* are located in a cluster, containing 9 *REM* genes in total, on the fourth chromosome of *Arabidopsis* and they show a high level of homology, which might indicate a possible functional redundancy.

An *in situ* hybridization analysis showed that *REM34, REM35* and *REM36* share the same expression pattern and that they are expressed in the IM, FM and during early stages of flower formation, although no expression was observed in the developing sepals (Mantegazza *et al.*, 2014) (Figure I-6B).

REM34 was also found to be co-expressed with the FMI genes *LEAFY* and *APETALA1,* which are responsible for the specification of floral meristem identity. The degree of correlation between the expression patterns of different genes is considered to be a good indicator of their functional association, thus the co-expression analysis can be a useful tool when investigating the function of genes (Usadel *et al.*, 2009; Mantegazza *et al.*, 2014).

The available single insertional available mutants for *REM34, REM35* and *REM36* showed no visible phenotype and, because of the position in linkage of these genes on the *Arabidopsis* genome, it is difficult to obtain multiple mutant combinations by crossing.

In this thesis I focused on the functional analysis of *REM34, REM35* and *REM36* using both an RNAi silencing and CRISPR-Cas9 mutagenesis approach. These studies showed that these *REM* genes play a role in phyllotaxis and male and female gametophyte development.

II. Results and Discussion

II.I Strategies to Functionally characterize in linkage redundant genes

REM_RNAi and 35S:REM34-EAR lines construction and chatacterization

REM34, *REM35* and *REM36* are located in a cluster, containing 9 *REM* gene in total, on the fourth chromosome of Arabidopsis. This cluster is thought to derive from a duplication event involving chromosomes II and IV, which occurred about 4 to 14 million years ago. In addition, this cluster of genes sustained recent tandem duplication events, as indicated by their similar intron/exon structures in which the position of the B3 DNA binding domains is highly conserved (Romanel *et al.*, 2009).

As a result of these duplications events, *REM34*, *REM35* and *REM36* are homologous, sharing around 70% of sequence identity. Furthermore, they share the same expression pattern during the first stages of flowed development (Mantegazza, *et al.*, 2014). *REM34*, *REM35* and *REM36* are thus likely to be functionally redundant, as this is a common phenomenon between genes that share an high degree of homology and the same expression patter (Briggs et al., 2006). As mentioned above, the *REM34* cluster is composed of 9 genes in total, however, *REM34, REM35* and *REM36* show unique characteristics compared to the other members of the same clusters, such as the presence of several FMI genes binding sites in their regulatory regions, and their sequences shows a higher level of homology compared to the other *REMs.* As so, the analysis performed by Mantegazza *et al.´*2014), suggested that among the 9 *REM* genes belonging to the *REM34* cluster, *REM34, REM35* and *REM36* might have overlapping functions during the reproductive development of Arabidopsis.

Single insertional knock-down mutants were available only for *REM34* and *REM36*, while no suitable insertional line was available for *REM35* (Mantegazza, *et al.*, 2014). *REM34*, *REM35* and *REM36* are located in linkage in a 7,5 kb region, it is thus unlikely that multiple mutant combinations can be produced by crossing the single insertional lines available.

We thus decided to employ two different approaches, the first based on a multiplexed RNA interference (RNAi) technology and the second on the fusion of REM34 with the EAR repressive domain, with the aim of modifying their expression and identifying their role during inflorescence development.

To achieve the simultaneous silencing of *REM34*, *REM35* and *REM36* we decided to implement a multi-fragments RNAi approach, previously proven successful in silencing up to six targets in Arabidopsis thaliana (Czarnecki *et al.*, 2016). Here, the multiple RNA interference technology was used to express a single chimeric double stranded RNA that targeted the three *REM* genes under the control of *CaMV35S* promoter. The generation of a single RNA hairpin, containing the three interfering fragments, provides multiple advantages: it allows the silencing of multiple genes in with a single transformation event; it prevents the employment of multiple *CaMV35S* promoters, which are more likely to be silenced in plants and it allows the achievement of an uniform downregulation of all the target genes in all the different plant tissues. (Figure II-1A).

The interfering fragments were selected with the aid of BLASTn in three specific regions of the coding sequences of the three target genes. For *REM34* and *REM36* it was possible to choose three highly specific fragments with no expected off targets. The fragment chosen to target *REM35* had a partial complementarity with *REM36* and, at a lower level, with *REM37*, one other member of the *REM34* cluster, whose expression is almost undetectable in most of Arabidopsis tissues (Mantegazza, Gregis, Mendes, *et al.*, 2014; Klepikova *et al.*, 2016).

Forty *REM_RNAi* T1 lines were obtained, all characterized by defects in the inflorescence architecture and by a partial sterility. We evaluated the downregulation of *REM34*, *REM35* and *REM36* in nine of them: all of the analyzed lines showed a down-regulation of at least 50% of *REM34* and *REM35*, while the level of silencing of *REM36* was highly variable (Figure II-1B).

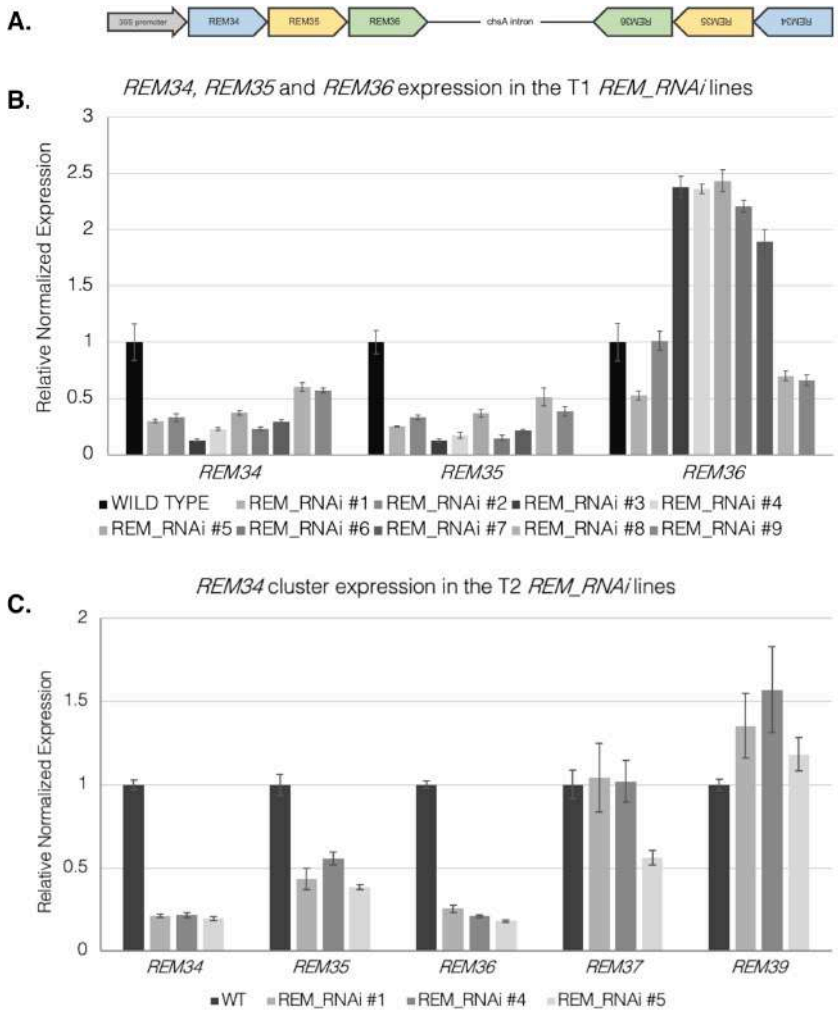

Figure II-1 Multiple RNA interference approach

A. Schematic representation of the RNAi construct. The *REM34-REM35-REM36* sense and antisense fragments are separated by the chsA intron, which allows the hairpin structure formation. B. qRT-PCR on nine different *REM_RNAi* T1 inflorescences, showing a strong downregulation of *REM34* and *REM35* and different levels of *REM36* expression. C. qRT-PCRs, performed on three different T2 *REM_RNAi* #1 plants, to evaluate the specificity of the three fragments chosen for the RNA interference construct. Two genes were selected: *REM37*, which was the possible off target of one of the fragments, and *REM39*, which is the *REM* gene with the higher expression in the tissues of interest belonging to the cluster of *REM34*, *REM35* and *REM36* (Mantegazza et al., 2014). Downregulation of neither *REM37* nor *REM39* was detrcted, confirming the specificity of the silencing. The expression levels of *REM34*, *RERM35* and *REM36* were also measured, to make sure that the silencing of the target genes was maintained in the T2 generation.

The silencing of the *REM34*, *REM35* and *REM36* was confirmed in the T2 generation, where, to evaluate the specificity of the RNAi fragments, the expression of *REM37* and *REM39* was also measured (Figure II-1C). *REM37* was chosen as it was found to be the possible off target of the *REM35* interference fragment while *REM39* expression was tested as it belongs to the same cluster of *REM34* and it is highly expressed in the same tissues of the genes of interest.

None of the possible off targets was downregulated in the *REM_RNAi* lines, indicating that the construct is able to silence in an efficient and specific way only the three genes of interest, *REM34*, *REM35* and *REM36*.

To confirm the results obtained in the *REM_RNAi* lines and further characterize the role of *REM34*, *REM35* and *REM36* during inflorescence development, the Chimeric Repressor Silencing Technology (CRES-T) was also employed. The CRES-T technique relies on the expression of the transcription factor of interest, fused with the dominant EAR-motif repressive domain, thus converting the transcription factor into a dominant repressor (Figure II-2A).

Five transgenic T1 lines, with different levels of overexpression of the *REM34-EAR* mRNA, were obtained (Figure II-2B). Interestingly, these lines exhibited a similar mutated phyllotaxis pattern and partial sterility as the *REM_RNAi* lines, further confirming that these phenotypes were likely caused by the perturbation of *REM34*, *REM35* and *REM36* function in the inflorescence of Arabidopsis.

The overexpression of the chimeric REM34-EAR protein could in theory cause the co-suppression of *REM34* and its homologues *REM35* and *REM36*, which could also be the cause of the similarity between the REM34-EAR and *REM_RNAi* lines.

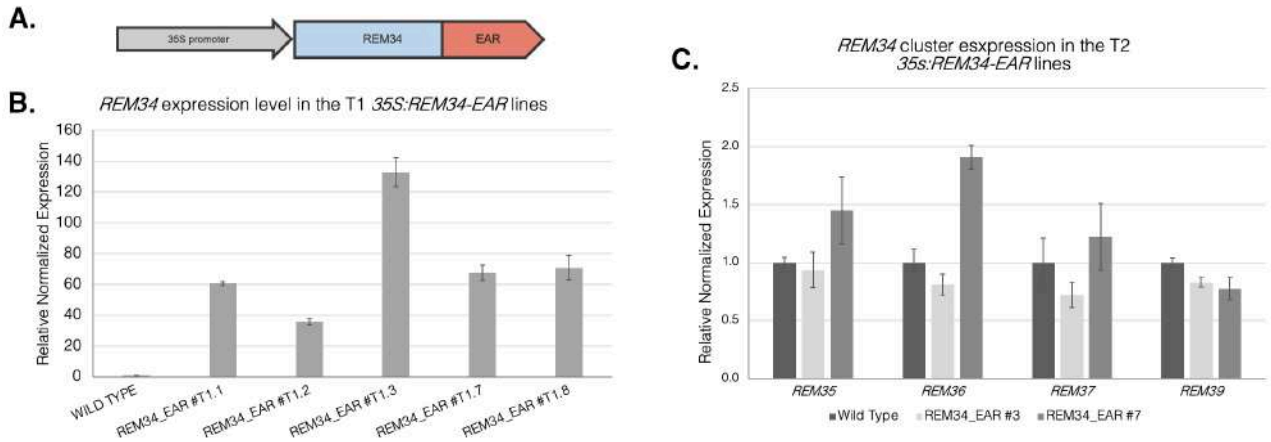

Figure II-2 *35S:REM34-EAR* lines

A. Schematic representation of the *35S:REM34-EAR* construct. The C-terminal of the *REM34* CDS was fused in frame with the EAR repressive motif, the expression of the chimeric protein is driven by the *CaMV35S* constitutive promoter. B. qRT-PCR for the evaluation of the *REM34_EAR* overexpression in five T1 transgenic lines, compared to the wild type all the analyzed lines show different levels of overexpression of *REM34,* the lines #1 and #7 were chosen to further investigate the effect of the overexpression of the dominant repressor REM34-EAR protein. C. qRT-PCR on inflorescence of the T2 *35S:REM34-EAR* #1 and #7 lines, the level of expression of different members of the *REM34* cluster was evaluated to ensure that the overexpression of *REM34* was not causing the downregulation of its homologous genes.

To exclude this possibility, the expression levels of *REM35*, *REM36*, *REM37* and *REM39* were measured: which revealed that none of the members of the *REM34* cluster was found to be downregulated, suggesting that the observed phenotypes were indeed caused by the action of the constitutive REM34-EAR repressor (Figure II-2C). The level of expression of the endogenous *REM34* was not taken into account, as the perturbation of *REM34* expression alone does not cause the phenotypical defects observed in the analyzed lines (Franco-Zorrilla *et al.*, 2002; Mantegazza, Gregis, Mendes, *et al.*, 2014).

The Arabidopsis genome is characterized by the extensive presence of duplicated chromosomal segments, suggesting an evolutionary model involving one or more cycles of genome duplications followed by gene loss and gene divergence. Besides the *REM* transcription factors, many other gene families appear to be organized in tandem arrays, further supporting the hypothesis of the evolution of the genome through gene duplication and specialization events (Bevan and Walsh, 2005). Functional redundancy between paralogous genes and the presence of in linkage homologous genes are diffused events in Arabidopsis and other plant species, making it crucial to develop fast and efficient tolls to overcome these difficulties.

In this study, we implemented two techniques, the RNAi and CRES-T, to allow the functional characterization of in-tandem redundant genes. The fusion of the EAR repressive motif to a transcription factor of interest was already found to be an efficient strategy when dealing with redundant transcription factors (Hiratsu *et al.*, 2003) and here we further proof that this tool is reliable also in the case of highly duplicated families, such as the one of the REM transcription factor. Indeed, the analysis of the expression of *REM35, REM36, REM37* and *REM39* in these lines showed that the overexpression of the *REM34-EAR* chimeric protein does not cause the silencing of other members of the *REM* family. The only CRES-T approach downside is that this technique is only appliable when dealing with transcriptional activators, while it would not be effective to functional characterize genes that work as transcriptional repressors.

The indication that both approaches gave the same phenotypical defects, when applied to study the *REM34* cluster function, provides solid evidence that both methods are reliable and useful tool to characterize in linkage and/or redundant genes and suggest that these genes might work as transcriptional activators.

CRISPR/Cas9 Genome Editing System

The two strategies described above were proved to be very efficient in helping in the functional characterization of *REM34*, *REM35* and *REM36*, but they do not produce complete knock-out mutants. Furthermore, *REM_RNAi* transgenic construct might be silenced over generations (Meins *et al.*, 2005). Therefore, we decided to exploit the CRISPR/Cas9 genome editing technology to generate single and multiple mutant combinations of the three genes of interest.

Following the protocol described by Fauser et al., 2014, we designed three protospacers, specific for the coding sequences of *REM34*, *REM35* and *REM36* and cloned them into the *pDE_Cas9* vector, in which the *Cas9* expression is driven by the constitutive *pUBI* promoter,

obtaining in this way three different constructs: *pDE_Cas9-REM34*, *pDE_Cas9-REM35* and *pDE_Cas9-REM36* (Figure II-3A).The protospacers were designed with the aid of the CRISP-P 2.0 software (Liu *et al.*, 2017) and they were selected for their specificity and absence of off-targets in the Arabidopsis genome.

To generate the three single mutants, the three different constructs were transformed into wild type Col-0 Arabidopsis plants. At least 15 transformant T1 plants for each construct were obtained and, for each of them, the region around the protospacer was amplified from genomic DNA extracted from inflorescences and sequenced, to detect the mutations induced by the CRISPR/Cas9 system. Among the 15 analyzed T1 plants carrying the *pDE_Cas9-REM34* construct, one was characterized by the insertion of a T in the protospacer sequence while all the other showed no changes in their sequence; two of the 15 plants carrying the *pDE_Cas9-REM35* presented an A insertion in their protospacer and, finally, an A insertion was found in the protospacer region of two of the *pDE_Cas9-REM36* plants (Figure II-3B).

In this generation, the plants are likely to be chimeric and the mutations observed are inherited by the successive generation only if they arise in the germ cell line. In addition, the plants of the T1 generation are still characterized by the presence of the *pDE_Cas9* transgene.

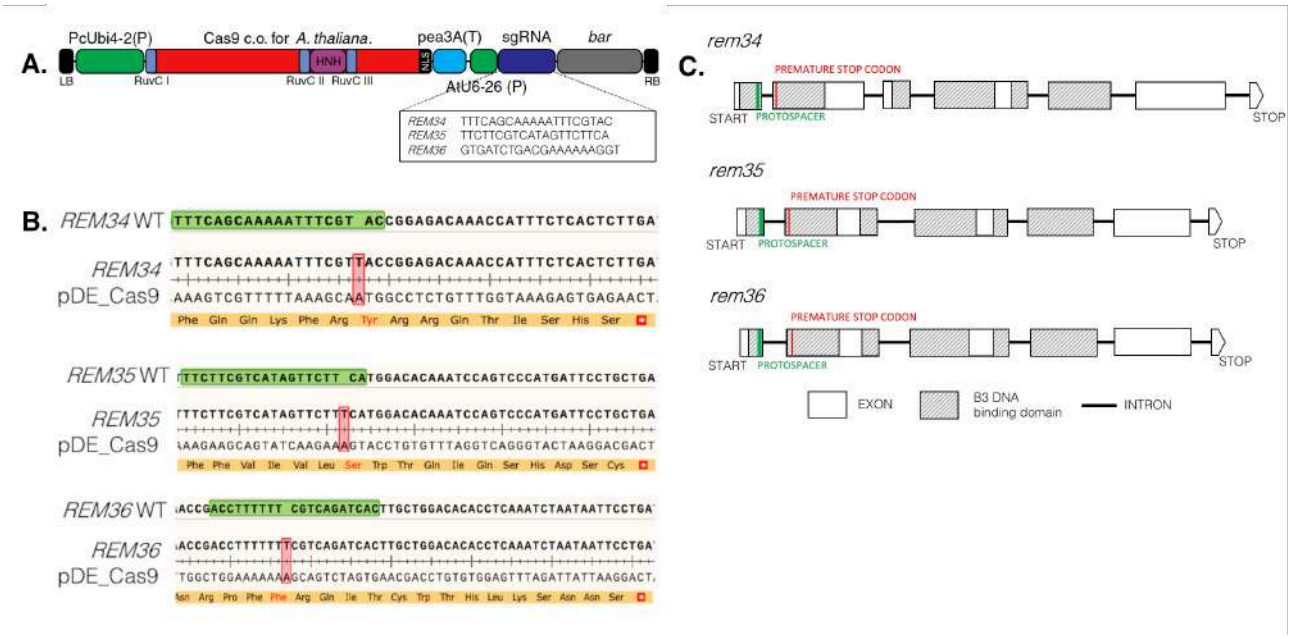

Figure II-3 CRISPR/Cas9 Genome Editing System.

A. Schematic representation of the construct employed for the editing of *REM34, REM35* and *REM36.* The Cas9 expression is driven by the PcUbi4-2 promoter, the basta resistance (bar) cassette allows the selection of transformant plants. The sequences of the three protospacers are indicated in the box. Adapted from Fauser *et al.,* 2014. B. Alignments of the *REM34, REM35* and *REM36* wild type and mutated sequences. For all the three genes the wild type sequences is indicated on top of the alignment and the protospacer is underlined in green. The mutated sequences, with the nucleotide insertion indicated in red, is showed below. For each gene, the aminoacidic sequence is also shown, and the newly formed stop codon is indicated by the red asterisk. C. Schematic representation of the structure of *REM34, REM35* and *REM36.* The three genes are characterized by three repetitions of the B3 DNA binding domain, indicated by the striped boxes. The premature stop codon location is indicated in red and the protospacer region in green.

To allow the segregation of the transgene and test whether the identified mutations were inherited by the following generation, the T1 plants showing a mutation in the target region were propagated to the T2 generation, where it was possible to obtain single homozygous mutated lines for *rem34*, *rem35* and *rem36* without the CRISPR/Cas9 construct.

REM34, *REM35* and *REM36* share a similar structure, which is characterized by the repetition in tandem of three B3 DNA binding domains. To disrupt their function as transcription factors, all the protospacers were designed to target the first of the DNA binding domain; the three mutants are characterized by the insertion of a single nucleotide which causes a frameshift in the CDS, inducing the formation of a premature stop codon at the beginning of the first B3 domain (Figure II-3C).

Since *REM34*, *REM35* and *REM36* are in close linkage on chromosome 4, it was not feasible to cross the single mutants to obtain multiple mutant combinations. Once the *rem34*, *rem35* and *rem36* homozygous single mutants were obtained and the Cas9 transgene was lost by segregation, they were re-transformed with a different *pDE_Cas9* construct, specific for one of the other *REM* genes of interest, to generate all the possible double mutants combinations.

Among the six T1 *rem34* plants, carrying the *pDE_Cas9-REM35* construct, three displayed an A insertion in the region of the protospacer. 14 T1 *rem34* plants, with the *pDe_Cas9-REM36* construct, were obtained four of which were found to have a A insertion in the protospacer. Finally, two of the 19 *rem35* plants transformed with the *pDE_Cas9-REM36* construct, were found to carry an A insertion in the *REM36* coding sequence. In the following generations, all the different double mutant, without the *pDE_Cas9* transgene, were isolated. To obtain the double mutants, we employed the same protospacers used to generate the three single mutants. As a consequence, the mutations produced by the action of the Cas9 were the same in the single and double mutants, and are the ones described in the Figure II-3B and C.

Besides from the strategy described above, three different CRISPR/Cas9 multiplexed genome-editing system were also employed, all of which relied on the expression of multiple gRNAs in a single construct. While in the first multiplex strategy employed, the Cas9 expression was driven by the constitutive *pUBI* promoter, the other two relied on the use of promoters specific for the reproductive tissues, which are more likely to generate mutation in the germ lines (Lowder *et al.*, 2015; Wang *et al.*, 2015).

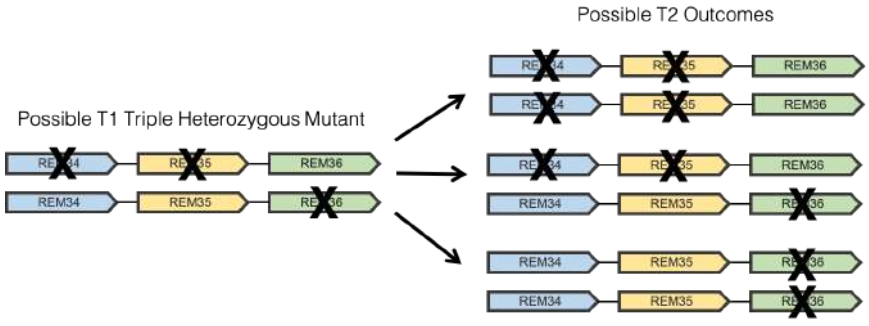

Figure II-4 Possible inheritance pattern of the mutations induced by a multiplexed CRISPR/Cas9 genome editing approach.

These methods were found to be able to generate some multiple mutant combinations, but never in homozygosity. This might be due to the fact that the target genes *REM34*, *REM35* and *REM36* are in tandem and the mutant alleles are not always generated *in cis,* therefore the mutants alleles are not always in the same haplotype (Figure II-4).

Therefore, we believe that the most efficient strategy, to generate multiple mutants of in linkage genes in Arabidopsis, was to utilize one single gRNA at the time, generating first the single mutants of interest and later all the possible double mutants combinations.

II.II Role of *REM34*, *REM35* and *REM36* in gametophytes development

REM_RNAi and 35S:REM34-EAR have a reduced seed set

At the start of my PhD thesis research the CRISPR-Cas9 induced mutants were not yet available. Therefore, to functionally characterize the role of *REM34*, *REM35* and *REM36* during Arabidopsis' inflorescence development, plants containing either the *REM_RNAi* construct, in which the three target genes were simultaneously silenced, or expressing the *REM34-EAR* chimeric protein, where *REM34* is constitutively expressed and acts as a dominant repressor, were used. Both approaches led to the generation of T1 plants with short siliques, which hinted to fertility problems.

To examine in depth this defect, three *REM_RNAi* (#1, #4 and #5) and two *35S:REM34-EAR* (#1 and #7) lines were propagated to the T2 generation, where their silique length and seed set were evaluated.

The *REM_RNAi* #T2.1 line showed a decrease of 35.3% in the silique length and a 19.4% reduction in total ovule number. Furthermore, on average 66% of the ovules failed to be fertilized. The other two *REM_RNAi* lines, #4 and #5, showed a similar phenotype even if the percentage of unfertilized ovules was lower, 35.3 and 45.4%, respectively (Figure II-5). These defects were confirmed in the *35S:REM34-EAR* lines, in which the T2 generation of the #1 and #7 lines were found to show a decrease in the silique length of 23.1 and 25.0%, respectively, and the presence of 55.0 and 42.6% aborted ovules (Figure II-5).

We chose the *CaMV35S* constitutive promoter to drive the *REM_RNAi* fragments and *REM34-EAR* expression, as it has been shown that such promoter can be successfully employed to study the function of genes involved in gametophytic development (Acosta-García and Vielle-Calzada, 2004; Mendes *et al.*, 2016). Such promoter is highly active in the sporophytic reproductive tissues, but its activity seems to be low during female and male gametophyte development. Is thus possible that the observed gametophytic phenotypes are caused by the silencing of *REM34*, *REM35*, and *REM36* in the female and male sporophytic cells, rather than from a defect in the gametophyte themselves. However, it is also important to consider that the RNAi construct is dominant and that it can trigger a non-cell autonomous and systemic silencing signal which might be maintained throughout the different phases of plant development (Mlotshwa *et al.*, 2002; Melnyk *et al.*, 2011; Skopelitis *et al.*, 2018).

To evaluate whether the sterility observed in the *REM_RNAi* T2 segregating lines was exacerbated in plants carrying the construct in homozygosity, as expected if the defect was gametophytic, the *REM_RNAi* #1 line was propagated to the T3 generation, where plants

homozygous for the *REM_RNAi* construct were selected. Interestingly, the percentage of ovule abortion was the same in the *REM_RNAi* #T2.1 and the *REM_RNAi* #T3.1, suggesting that the silencing of the three *REM* genes was probably acting both at the sporophytic and gametophytic level (Figure II-3C).

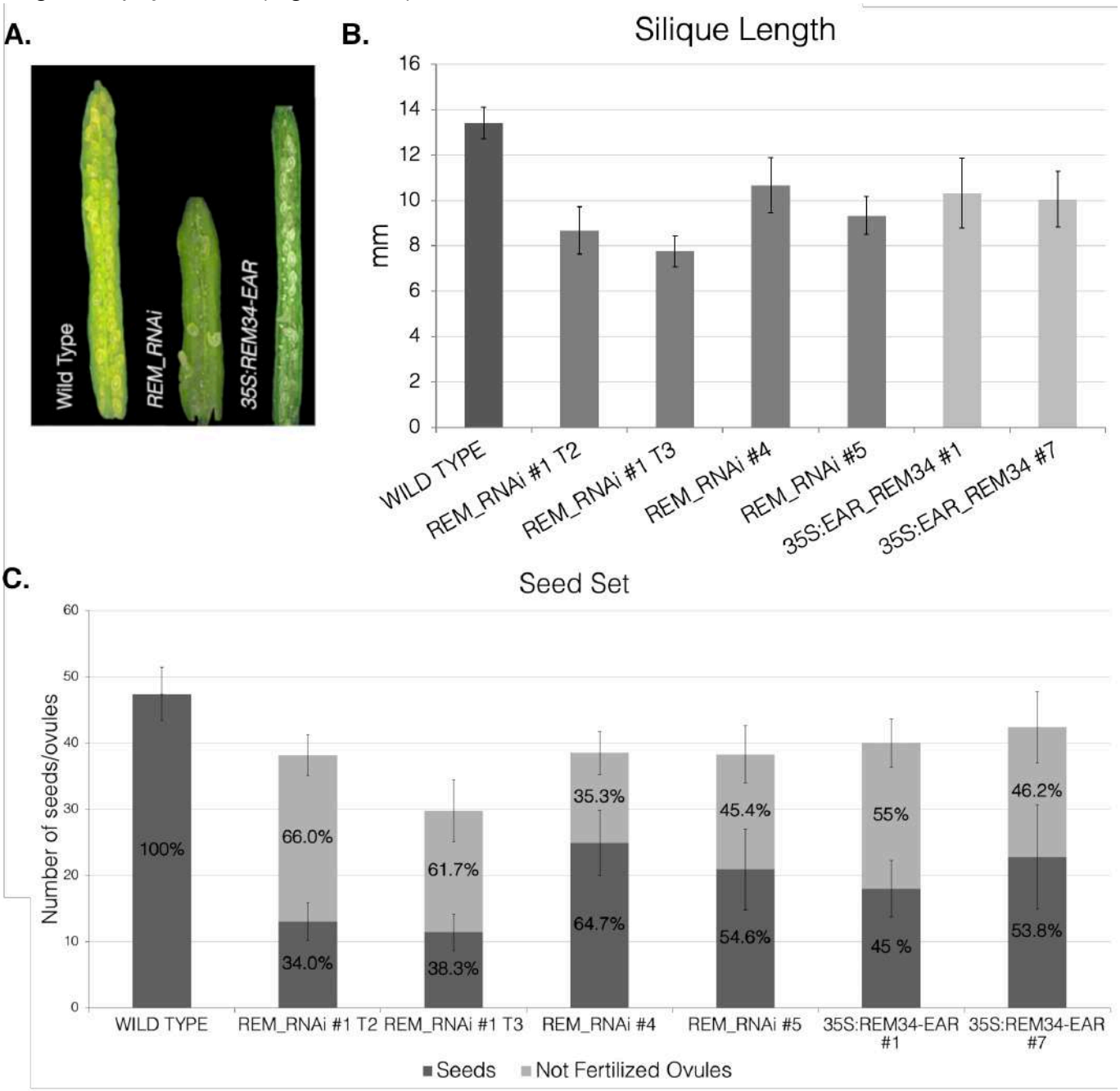

Figure II-5 Partial sterility phenotype of the REM_RNAi and 35S:REM34-EAR lines

A. Example of a wild type, *REM_RNAi* and *35S:REM34-EAR* line seed set. B. Graph showing the mean length of 10 wild type and 10 *REM_RNAi #1* T2*, #T1* T3*, #T4*, #*5* and *35S:REM34-EAR #1* and 7 siliques. A wild type silique measures on average 13.4 mm, the siliques from the different *REM_RNAi* and *35S:REM34-EAR* lines were found to measure on average between 7.8 and 10.7 mm. ($p < 0.01$ for all comparison with the wild-type, ANOVA and *post hoc* Tukey HSD test were used). C. Graph showing the mean number of ovules/silique in the wild-type and *REM_RNAi* and *35S:REM34-EAR* plants, divided in seeds and not fertilized ovules. Compared to the wild-type situation, in which each silique contains on average 47.4 ovules, the *REM_RNAi* siliques have on average 29.8 to 38.5 ovules while the *35S:REM34-EAR* lines show a reduction of about 10% in the total seed set ($p < 0.01$ for all comparison with the wild-type, ANOVA and *post hoc* Tukey HSD test were used). On each histogram bar, the percentage of seeds and not fertilized ovules/siliqua are shown: on average between 35.3 and 66.0% of ovules, depending from the analyzed line, failed to be fertilized, while no aborted ovules were detected in the wild type situation ($p < 0.01$ for all comparison with the wild type, ANOVA and *post hoc* Tukey HSD test were used).

These analyses allowed also the exclusion of the possibility that the reduced seed set was linked to the presence of a heterozygous T-DNA insertion (Curtis *et al.*, 2009; Clark and Krysan, 2010) and suggests that either the sporophytic silencing of *REM34*, *REM35*, and *REM36* affects the gametophyte or that the mobile siRNA diffuses from the sporophyte to the gametes, causing the partial sterility observed both in the *REM_RNAi* and in the *35S:REM34-EAR* lines.

To understand if the reduced seed set was due to problems in the female or the male gametophyte, we performed reciprocal crosses between T3 *REM_RNAi* #1, homozygous for the T-DNA triggering the RNAi silencing, and wild type plants. As a control, both T3 *REM_RNAi* #1 and wild-type plants were manually self-pollinated, to evaluate how the manipulation of the flower was affecting the fertility of the analyzed plants (Figure II-6).

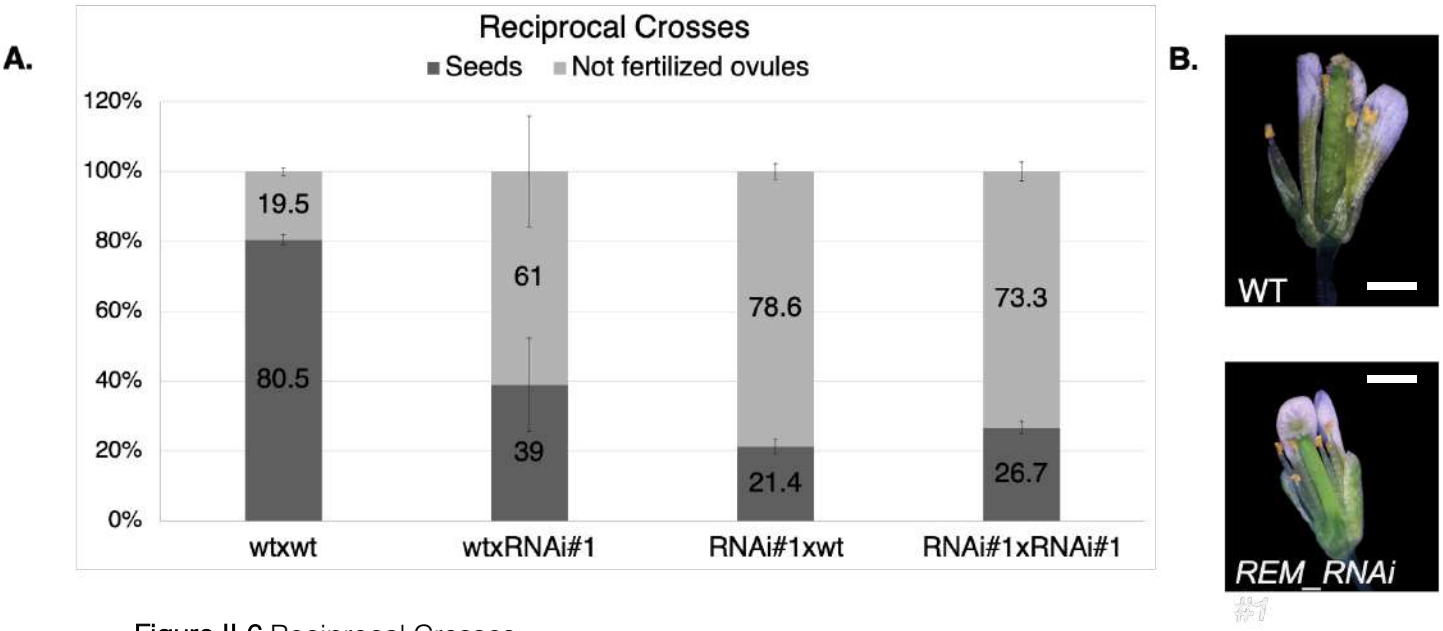

Figure II-6 Reciprocal Crosses

A. Reciprocal crosses analysis between wild type and T3 *REM_RNAi* #1 plants, homozygous for the construct. As a control, both wild type x wild type and *REM_RNAi* #1 x *REM_RNAi* #1 crosses were performed. Crosses are indicated female x male. ($p < 0.01$ for all comparison with the wild type of the non-fertilized ovules number, ANOVA and post hoc Tukey HSD test were used). **B.** Example of a wild type and *REM_RNAi* line flower, compared to the wild type *REM_RNAi* anthers appear to contain less pollen, which does not adhere well to the stigma. Scale bar 20 mm.

When *REM_RNAi* pistils were pollinated with *REM_RNAi* pollen, 73.3% of the ovules failed to be fertilized while wild type lines manually pollinated with wild type pollen showed a 19% decrease in fertility, suggesting that the manual pollination was only slightly affecting the efficiency of the fertilization process. When *REM_RNAi* pistils were pollinated with wild type pollen, the percentage of unfertilized ovules was 78.6%, indicating a strong defect of the female reproductive organs of the *REM_RNAi* lines. Interestingly, when wild type pistils were pollinated with *REM_RNAi* pollen, 61.0% of the ovules were not fertilized. Moreover, we observed a high variability in the number of unfertilized ovules using *REM_RNAi* pollen.

Macroscopical inspection revealed a decrease in pollen grain number compared to wild type anthers and a lack of adherence of the pollen to the wild type stigma. All these considerations strongly suggest that both female and male reproductive organs are affected in the *REM_RNAi* lines.

REM34, REM35 and REM36 expression pattern during sporogenesis and gametogenesis

Reciprocal crosses between wild type and *REM_RNAi* plants suggested that *REM34*, *REM35* and *REM36* could play a role in both female and male gametophyte development, however, a detailed analysis of the expression levels of these genes was only available for the inflorescence meristem, flower meristem and during the first stages of flower development (Franco-Zorrilla *et al.*, 2002; Mantegazza, Gregis, Mendes, *et al.*, 2014), while their pattern of expression during sporogenesis and gametogenesis was not investigated yet.

Consequently, an RNA *in situ* hybridization analysis for *REM34*, *REM35*, and *REM36* in both female and male reproductive organs was performed, to understand where and when these genes are expressed during flower development and to further understand if they play a role during the sporophytic or gametophytic development of the reproductive tissues.

In Arabidopsis, pollen mother cells differentiate inside young anthers, while ovule primordia arise from the placenta, at stage 8 of flower development and their differentiation is completed at stage 13 (flower and gametophytes developmental stages are defined accordingly to Schneitz et al., 1995 and Smyth et al., 1990.)

Our analysis revealed that the timing of expression of the three *REM* genes coincided with male and female sporogenesis. Indeed, at stage 8/9 of flower development, a hybridization signal for *REM34*, *REM35* and *REM36* was detected in the anthers, where the pollen mother cells differentiate, and within the carpels and, where the signal was stronger in the placenta and ovule primordia (Figure II-7A). At stage 10, which coincides with the last steps of sporogenesis, a strong signal was detected in developing ovules and pollen (Figure II-7B).

During subsequent stages of flower development, stages 11–12, both female and male initiate gametophyte development. A decrease in the signal was clearly observable in anthers; during these stages, pollen reaches maturity, and the vegetative and generative cells differentiate, after undergoing two mitotic divisions (Park *et al.*, 1998). In contrast, a strong signal was detected during ovule development when the surviving megaspore undergoes three rounds of mitosis and passes from stages 3I to 3V. Interestingly, when the ovule is at its very last stage of development 3-VI, a strong signal was detected in the funiculus, in the innermost integument and, inside the mature female gametophyte, in the central cell region (Figure II-7D).

The expression analysis of *REM34*, *REM35*, and *REM36* highlighted the fact that, as already reported for the inflorescence meristem tissues, they shared the same expression pattern also during anther/pollen and carpel/ovule development.

They were indeed expressed, during sporogenesis, in the female and male reproductive tissues, both during the sporophytic and gametophytic phase.

During gametogenesis, their expression level decreased in the anthers and pollen grains, while a strong signal persisted in the female gametophyte and the surrounding sporophytic tissue.

These evidences, combined with the phenotypes observed in the *REM_RNAi* lines, denote an important role for these genes during the development and production of viable male and female structures and gametes, in both sporophytic and gametophytic organs.

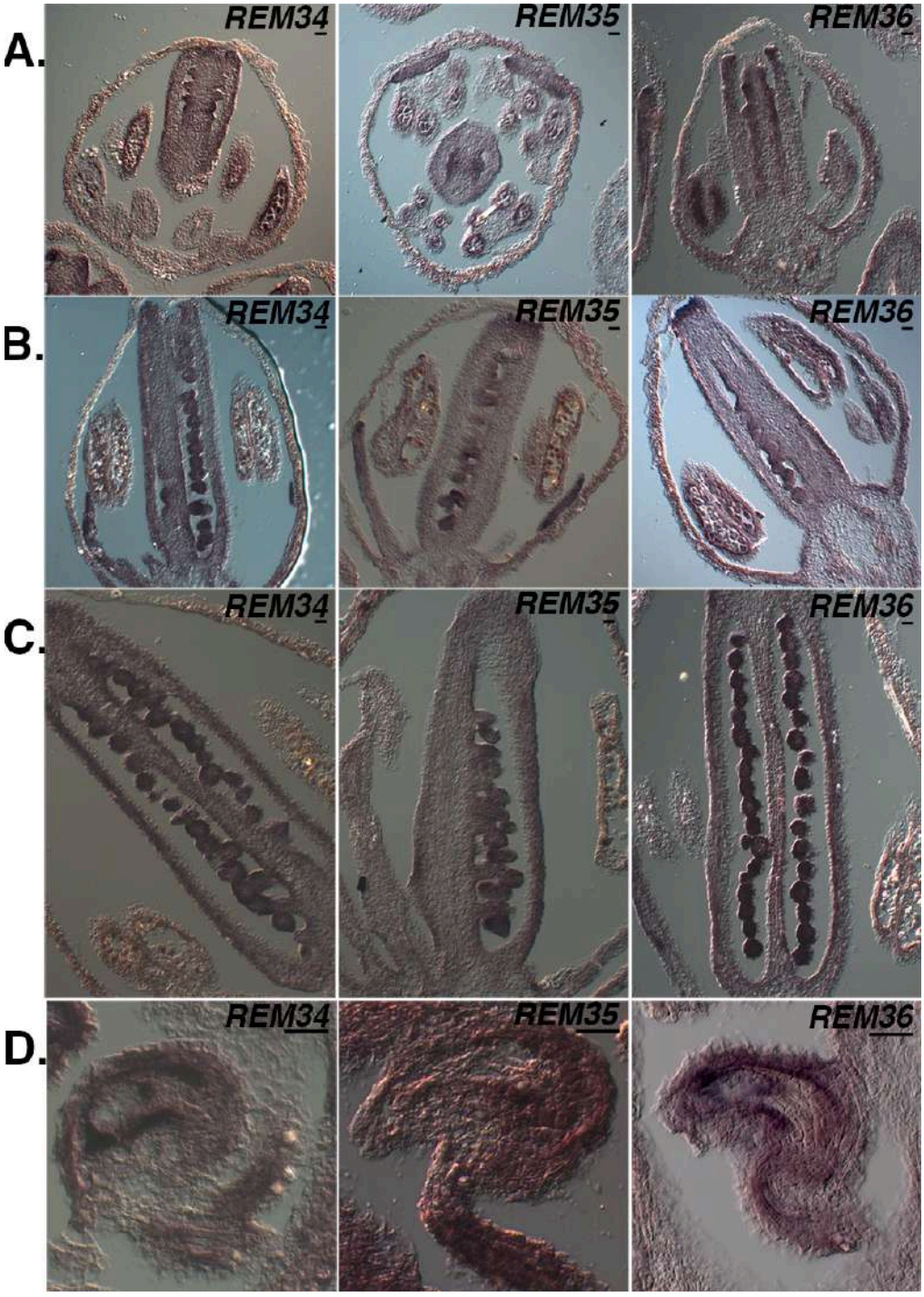

Figure II-7 REM34, REM35 and REM36 in situ hybridization analysis

A. In flowers at ST8-9, the signal in the carpel is restricted in the tissue of the placenta and ovules primordia. At the same stage, a clear signal is also visible in the anthers. B. At ST 10-11, the signal is present in the ovules, which are completing megagametogenesis, and in the anthers, where the pollen grains are undergoing the first mitotic division. C. At ST12, when pollen reaches maturity, the signal is no longer visible in the anthers. D. In flowers at anthesis, the target genes are expressed in the mature female gametophytes, in particular in the funiculus, inner integuments, and central cell. (bar = 20 µm).

REM_RNAi and 35S:REM34-EAR lines are characterized by a post-meiotic defect of both female and male gametophyte

The expression profile of *REM34*, *REM35*, and *REM36* suggests that these genes play a role during ovule and pollen development. Furthermore, the reciprocal crosses showed that between 73.3% and 78.6% of the ovules in the *REM_RNAi* homozygous background could not be fertilized with wild type pollen. In a similar way, *REM_RNAi* derived pollen was able to fertilize only 40% of wild type ovules.

Based on this evidence, we hypothesized that both gametophytic defects in the *REM_RNAi* lines might be due to an arrest in their development.

Therefore, a detailed evaluation of female gametophyte development was carried out in the T3 *REM_RNAi* #1 homozygous line. In this line, 42.9% (227/529) of the ovules failed to complete their development and showed an arrest in the FG1 stage (Figure II-8A). These ovules were characterized by an embryo sac containing one large cell, the functional megaspore, with a single nucleus; the rest of the ovules completed their development reaching the FG7 stage. The same phenotype was observed in the T2 of the RNAi #4 and #5 lines, both derived from hemizygous mothers (Figure II-8B).

The phenotype of the aborted ovules was further evaluated in cleared mature carpels of the T2 *35S:REM34-EAR* #1 and #7 lines. Also in these lines, we detected both mature ovules at FG7 stage, with the seven cells clearly distinguishable, and ovules at FG1 stage, characterized by a single cell embryo sac (Figure II-8B). The FG1 stage is the stage that defines the end of sporogenesis, when the Megaspore Mother Cell (MMC) acquires the identity of Functional Megaspore and subsequently will undergo three mitotic divisions that give rise to the mature embryo sac.

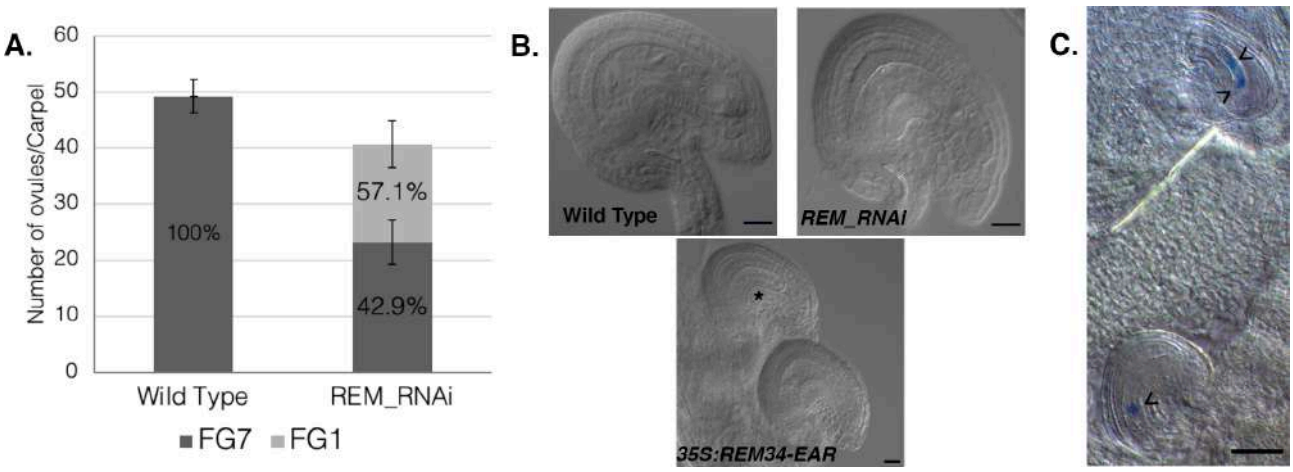

Figure II-8 Female Gametophyte Analysis.

A. Analysis of cleared mature carpels of both wild type (n = 11) and *REM_RNAi* #1(n = 13). In wild type mature carpels, all the ovules reach the FG7 stage (542/542 ovules), while in the *REM_RNAi* line, 227/529 ovules are arrested at the FG1 stage. B. Cleared ovules collected from wild type, *REM_RNAi and 35S:REM34-EAR* mature carpels. In the wild type situation, 100% of the embryo sac reaches the FG7 stage, while in the RNAi and EAR carpels it is possible to detect ovules blocked in the FG1 stage, marked by an asterisk, and mature ovules (bar = 20 µm). D. *pSUF4:SUF4-GUS* in the *REM_RNAi* line: in the uppermost ovule, two nuclei are stained, indicating the progression of gametogenesis till FG4 stage. In the lowest ovule only one nucleus is stained indicating an arrest in FG1 stage. The arrowheads marked nuclei (bar = 50 µm).

To confirm that, in the *REM_RNAi* lines, the defective female gametophytes were arrested in the FG1 stage, after meiosis, we crossed the *pSUF4:SUF4-GUS* marker line with the *REM_RNAi* plants. In the *pSUF4:SUF4-GUS* marker line, *GUS* expression is not detectable during megasporogenesis, but it becomes visible after meiosis, once the functional megaspore is formed, and marks all the nuclei of the embryo sac (Resentini *et al.*, 2017).

In *REM_RNAi* pistils, it was possible to observe both wild type like ovules, with more than one nucleus and ovules arrested in the FG1 stage, with the nucleus of the functional megaspore, expressing the *GUS* reporter suggesting that the defect in female gametophyte development was post-meiotic (Figure II-8C).

In parallel, to understand the cause of the male gametophyte defect, an in vitro germination assay was carried out which showed a 30% decrease in the germination rate of the *REM_RNAi* pollen compared to the wild type (Figure II-9A and B). The growth rate of *REM_RNAi* pollen tubes and their ability to target correctly ovules were also evaluated in vivo by means of aniline blue staining.

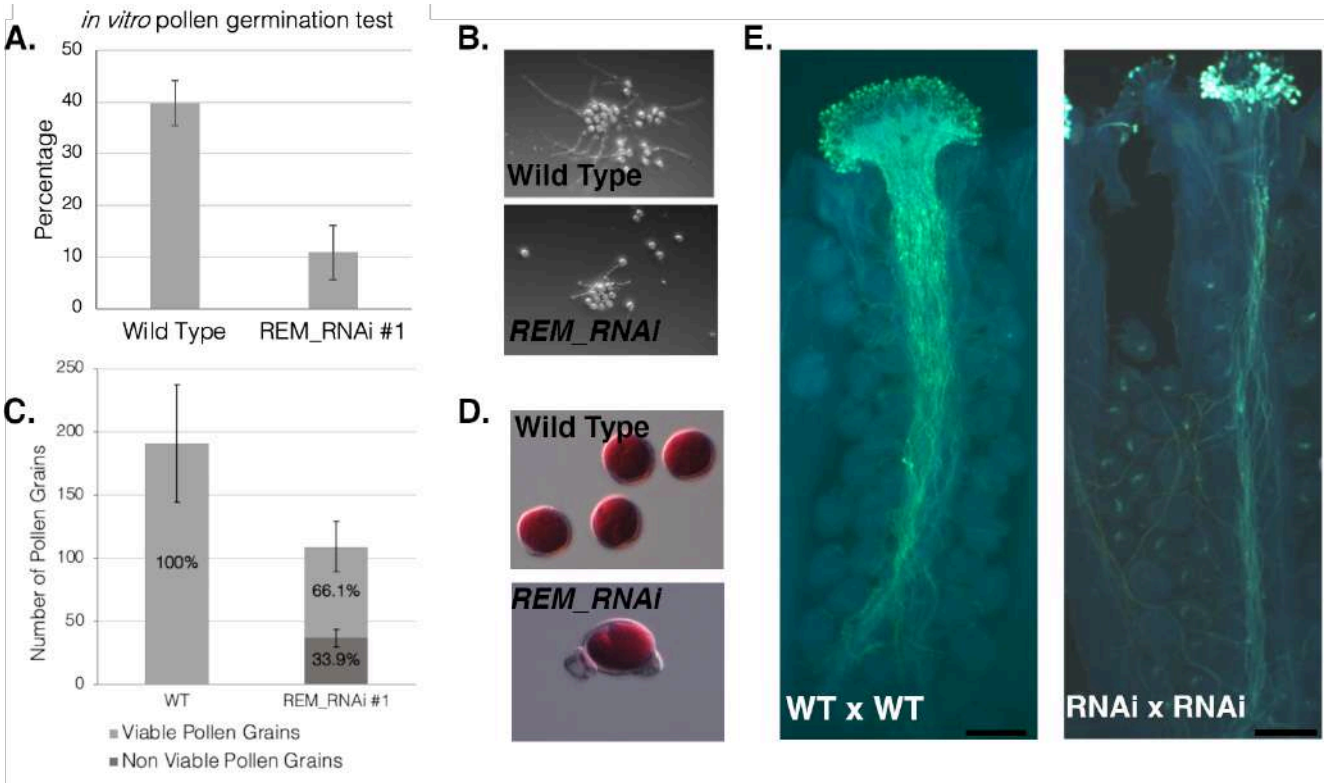

A. *REM_RNAi* #1 pollen germination test *in vitro* showed a 30% decrease in the germination capability in the *REM_RNAi* grains compared to the wild type. **B.** Example of the i*n vitro* germination test of wild type and *REM_RNAi* #1 pollen grains, plates were imaged 24 h after plating (bar = 100 µm), compared to the wild type, where the majority of pollen grains were able to produce the pollen tube, only a few grains germinated 24h after plating **C.** Mature anthers from wild-type and *REM_RNAi#1* flowers were dissected, the released pollen was collected and treated with Alexander's staining to discriminate between viable and non-viable pollen grains. In the wild type, 100% of the pollen grains resulted vital while 33.9% of *REM_RNAi#*1 pollen was found to be non-vital. (wt n = 1,337, *REM_RNAi #1= 874*; $p < 0.01$ for all comparison with the wild-type, ANOVA and *post hoc* Tukey HSD test were used). **D.** Pollen grains, collected from mature anthers of both wild-type and *REM_RNAi #*1 anthers, were stained with Alexander's staining to check pollen grain viability. While all the wild type grains were viable, some *REM_RNAi#*1 pollen grains appeared shrunken and unable to be stained in red (bar = 20 µm). **E.** Aniline staining was employed to visualize pollen grains adhesion to the stigma and pollen tube germination and growth. Compared to the wild type situation, a lower number of *REM_RNAi* #1 grains were able to adhere to the stigma and to germinate. In both cases the pollen tubes grow correctly until the end of the transmitting tract, In *REM_RNAi #1* x *REM_RNAi #1* cross, several ovules are not targeted by a pollen tube, as these are blocked in FG1 stage and so synergids are not properly formed (Bar=100µm).

The *REM_RNAi* pollen tubes did not show any growth defect: they reached the end of the pistil in the same time as the wild type pollen tubes, and the mature ovules were correctly targeted (Figure II-9E). We noticed that, as mentioned before, the *REM_RNAi* pollen number appeared to be lower, and they did not adhere well to the stigma papillae, which could explain the high variability observed in the backcrosses between wild-type pistils and *REM_RNAi* pollen.

To calculate the percentage of viable pollen grains, mature anthers were collected from *REM_RNAi* and wild type plants and treated with Alexander's stain, which colors viable pollen red. While in the wild type, all the collected pollen was viable, in the *REM_RNAi* anthers, 33.9% of the grains were not stained, indicating that those pollen grains were non-viable and did not appear to contain any cytoplasm (Figure II-9C and D).

The percentage of non-viable pollen grains in the *REM_RNAi* line corresponds to the decreased germination capability observed in vitro, suggesting that the grains which are unable to produce the pollen tube are the degenerated ones.

We decided to follow *REM_RNAi* pollen development, employing DAPI to visualize nuclei division, to detect when the degeneration of the nuclei was occurring. At the microspore stage, both *REM_RNAi* and wild type grains were characterized by the presence of a single bright nucleus localized at the center of the cell, indicating that the pollen went through sporogenesis and meiosis correctly. After meiosis, in wild type, the microspore undergoes gametogenesis which consist of a first mitotic division that produced one vegetative and one sperm nucleus. Subsequently, the second round of mitosis leads to the formation of the mature pollen grain, which contained two small sperm cells each with a bright and elongated nucleus and the vegetative cell.

In *REM_RNAi* anthers, however, after the first mitotic round, some grains were characterized by the lack of nuclei; this phenotype was detectable also at the tricellular stage, where *REM_RNAi* anthers displayed both viable pollen grains, with two sperm cell nuclei and a distinct vegetative nucleus, and not viable pollen grains, in which no DNA was detectable (Figure II-10 A-F).

The degeneration of the pollen grains was detected also in the T2 of the RNAi #4 and #5 lines, where the DAPI staining of mature anthers confirmed the presence of both fully developed and defective grains (Figure II-10G and H). This analysis suggests that the degeneration of pollen grains observed in the *REM_RNAi* lines could be due to a post-meiotic block, a similar defect to the one observed in the female gametophytes.

To confirm the post meiotic block in the male gametophyte, mature pollen of the T2 *35S:REM34-EAR* #1 and #7 lines were stained with DAPI. Similarly to what was observed in the *REM_RNAi* lines, some pollen grains were able to reach the tricellular stage while others appeared shrunken and degenerated, with no visible nuclei (Figure II-10 I).

Our analyses showed that *REM34*, *REM35* and *REM36* are expressed throughout female and male gametophyte development in both gametes and in the sporophytic tissues surrounding them. Furthermore, *REM_RNAi* and *35S:REM34-EAR* lines are characterized by a reduced seed set. This sterility problem is due to a block in both female and male gametophyte development, that are able to go through sporogenesis correctly, giving rise to haploid spores, but cannot undergo the mitotic rounds which are necessary for the correct

gametogenesis. Thus, in Arabidopsis, *REM34*, *REM35*, and *REM36* transcription factors seem to be required post-meiotically for gametophytic development.

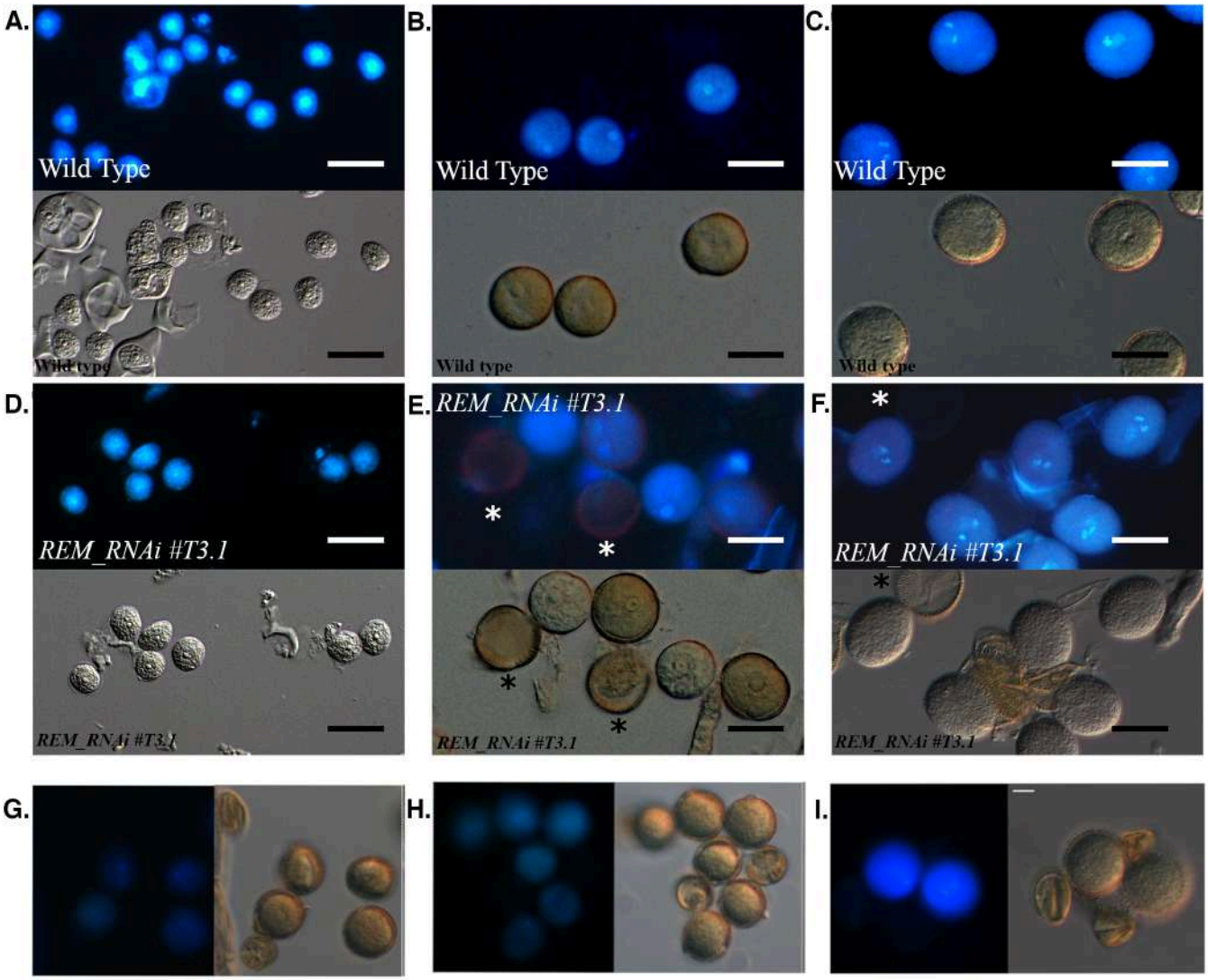

Figure II-10 Pollen development in the *REM_RNAi* and *35S:REM34-EAR* lines

A-F. DAPI staining of wild type and *REM_RNAi #*1 pollen grains at different developmental stages. At the microspore stage (A and D), all the grains contain a well-defined central nucleus. At the bicellular stage in all wild type grains (B), the sperm and vegetative nuclei are distinguishable, while in the *REM_RNAi #*1 lines (E), some grains, marked with an asterisk, do not display any nucleus. Wild type mature pollen grains (C), characterized by the presence of two sperm cells and one vegetative nucleus.*REM_RNAi#*1 mature pollen (F), the asterisk marks a mutant pollen grain without nucleus (bar = 10 µm). G-H. DAPI stained pollen, collected from the *REM_RNAi* #4 and #5 mature anthers, some grains do not contain any nuclei and appear to be degenerated. I. Pollen grain collected from mature *35S:REM34-EAR* anthers, show the same phenotype described for the *REM_RNAi* lines

REM34 and REM35 interaction

Different studies on the *REM* gene family showed that these transcriptional factors are likely to act forming complexes with themselves or with other regulatory proteins (Romanel et al., 2009; Swaminathan et al., 2008). In particular, VDD and VAL, two functionally characterized *REM* factors involved in synergid degeneration upon fertilization, carry out their function forming hetero and homodimers (Mendes *et al.*, 2016). To understand if also

REM34, REM35, and REM36 could function via dimer formation, yeast two-hybrid assays were performed.

This approach revealed that REM35 is able to interact strongly with itself and also with REM34, while no interactions were detected with REM36 (Figure II-11A). All the interactions observed in the yeast two-hybrid assays were confirmed in vivo with a Bimolecular Fluorescence Complementation (BiFC) assay in *Nicotiana benthamiana* leaves (Figure II-11 B).

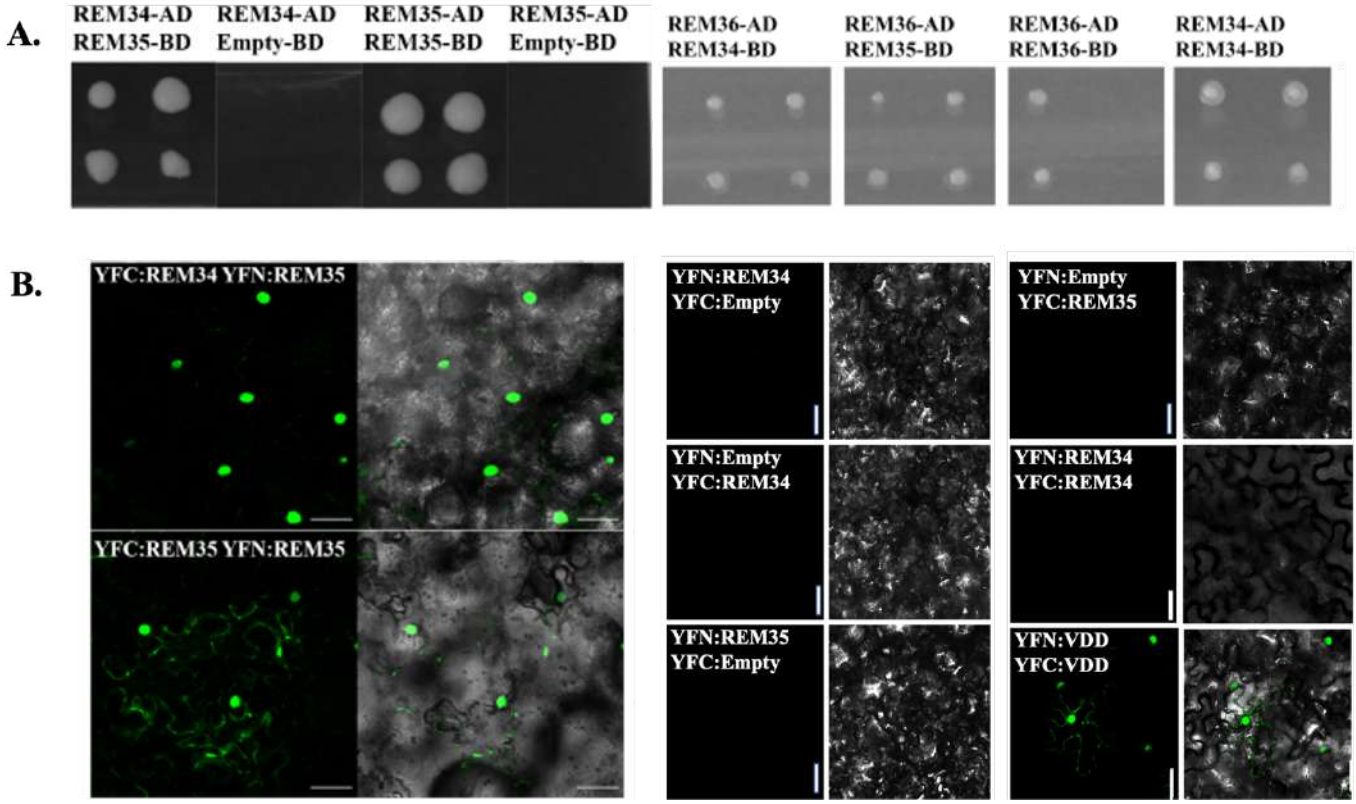

Figure II-11 REM34 and REM35 interaction.

A. Yeast two hybrid assays showing the interactions between REM34 and REM35 and REM35 and REM35, on –L-W-H + 2.5 3-AT selective media. Empty pDEST32 vector was employed as a negative control. In the Y2H assays, no interactions were detected for REM36 and REM34 homodimers. B. BiFC experiments in tobacco leaf cells showing the reconstitute YFP fluorescence (green) between REM34 and REM35 fusions to the C- and N-terminal fragments of YFP, respectively. REM35 fusions to the C- and N-terminal fragments of YFP (bar = 50 µm). Negative and positive controls for the BiFC experiment: all the constructs were cotranformed with the corresponding empty vector to test for false positive interaction. The REM34_REM34 interaction, which was found to be negative in the Y2H screening, was also employed as a negative control. Finally, as a positive control, the VDD_VDD interaction (M. Mendes et al, 2014) was tested.

This finding suggests that REM35 could act as a homodimer and as a heterodimer, together with REM34. It is interesting to notice that the same interaction behavior was reported also for VDD and VAL, suggesting that these characteristics might well be a common feature for the REM family and, in perspective of the guilt-by-association principle, it would be informative to analyze all possible REM protein interactions. The same approach was shown to be extremely useful for the characterization of MADS domain transcription factor family, for which extensive protein–protein interaction studies effectively guided genetic studies and functional characterization of many of them (de Folter *et al.*, 2005; Gregis *et al.*, 2006; Fornara *et al.*, 2008; Immink *et al.*, 2009).

Downregulation of REM34, REM35, and REM36 Altered Expression of Genes Involved in Post-Meiotic Divisions

As described above, the downregulation of *REM34*, *REM35*, and *REM36* resulted in a post-meiotic arrest in both female and male gametophytes, suggesting that these transcription factors could be involved in regulating mitosis progression during gametogenesis.

To elucidate the molecular mechanism behind this block, we measured the expression levels of genes that control gametogenesis by q-RTPCR. We focused on genes that, when mutated or overexpressed, cause similar defects to those observed in the *REM_RNAi* gametophytes. Those genes were divided into three categories, based on the biological process in which they are involved in: ribosome biogenesis (*MIDASIN MDS*, NOTCHLES *NLE*), cell cycle control (*RETINOBLASTOMA-RELATED PROTEIN RBR*, *CYCLIN-DEPENDENT KINASE INHIBITOR KRP6*), and chromatin regulation (*HISTONE ACETYL TRANSFERASE HAM1*, *HAM2*) (Figure II-12).

MDS, which, together with *NLE*, is involved in the biogenesis of the 60S ribosomal subunit and is essential during megagametogenesis (Chantha *et al.*, 2010), was shown to be downregulated in the *REM_RNAi* lines. *KRP6*, a CDK inhibitor whose overexpression causes a block in mitosis progression during female and male gametophytic development, was also downregulated in the *REM_RNAi* lines.

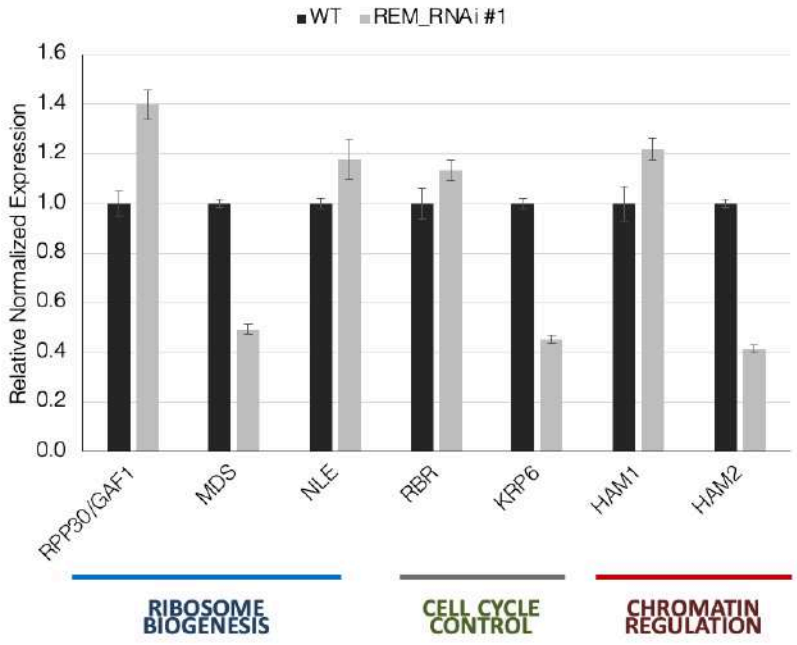

Figure II-12 Possible targets of REM34, REM35 and REM36

Expression analysis of genes involved in gametophyte development by qRT-PCR. Selected gene expression in inflorescence of wild-type and *REM_RNAi #T3.1*. The expression of selected genes was normalized to that of UBI, and the expression level in Col was set to 1. The possible targets were classified accordingly to their biological function: ribosome biogenesis, cell cycle control and chromatin regulation

Among the downregulated genes, the one that stands out most is *HAM2*, a HAT that, together with its homolog *HAM1*, belongs to the MYST clade of the *HAT* family and was shown to be involved in post-meiotic control of female and male gametophytic development. The *ham1 ham2* double mutant is lethal, while keeping one of the two genes heterozygous for the mutant allele resulted in a post-meiotic arrest during both female and male

gametophyte developments (Latrasse *et al.*, 2008), a phenotype similar to the one observed in the *REM_RNAi* as well as in the *35S:REM34-EAR* lines.

The downregulation of *HAM2* in the *REM_RNAi* background, and the phenotypical similarity between the *REM_RNAi* lines and the *HAM* downregulation suggest that these genes might be involved in the control of the same biological processes throughout Arabidopsis development. The observed downregulation of the other analyzed target genes could, for instance, be due to the general deregulation of transcription caused by the reduced expression of the chromatin remodeling factor *HAM2*. Further analysis will be needed to confirm the possible interaction between *REM34*, *REM35* and *REM36* and the HATs *HAM1* and *HAM2*.

It is finally worth mentioning that, in mammals, the MYST protein family was found to be involved in many fundamental cell functions such as cell cycle progression and DNA repair (Pillus, 2008; Sapountzi and Côté, 2011). Furthermore, the human *MYST4* acetylase was found to be involved in the control of gametogenesis as well (McGraw *et al.*, 2007).

While not much is known about the *REM* gene family, substantial information is available for other transcription factor families characterized by the presence of the B3 DNA binding domain. In particular, the well-characterized *ARF* family, known to play a crucial role in regulating auxin responses, and the *RAV* family, which was found to be involved in hormonal regulation during different stages of Arabidopsis development (Swaminathan *et al.*, 2008). Auxin was found to be involved in gametogenesis (Pagnussat *et al.*, 2009; Panoli *et al.*, 2015). For instance, the perturbation of auxin transport in the embryo sac causes an arrest in the earliest stages of megagametogenesis (Ceccato *et al.*, 2013). Auxin biosynthesis was also recently shown to be essential for the transition from microsporogenesis to microgametogenesis, in the male gametophyte (Yao *et al.*, 2018). Because of the phenotypic similarities between the auxin defective mutant and the *REM_RNAi* lines and because of the linkage between transcription factors containing the B3 DNA binding domain and the regulation of hormonal responses, it is tempting to speculate that the role of *REM34*, *REM35*, and *REM36* in gametogenesis could be based on the regulation of hormonal related processes.

It is finally worth mentioning that this post-meiotic block, while strongly confirmed by the analyses on the different generations of both *REM_RNAi* and *35S:REM34-EAR* lines, do not appear neither in the three *rem34, rem35* and *rem36* single mutant or in the *rem34 rem35, rem34 rem36* and *rem35 rem36* double mutant. This evidence suggests that *REM34, REM35* and *REM36* act redundantly in the control of the gametophytes development and only the downregulation of the three of them or the overexpression of a dominant negative version of one of them, as in the case of the REM34-EAR chimeric protein, is sufficient to trigger an arrest in the female and male gametophytic development.

It might also be possible that, since the *REM* gene family is very abundant and highly duplicated, other members of the same family can partially complement the loss of two out of the three genes of interest, but cannot complement the simultaneous downregulation of *REM34, REM35* and *REM36.* To verify this hypothesis, the CRISPR/Cas9 genome editing system could be employed to create a triple knock-out mutant.

II.III Role of *REM34, REM35* and *REM36* in inflorescence architecture determination

REM34, REM35 and REM36 are involved in the establishment of the phyllotactic pattern

The mis regulation of *REM34, REM35* and *REM36* in the *REM_RNAi* and *35S:REM34-EAR* lines was found to cause both a partial sterility, linked to a post-meiotic block in both female and male gametophyte development (as described above), and evident defects in the phyllotactic pattern, which is the geometrical arrangement of the flowers around the main stem of the plant. While the gametophytic defect was only visible in the *REM_RNAi* and *35S:REM34-EAR* lines, the alteration of the phyllotaxis was present also in the CRISPR/Cas9 single and double knock-out mutants. As the *rem34 rem35* double mutant was obtained only recently, it was not included in the analysis described above.

Wild type Arabidopsis plants are characterized by a spiral phyllotactic pattern, in which successive siliques arise at an angle of 137.5° from each other. The *REM_RNAi* and *35S:REM34-EAR* lines are, on the other hand, characterized by an aberrant phyllotaxis, with siliques arising at narrower or wider angles compared to the wild type (Figure II-13).

To better characterize the alteration of the phyllotactic pattern of these lines, the angles between successive siliques of 10 fully matured wild type, *REM_RNAi #1, #4, #5* and *35S:REM34-EAR #1* and #7 were measured. In the wild type, as expected, 60% of the angles (76 out of 125 measured angles) had a value included between 130° and 150° and the phyllotactic graph shows a single prominent peak, around those values, with few outliers. The phyllotactic pattern of the three analyzed *REM_RNAi* lines is instead characterized by the presence of three distinct peaks of values: the canonical 140°, which accounts for around 30% of the total measured angles, and two non-canonical peaks at 90° and 180°, in which are included on average 40% of the total angles. The other angles are distributed at different values with no prominent peaks (Figure II-13). The same mutated phyllotactic pattern, with the angles between successive siliques distributed in three peaks at 90°, 140° and 180°, is displayed also by the two analyzed *35S:REM34-EAR* lines (Figure II-13). The same analysis was performed for the three *rem34, rem35* and *rem36* single mutants and for the *rem34 rem36* and *rem35 rem36* double mutants. The *rem34* single mutant had a disorganized phyllotactic pattern, with a wider distribution of angles around the 130° canonical value compared to wild type and a second smaller peak, of the 10% of the total measured angles, at 180°. The *rem35* and *rem36* single mutants are instead characterized by phyllotactic pattern similar to the one observed in the *REM_RNAi* and *35S:REM34-EAR* lines, with three distinct peaks: 10% of the siliques had a divergence angle of 90°, 30% were distributed around the canonical 130° value and 15% showed a divergence angle of 180° (Figure II-13).Finally, the two double mutants *rem34 rem36* and *rem35 rem36* show a highly disorganized phyllotactic pattern, with several peaks at different degrees (Figure II-13).

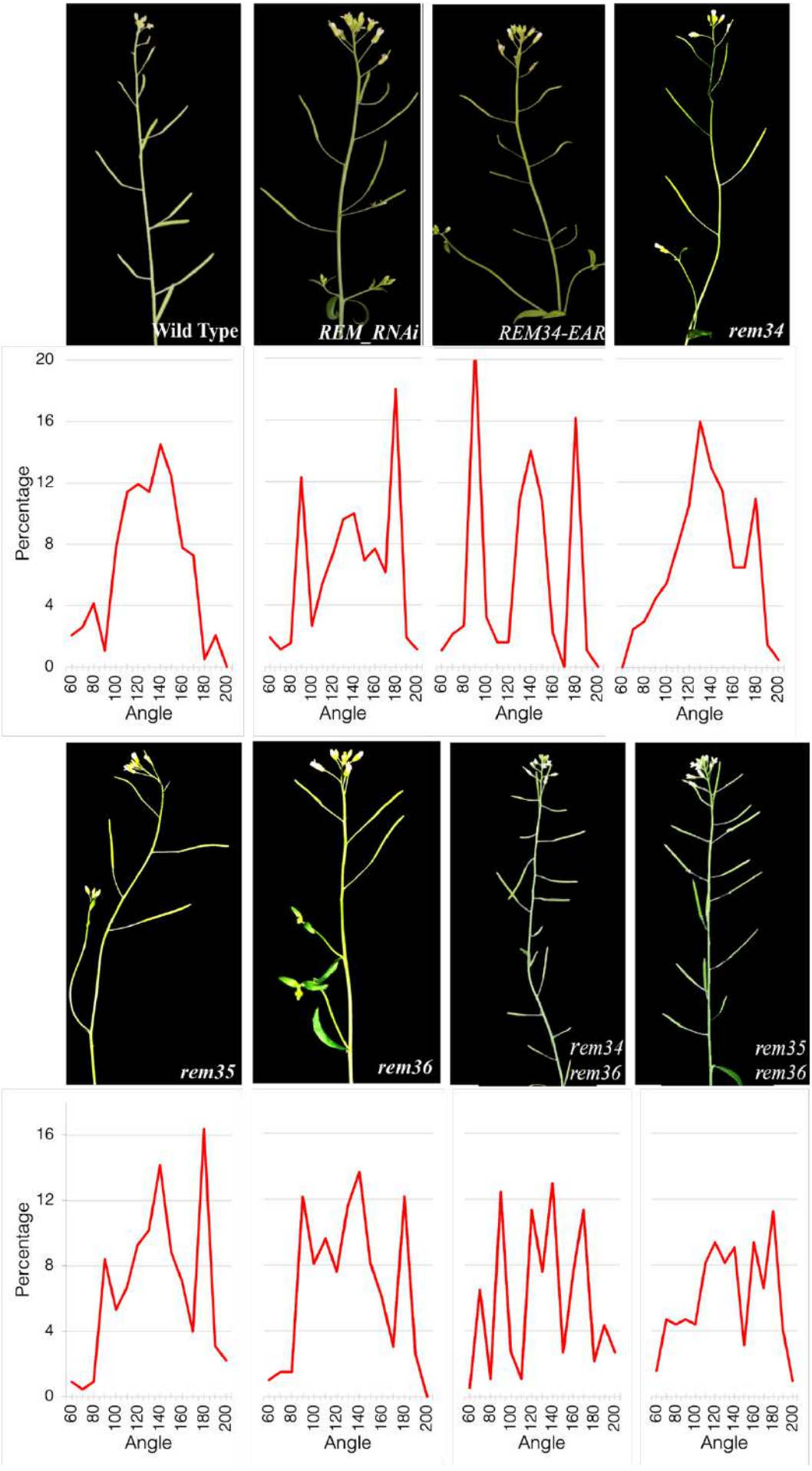
Wild Type
REM_RNAi
REM34-EAR
rem34
rem35
rem36
rem34
rem36
rem35
rem36
Percentage
Angle
0
4
8
12
16
20
60
80
100
120
140
160
180
200

Figure II-13 Phyllotactic pattern analysis.

The angles between successive siliques were measured in 10 wild type (n=125), *REM-RNAi* #1 (n=140), #4 (n=142) and #5 (n=192), *35S:REM34-EAR* #1 (n=208) and #7 (n=169). In the wild type the majority of the angles are distributed around the 140° canonical angles, with few exceptions. In the *REM_RNAi* and *35S:REM34-EAR* lines instead the angles are distributed around three values: 90°, 140° and 180°.
The phyllotactic pattern of the *rem34, rem35* and *rem36* single mutants was also analyzed; the *rem34* mutant is characterized by a wider distribution of the angles, the *rem35* and *rem36* single mutants instead show the same pattern described for the *REM_RNAi* and *35S:REM34-EAR* lines. The phyllotactic pattern of the two double mutants is highly disorganized, with multiple peaks.

The analysis performed on the different single and double mutants combinations allowed better understanding the role of the different *REM* genes of interest and suggested that *REM35* and *REM36* are the main players involved in the establishment of the correct phyllotactic pattern, while *REM34* plays a less prominent role.

This analysis also underlined the highly redundant role that these genes play in the regulation of the inflorescence architecture, as the double mutants were characterized by a much more disorganized phyllotactic pattern compared to the three single mutants.

Alterations in the phyllotactic pattern of Arabidopsis can lead to changes in the rate of production of new organs and, consequently, change also in the number of siliques that develop on the inflorescence. In particular, plants with an alternated or decussated phyllotaxis, in which successive organs arise at angles of 90° or 180°, can in theory produce more fruits than plants in which the phyllotactic pattern is spiral, without drastically changing the total high or life span of the plant itself.

To test how the mutated phyllotactic pattern of the *REM_RNAi* lines and of the *rem34, rem35* and *rem36* single mutants was affecting the overall silique production of these plants, silique number and the rate of new flower production were evaluated.

We decided to focus these analyses on the *RNAi* lines as well as the three single mutants, as they are characterized by a mutated but regular phyllotaxis pattern. The double mutants were not considered, as their highly disorganized phyllotaxis is not likely to lead to improvement in siliques production.As a start, the number of newly opened flowers was measured every day from bolting of the plant to its complete maturation (around 10 days) for 10 plants each of WT, RNAi, *rem34*, *rem35* and *rem36*. The *REM_RNAi* line was able to produce on average 30 new flowers in 10 days, compared to the 18 produced by the wild type, suggesting a high increase in the rate of flower production; the single mutants were instead characterized by a intermediated phenotype between the *REM_RNAi* and wild type lines (Figure II-15A).

To further confirm this increase in the flower production ability of these lines, the plastochron, which is the time interval between two recurring successive events (such as flower initiation), was measured in the first 4 days after bolting, the phase in which the rate of flower production is highest. The *REM_RNAi* line it is able to produce a new flower on average every 7.5 hours, while the time required for wild type plants was 12.3 hours. The three knock-out lines present, also in this case, an intermediate phenotype between the WT and the RNAi lines (9h for *rem34,* 10h for *rem35* and 10.1h for *rem36*) (Figure II-15B).

While in the *REM_RNAi* lines this increase in yield was negatively counterbalanced by a reduction in seed set, the *rem34, rem35* and *rem36* single mutants did not exhibit any decrease in the total seed number (data not shown), making these genes an interesting target for crop improvement, especially in species closely related to Arabidopsis, such as *Brassica napus.*

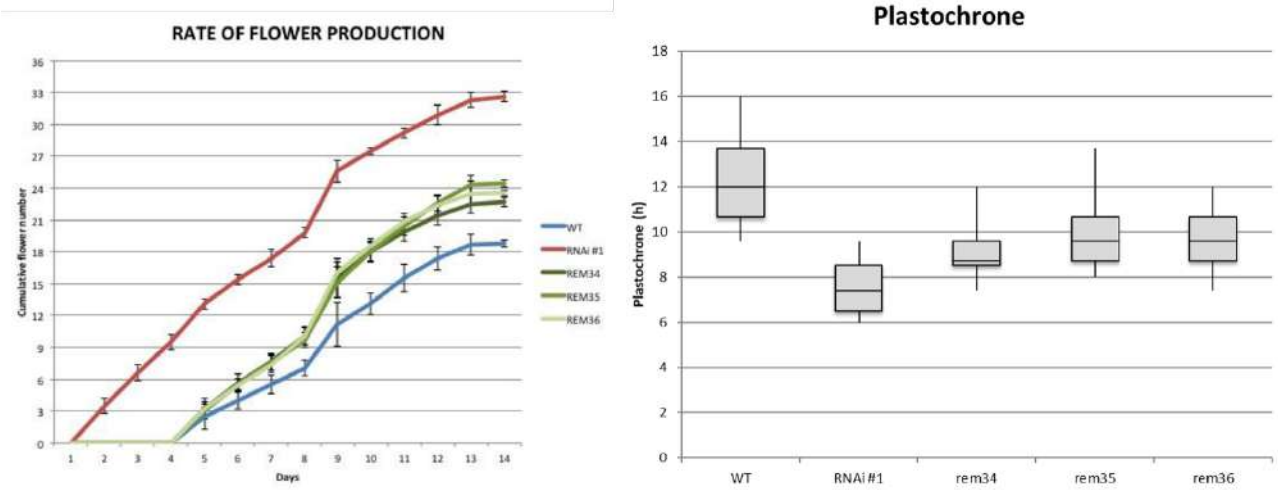

Figure II-13 rate of flowers production and plastochron

A. The cumulative number of newly opened flowers was measured in 10 wild type, *REM_RNAi* and *rem34, rem35* and *rem36* single mutants. Ten days after bolting *REM_RNAi* lines are able to produce on average 12 flowers more than the wild type. The three single mutants also show an increase in the rate of flowers productions. B. The platochron, the time interval between new flowers production was measured in the first 4 days after bolting. Wild type plants are able to produce a new flower every 12 hours, while this time is reduced both in the *REM_RNAi* and *rem34, rem35* and *rem36* single mutants.

Auxin signaling is impaired in the rem mutant lines

The establishment of the phyllotactic pattern is mainly driven by the polar distribution of the hormone auxin at the inflorescence meristem level. This hormone accumulates in initiation sites, where a new primordium has to arise, and controls the first steps in the formation of new organs. The areas surrounding the primordia are depleted of auxin and therefore primordium initiation is inhibited in these sites. The spatiotemporal regulation of auxin fluxes at the meristem level is thus fundamental to ensure a correct phyllotaxis.

Different tools were recently developed, to allow following *in vivo* auxin fluxes in the different tissues of plants. Among them the most used ones are the DII-Venus fusion protein, that marks auxin minima, and the *DR5* auxin responsive synthetic promoter, expressed in auxin maxima regions.

The current hypothesis is that auxin signaling relies on the dynamic interaction of the ARF transcription factor with their repressors Aux/IAA: in low auxin concentrations the ARFs are bound to the AuxRE motif in the promoter of their target genes, but they cannot activate transcription, as their activity is inhibited by their interaction with the Aux/IAA repressors. When auxin enters the cell, it can directly bind the TIR1/AFB subunit of the SCF-type E3 ubiquitin-ligase complex, which is then able to target the Aux/IAA protein, causing their degradation. As a consequence, the inhibition on the ARFs is removed and their target are derepressed.

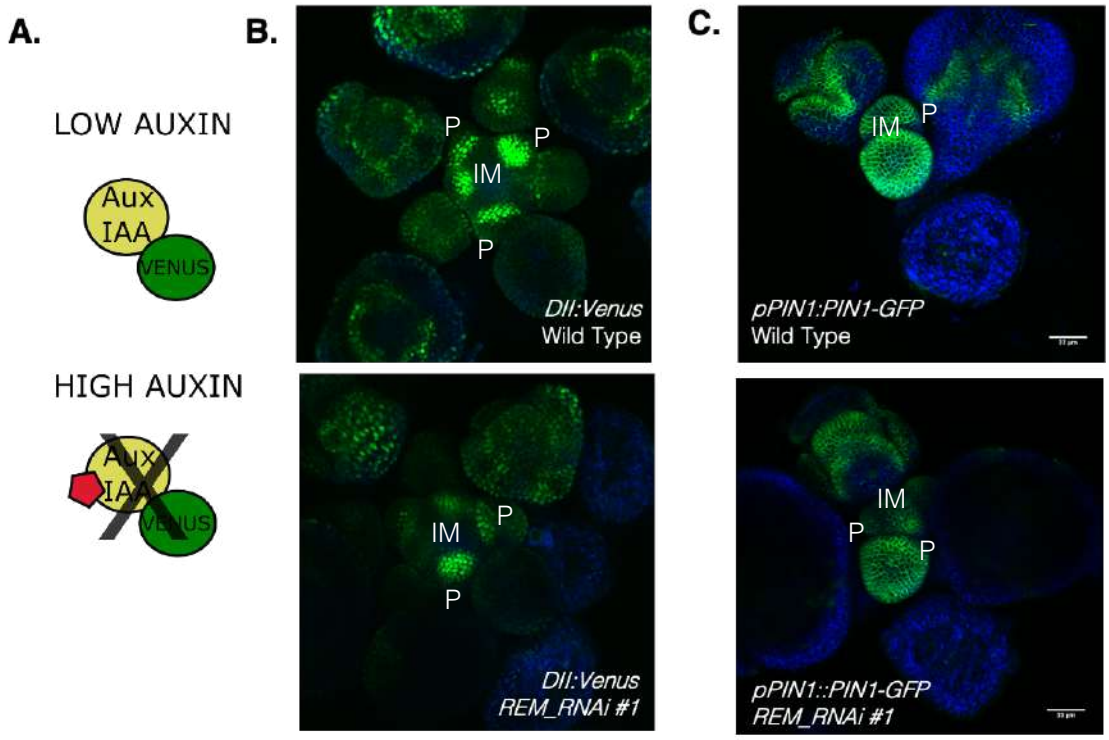

Figure II-16 Auxin behavior in the *REM_RNAi* lines

A. The *DII:Venus* marker line allows to visualize auxin minima areas in plant tissues, relying on the degradation mechanism of the Aux/IAA repressors. B. In both wild type and *REM_RNAi* lines the fluorescence signal marks the area around the primordia, suggesting that auxin is correctly distributed in the inflorescence meristem C. The PIN1 auxin carrier was correctly distributed on the membranes of both wild type and *REM_RNAi* lines, further confirming that the flux of auxin is correctly maintained in the *REM_RNAi* lines. IM: Inflorescence Meristem, P: Flower Primordium

The DII-Venus reporter line takes advantage of the Aux/IAA degradation mechanism to allow the visualization of regions of auxin minima: in this marker line the auxin interaction domain (domain II or DII) of the IAA28, fused in frame with the Venus fluorescence reporter, is expressed constitutively; when auxin levels are high, the DII-Venus chimeric protein is rapidly targeted and degraded, thus a fluorescence signal is not visible in areas of auxin maxima (Figure II-16A) (Brunoud *et al.*, 2012).

In both wild type and *REM_RNAi* inflorescence meristem, the DII-Venus signal is detectable in the boundary regions between the IM and the developing primordia, which are the expected auxin-depleted regions of this tissue (Figure II-16B).

This observation suggests that auxin is correctly distributed in the inflorescence meristem and that the auxin-induced degradation of the Aux/IAA repressors is taking place correctly.

To further investigate whether auxin transport is affected in the *REM_RNAi* lines, we chose to visualize the distribution of the PIN1 auxin carrier, which is the main carrier driving auxin polar flux at the IM level. Also in this case, no differences were detected between wild type or *REM_RNAi* plants expressing the *pPIN1:PIN1-GFP* marker line: in both backgrounds PIN1 was correctly located on the membranes of the meristem cells and its distribution was clearly polarized on one side of the cell, ensuring in this way the correct establishment of the polar auxin flux towards the incipient primordia (Figure II-16C).

Auxin signaling relies both on the Aux/IAA auxin-dependent degradation and on the correct functioning of the ARF transcription factors, consequently, if one of these processes is impaired in the plant, the developmental pathways that are driven by auxin are likely to be affected. The *REM_RNAi* and *35S:REM34-EAR lines*, as well as the single and double knock-out mutants, showed an aberrant phyllotactic pattern, consistent with defects in auxin signaling during their reproductive development; however, auxin distribution and Aux/IAA degradation was not impaired in these lines. This suggests the possibility that ARF activity might be affected in lines in which *REM34, REM35* and *REM36* are downregulated or mutated.

To test this hypothesis, we employed the *DR5v2-ntdTomato/DR5-n3GFP* double reporter line (Liao *et al.*, 2015). The DR5 synthetic promoter is one of the most used reporters of auxin response and is composed by repetitions in tandem of the AuxRE (CTCTGT) motif which drive the expression of a reporter protein, allowing the visualization of areas in which these sites are highly transcribed (Figure II-17A).

The *DR5v2-ntdTomato/DR5-n3GFP* contains both the canonical DR5 promoter, consisting of 9 repetitions in tandem of the CTCTGT motif, and a second version of the same promoter, the DR5v2, with a different AuxRE sequence (TGTCGG), found to be more sensitive to auxin. In the wild type inflorescence meristems, both reporters were visible and the *DR5:GFP* signal was, as expected, marking the developing primordia, which are the areas of auxin maxima. However, in the *REM_RNAi* background both the *DR5* and the *DR5v2* promoters were active in the inflorescence meristem (Figure II-17B).

To verify whether the reporter constructs were in some way silenced in the *REM_RNAi* background, we also investigated their activity in roots of both wild type and *REM_RNAi* lines which showed that in both genotypes a strong signal was detectable in the expected auxin maxima region (Figure II-17B).

This allowed to rule out the hypothesis absence of the reporter expression in the *REM_RNAi* plants was due to silencing of the construct. Therefore, these results indicate that the signaling of auxin and, in particular, the transcriptional activation activity of the ARFs on DR5-containing promoters, is impaired in Arabidopsis reproductive tissues, when *REM34, REM35* and *REM36* are downregulated.

Two possible hypotheses could explain this impairment: auxin concentration in the *REM_RNAi* meristem does not reach the threshold necessary to activate the *DR5* promoter, or auxin is present in the correct quantity in the analyzed tissues but the signaling cascade is impaired, in absence of *REM34, REM35* and *REM36* activity.

To understand which of these hypotheses was correct, wild type and *REM_RNAi* plants, carrying the *DR5v2-ntdTomato/DR5-n3GFP* reporter line, were treated with exogenous auxin. If the loss of the *DR5* activity in the *REM_RNAi* background is due to a lack of auxin in the inflorescence meristem, the exogenous application of this hormone should rescue the marker line expression.

If, on the other hand, auxin levels are correct but the signaling pathway of this hormone is defective, auxin treatments should not have an effect on the *DR5* promoter activity in the *REM_RNAi* background.

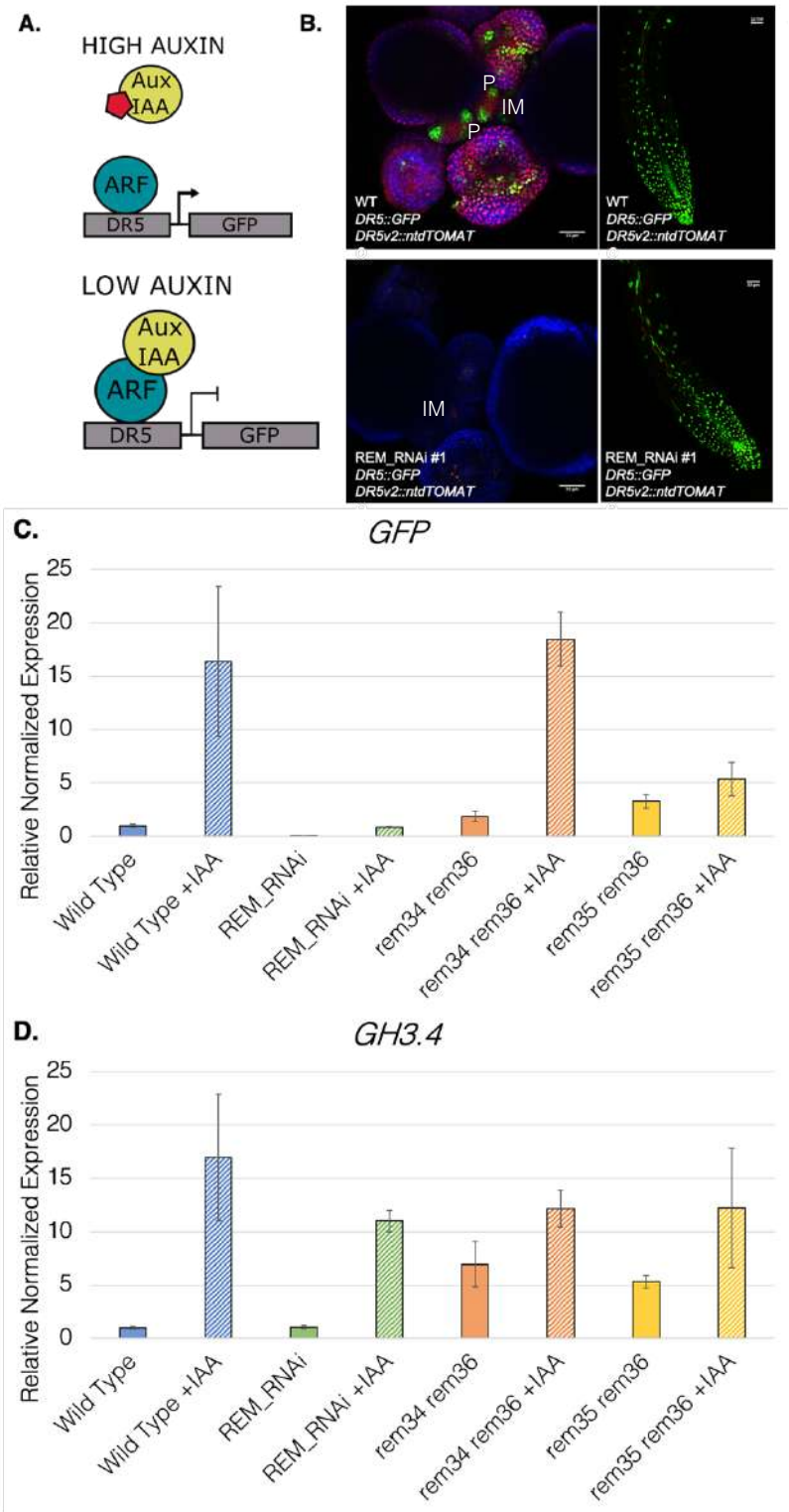

Figure II-17 Analysis of the *DR5:GFP* marker line in the *REM_RNAi* line

A. In the *DR5.GFP* marker line, the *GFP* expression is driven by the synthetic *DR5* auxin responsive promoter, which is only active when auxin concentration is high in the cell B. In the wild type inflorescence meristem, the *DR5* signal is visible in the flower primordia, which correspond to the area of auxin maxima, while in the *REM_RNAi* lines no signal is detectable, at least 5 plants for genotype were imaged. In the root meristems of both wild type and *REM_RNAi* lines the *DR5* signal is detectable, confirming that the marker line is functional in the *REM_RNAi* lines. Scale bar 33 µm, IM: Inflorescence Meristem P: Flower Primordium C. qRT-PCR to measure *GFP* and *GH3.4* expression in the wild type, *REM_RNAi* and *rem34 rem36* and *rem35 rem36* double mutant. The *GFP* expression, driven by the *DR* promoter, increases after exogenous auxin application, while in the *REM_RNAi* line the *GFP* expression is not rescued by exogenous auxin. To verify whether the auxin application, the *GH3.4* auxin responsive genes expression level was measured.

In wild type inflorescences, real time PCR analysis showed that *GFP* expression levels increased after a 3h application of 10μM IAA. In the *REM_RNAi* line, *GFP* transcripts were almost undetectable in the mock-treated inflorescence and, interestingly, the exogenous auxin application did not result in increased *GFP* transcript levels (Figure II-17C). To ensure that the auxin treatments were performed correctly on both lines, the level of expression of *GH3.4,* a member of the *GH3* auxin-responsive family (Hagen and Guilfoyle, 2002), was measured in untreated and treated inflorescence of both wild type and *REM_RNAi* plants. In this case, the *GH3.4* was found to be induced by auxin application in both backgrounds, suggesting that the auxin treatments were correctly performed.

As exogenous auxin application did not increase the *DR5*-driven *GFP* transcription levels in the *REM_RNAi* lines, it was possible to rule out the hypothesis that the lack of *DR5:GFP* signal was caused by low auxin concentration in the inflorescence. However, these findings strongly suggested that, in the *REM_RNAi* lines, auxin perception is impaired.

Preliminary analyses were also performed on the *DR5v2-ntdTomato/DR5-n3GFP* reporter line in the *rem34 rem36* and *rem35 rem36* double mutants, while the *rem34 rem35* double mutant was not included in this analysis as it was obtained only recently, and the experiments are still ongoing.

First, to assess whether the *DR5:GFP* marker line was detectable in the double mutants background, the *GFP* transcript levels were measured in mock-treated inflorescences. Surprisingly, in contrast to what was found in the *REM_RNAi* lines, the levels of *GFP* expression were upregulated in the double mutants inflorescences. Furthermore, exogenous auxin applications were found to be able to increase the *GFP* transcript levels in both *rem34 rem36* and *rem35 rem36* mutant backgrounds. Also in this case, as a control, the expression levels of *GH3.4* were measured in both mock and auxin-treated plants. *GH3.4* was found to be upregulated in the mock-treated inflorescence and exogenous auxin application was able to increase the expression level of this gene (Figure II-17C).

These findings are not easily interpretable but, taken together, suggest that the auxin signaling pathway is partially impaired when *REM34, REM35* and *REM36* expression is perturbed. Furthermore, the analysis on the two double mutants, *rem34 rem36* and *rem35 rem36,* suggest that these three genes play both synergistic and antagonistic roles in the control of the auxin response: while the downregulation of the three of them causes the silencing of the *DR5* promoter, the mutation of only two of them and, in particular, of *REM35* causes an increased activity of the same promoter and the overexpression of the auxin-responsive gene *GH3.4.* To further elucidate the complex relationship between these genes and the different roles that each one of them plays in the control of inflorescence development, it would be important to perform the same analyses as described here using *rem34, rem35* and *rem36* single mutants and the double and triple mutant combinations.

Cytokinin signaling and meristem size in the REM_RNAi lines

Although auxin is the main signaling molecule involved in the correct phyllotaxis establishment, different other internal and external factors contribute to the precise spatiotemporal regulation of this phenomenon.

It has been demonstrated, for instance, that meristem size can negatively influence the robustness of the phyllotactic pattern. It is also know that, besides from genetic cues, also day length can influence meristem size (Landrein *et al.*, 2015b). To check whether the permutations detected in the phyllotaxy of the *REM_RNAi,* single and double mutant combinations were maintained under different growing conditions, the phyllotactic pattern of these lines was evaluated after growing the plants for 4 weeks in short day conditions, before moving them in long day inductive conditions. Plants grown in this way present a larger inflorescence meristem, compared to the ones only grown in long day conditions, and are thus more prone to show a disorganized phyllotactic pattern (Landrein *et al.*, 2015a).

In these conditions wild type plants show a more disorganized phyllotaxis with a wider distribution of angles around the canonical 140°. The *REM_RNAi* and *rem34, rem35* and *rem36* single mutants however, were, also in these conditions, characterized by mutated phyllotactic pattern, characterized by angles distributed around three main values of 90°, 140° and 180°, suggesting that this pattern is highly specific for the downregulation or mutation of *REM34, REM35* and *REM36* and is independent from the environmental conditions (Figure II-18A).

We next investigated whether the impairment of auxin signaling reported in the different *REM* mutant or transgenic lines was directly or indirectly affecting inflorescence meristem size and morphology, causing in this way the permutations registered in the phyllotactic pattern of these plants. It has indeed been reported that auxin signaling can negatively influence the size of the inflorescence meristem in Arabidopsis (Shi *et al.*, 2018; Luo *et al.*, 2018). 5 wild type and 5 *REM_RNAi* inflorescences were imaged by Scanning Electron Microscopy (SEM), and the inflorescence meristem size was measured. No statistically significant differences between wild type and *REM_RNAi* meristems were detected, suggesting that *REM34, REM35* and *REM36* influence auxin signaling in the inflorescence, without affecting the size of the IM (Figure II-18B).

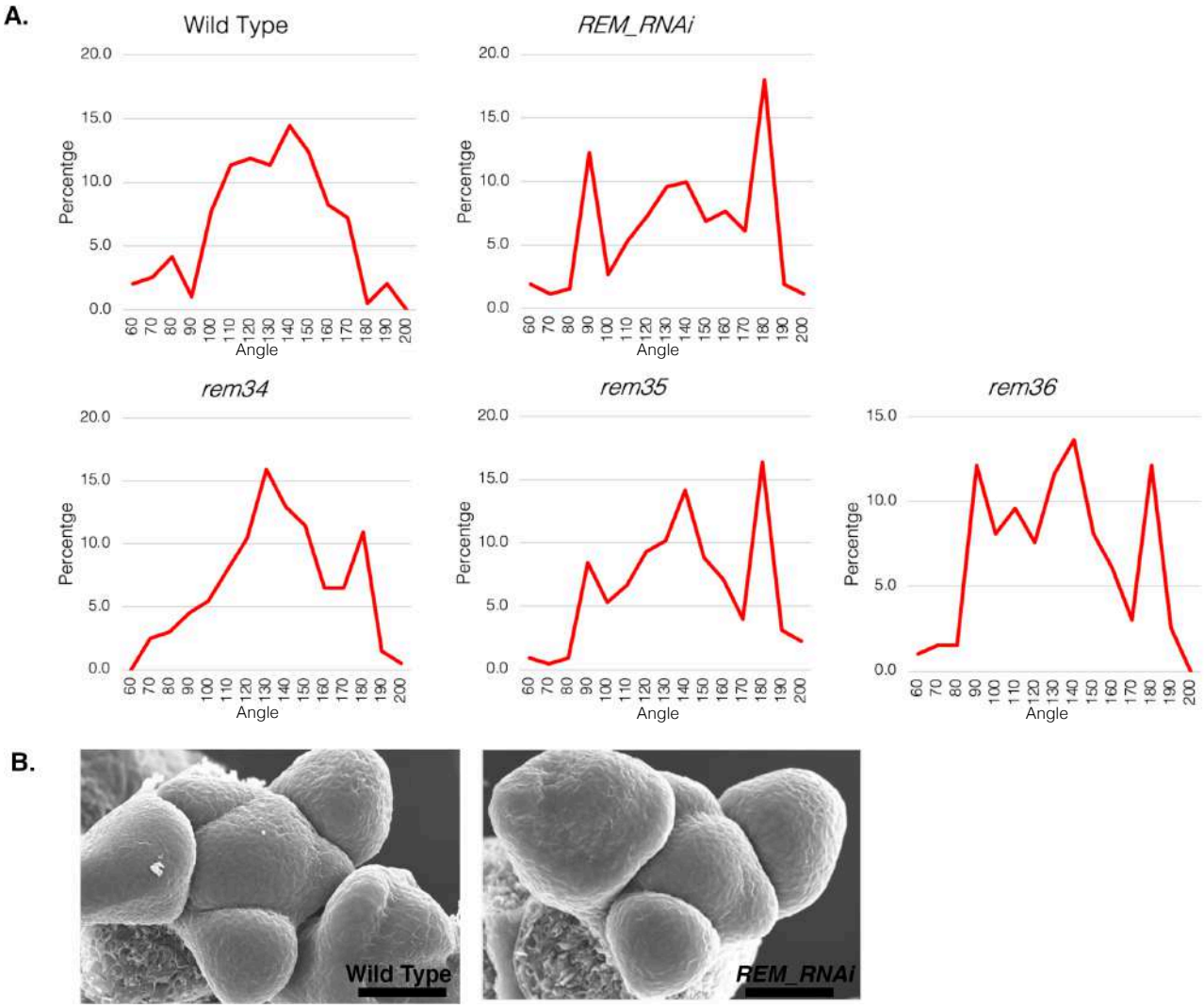

Figure II-18

A. Growth conditions affect meristem size in Arabidopsis, thus changing the organization of phyllotaxis. In particular, plants grown under short day conditions are usually characterized by bigger inflorescence meristems and a more disorganized phyllotactic pattern, compared to those grown in long day conditions only. To test whether the mutated phyllotactic pattern typical of the *REM_RNAi* line as well of the *rem34, rem35* and *rem36* mutants was affected by the growing conditions of the plants, successive siliques angles of 10 plants for each genotype were measured. In these conditions wild type plants are characterized by a wider distribution of angels around the canonical 140° values. In the *REM_RNAi* and single mutants background the angles are distributed around three main values: 90°, 140° and 180°, with a similar distribution to the one described above, suggesting that growing conditions do not affect the phyllotaxis of these line **B.** Scanning electron microscopy of meristems of both wild type and *REM_RNAi* plant, no differences in the morphology of the inflorescence meristem were detected and the meristem size was not affected in the *RNAi* lines. Scale bar 30 µm

Finally, cytokinin signaling was found to play a crucial role in the temporal regulation of new organ formation in the inflorescence meristem (Besnard, Refahi, *et al.*, 2014a), and the crosstalk between auxin and cytokinin is known to be involved in the control of many plant developmental processes (reviewed in Chandler and Werr, 2015). With the aid of the *TCSn:GFP* marker line, which allows the visualization of cytokinin dynamics, we were able to prove that the cytokinin signaling and its distribution is not affected in *REM_RNAi* lines (Figure II-19A).

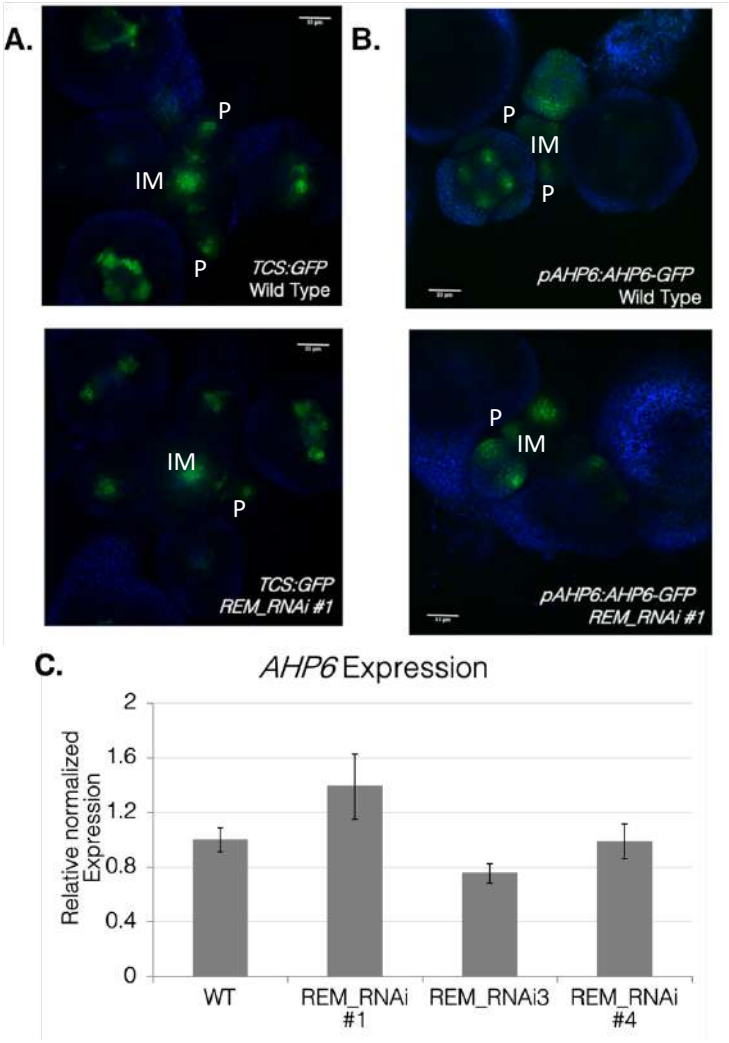

Figure II-19 Cytokinin signaling is not affected in the *REM_RNAi* line

A. The synthetic *TCS* promoter, which is induced by cytokinin, is expressed correctly in the *REM_RNAi* lines, suggesting that the cytokinin signal is not affected by the downregulation of *REM35, REM35* and *REM36* Scale bar 33 µm; IM: Inflorescence Meristem P: Flower Primordia. **B.** *AHP6* expression, which is a negative regulator of cytokinin and it is involved in the temporal regulation of primordia initiation, is not affected in the *REM_RNAi* lines. Scale bar 33 µm **C.** AHP6 protein is correctly present in the newly developing primordia, further confirming the cytokinin signaling is not impaired in the *REM_RNAi* lines.

The negative regulator of cytokinin signaling AHP6 is the factor that, in the inflorescence meristems, controls the crosstalk between auxin and cytokinin and determines the time intervals between new primordia emergence. Since *REM34, REM35* and *REM36* are involved in the specification of the time in which new flowers are produced, as demonstrated by the shorter plastochron that characterizes the *REM_RNAi* and *rem* mutants, we decided to check whether AHP6 function was impaired in these lines. To do so, we measured the *AHP6* transcript levels and imaged the protein distribution in the *REM_RNAi* inflorescences. Neither the transcription nor the distribution of this enzyme was affected in the *REM_RNAi* background (Figure II-19B and C).

These analyses suggest that in the inflorescence meristem *REM34, REM35* and *REM36* are involved in auxin signaling, while they do not seem to be playing a direct role in the cytokinin pathway. Moreover, the analysis of the meristem morphology allowed to exclude the possibility that the perturbation of the phyllotactic pattern in the *REM* silencing lines are linked to changes in the dimension of the meristem itself.

Finally, the comparison of the phyllotaxy of the *REM_RNAi* and *rem* single mutants under grown under different day length conditions clearly showed that the mutated phyllotactic pattern of these lines, in which angles are distributed around three main values (90°, 140° and 180°), is not influenced by these different growing conditions. This suggest that the appearance of these two non-canonical angles, in the different *rem* background, might be linked directly to the action of *REM34, REM35* and *REM36* in the regulation of auxin signaling in Arabidopsis inflorescence meristem.

REM35 is able to interact with the Auxin Response Factor 19

The phenotypical analyses, carried out in the different *REM* mutated backgrounds, suggested that *REM34, REM35* and *REM36* play a role in the control of primordia initiation in the inflorescence meristem of Arabidopsis and can consequently influence the yield of the plant. The imaging of both auxin and cytokinin marker lines, in the inflorescence meristem of these plants, allowed to rule out the involvement of *REM34, REM35* and *REM36* in the control of the cytokinin pathway, and suggested that they mainly exert their function in the auxin signaling pathway. Finally, the application of exogenous auxin and the analysis of its effects on both the synthetic *DR5* promoter activity and on the *GH3.4* auxin responsive gene, clearly demonstrated a crucial role for *REM34, REM35* and *REM36* in regulating the transcriptional network downstream of auxin sensing in the cell.

To try to unravel the molecular mechanism through which *REM34, REM35* and *REM36* act, a yeast-2-hybrid screening, against a library of 96 transcription factors involved in the control of hormonal pathways in the inflorescence of Arabidopsis, was carried out in collaboration with the laboratory of Stefan de Folter (CINVESTAV, Irapuato, Mexico).

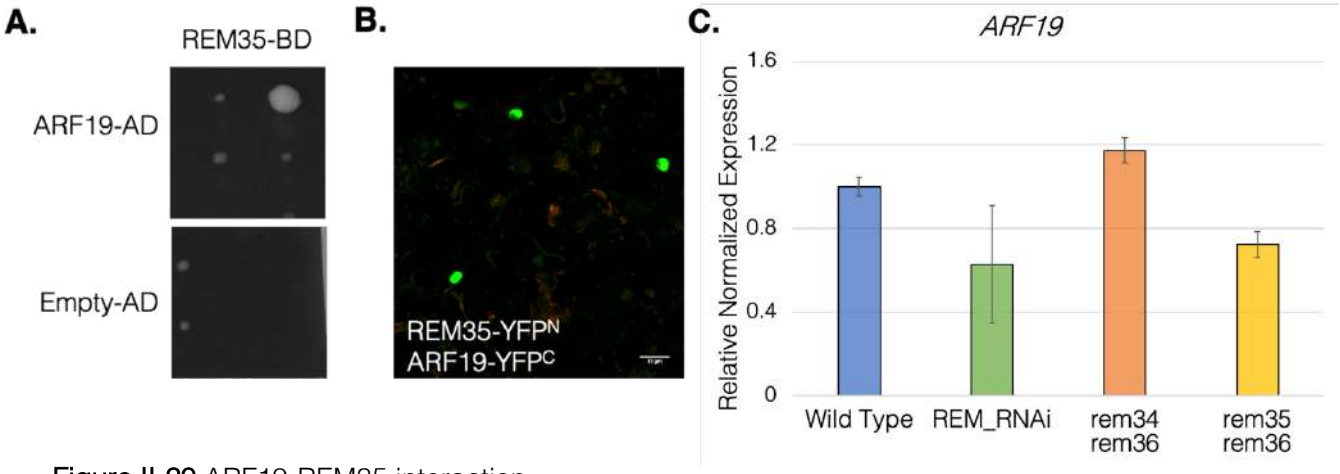

Figure II-20 ARF19-REM35 interaction

A. REM34, REM35 and REM36 CDS were cloned into the bait vector (pDONOR22-BD) and tested against a library of 96 transcription factors, cloned into the pray vector (pDONOR32-AD) involved in hormonal signaling in the inflorescence meristem of Arabidopsis. From this screening, it was found that REM35 is able to interact with ARF19, a transcription factor involved in auxin signaling and lateral organ development in the roots. **B.** The REM35 and ARF19 interaction was confirmed through BiFC assay, in which it is possible to see the reconstitute YFP fluorescence (green) between ARF19 and REM35 fusions to the C- and N-terminal fragments of YFP, respectively. The negative controls for the BiFC assay are shown in Figure II-11B **C.** As auxin signaling is often controlled by feedback loops, the expression of *ARF19* was measured in the *REM_RNAi* lines as well as the *rem34 rem36* and *rem35 rem36* double mutants. No downregulation of *ARF19* was detected, suggesting that *REM34, REM35* and *REM36* are not involved in the regulation of *ARF19.*

This analysis revealed that REM35, besides being able to form homodimers and heterodimers with REM34, is able to interact also with the Auxin Responsive Factor ARF19 (Figure II-20A). This finding, which was also confirmed *in vivo* with a BiFC assay (Figure II-20B), further confirmed a central involvement of these *REM* genes in the regulation of auxin signaling in the inflorescence meristem.

According to the available expression data (Klepikova *et al.*, 2016), *ARF19* is expressed in the inflorescence meristem throughout the reproductive development of Arabidopsis, however its role in these tissues is still uncharacterized.

Despite this lack of information about the role of *ARF19* in inflorescence development, it investigated in other plant tissues. For instance, it has been demonstrated that this transcription factor, together with its homolog *ARF7*, controls lateral root emergence and development (Okushima *et al.*, 2005).

In particular, *ARF19* and *ARF7* regulate the initiation and the earliest stages of lateral root primordia formation, by directly binding to the AuxRE elements of the promoters of different members of the *Lateral Organ Boundaries (LBD)* transcription factor family (Okushima *et al.*, 2007; Lee *et al.*, 2009). It is tempting to speculate that *ARF19* might control primordia initiation also in the shoot apex together with *REM34, REM35* and *REM36.*

Auxin signaling appears to be generally perturbed in the *REM_RNAi* lines and in the *rem* mutants background, we thus decided to test whether this mis-regulation was linked to a direct regulation of *ARF19* expression by the *REM* transcription factors. The expression level of *ARF19* was not found to be different in the wild type, *REM_RNAi, rem34 rem36* and *rem35 rem36* double mutants, excluding this scenario (Figure II-20C).

Taken together, the discovery of a physical interaction between, REM35 and ARF19 and the fact that no differences were found in *ARF19* transcript level in the analyzed genetic backgrounds strongly suggest that *REM34, REM35* and *REM36* act in a putative complex with ARF19 to regulate auxin signaling.

The role of ARF7 and ARF19 in the phyllotaxis

The evidences presented above hint that ARF19 could control together with REM34, REM35 and REM36 in the control of primordia formation and phyllotaxy in the Arabidopsis inflorescence meristem.

Since a detailed investigation of the phenotype of the inflorescence architecture of *arf19* mutant was not available yet, we fist carried out a measurement of the phyllotaxis pattern of this line. At the same time, since it is know that *ARF7* acts redundantly to *ARF19* in root development (Okushima *et al.*, 2005), we analyzed also the *arf7* and *arf7 arf19* double mutant to understand if this redundancy relationship was maintained also in the shoots.

The phyllotaxy of *arf7, arf19* and of the *arf7 arf19* double mutant showed similar permutations to the one observed in the *REM_RNAi* line, also in this case the successive angles between siliques were distributed around three main values: 90°, 140° and 180°. This permutated pattern was present in all the mutants analyzed but was more evident in the *arf7 arf19* double mutant where 45% of the siliques (75/165) showed a divergence angle

ranging from 130° to 150°, while 34% of them (56/165) are characterized by a divergence angle of 90° or 180° (Figure II-21).

Higher-order mutants, which carry different combinations of the *rem34, rem35* and *rem36* crossed with *arf7* and *arf19,* displayed a similar phyllotactic pattern (Figure II-20), with no additional permutations, suggesting that these genes control inflorescence architecture by acting on the same pathway.

The finding that the REM35 can physically interact with ARF19 further sustains the hypothesis that the members of these two transcriptional factor families collaborate in the control of primordia specification in the inflorescence meristem of Arabidopsis.

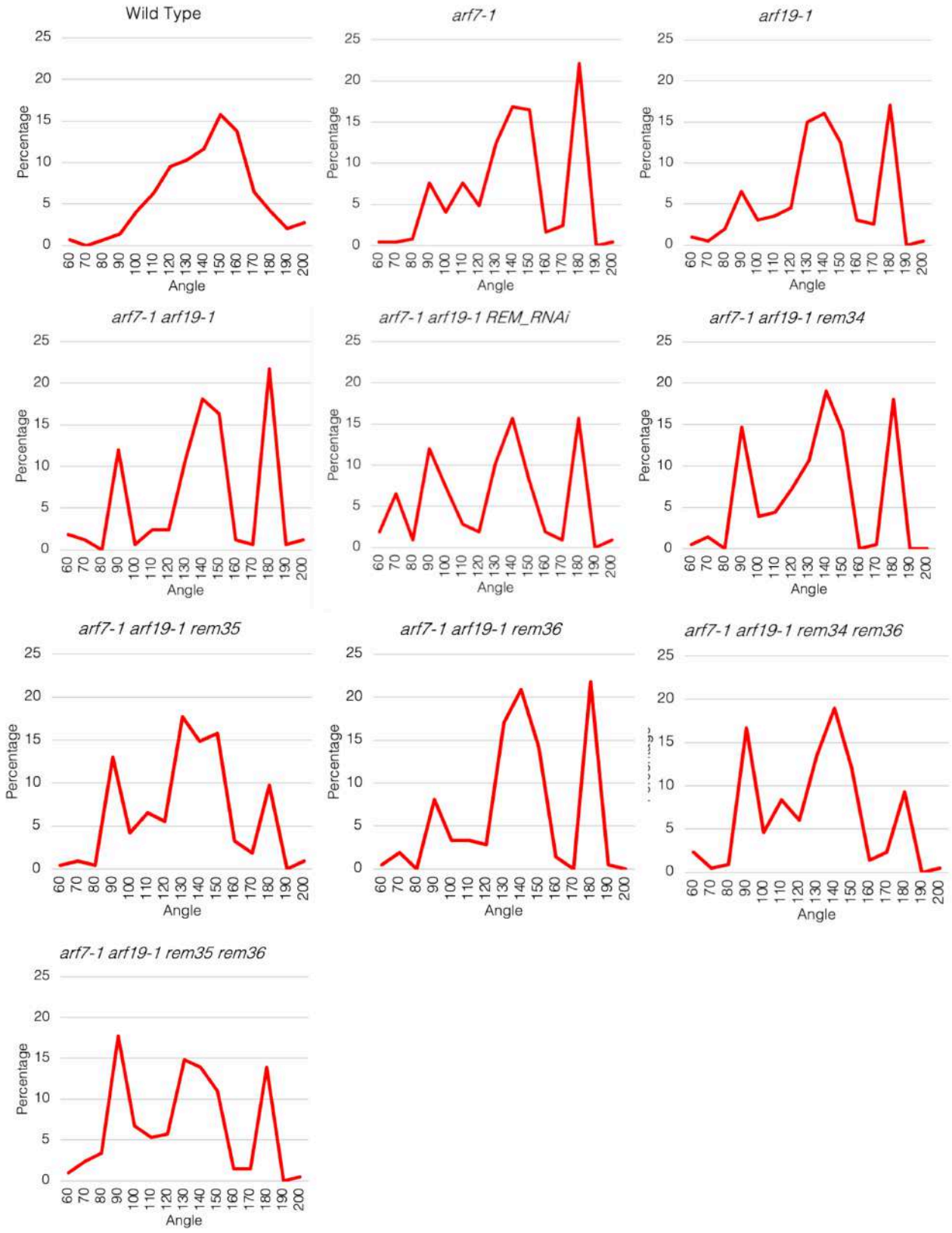

Figure II-21 ARF7 and ARF19 are involved in phyllotaxy control

The angles between successive siliques were measured in 10 wild type, *arf7, arf19, arf7 arf19* plants, as well as in the multiple order mutants *arf7 arf19 REM_RNAi, arf7 arf19 rem34, arf7 arf19 rem35, arf7 arf19 rem36, arf7 arf19 rem34 rem36* and *arf7 arf19 rem35 rem36.* Compared to the wild type, all the analyzed mutant show an aberrant phyllotactic pattern.

REM34, REM35 and REM36 negatively regulate the expression of the ARF19 target LBD18

As described above, *ARF7* and *ARF19* are involved in lateral organ development in the roots, and the *arf7 arf19* double mutant is characterized by the absence of lateral roots. In particular, these Auxin Responsive Factors regulate lateral root initiation by controlling the expression of *PUCHI* and *LBD18* (Kang *et al.*, 2013).

To investigate whether the REM35-ARF19 complex is involved in the control of lateral organ initiation in the shoot, by acting on the same targets that are regulated by ARF19 in the roots, the *LBD18* expression level was measured in inflorescences of wild type, *REM_RNAi,* the *rem34 rem35* and the *rem35 rem36* double mutants (Figure II-22A). Interestingly, *LBD18* appeared to be upregulated in all the lines mutated for the *REM* genes of interest, suggesting that these *REM* factors function as negative regulators of *LBD18* expression.

To further test this hypothesis, lines overexpressing *REM35* fused with the RFP reporter were generated, in which *REM35* is ectopically expressed also in the roots (Figure II-22B).

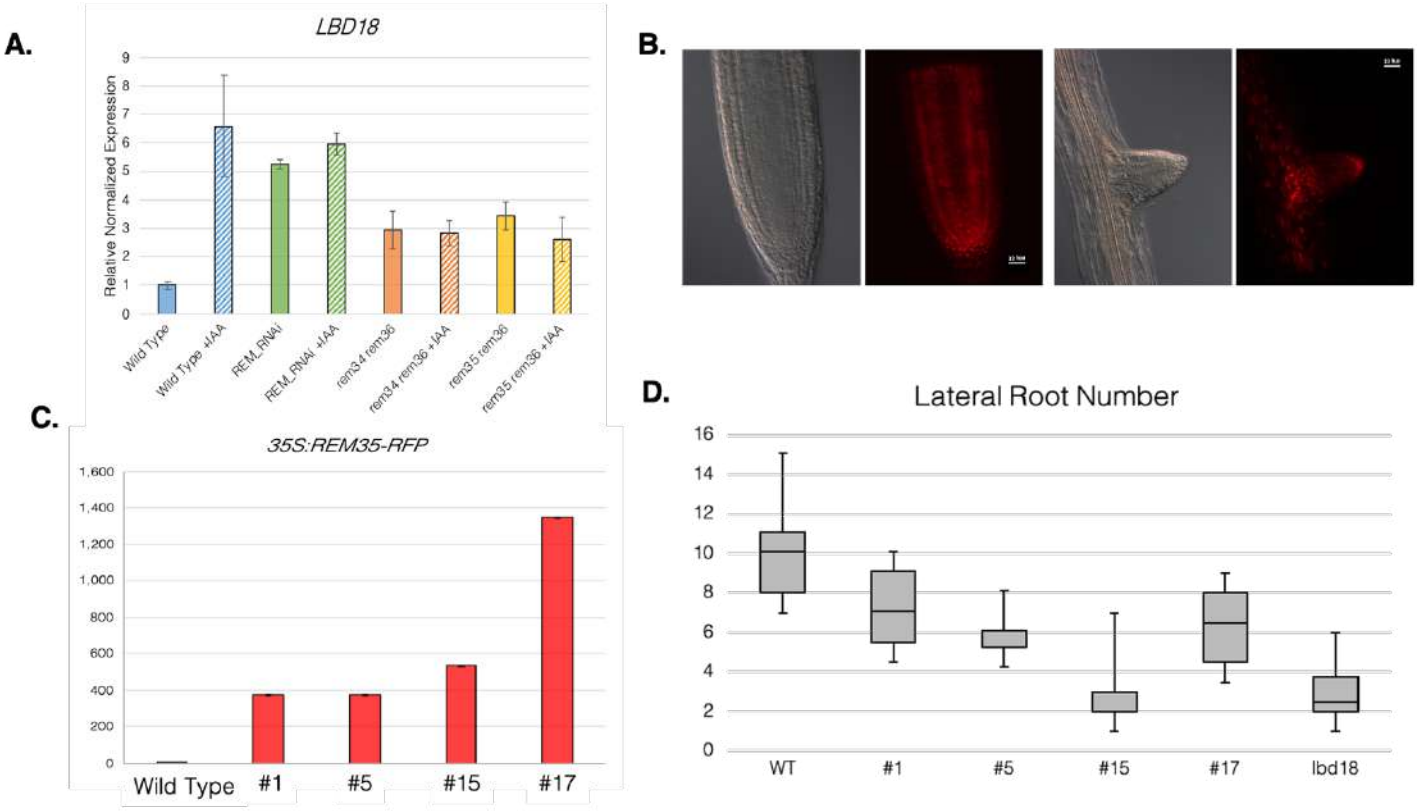

Figure II-22 Lateral root development is impaired in the REM35 overexpressing lines

A. *LBD18* expression is upregulated in inflorescence of the RNAi and double mutants lines, suggesting that the rems act as negative regulators of *LBD18* in this tissue. B. Roots of the *35s:REM35-RFP* overexpressing lines, showing the ectopic presence of the REM35-RFP protein in the roots, where this transcription factor is normally absent. The nuclear localization of the RFP signal suggests that the transcription factor is correctly localized in the nuclei. C. The overexpression level of *REM35* wan assessed in 4 different *35S.REM35-RFP* lines, all off which showed different levels of overexpression of *REM35.* D. Compared to the wild type, the four *35S:REM35-RFP* lines show a decrease number of lateral roots, similarly to what is observable in the *lbd18* mutant. 10 to 15 plants for each genotype were analyzed, the experiment was repeated twice; ANOVA and post hoc Tukey HSD test were used, $p < 0.1$ for all the comparison with the wild type.

Four lines, showing different levels of overexpression of *REM35,* were chosen to investigate the number of lateral roots, comparing it to both the wild type and the *lbd18* mutants (Figure II-22C). All the analyzed lines showed a decreased ability to produce lateral roots, showing a phenotype similar to the *lbd18* mutant. This finding confirmed our hypothesis that *REM34, REM35* and *REM36* might work as negative regulators of the ARF19 target *LBD18.*

To further understand the molecular mechanism through which *REM34, REM35* and *REM36* control auxin signaling during inflorescence development further experiment are needed.

Further analyses are indeed required to clarify the mechanism of interaction between ARF19 and REM35. It has indeed been proven that ARFs can interact with other regulatory transcription factors both with the B3 domain and with the PB1 dimerization domain and that these interactions modulate ARFs activity and target specificity (Shin *et al.*, 2007; Pandey *et al.*, 2018). To better understand how *REM34, REM35* and *REM36* are involved in the modulation of auxin signaling it would thus be informative to understand with which ARF19 domain they are able to interact and how this interaction affects ARF19 activity as a transcriptional activator. Preliminary evidences, based on the analysis of *LBD18* expression, suggest that these genes might act inhibiting ARF19 function.

Furthermore, Chromatin Immuno-Precipitation (ChIP) assays could be performed to verify whether REM34, REM35 or REM36 can directly bind the promoters of their putative target, such as *LBD18.* For this purpose, tagged versions of REM34 and REM35, fused with a fluorescence marker and expressed under the control of their native promoters, were generated and are currently under analysis.

III. CONCLUSIONS AND FUTURE PROSPECTIVES

The REM transcription factor family, in Arabidopsis, is composed of 45 genes preferentially expressed during the reproductive development of this plant. Although these genes are widespread in both monocot and dicot species, their function remains elusive. The main aim of this thesis was to study *REM34, REM35* and *REM36,* three members of the poorly characterized *REM* family, for their role in Arabidopsis reproductive development. We chose to focus on these three members of the *REM* family as a deep analysis performed on this family in our lab suggested that *REM34, REM35* and *REM36* might play an important role during inflorescence development (Mantegazza, Gregis, Mendes, *et al.*, 2014)

As a first step to determine the function of *REM34, REM35* and *REM36* during inflorescence meristem development, we had to implement different techniques to perturb the function of these genes, taking into account the fact that they are likely to be redundant and are located in linkage in the genome. We employed both a multiplexed *RNAi* approach, through which the expression of the three target genes was reduced, and the CRES-T technology, which relied on the overexpression of *REM34* fused to the EAR repressor domain. Several morphological and molecular analyses, performed on both lines, clearly showed how this multiplexed RNA interference approach is effective and fast in helping in the characterization of redundant and/or in linkage genes, a situation which is not rare in plants, whose genomes are usually characterized by duplication events.

At the same time, the CRISPR/Cas9 genome editing system was also successfully employed to create single and multiple mutant combinations. In particular, we were able to obtain the three single mutants *rem34, rem35* and *rem36* and the three possible double mutant combinations *rem34 rem35, rem34 rem36* and *rem35 rem36.* The characterization of these mutants showed that these genes are redundant and have overlapping functions in the control of inflorescence meristem development. As the *rem34 rem35* mutant was obtained only recently, it was not included in most of the analysis described here but the experiments on this line are still ongoing. Furthermore, this line is currently being employed to generate the *rem34 rem35 rem36* triple mutant, with the CRISPR/Cas9 system described above.

The phenotypical characterization of the *REM_RNAi* and *35S:REM34-EAR* lines as well as the single and double mutants showed that both lines have a defective phyllotactic pattern while only the *REM_RNAi* and *35S:REM34-EAR* plants are characterized by a partial sterility. The analysis of both female and male gametophytes of these lines revealed a post-meiotic block in their development: while these plants can produce haploid spores, those spores cannot undergo gametogenesis and give rise to a completely developed gamete. To do so, they regulate the expression of different targets both directly and indirectly along the genetic network that controls gametophytic development in *Arabidopsis*.

The analysis of the expression pattern of *REM34*, *REM35* and *REM36* in the reproductive organs of Arabidopsis, together with the analyses performed on both hemizygous and homozygous lines, suggested that these three genes can influence gametogenesis acting mainly at the sporophytic level. The observation that *REM34*, *REM35*, and *REM36* are expressed throughout all stages of gametogenesis in the embryo sac leaves of course the possibility open that they directly play a function in the female gametophyte. The employment of an embryo sac specific promoter could be useful in order to validate this hypothesis and to be able to better distinguish between the sporophytic and gametophytic roles of *REM34*, *REM35*, and *REM36*.

These finding suggest that *REM34, REM35* and *REM36* might be crucial for gametogenesis acting redundantly, as demonstrated by the finding that the single knock-out mutants do not show this phenotype.

The analysis of the *rem34 rem35 rem36* triple mutants, currently under generation, could help to clarify the cause of this post-meiotic block individuating the exact step in which *REM34, REM35* and *REM36* are required.

The analysis of the inflorescence architecture of the *REM_RNAi, 35S:REM34-EAR,* single and double mutant plants revealed that all these lines are characterized by a mutated phyllotactic pattern, in which the divergence angles are distributed around three main values: 90°, 140°and 180°, compared to the wild type, in which there is only one canonical angle, 140°.

Such defects were found to be linked with permutations in the auxin perception at the inflorescence meristem level. Furthermore, we showed that REM35 can interact with REM34 and ARF19, a transcription factor involved in the regulation of the auxin signaling cascade.

While the role of ARF19 was well characterized in the root apical meristem (Okushima *et al.*, 2007; Hardtke *et al.*, 2004; Lee *et al.*, 2009), its function in the inflorescence meristem was still unclear.

We carried out a phenotypical analysis on the phyllotactic pattern of *arf7, arf19* and *arf7 arf19* double mutants, though which we showed that these mutants have similar defects as the ones displayed by the *REM_RNAi* and by the different *rem* mutants.

ARF7 and *ARF19* control lateral organ development in the roots, by regulating the expression of their targets *PUCHI* and *LBD18* (Kang *et al.*, 2013). To verify whether they are involved in controlling lateral organ development, and thus the phyllotaxy, in the inflorescence by acting on the same targets, together with *REM34, REM35* and *REM36* the level of expression of *LBD18* was measured in the *REM_RNAi* and *rem34 rem35, rem35 rem36* double mutants. Unexpectedly, *LBD18* was upregulated in these lines, suggesting that the *REM* factors act as negative regulators of this gene. To further confirm this observation, we chose to overexpress *REM35*, expanding its expression also in the root, and evaluate the root phenotype, comparing it with the wild type and with the *lbd18* mutant, in which the lateral root number is strongly reduced. Also the lines overexpressing *REM35* show a decreased lateral root number, further suggesting that it is a repressor of *LBD18*.

It is not known whether *REM34, REM35* and *REM36* can directly bind the DNA and if they can do this in a sequence specific way, however there are structural evidences supporting the idea that the B3 domain of these proteins can function as a dimerization domain with other proteins. The ARFs transcription factor are also characterized by the presence of the B3 domain, which acts both as a sequence specific DNA binding domain and as a dimerization domain (Shin *et al.*, 2007).

Different hypothesis can be made, on the mechanism in which REM35 and ARF19 interact and the role that this complex plays in the regulation of LBD18. It is possible to speculate that REM35 interacts with the B3 domain of ARF19, regulating its target specificity, as already reported for the MYB77-ARF7 interaction (Shin *et al.*, 2007), this hypothesis would not however explain the opposite effect that REM34, REM35, REM36 and ARF19 appear to have on their targets (Figure III-1A). It is also tempting to speculate that a possible interaction between the B3 DNA binding domain of ARF19 and REM35 prevents the binding of ARF19 to its target regions in the genome, inhibiting its function as a transcriptional activator, which could also explain why the target of ARF19 *LBD18* is upregulated in the *rem* mutated backgrounds (Figure III-1B).

Finally, one other explanation of the negative effect that *REM34, REM35* and *REM36* seem to have on *LBD18* expression might be that these genes are involved in mediating the interaction of ARF19 with the Aux/IAA-TOPLESS complex, which is in charge of recruiting histone deacetylases that keep the chromatin of ARFs targets in a repressive state (Figure III-1C).

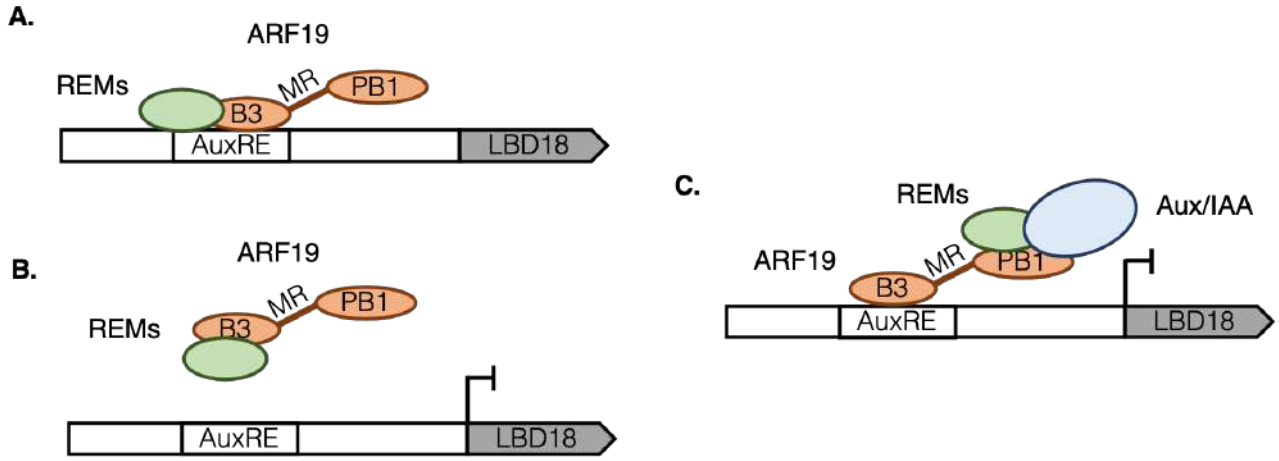

Figure III-1 Possible mechanisms of action of *REM34, REM35* and *REM36*

A. ARF19 binds DNA through the B3 DNA binding domain, it is thus possible that REM34 and REM35 regulate target specificity of this transcription factor interacting with the B3 domain. B. It is also possible that REM35, interacting with the B3 binding domain of ARF19, prevents the binding of this domain to the DNA C. REM35 could bind the PB1 binding domain of ARF19, facilitating the interaction with the Aux/IAA repressors.

Auxin signaling seems to be affected in different ways in the *REM_RNAi* lines and in the double mutants, for instance the *DR5* auxin responsive promoter is not functional in the *RNAi* plants but seems to be overexpressed in the *rem34 rem36* and *rem35 rem36* double mutants. The different level of expression of the *DR5:GFP* marker line in the different analyzed backgrounds might be explained by the hypothesis that *REM34, REM35* and *REM36* are able to interact with different members of the *ARF* gene family, which can act both as activators and repressor of transcription. The analysis of the *rem34 rem35 rem36* triple mutant, as well as of the three single mutants, could help unravel the role that each one of these genes plays singularly in modulation auxin response. Furthermore, protein-protein interaction analysis between REM34, REM35 and REM36 and the 23 ARFs of Arabidopsis might help elucidating the mechanisms through which these genes modulate auxin response.

While a putative DNA consensus sequence for REM34 has been proposed (Franco-Zorrilla *et al.*, 2014), it is still unclear whether the REMs transcription factors can bind DNA in a sequence specific way. ChIP experiments, performed on *LBD18* promoter employing the *pREM34:REM34-GFP* and *pREM35:REM35-RFP*, which were generated and validated

(data not shown), could help in understand whether these genes regulate their target binding specific sequences in their promoter or if their sequence specificity is given by the interaction with other factors, such as ARF19.

The characterization of the inflorescence architecture of the different *rem* mutant and of *arf7* and *arf19* mutants clearly showed that these genes are involved in phyllotaxis regulation. The highly repetitive spiral phyllotactic pattern of Arabidopsis, in which successive flower primordia arise from the inflorescence meristem at a divergence angle of 137.5°, is the result of geometrical and chemical constrains; in particular, the spatio-temporal regulation of the perception of the hormone auxin, which is the morphogen in charge of triggering new primordia initiation, in the inflorescence meristem is the signal that gives rise to this organized developmental pathway. As reiterative processes driven by the perception of morphogenic signals are common phenomena in the development of different organisms (Shyer *et al.*, 2013; Corson *et al.*, 2017; Marcon and Sharpe, 2012), understanding how phyllotaxis is established in Arabidopsis might be useful to clarify the general mechanism behind such pathways.

A key factor that determines the spatial and temporal interval between successive events is the precise regulation of the production and of the perception of the signals which trigger such events. In Arabidopsis, this morphogenic signal is auxin. Recently it has been demonstrated that, in roots, auxin perception is spatially regulated by the cytoplasmatic-nuclear partitioning of ARF proteins. In particular, ARF7 and ARF19 were found to accumulate in cytoplasmatic aggregates in regions where the plants do not need to respond to auxin. These aggregate are, on the other hand, not present in auxin-responsive regions, such as the root tip, where these transcription factors localize in the nuclei (Powers *et al.*, 2019). These aggregates are easily reverted into monomeric proteins, which can thus quickly enter the nucleus and trigger auxin response.

It is possible that the same cellular partitioning of ARF7 and ARF19 is conserved also in the inflorescence meristem and it is tempting to speculate that the plasticity of such protein aggregates is one of the regulatory mechanisms behind phyllotaxis establishment. to verify this hypothesis, it would be important to characterize the cellular localization and distribution of ARF7 and ARF19 in the inflorescence meristem and, since ARF19 is able to interact with REM35 and REM34, it would be interesting to understand whether the REM genes are also involved in the regulation of the formation and/or disaggregation of the ARF aggregates. To

do so, it would be possible to employ the *pREM34:REM34-GFP* and *pREM35:REM35-RFP* marker lines, which were produced and validated during this thesis (Data not shown).

It is finally worth mentioning that the phenotypical analysis of the *rem34, rem35* and *rem36* single mutants showed that the mutations in the phyllotactic pattern led to an increased yield of these lines, which is due to a higher rate of flower production without affecting the total high of the plant. As so, these genes might be promising targets for crop improvement. In particular, in *Brassica napus,* a cultivated Brassicaceae relative of *Arabidopsis thaliana*, the *REM34* cluster appears to be conserved and could be thus an interesting target to improve seeds production in this specie.

IV. MATERIALS and METHODS

IV.I Plant material and growth conditions

All experiments were performed in *Arabidopsis thaliana* ecotype Columbia-0 (Col-0). Plants were grown in a controlled environment at 20–22°C either under long day conditions (16 h light/8 h dark) or under short day (8 h light/16 h dark) conditions for 4 weeks after germination and then transferred to long day conditions.

When necessary, seeds of Arabidopsis were germinated on MS plates (Murashige & Skoog Medium, supplemented with 1% sucrose and solidified with 0,7% Plant Agar) with the appropriate selection.

BASTA® selection was performed on seedlings, which were sprayed 3 times/week with BASTA solution (Bayern, working concentration on soil 50 µg/mL). Tobacco plants were germinated and grown at 20–22°C under long day conditions.

The *suf4-1 pSUF4*:*SUF4-GUS* seeds were donated by Scott Michaels. (University of Wisconsin, USA). The *DR5:GFP/DR5v2:Tomato* and *R2D2* marker lines were donated by Dolf Weijers (Wageningen University, Netherlands). The *TCSn:GFP* and *pPIN1:PIN1-GFP* reporter lines were provided by Jiří Friml (Ghent University, Belgium). The *pAHP6:AHP6-GFP* line was provided by Anthony Bishopp (University of Helsinki, Finland). The *arf7-1 arf19-1* double mutant was obtained from the Nottingham Arabidopsis Stock Centre (N24629).

IV.II Constructs

RNA Interference and 35S:EAR-REM34

The *REM_RNAi* and *35S:EAR-REM34* construct were already available in the laboratory. The DNA fragments specific for the coding sequence of *REM34*, *REM35*, and *REM36* silencing were amplified with the following primers: *REM34* fw GGT CTC ACA CCT GAA GTT TCC AAA GGA AAG G – rv GGT CTC TAT CTC TCT CCA ACC TCT TC; *REM35* fw GGT CTC AAG ATT CCA AGT CCA AGG ACA AG – rv GGT CTC GTG TCA ACA ATA ATC TGT TTC; *REM36* fw GGT CTC GCC TTA ATC ATC CCA CAA GCA CAC – rv CAC CAT GGC GGA TCC ACC ACA TTT C. The specificity of the selected fragment was checked by BLAST against the Arabidopsis genome. Both constructs were transformed into Arabidopsis plants using the floral-dip method (Clough and Bent, 1998).

CRISPR/Cas9 Genome Editing System

The pDE-Cas9-REM34, pDE-Cas9-REM35 and pDE-Cas9-REM36 constructs were cloned following the protocol published by Fauser *et al.*, 2014. The three protospacers were selected with the aid of the CRISP-P 2.0 software (http://crispr.hzau.edu.cn/CRISPR2) and are: *REM34* TTT CAG CAA AAA TTT CGT AC; *REM35* TTC TTC GTC ATA GTT CTT CA; *REM36* GTG ATC TGA CGA AAA AAG GT.

REM35 Overexpression Line

To obtain the *35S:REM35-RFP* constructs, the *35S CaMV,* the *REM35* CDS (fw GGG GAC AAG TTT GTA CAA AAA AGC AGG CTT CAT GGA TGA TCC AGC AAT TTC – rv GGG GAC CAC TTT GTA CAA GAA AGC TGG GTC TTA CTT GAG GAT TTT GTT GAT TTC CG) and the mRFP (Red Fluorescence Protein) were cloned into the *pGHW7* multiplex Gateway vector.

IV.III Phenotypical analyses

Divergence Angles Measurement

The phyllotactic patter was measured as described before (Peaucelle *et al.*, 2007) on 2 months old plants using a 3D clockwise protractor. The first 3 cm of the stem were not taken into account because elongation of is incomplete in this region. The divergence angle was measured taking in account the insertion point of the two successive floral pedicels, without considering the outgrowth direction of the flower. The clockwise or anticlockwise orientation of the phyllotaxis was determined by following the direction that gives the smallest average divergence angle. The measurement was performed on at least 10 plants for each genotype.

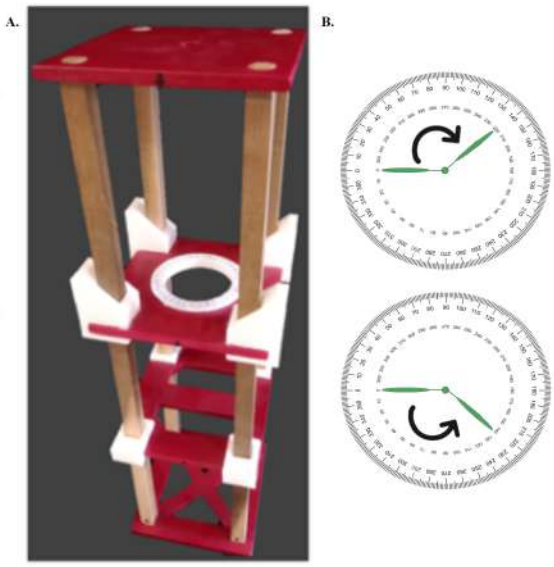

Figure IV-1 3D Protractor
A. Stems were fixed to the apex pointing down through the center of the structure in which a sliding 3D protractor allowed to measure the successive organ. The precision of the protractor is of +/- 10° **B.** Divergence angles are measured between the insertion point of the pedicel of two successive branches in clockwise or anticlockwise orientation.

Plastochrone Measurement

The plastochrone, which is the time that a plant needs to produce a new flower (hours/number of flowers) was evaluated in at least 10 plants for each genotype. The number of newly opened flowers was measured every day for 10 days, starting from the day after bolting. This measurement was performed at the same time of the day during the entire experiment. ANOVA and post hoc Tukey HSD test were used to assess the p-value.

Silique Length, Seed Number Evaluation, and Reciprocal Crosses

For at least 3 plants for each line, 10 siliques were dissected in order to evaluate the number of seed, aborted seed, and non-fertilized ovule employing a Leica® MZ 6 microscope.

For wild-type x *REM_RNAi* reciprocal crosses, stage 11-13 buds were emasculated, removing all floral organs except for the ovary. Anthers in the correct stage of development were than taken from other flowers and used to pollinate the stigma. The numbers of seeds and unfertilized ovules were assessed for at least five pistils for each cross, and three biological replicas of the experiment were performed. ANOVA and post hoc Tukey HSD test were used to assess the p-value.

Female Gametophyte Characterization

The female gametophytes analysis was performed as previously described by Brambilla *et al.*, 2007: flowers were emasculated and harvested on the next day. The emasculated pistils were left O/N at 4°C in a 1:9 acetic acid:ethanol solution. Samples were rehydrated by subsequent washes with ethanol 90 and 70% and incubated O/N at 4°C in clearing solution (160 g chloral hydrate, 50 g glycerol, and H2O to a final volume of 250 ml). Pistils at different developing states were separated from the other floral organs

and opened to evaluate the female gametophyte morphology with a Zeiss Axiophot® microscope equipped with differential interference contrast (DIC) optics. At least 10 carpels for each genotype were analyzed. ANOVA and post hoc Tukey HSD test were used to assess the p-value.

For the *suf4-1 pSUF4*:*SUF4-GUS* marker line analysis, β-Glucuronidase (GUS) assays were performed as described by Resentini *et al.*, 2017, pistils were dissected and fixed in acetone 90% and incubated O/N at 37°C and subsequently cleared as described above.

Male Gametophyte Characterization

In vitro pollen germination analysis was performed following the protocol by Bou Daher et al., 2009, with minor modifications: pollen grains were plated on small glass plates, containing 2.5 ml of pollen germination medium [PGM:18% sucrose, 0.01% boric acid, 1 mM CaCl2, 1 mM Ca(NO3)2, 1 mM MgSO4, 0.5% agarose pH = 7]. The plates were incubated overnight at 22°C, with wet paper to maintain humidity. The next day, pollen germination and growth were evaluated with a Zeiss Axiophot® microscope.

Aniline Blue Staining was performed on flowers emasculated and, after 24 h, pollinated. The pollinated ovaries were collected at two different time points: 5 and 24 h after pollination. Samples were fixed O/N and stained in absolute ethanol/glacial acetic acid 9:1, as described by Mori *et al.*, 2006. Subsequently, they were transferred into an 8M NaOH solution for 1 h at 50°C. Finally, the carpels were washed twice with ddH2O for 10 min and they were stained with aniline blue solution (aniline blue 2%, glycerol 1 M ddH2O) (Takeuchi and Higashiyama, 2016). Samples were stored at 4°C for 3 h or overnight and were imaged under UV light (350–400 nm) with a Zeiss Axiophot® microscope.

Pollen DAPI Staining was performed according to Park *et al.*, 1998: mature pollen was obtained by placing 3–4 open flowers in a microcentrifuge tube containing 300 μl of 4′,6-diamidino-2-phenylindole (DAPI) staining solution (0.1 M sodium phosphate (pH 7), 1 mM EDTA, 0.1% Triton X-100, 0.4 μg/ml DAPI high grade, Sigma). After brief vortexing and centrifugation, the pollen pellet was transferred to a microscope slide and observed with a Zeiss Axiophot® microscope. Pollen at earlier stages of maturation was also analyzed by dissecting single anthers. Anthers were disrupted on microscope slides and squashed in DAPI staining solution (1 μg/ml) under a coverslip.

Alexander Staining on pollen grains was performed as described by Peterson *et al.*, 2010. After fixation (performed with 6 alcohol:3 chloroform:1 acetic acid), the anthers were placed on a microscope slide with a few drops of staining solution (10 ml 95% alcohol, 1 ml malachite green (1% solution in 95% alcohol), 50 ml distilled water, 25 ml glycerol, 5 ml acid fuchsin (1% solution in water), 0.5 ml orange G (1% solution in water), 4 ml glacial acetic acid, and distilled water to a total of 100 ml). Samples were analyzed with a Zeiss Axiophot® microscope.

CLSM Analysis

For confocal imaging, the Laser Scanning Confocal Microscope Nikon A1 was used. For GFP, laser conditions were set at 488 nm of excitation and the signal was acquired considering an emission range between 500 and 600 nm. After removal of siliques and older flowers, the inflorescence was harvested approximately 1 cm from the SAM. With the help of a Leica® MZ 6 microscope floral buds were removed, leaving exposed only flower primordia and the inflorescence meristem. The steam of the inflorescence was included in a 2% solution of low melting agar.

For female and male gametophytes analysis inflorescences were fixed as described by Braselton *et al.*, 1996.

IV.IV Protein -Protein Interactions

Yeast-2-Hybrid (Y2H)

The AH109 yeast strain was used for the Yeast-2-Hybrid assay, and yeast transformation was performed as described by de Folter and Immink, 2011. The coding sequences of *REM34*, *REM35*, and *REM3* were cloned in the GAL4 system Gateway vectors (pGADT7 and pGBKT7; Clontech Laboratories, Inc.). The protein-protein interaction assays were performed on selective yeast synthetic dropout medium lacking Leu, Trp, Ade, and His, and supplemented with different concentrations of 3-aminotriazole (1, 2.5, or 5 mm of 3-AT). Plates were grown for 5 days at 20°C.

The CDS of the genes of interest were cloned with the following primers: *REM34* fw GGG GAC AAG TTT GTA CAA AAA AGC AGG CTT CAT GGC GGA TCC ACC ACA TTT CTC – rv GGG GAC CAC TTT GTA CAA GAA AGC TGG GTT CAA ACC AGA TTA CTG CTG AGG; *REM35* fw GGG GAC AAG TTT GTA CAA AAA AGC AGG CTT CAT GGA TGA TCC AGC AAT TTC; *REM36* fw GGG GAC AAG TTT GTA CAA AAA AGC AGG CTT CAT GGC GAA TCA TCC ACT A; *REM35/REM36* rv GGG GAC CAC TTT GTA CAA GAA AGC TGG GTC TTA CTT GAG GAT TTT GTT GAT TTC CG.

Bimolecular fluorescence complementation (BiFC)

The *REM34, REM35* and *REM36* coding sequences were cloned in the pYFPN43 and pYFPC43 vectors. Agrobacterium, co-transformed with the viral suppressor p19 construct, was used to infiltrate tobacco leaves. 3 days after inoculation, the abaxial surfaces of infiltrated leaves was imaged. As positive control, the VAL-VDD interaction was tested (Mendes *et al.*, 2016) while the constructs containing the CDS were co-transformed with the empty pYFN43 and pYFC43 vectors, as a negative control. REM34 homodimerization, which was not observed in the Y2H assays, was also employed as a negative control.

IV.V *In Situ* Hybridization Analysis

In situ hybridization analyses on *REM34*, *REM35*, and *REM36* were performed as described in Mantegazza *et al.*, 2014, employing the same probes described. Evaluation of the expression profile in the inflorescence and flower meristems, which was previously published, was used as a positive control.

IV.VI Gene Expression Analysis

Total RNA was extracted from whole inflorescences using lithium chloride. RNA samples were treated with DNase and retrotranscribed employing the iScript™ Reverse Transcription Suoermix (Bio-Rad). 1:10 dilutions of the cDNA were used as templates in qRT-PCRs, which was performed with the iQ SYBR Green Supermix (Bio-Rad) to detect target synthesis. All the experiments were performed with three technical replicates for each of the three biological replicates.

Auxin treatments were performed 5 days after bolting on primary inflorescences, using 15 µL of 10 µM IAA or water (mock), containing 0.01% Silwet L-77. 3h after treating, inflorescences were collected and immediately frozen in liquid nitrogen. RNA extraction and RT-PCR were performed as described above.

Primers employed for expression analysis are listed in the table below (Table IV-1).

CTGTTCACGGAACCCAATTC	Ubiquitin fw
GGAAAAAGGTCTGACCGACA	Ubiquitin rv
AGCTTGTGAGACTGCTCCAC	REM34 fw
CCTGATCGGAGACTGAGCAC	REM34 rv
CATTTGATGAAGGAGGGGAGAC	REM35 fw
CTTTCTAGCTCTGACCGAATCC	REM35 rv
TCACTTGCTGGACACACCTC	REM36 fw
TCGTCTCGAAGACAGTGTGC	REM36 rv
TGGCATAGAGTGGAAGTCGCATC	REM37 fw
GTCATTCGGGGTTTCCTATCC	REM37 rv
GGAGAAGTTTCTGCCGTGAG	REM39 fw
GGTCACTGGCCACTCTTCTC	REM39 rv
ACGTAAACGGCCACAAGTTC	eGFP fw (Che-Yang Liao et al 2015)
AAGTCGTGCTGCTTCATGTG	eGFP rv (Che-Yang Liao et al 2015)
CCTGTTCCTGGGGCATGG	tdTomato fw
TGATGACGGCCATGTTGTTG	tdTomato rv
GCAAGCTCAGTGGTGACTAC	MDS fw
ACATCCACTTTCTGACATGC	MDS rv
GTTAACCGTTGCTCACAGAC	NLE fw
GCCTTTGCAAGTAAACAATG	NLE rv
AGTCGCCTGCTGCTAAGACAAA	RBR fw
ATGACAGTCCTGAGCCACTTGG	RBR rv
CTTCTGATTCATCACCGGACTC	KRP6 fw (Liu J et al 2008)
ACACCAAACGACGAACTGTTCT	KRP6 rv (Liu J et al 2008)
ATGGGATCGTCTGCGGATACA	HAM1 fw (Latrasse et al., 2008)
GAATTCGTGAGAGCGAGTATCGCA	HAM1 rv (Latrasse et al., 2008)
CCTTTAACTCCTGATCAAGCTAT	HAM2 fw (Latrasse et al., 2008)
CTACAGCGCACTCTACTGAATC	HAM2 rv (Latrasse et al., 2008)
ATGAATCTCTACGTGCCGGG	GH3.4 fw
GACGTCCTGAAGTAGTCGCT	GH3.4 rv

Table IV-1 Primers employed for Expression Analyses

V. REFERENCES

Acosta-García, G. and Vielle-Calzada, J.-P. (2004) A classical arabinogalactan protein is essential for the initiation of female gametogenesis in Arabidopsis. *Plant Cell*, **16**, 2614–28. Available at: http://www.ncbi.nlm.nih.gov/pubmed/15377758 [

Andrés, F. and Coupland, G. (2012) The genetic basis of flowering responses to seasonal cues. *Nat. Rev. Genet.*, **13**, 627–639. Available at: https://pubmed.ncbi.nlm.nih.gov/22898651/

Bainbridge, K., Guyomarc'h, S., Bayer, E., Swarup, R., Bennett, M., Mandel, T. and Kuhlemeier, C. (2008) Auxin influx carriers stabilize phyllotactic patterning. *Genes Dev.*, **22**, 810–823.

Benková, E., Michniewicz, M., Sauer, M., Teichmann, T., Seifertová, D., Jürgens, G. and Friml, J. (2003) Local, Efflux-Dependent Auxin Gradients as a Common Module for Plant Organ Formation. *Cell*, **115**, 591–602.

Berger, F. and Twell, D. (2011) Germline Specification and Function in Plants. *Annu. Rev. Plant Biol.*, **62**, 461–484. Available at: http://www.ncbi.nlm.nih.gov/pubmed/21332359

Berke, L. and Snel, B. (2015) The plant Polycomb repressive complex 1 (PRC1) existed in the ancestor of seed plants and has a complex duplication history. *BMC Evol. Biol.*, **15**. Available at: https://pubmed.ncbi.nlm.nih.gov/25881027/

Besnard, F., Refahi, Y., Morin, V., et al. (2014a) Cytokinin signalling inhibitory fields provide robustness to phyllotaxis. *Nature*, **505**, 417–21. Available at: http://www.ncbi.nlm.nih.gov/pubmed/24336201.

Besnard, F., Refahi, Y., Morin, V., et al. (2014b) Cytokinin signalling inhibitory fields provide robustness to phyllotaxis. *Nature*, **505**, 417–421.

Besnard, F., Rozier, F. and Vernoux, T. (2014) The AHP6 cytokinin signaling inhibitor mediates an auxin-cytokinin crosstalk that regulates the timing of organ initiation at the shoot apical meristem. *Plant Signal. Behav.*, 4–7.

Bevan, M. and Walsh, S. (2005) The Arabidopsis genome: a foundation for plant research. *Genome Res.*, **15**, 1632–42. Available at: http://www.ncbi.nlm.nih.gov/pubmed/16339360

Boer, D.R., Freire-Rios, A., Berg, W.A.M. Van Den, et al. (2014) Structural basis for DNA binding specificity by the auxin-dependent ARF transcription factors. *Cell*, **156**, 577–589. Available at: https://pubmed.ncbi.nlm.nih.gov/24485461/

Bou Daher, F., Chebli, Y. and Geitmann, A. (2009) Optimization of conditions for germination of cold-stored Arabidopsis thaliana pollen. *Plant Cell Rep.*, **28**, 347–357.

Brambilla, V., Battaglia, R., Colombo, M., Masiero, S., Bencivenga, S., Kater, M.M. and Colombo, L. (2007) Genetic and Molecular Interactions between BELL1 and MADS Box Factors Support Ovule Development in Arabidopsis. *Plant Cell Online*, **19**, 2544–2556.

Braselton, J.P., Wilkinson, M.J. and Clulow, S.A. (1996) Feulgen staining of intact plant tissues for confocal microscopy. *Biotech. Histochem.*, **71**, 84–7. Available at: http://www.ncbi.nlm.nih.gov/pubmed/9138536

BRIGGS, G., OSMONT, K., SHINDO, C., SIBOUT, R. and HARDTKE, C. (2006) Unequal genetic redundancies in Arabidopsis – a neglected phenomenon? *Trends Plant Sci.*, **11**, 492–498. Available at: http://www.ncbi.nlm.nih.gov/pubmed/16949326

Brunoud, G., Wells, D.M., Oliva, M., et al. (2012) A novel sensor to map auxin response and distribution at high spatio-temporal resolution. *Nature*, **482**, 103–106.

Burian, A., Raczyńska-Szajgin, M., Borowska-Wykręt, D., Piatek, A., Aida, M. and Kwiatkowska, D. (2015) The CUP-SHAPED COTYLEDON2 and 3 genes have a post-meristematic effect on Arabidopsis thaliana phyllotaxis. *Ann. Bot.*, **115**, 807–820.

Busch, W., Miotk, A., Ariel, F.D., et al. (2010) Transcriptional control of a plant stem cell niche. *Dev. Cell*, **18**, 841–853. Available at: http://dx.doi.org/10.1016/j.devcel.2010.03.012.

Calderón Villalobos, L.I.A., Lee, S., Oliveira, C. De, et al. (2012) A combinatorial TIR1/AFB-Aux/IAA co-receptor system for differential sensing of auxin. *Nat. Chem. Biol.*, **8**, 477–485. Available at: https://www.nature.com/articles/nchembio.926

Ceccato, L., Masiero, S., Sinha Roy, D., Bencivenga, S., Roig-Villanova, I., Ditengou, F.A., Palme, K., Simon, R. and Colombo, L. (2013) Maternal Control of PIN1 Is Required for Female Gametophyte Development in Arabidopsis. *PLoS One*, **8**, 2–8.

Cecchetti, V., Celebrin, D., Napoli, N., Ghelli, R., Brunetti, P., Costantino, P. and Cardarelli, M. (2017) An auxin maximum in the middle layer controls stamen development and pollen maturation in Arabidopsis. *New Phytol.*, **213**, 1194–1207. Available at: http://www.ncbi.nlm.nih.gov/pubmed/27659765

Chandler, J.W., Jacobs, B., Cole, M., Comelli, P. and Werr, W. (2011) DORNRÖSCHEN-LIKE expression marks Arabidopsis floral organ founder cells and precedes auxin response maxima. *Plant Mol. Biol.*, **76**, 171–185.

Chandler, J.W. and Werr, W. (2015) Cytokinin-auxin crosstalk in cell type specification. *Trends Plant Sci.*, **20**, 291–300. Available at: http://www.cell.com/article/S1360138515000485/fulltext

Chantha, S.C., Gray-Mitsumune, M., Houde, J. and Matton, D.P. (2010) The MIDASIN and NOTCHLESS genes are essential for female gametophyte development in Arabidopsis thaliana. *Physiol. Mol. Biol. Plants*, **16**, 3–18.

Chen, Z.H., Bao, M.L., Sun, Y.Z., Yang, Y.J., Xu, X.H., Wang, J.H., Han, N., Bian, H.W. and Zhu, M.Y. (2011) Regulation of auxin response by miR393-targeted transport inhibitor response protein 1 is involved in normal development in Arabidopsis. *Plant Mol. Biol.*, **77**, 619–629. Available at: https://pubmed.ncbi.nlm.nih.gov/22042293/

Cheng, C.-Y., Mathews, D.E., Schaller, G.E. and Kieber, J.J. (2013) Cytokinin-dependent specification of the functional megaspore in

the Arabidopsis female gametophyte. *Plant J.*, **73**, 929–40. Available at: http://www.ncbi.nlm.nih.gov/pubmed/23181607

Cheng, Y., Dai, X. and Zhao, Y. (2006a) Auxin biosynthesis by the YUCCA flavin monooxygenases controls the formation of floral organs and vascular tissues in Arabidopsis. *Genes Dev.*, **20**, 1790–9. Available at: http://www.ncbi.nlm.nih.gov/pubmed/16818609

Cheng, Y., Dai, X. and Zhao, Y. (2006b) Auxin biosynthesis by the YUCCA flavin monooxygenases controls the formation of floral organs and vascular tissues in Arabidopsis. *Genes Dev.*, **20**, 1790–1799.

Cheng, Y., Dai, X. and Zhao, Y. (2007) Auxin synthesized by the YUCCA flavin monooxygenases is essential for embryogenesis and leaf formation in Arabidopsis. *Plant Cell*, **19**, 2430–2439. Available at: /pmc/articles/PMC2002601/?report=abstract

Cherenkov, P., Novikova, D., Omelyanchuk, N., Levitsky, V., Grosse, I., Weijers, D. and Mironova, V. (2018) Diversity of cis-regulatory elements associated with auxin response in Arabidopsis thaliana. *J. Exp. Bot.*, **69**, 329–339.

Chung, Y., Zhu, Y., Wu, M.F., et al. (2019) Auxin Response Factors promote organogenesis by chromatin-mediated repression of the pluripotency gene SHOOTMERISTEMLESS. *Nat. Commun.*, **10**. Available at: https://pubmed.ncbi.nlm.nih.gov/30792395/

Clark, K.A. and Krysan, P.J. (2010) Chromosomal translocations are a common phenomenon in Arabidopsis thaliana T-DNA insertion lines. *Plant J.*, **64**, 990–1001. Available at: http://www.ncbi.nlm.nih.gov/pubmed/21143679

Clough, S.J. and Bent, A.F. (1998) Floral dip: a simplified method for Agrobacterium-mediated transformation of Arabidopsis thaliana. *Plant J.*, **16**, 735–43. Available at: http://www.ncbi.nlm.nih.gov/pubmed/10069079

Coen, E.S. and Meyerowitz, E.M. (1991) The war of the whorls: genetic interactions controlling flower development. *Nature*, **353**, 31–37.

Comelli, P., Glowa, D., Chandler, J.W. and Werr, W. (2016) Founder-cell-specific transcription of the DORNRÖSCHEN-LIKE promoter and integration of the auxin response. *J. Exp. Bot.*, **67**, 143–155.

Comelli, P., Glowa, D., Frerichs, A., Engelhorn, J., Chandler, J.W. and Werr, W. (2020) Functional dissection of the DORNRÖSCHEN-LIKE enhancer 2 during embryonic and phyllotactic patterning. *Planta*, **251**, 1–15. Available at: https://doi.org/10.1007/s00425-020-03381-7.

Corson, F., Couturier, L., Rouault, H., Mazouni, K. and Schweisguth, F. (2017) Self-organized Notch dynamics generate stereotyped sensory organ patterns in Drosophila. *Science (80-.).*, **356**. Available at: http://science.sciencemag.org/

Cui, D., Zhao, J., Jing, Y., Fan, M., Liu, J., Wang, Z., Xin, W. and Hu, Y. (2013) The Arabidopsis IDD14, IDD15, and IDD16 Cooperatively Regulate Lateral Organ Morphogenesis and Gravitropism by Promoting Auxin Biosynthesis and Transport. *PLoS Genet.*, **9**.

Curtis, M.J., Belcram, K., Bollmann, S.R., Tominey, C.M., Hoffman, P.D., Mercier, R. and Hays, J.B. (2009) Reciprocal chromosome translocation associated with TDNA-insertion mutation in Arabidopsis: genetic and cytological analyses of consequences for gametophyte development and for construction of doubly mutant lines. *Planta*, **229**, 731–45. Available at: http://link.springer.com/10.1007/s00425-008-0868-0

Czarnecki, O., Bryan, A.C., Jawdy, S.S., Yang, X., Cheng, Z.M., Chen, J.G. and Tuskan, G.A. (2016) Simultaneous knockdown of six non-family genes using a single synthetic RNAi fragment in Arabidopsis thaliana. *Plant Methods*, **12**, 1–11.

Ding, Z., Wang, B., Moreno, I., et al. (2012) ER-localized auxin transporter PIN8 regulates auxin homeostasis and male gametophyte development in Arabidopsis. *Nat. Commun.*, **3**.

Douady, S. and Couder, Y. (1996) Phyllotaxis as a dynamical self organizing process part I: The spiral modes resulting from time-periodic iterations. *J. Theor. Biol.*, **178**, 255–273.

Ebel, C., Mariconti, L. and Gruissem, W. (2004) Plant retinoblastoma homologues control nuclear proliferation in the female gametophyte. *Nature*, **429**, 776–780. Available at: http://www.nature.com/articles/nature02637

Fal, K., Liu, M., Duisembekova, A., Refahi, Y., Haswell, E.S. and Hamant, O. (2017) Phyllotactic regularity requires the paf1 complex in Arabidopsis. *Dev.*, **144**, 4428–4436.

Farcot, E., Lavedrine, C. and Vernoux, T. (2015) A modular analysis of the auxin signalling network. *PLoS One*, **10**. Available at: /pmc/articles/PMC4373724/?report=abstract

Fauser, F., Schiml, S. and Puchta, H. (2014) Both CRISPR/Cas-based nucleases and nickases can be used efficiently for genome engineering in Arabidopsis thaliana. *Plant J.*, **79**, 348–359.

Finet, C., Fourquin, C., Vinauger, M., Berne-Dedieu, A., Chambrier, P., Paindavoine, S. and Scutt, C.P. (2010) Parallel structural evolution of auxin response factors in the angiosperms. *Plant J.*, **63**, 952–959. Available at: https://pubmed.ncbi.nlm.nih.gov/20626651/

Folter, S. de and Immink, R.G.H. (2011) Yeast protein-protein interaction assays and screens. *Methods Mol. Biol.*, **754**, 145–65. Available at: http://www.ncbi.nlm.nih.gov/pubmed/21720951

Folter, S. de, Immink, R.G.H., Kieffer, M., et al. (2005) Comprehensive Interaction Map of the Arabidopsis MADS Box Transcription Factors. *PLANT CELL ONLINE*, **17**, 1424–1433.

Fornara, F., Gregis, V., Pelucchi, N., Colombo, L. and Kater, M. (2008) The rice StMADS11-like genes OsMADS22 and OsMADS47 cause floral reversions in Arabidopsis without complementing the svp and agl24 mutants. *J. Exp. Bot.*, **59**, 2181–2190. Available at: https://academic.oup.com/jxb/article-lookup/doi/10.1093/jxb/ern083

Franco-Zorrilla, J.M., Cubas, P., Jarillo, J.A., Fernández-Calvín, B., Salinas, J. and Martínez-Zapater, J.M. (2002) AtREM1, a member of a new family of B3 domain-containing genes, is preferentially expressed in reproductive meristems. *Plant Physiol.*,

128, 418–27. Available at: http://www.ncbi.nlm.nih.gov/pubmed/11842146

Franco-Zorrilla, J.M., López-Vidriero, I., Carrasco, J.L., Godoy, M., Vera, P. and Solano, R. (2014) DNA-binding specificities of plant transcription factors and their potential to define target genes. *Proc. Natl. Acad. Sci. U. S. A.*, **111**, 2367–72. Available at: http://www.pubmedcentral.nih.gov/articlerender.fcgi?artid=3926073&tool=pmcentrez&rendertype=abstract.

Galvan-Ampudia, C.S., Cerutti, G., Legrand, J., et al. (2020) Temporal integration of auxin information for the regulation of patterning. *Elife*, **9**, 1–65.

Galvan-Ampudia, C.S., Chaumeret, A.M., Godin, C. and Vernoux, T. (2016) Phyllotaxis: from patterns of organogenesis at the meristem to shoot architecture. *Wiley Interdiscip. Rev. Dev. Biol.*, **5**, 460–473.

Gray, W.M., Kepinski, S., Rouse, D., Leyser, O. and Estelle, M. (2001) Auxin regulates SCFTIR1-dependent degradation of AUX/IAA proteins. *Nature*, **414**, 271–276. Available at: www.nature.com

Gregis, V., Sessa, A., Colombo, L. and Kater, M.M. (2008) *AGAMOUS-LIKE24* and *SHORT VEGETATIVE PHASE* determine floral meristem identity in Arabidopsis. *Plant J.*, **56**, 891–902. Available at: http://doi.wiley.com/10.1111/j.1365-313X.2008.03648.x

Gregis, W.V., Sessa, A., Colombo, L., Kater, M.M., Gregis, V., Sessa, A., Colombo, L. and Kater, M.M. (2006) AGL24, SHORT VEGETATIVE PHASE, and APETALA1 Redundantly Control AGAMOUS during Early Stages of Flower Development in Arabidopsis. *PLANT CELL ONLINE*, **18**, 1373–1382.

Guédon, Y., Refahi, Y., Besnard, F., Farcot, E., Godin, C. and Vernoux, T. (2013) Pattern identification and characterization reveal permutations of organs as a key genetically controlled property of post-meristematic phyllotaxis. *J. Theor. Biol.*, **338**, 94–110. Available at: http://dx.doi.org/10.1016/j.jtbi.2013.07.026.

Guilfoyle, T.J. and Hagen, G. (2007) Auxin response factors. *Curr. Opin. Plant Biol.*, **10**, 453–460.

Hafidh, S., Fíla, J. and Honys, D. (2016) Male gametophyte development and function in angiosperms: a general concept. *Plant Reprod.*, **29**, 31–51.

Hagen, G. and Guilfoyle, T. (2002) *Auxin-responsive gene expression: genes, promoters and regulatory factors*, Auxin Molecular Biology.

Hardtke, C.S., Ckurshumova, W., Vidaurre, D.P., Singh, S.A., Stamatiou, G., Tiwari, S.B., Hagen, G., Guilfoyle, T.J. and Berleth, T. (2004) Overlapping and non-redundant functions of the Arabidopsis auxin response factors MONOPTEROS and NONPHOTOTROPIC HYPOCOTYL 4. *Development*, **131**, 1089–1100. Available at: https://pubmed.ncbi.nlm.nih.gov/14973283/

Heisler, M.G., Ohno, C., Das, P., Sieber, P., Reddy, G. V., Long, J.A. and Meyerowitz, E.M. (2005) Patterns of Auxin Transport and Gene Expression during Primordium Development Revealed by Live Imaging of the Arabidopsis Inflorescence Meristem. *Curr. Biol.*, **15**, 1899–1911. Available at: http://www.sciencedirect.com/science/article/pii/S0960982205012133

Hiratsu, K., Matsui, K., Koyama, T. and Ohme-Takagi, M. (2003) Dominant repression of target genes by chimeric repressors that include the EAR motif, a repression domain, in Arabidopsis. *Plant J.*, **34**, 733–739.

Huanca-Mamani, W., Garcia-Aguilar, M., Leon-Martinez, G., Grossniklaus, U. and Vielle-Calzada, J.-P. (2005) CHR11, a chromatin-remodeling factor essential for nuclear proliferation during female gametogenesis in Arabidopsis thaliana. *Proc. Natl. Acad. Sci.*, **102**, 17231–17236. Available at: http://www.pnas.org/cgi/doi/10.1073/pnas.0508186102.

Immink, R.G., Tonaco, I.A., Folter, S. de, Shchennikova, A., Dijk, A.D. van, Busscher-Lange, J., Borst, J.W. and Angenent, G.C. (2009) SEPALLATA3: the "glue" for MADS box transcription factor complex formation. *Genome Biol.*, **10**, R24. Available at: http://genomebiology.biomedcentral.com/articles/10.1186/gb-2009-10-2-r24

Ingouff, M., Jullien, P.E. and Berger, F. (2006) The female gametophyte and the endosperm control cell proliferation and differentiation of the seed coat in Arabidopsis. *Plant Cell*, **18**, 3491–501. Available at: http://www.ncbi.nlm.nih.gov/pubmed/17172356

Johnston, A.J., Matveeva, E., Kirioukhova, O., Grossniklaus, U. and Gruissem, W. (2008) A Dynamic Reciprocal RBR-PRC2 Regulatory Circuit Controls Arabidopsis Gametophyte Development. *Curr. Biol.*, **18**, 1680–1686. Available at: http://dx.doi.org/10.1016/j.cub.2008.09.026.

Jönsson, H., Heisler, M.G., Shapiro, B.E., Meyerowitz, E.M. and Mjolsness, E. (2006) An auxin-driven polarized transport model for phyllotaxis. *Proc. Natl. Acad. Sci. U. S. A.*, **103**, 1633–8. Available at: http://www.ncbi.nlm.nih.gov/pubmed/16415160

Kang, N.Y., Lee, H.W. and Kim, J. (2013) The AP2/EREBP gene PUCHI co-acts with LBD16/ASL18 and LBD18/ASL20 downstream of ARF7 and ARF19 to regulate lateral root development in arabidopsis. *Plant Cell Physiol.*, **54**, 1326–1334. Available at: www.pcp.oxfordjournals.org

Kierzkowski, D., Lenhard, M., Smith, R. and Kuhlemeier, C. (2013) Interaction between Meristem tissue layers controls phyllotaxis. *Dev. Cell*, **26**, 616–628. Available at: http://dx.doi.org/10.1016/j.devcel.2013.08.017.

Klepikova, A. V., Kasianov, A.S., Gerasimov, E.S., Logacheva, M.D. and Penin, A.A. (2016) A high resolution map of the *Arabidopsis thaliana* developmental transcriptome based on RNA-seq profiling. *Plant J.*, **88**, 1058–1070. Available at: http://www.ncbi.nlm.nih.gov/pubmed/27549386

Landrein, B., Refahi, Y., Besnard, F., Hervieux, N., Mirabet, V., Boudaoud, A., Vernoux, T. and Hamant, O. (2015a) Meristem size contributes to the robustness of phyllotaxis in Arabidopsis. *J. Exp. Bot.*, **66**, 1317–1324.

Landrein, B., Refahi, Y., Besnard, F., Hervieux, N., Mirabet, V., Boudaoud, A., Vernoux, T. and Hamant, O. (2015b) Meristem size contributes to the robustness of phyllotaxis in Arabidopsis. *J. Exp. Bot.*, **66**, 1317–1324.

Larsson, E., Vivian-Smith, A., Offringa, R. and Sundberg, E. (2017) Auxin homeostasis in arabidopsis ovules is anther-dependent at maturation and changes dynamically upon fertilization. *Front. Plant Sci.*, **8**, 1–14.

Latrasse, D., Benhamed, M., Henry, Y., Domenichini, S., Kim, W., Zhou, D.X. and Delarue, M. (2008) The MYST histone acetyltransferases are essential for gametophyte development in arabidopsis. *BMC Plant Biol.*, **8**, 1–16.

Lee, H.W., Kim, N.Y., Lee, D.J. and Kim, J. (2009) LBD18/ASL20 regulates lateral root formation in combination with LBD16/ASL18 downstream of ARF7 and ARF19 in Arabidopsis. *Plant Physiol.*, **151**, 1377–1389.

Leibfried, A., To, J.P.C., Busch, W., Stehling, S., Kehle, A., Demar, M., Kieber, J.J. and Lohmann, J.U. (2005) WUSCHEL controls meristem function by direct regulation of cytokinin-inducible response regulators. *Nature*, **438**, 1172–1175.

Levy, Y.Y. (2002) Multiple Roles of Arabidopsis VRN1 in Vernalization and Flowering Time Control. *Science (80-.).*, **297**, 243–246. Available at: http://www.sciencemag.org/cgi/doi/10.1126/science.1072147

Li, N., Yuan, L., Liu, N., Shi, D., Li, X., Tang, Z., Liu, J., Sundaresan, V. and Yang, W.-C. (2009) SLOW WALKER2, a NOC1/MAK21 Homologue, Is Essential for Coordinated Cell Cycle Progression during Female Gametophyte Development in Arabidopsis. *PLANT Physiol.*, **151**, 1486–1497. Available at: http://www.ncbi.nlm.nih.gov/pubmed/19734265

Liao, C.-Y., Smet, W., Brunoud, G., Yoshida, S., Vernoux, T. and Weijers, D. (2015) Reporters for sensitive and quantitative measurement of auxin response. *Nat. Methods*, **12**, 1098–1098.

Lieberman-Lazarovich, M., Yahav, C., Israeli, A. and Efroni, I. (2019) Deep Conservation of cis-Element Variants Regulating Plant Hormonal Responses. *Plant Cell*, **31**, 2559–2572.

Liu, H., Ding, Y., Zhou, Y., Jin, W., Xie, K. and Chen, L.L. (2017) CRISPR-P 2.0: An Improved CRISPR-Cas9 Tool for Genome Editing in Plants. *Mol. Plant*, **10**, 530–532.

Liu, J., Zhang, Y., Qin, G., et al. (2008) Targeted Degradation of the Cyclin-Dependent Kinase Inhibitor ICK4/KRP6 by RING-Type E3 Ligases Is Essential for Mitotic Cell Cycle Progression during Arabidopsis Gametogenesis. *Plant Cell Online*, **20**, 1538–1554. Available at: http://www.plantcell.org/cgi/doi/10.1105/tpc.108.059741.

Liu, X., Dinh, T.T., Li, D., et al. (2014) AUXIN RESPONSE FACTOR 3 integrates the functions of AGAMOUS and APETALA2 in floral meristem determinacy. *Plant J.*, **80**, 629–641. Available at: https://pubmed.ncbi.nlm.nih.gov/25187180/

Liu Zhan Bin, Ulmasov, T., Shi Xiangyang, Hagen, G. and Guilfoyle, T.J. (1994) Soybean GH3 promoter contains multiple auxin-inducible elements. *Plant Cell*, **6**, 645–657.

Ljung, K., Bhalerao, R.P. and Sandberg, G. (2001) Sites and homeostatic control of auxin biosynthesis in Arabidopsis during vegetative growth. *Plant J.*, **28**, 465–474. Available at: https://onlinelibrary.wiley.com/doi/full/10.1046/j.1365-313X.2001.01173.x

Long, J.A., Ohno, C., Smith, Z.R. and Meyerowitz, E.M. (2006) TOPLESS regulates apical embryonic fate in Arabidopsis. *Science (80-.).*, **312**, 1520–1523. Available at: https://science.sciencemag.org/content/312/5779/1520

Lowder, L.G., Zhang, D., Baltes, N.J., et al. (2015) A CRISPR/Cas9 Toolbox for Multiplexed Plant Genome Editing and Transcriptional Regulation. *Plant Physiol.*, **169**, 971–85. Available at: http://www.ncbi.nlm.nih.gov/pubmed/26297141%5Cnhttp://www.pubmedcentral.nih.gov/articlerender.fcgi?artid=PMC4587453.

Luo, L., Zeng, J., Wu, H., Tian, Z. and Zhao, Z. (2018) A Molecular Framework for Auxin-Controlled Homeostasis of Shoot Stem Cells in Arabidopsis. *Mol. Plant*, **11**, 899–913. Available at: https://doi.org/10.1016/j.molp.2018.04.006

Ma, Y., Miotk, A., Šutiković, Z., et al. (2019) WUSCHEL acts as an auxin response rheostat to maintain apical stem cells in Arabidopsis. *Nat. Commun.*, **10**, 1–11.

Mandel, T., Moreau, F., Kutsher, Y., Fletcher, J.C., Carles, C.C. and Williams, L.E. (2014) The ERECTA receptor kinase regulates Arabidopsis shoot apical meristem size, phyllotaxy and floral meristem identity. *Dev.*, **141**, 830–841.

Mansfield, S.G. and Briarty, L.G. (1991) Early embryogenesis in *Arabidopsis thaliana* . II. The developing embryo. *Can. J. Bot.*, **69**, 461–476. Available at: http://www.nrcresearchpress.com/doi/10.1139/b91-063

Mantegazza, O., Gregis, V., Chiara, M., Selva, C., Leo, G., Horner, D.S. and Kater, M.M. (2014) Gene coexpression patterns during early development of the native Arabidopsis reproductive meristem: Novel candidate developmental regulators and patterns of functional redundancy. *Plant J.*, **79**, 861–877.

Mantegazza, O., Gregis, V., Mendes, M.A., Morandini, P., Alves-Ferreira, M., Patreze, C.M., Nardeli, S.M., Kater, M.M. and Colombo, L. (2014) Analysis of the arabidopsis REM gene family predicts functions during flower development. *Ann. Bot.*, **114**, 1507–1515.

Marcon, L. and Sharpe, J. (2012) Turing patterns in development: What about the horse part? *Curr. Opin. Genet. Dev.*, **22**, 578–584. Available at: http://dx.doi.org/10.1016/j.gde.2012.11.013.

Mashiguchi, K., Tanaka, K., Sakai, T., et al. (2011) The main auxin biosynthesis pathway in Arabidopsis. *Proc. Natl. Acad. Sci.*, **108**, 18512–18517.

Matias-Hernandez, L., Battaglia, R., Galbiati, F., Rubes, M., Eichenberger, C., Grossniklaus, U., Kater, M.M. and Colombo, L. (2010) VERDANDI is a direct target of the MADS domain ovule identity complex and affects embryo sac differentiation in Arabidopsis. *Plant Cell*, **22**, 1702–15. Available at: http://www.pubmedcentral.nih.gov/articlerender.fcgi?artid=2910977&tool=pmcentrez&rendertype=abstract%5Cnhttp://www.plantcell.org/content/22/6/1702.short.

McCarty, D.R., Hattori, T., Carson, C.B., et al. (1991) The Viviparous-1 developmental gene of maize encodes a novel transcriptional activator. *Cell*, **66**, 895–905. Available at: http://www.ncbi.nlm.nih.gov/pubmed/1889090

McGraw, S., Morin, G., Vigneault, C., Leclerc, P. and Sirard, M.-A. (2007) Investigation of MYST4 histone acetyltransferase and its involvement in mammalian gametogenesis. *BMC Dev. Biol.*, **7**, 123. Available at: http://www.ncbi.nlm.nih.gov/pubmed/17980037

Meins, F., Si-Ammour, A. and Blevins, T. (2005) RNA silencing systems and their relevance to plant development. *Annu. Rev. Cell Dev. Biol.*, **21**, 297–318. Available at: https://pubmed.ncbi.nlm.nih.gov/16212497/.

Melnyk, C.W., Molnar, A. and Baulcombe, D.C. (2011) Intercellular and systemic movement of RNA silencing signals. *EMBO J.*, **30**, 3553–3563. Available at: http://emboj.embopress.org/cgi/doi/10.1038/emboj.2011.274

Mendes, M.A., Guerra, R.F., Castelnovo, B., et al. (2016) Live and let die: a REM complex promotes fertilization through synergid cell death in Arabidopsis. *Development*, **143**, 2780–2790.

Mir, R., Aranda, L.Z., Biaocchi, T., Luo, A., Sylvester, A.W. and Rasmussen, C.G. (2017) A DII domain-based auxin reporter uncovers low auxin signaling during telophase and early G1. *Plant Physiol.*, **173**, 863–871.

Mlotshwa, S., Voinnet, O., Mette, M.F., Matzke, M., Vaucheret, H., Ding, S.W., Pruss, G. and Vance, V.B. (2002) RNA silencing and the mobile silencing signal. *Plant Cell*, **14**, S289–S301. Available at: www.plantcell.org/cgi/doi/10.1105/tpc.001677.

Mori, T., Kuroiwa, H., Higashiyama, T. and Kuroiwa, T. (2006) GENERATIVE CELL SPECIFIC 1 is essential for angiosperm fertilization. *Nat. Cell Biol.*, **8**, 64–71.

Müller, C.J., Larsson, E., Spíchal, L. and Sundberg, E. (2017) Cytokinin-auxin crosstalk in the gynoecial primordium ensures correct domain patterning. *Plant Physiol.*, **175**, 1144–1157.

Muralla, R., Lloyd, J. and Meinke, D. (2011) Molecular Foundations of Reproductive Lethality in Arabidopsis thaliana G. Chua, ed. *PLoS One*, **6**, e28398. Available at: http://dx.plos.org/10.1371/journal.pone.0028398

Muto, H., Nagao, I., Demura, T., Fukuda, H., Kinjo, M. and Yamamoto, K.T. (2006) Fluorescence Cross-Correlation Analyses of the Molecular Interaction between an Aux/IAA Protein, MSG2/IAA19, and Protein-Protein Interaction Domains of Auxin Response Factors of Arabidopsis Expressed in HeLa Cells. *Plant Cell Physiol.*, **47**, 1095–1101. Available at: https://academic.oup.com/pcp/article/47/8/1095/2329665

O'Malley, R.C., Huang, S.S.C., Song, L., Lewsey, M.G., Bartlett, A., Nery, J.R., Galli, M., Gallavotti, A. and Ecker, J.R. (2016) Cistrome and Epicistrome Features Shape the Regulatory DNA Landscape. *Cell*, **165**, 1280–1292. Available at: http://dx.doi.org/10.1016/j.cell.2016.04.038.

Okada, K., Ueda, J., Komaki, M.K., Bell, C.J. and Shimura, Y. (1991) Requirement of the Auxin Polar Transport System in Early Stages of Arabidopsis Floral Bud Formation. *Plant Cell*, **3**, 677–684. Available at: http://www.plantcell.org/content/3/7/677.full.pdf+html.

Okushima, Y., Fukaki, H., Onoda, M., Theologis, A. and Tasaka, M. (2007) ARF7 and ARF19 regulate lateral root formation via direct activation of LBD/ASL genes in Arabidopsis. *Plant Cell*, **19**, 118–130.

Okushima, Y., Overvoorde, P.J., Arima, K., et al. (2005) Functional Genomic Analysis of the AUXIN RESPONSE FACTOR Gene Family Members in Arabidopsis thaliana : Unique and Overlapping Functions of ARF7 and ARF19. , **17**, 444–463.

Pagnussat, G.C., Alandete-Saez, M., Bowman, J.L. and Sundaresan, V. (2009) Auxin-Dependent Patterning and Gamete Specification in the Arabidopsis Female Gametophyte. *Science (80-.).*, **324**.

Pagnussat, G.C., Yu, H.J., Ngo, Q.A., et al. (2005) Genetic and molecular identification of genes required for female gametophyte development and function in Arabidopsis. *Development*, **132**, 603–614. Available at: https://pubmed.ncbi.nlm.nih.gov/15634699/

Pandey, S.K., Lee, H.W., Kim, M.-J., Cho, C., Oh, E. and Kim, J. (2018) LBD18 uses a dual mode of a positive feedback loop to regulate ARF expression and transcriptional activity in Arabidopsis. *Plant J.*, **95**, 233–251. Available at: http://doi.wiley.com/10.1111/tpj.13945

Panoli, A., Martin, M.V., Alandete-Saez, M., et al. (2015) Auxin Import and Local Auxin Biosynthesis Are Required for Mitotic Divisions, Cell Expansion and Cell Specification during Female Gametophyte Development in Arabidopsis thaliana H. Candela, ed. *PLoS One*, **10**, e0126164. Available at: https://dx.plos.org/10.1371/journal.pone.0126164

Paponov, I.A., Paponov, M., Teale, W., Menges, M., Chakrabortee, S., Murray, J.A.H. and Palme, K. (2008) Comprehensive transcriptome analysis of auxin responses in Arabidopsis. *Mol. Plant*, **1**, 321–337. Available at: http://dx.doi.org/10.1093/mp/ssm021.

Parcy, F., Bomblies, K. and Weigel, D. (2002) Interaction of LEAFY, AGAMOUS and TERMINAL FLOWER1 in maintaining floral meristem identity in Arabidopsis. *Development*, **129**.

Park, S.K., Howden, R. and Twell, D. (1998) The Arabidopsis thaliana gametophytic mutation gemini pollen1 disrupts microspore polarity, division asymmetry and pollen cell fate. *Development*, **125**, 3789–3799.

Peaucelle, a., Louvet, R., Johansen, J.N., et al. (2011) The transcription factor BELLRINGER modulates phyllotaxis by regulating the expression of a pectin methylesterase in Arabidopsis. *Development*, **138**, 4733–4741.

Peaucelle, A., Louvet, R., Johansen, J.N., Höfte, H., Laufs, P., Pelloux, J. and Mouille, G. (2008) Arabidopsis Phyllotaxis Is Controlled by the Methyl-Esterification Status of Cell-Wall Pectins. *Curr. Biol.*, **18**, 1943–1948.

Peaucelle, A., Morin, H., Traas, J. and Laufs, P. (2007) Plants expressing a miR164-resistant CUC2 gene reveal the importance of post-meristematic maintenance of phyllotaxy in Arabidopsis. *Development*, **134**, 1045–1050.

Peterson, R., Slovin, J.P. and Chen, C. (2010) pollen grains on m er al.

Pillus, L. (2008) MYSTs mark chromatin for chromosomal functions. *Curr. Opin. Cell Biol.*, **20**, 326–33. Available at: http://www.ncbi.nlm.nih.gov/pubmed/18511253 [Accessed December 3, 2018].

Pinon, V., Prasad, K., Grigg, S.P., Sanchez-Perez, G.F. and Scheres, B. (2013) Local auxin biosynthesis regulation by PLETHORA transcription factors controls phyllotaxis in Arabidopsis. *Proc. Natl. Acad. Sci. U. S. A.*, **110**, 1107–1112.

Powers, S.K., Holehouse, A.S., Korasick, D.A., et al. (2019) Nucleo-cytoplasmic Partitioning of ARF Proteins Controls Auxin Responses in Arabidopsis thaliana. *Mol. Cell*, **76**, 177-190.e5.

Prasad, K., Grigg, S.P., Barkoulas, M., et al. (2011) Arabidopsis PLETHORA transcription factors control phyllotaxis. *Curr. Biol.*, **21**, 1123–1128.

Prusinkiewicz, P., Erasmus, Y., Lane, B., Harder, L.D. and Coen, E. (2007) Evolution and development of inflorescence architectures. *Science (80-.).*, **316**, 1452–1456.

Refahi, Y., Brunoud, G., Farcot, E., Jean-Marie, A., Pulkkinen, M., Vernoux, T. and Godin, C. (2016) A stochastic multicellular model identifies biological watermarks from disorders in self-organized patterns of phyllotaxis. *Elife*, **5**, 1–51.

Reinhardt, D., Frenz, M., Mandel, T. and Kuhlemeier, C. (2004) Microsurgical and laser ablation analysis of leaf positioning and dorsoventral patterning in tomato. *Development*, **132**, 15–26. Available at: http://www.ncbi.nlm.nih.gov/pubmed/15563522 [Accessed April 11, 2017].

Reinhardt, D., Mandel, T. and Kuhlemeier, C. (2000) Auxin regulates the initiation and radial position of plant lateral organs. *Plant Cell*, **12**, 507–518. Available at: www.plantcell.org [Accessed July 14, 2020].

Reinhardt, D., Pesce, E.-R., Stieger, P., Mandel, T., Baltensperger, K., Bennett, M., Traas, J., Friml, J. and Kuhlemeier, C. (2003) Regulation of phyllotaxis by polar auxin transport. *Nature*, **426**, 255–260. Available at: http://eutils.ncbi.nlm.nih.gov/entrez/eutils/elink.fcgi?dbfrom=pubmed&id=14628043&retmode=ref&cmd=prlinks%5Cnpapers3://publication/doi/10.1038/nature02081.

Resentini, F., Cyprys, P., Steffen, J.G., et al. (2017) SUPPRESSOR OF FRIGIDA (SUF4) Supports Gamete Fusion via Regulating Arabidopsis EC1 Gene Expression. *Plant Physiol.*, **173**, 155–166. Available at: http://www.ncbi.nlm.nih.gov/pubmed/27920160 [Accessed October 27, 2018].

Richter, R., Kinoshita, A., Vincent, C., Martinez-Gallegos, R., Gao, H., Driel, A.D. van, Hyun, Y., Mateos, J.L. and Coupland, G. (2019) Floral regulators FLC and SOC1 directly regulate expression of the B3-type transcription factor TARGET OF FLC AND SVP 1 at the Arabidopsis shoot apex via antagonistic chromatin modifications. *PLoS Genet.*, **15**, e1008065.

Rijpkema, A.S., Vandenbussche, M., Koes, R., Heijmans, K. and Gerats, T. (2010) Variations on a theme: Changes in the floral ABCs in angiosperms. *Semin. Cell Dev. Biol.*, **21**, 100–107.

Romanel, E.A.C., Schrago, C.G., Couñago, R.M., Russo, C.A.M. and Alves-Ferreira, M. (2009) Evolution of the B3 DNA binding superfamily: New insights into REM family gene diversification. *PLoS One*, **4**.

Sapountzi, V. and Côté, J. (2011) MYST-family histone acetyltransferases: beyond chromatin. *Cell. Mol. Life Sci.*, **68**, 1147–1156. Available at: http://link.springer.com/10.1007/s00018-010-0599-9 [Accessed December 3, 2018].

Sassi, M., Ali, O., Boudon, F., et al. (2014) *An Auxin-Mediated Shift toward Growth Isotropy Promotes Organ Formation at the Shoot Meristem in Arabidopsis*,.

Schneitz, K., Hulskamp, M. and Pruitt, R.E. (1995) Wild-type ovule development in Arabidopsis thaliana: a light microscope study of cleared whole-mount tissue. *Plant J.*, **7**, 731–749. Available at: http://doi.wiley.com/10.1046/j.1365-313X.1995.07050731.x [Accessed October 10, 2019].

Shi, B., Guo, X., Wang, Y., Xiong, Y., Wang, J., Hayashi, K. ichiro, Lei, J., Zhang, L. and Jiao, Y. (2018) Feedback from Lateral Organs Controls Shoot Apical Meristem Growth by Modulating Auxin Transport. *Dev. Cell*, **44**, 204-216.e6. Available at: https://doi.org/10.1016/j.devcel.2017.12.021 [Accessed August 7, 2020].

Shi, D.-Q., Liu, J., Xiang, Y.-H., Ye, D., Sundaresan, V. and Yang, W.-C. (2005) SLOW WALKER1, essential for gametogenesis in Arabidopsis, encodes a WD40 protein involved in 18S ribosomal RNA biogenesis. *Plant Cell*, **17**, 2340–54. Available at: http://www.ncbi.nlm.nih.gov/pubmed/15980260 [Accessed November 2, 2018].

Shin, R., Burch, A.Y., Huppert, K.A., Tiwari, S.B., Murphy, A.S., Guilfoyle, T.J. and Schachtman, D.P. (2007) The Arabidopsis transcription factor MYB77 modulates auxin signal transduction. *Plant Cell*, **19**, 2440–2453. Available at: /pmc/articles/PMC2002618/?report=abstract [Accessed August 10, 2020].

Shyer, A.E., Tallinen, T., Nerurkar, N.L., Wei, Z., Gil, E.S., Kaplan, D.L., Tabin, C.J. and Mahadevan, L. (2013) Villification: How the gut gets its villi. *Science (80-.).*, **342**, 212–218. Available at: http://science.sciencemag.org/ [Accessed July 14, 2020].

Si-Ammour, A., Windels, D., Arn-Bouldoires, E., Kutter, C., Ailhas, J., Meins, F. and Vazquez, F. (2011) miR393 and secondary siRNAs regulate expression of the TIR1/AFB2 auxin receptor clade and auxin-related development of Arabidopsis leaves. *Plant Physiol.*, **157**, 683–691. Available at: www.plantphysiol.org/cgi/doi/10.1104/pp.111.180083 [Accessed August 9, 2020].

Simonini, S., Bencivenga, S., Trick, M. and Østergaard, L. (2017) Auxin-induced modulation of ETTIN activity orchestrates gene expression in arabidopsis. *Plant Cell*, **29**, 1864–1882.

Skopelitis, D.S., Hill, K., Klesen, S., Marco, C.F., Born, P. von, Chitwood, D.H. and Timmermans, M.C.P. (2018) Gating of miRNA movement at defined cell-cell interfaces governs their impact as positional signals. *Nat. Commun.*, **9**, 1–10. Available at: www.nature.com/naturecommunications.

Smith, R.S., Guyomarc'h, S., Mandel, T., Reinhardt, D., Kuhlemeier, C. and Prusinkiewicz, P. (2006) A plausible model of phyllotaxis. *Proc. Natl. Acad. Sci. U. S. A.*, **103**, 1301–1306. Available at: www.pnas.orgcgidoi10.1073pnas.0510457103 [Accessed July 14, 2020].

Smyth, D.R., Bowman, J.L. and Meyerowitz, E.M. (1990) Early flower development in Arabidopsis. *Plant Cell*, **2**, 755–767. Available at: http://www.ncbi.nlm.nih.gov/pubmed/2152125.

Snow, M. and Snow, R. (1932) Experiments on Phyllotaxis. I. The Effect of Isolating a Primordium. *Philos. Trans. R. Soc. London B Biol. Sci.*, **221**. Available at: http://rstb.royalsocietypublishing.org/content/221/474-482/1 [Accessed April 11, 2017].

Stepanova, A.N., Robertson-Hoyt, J., Yun, J., Benavente, L.M., Xie, D.Y., Doležal, K., Schlereth, A., Jürgens, G. and Alonso, J.M. (2008) TAA1-Mediated Auxin Biosynthesis Is Essential for Hormone Crosstalk and Plant Development. *Cell*, **133**, 177–191. Available at: https://pubmed.ncbi.nlm.nih.gov/18394997/

Strauss, S., Lempe, J., Prusinkiewicz, P., Tsiantis, M. and Smith, R.S. (2020) Phyllotaxis: is the golden angle optimal for light capture? *New Phytol.*, **225**, 499–510.

Su, Y.-H., Liu, Y.-B. and Zhang, X.-S. (2011) Auxin-Cytokinin Interaction Regulates Meristem Development. *Mol. Plant •*, **4**, 616–625.

Sung, S. and Amasino, R.M. (2004) Vernalization in Arabidopsis thaliana is mediated by the PHD finger protein VIN3. *Nature*, **427**, 159–164. Available at: http://www.nature.com/doifinder/10.1038/nature02195.

Swaminathan, K., Peterson, K. and Jack, T. (2008) The plant B3 superfamily. *Trends Plant Sci.*, **13**, 647–655.

Szemenyei, H., Hannon, M. and Long, J.A. (2008) TOPLESS mediates auxin-dependent transcriptional repression during Arabidopsis embryogenesis. *Science (80-.).*, **319**, 1384–1386. Available at: https://science.sciencemag.org/content/319/5868/1384

Takeuchi, H. and Higashiyama, T. (2016) Tip-localized receptors control pollen tube growth and LURE sensing in Arabidopsis. *Nature*, **531**, 245–248.

Tao, Y., Ferrer, J.L., Ljung, K., et al. (2008) Rapid Synthesis of Auxin via a New Tryptophan-Dependent Pathway Is Required for Shade Avoidance in Plants. *Cell*, **133**, 164–176. Available at: http://www.cbs.dtu.dk/services/TargetP/ [Accessed August 7, 2020].

The Arabidopsis Genome Initiative (2000) Analysis of the genome sequence of the flowering plant Arabidopsisthaliana. *Nature*, **408**, 796–815. Available at: http://www.nature.com/doifinder/10.1038/35048692

Uchida, N., Shimada, M. and Tasaka, M. (2013) ERECTA-family receptor kinases regulate stem cell homeostasis via buffering its cytokinin responsiveness in the shoot apical meristem. *Plant Cell Physiol.*, **54**, 343–351. Available at: https://pubmed.ncbi.nlm.nih.gov/22885615/

Ulmasov, T., Murfett, J., Hagen, G. and Guilfoyle, T.J. (1997) Aux/IAA proteins repress expression of reporter genes containing natural and highly active synthetic auxin response elements. *Plant Cell*, **9**, 1963–1971. Available at: https://pubmed.ncbi.nlm.nih.gov/9401121/ .

Usadel, B., Obayashi, T., Mutwil, M., et al. (2009) Co-expression tools for plant biology: Opportunities for hypothesis generation and caveats. *Plant, Cell Environ.*, **32**, 1633–1651.

Vernoux, T., Brunoud, G., Farcot, E., Morin, V., Daele, H. Van Den, et al. (2011) The auxin signalling network translates dynamic input into robust patterning at the shoot apex. *Mol. Syst. Biol.*, **7**. Available at: https://pubmed.ncbi.nlm.nih.gov/21734647/

Vernoux, T., Brunoud, G., Farcot, E., Morin, V., Daele, H. Van den, et al. (2011) The auxin signalling network translates dynamic input into robust patterning at the shoot apex. *Mol. Syst. Biol.*, **7**, 508. Available at: https://onlinelibrary.wiley.com/doi/abs/10.1038/msb.2011.39

Vernoux, T., Kronenberger, J., Grandjean, O., Laufs, P. and Traas, J. (2000) PIN-FORMED 1 regulates cell fate at the periphery of the shoot apical meristem. *Development*, **127**, 5157–5165.

Waltner, J.K., Peterson, F.C., Lytle, B.L. and Volkman, B.F. (2005) Structure of the B3 domain from *Arabidopsis thaliana* protein At1g16640. *Protein Sci.*, **14**, 2478–2483. Available at: http://doi.wiley.com/10.1110/ps.051606305

Wang, L., Kim, J. and Somers, D.E. (2013) Transcriptional corepressor TOPLESS complexes with pseudoresponse regulator proteins and histone deacetylases to regulate circadian transcription. *Proc. Natl. Acad. Sci. U. S. A.*, **110**, 761–766. Available at: /pmc/articles/PMC3545823/?report=abstract.

Wang, Y., Hou, Y., Gu, H., Kang, D., Chen, Z., Liu, J. and Qu, L.-J. (2012) The Arabidopsis APC4 subunit of the anaphase-promoting complex/cyclosome (APC/C) is critical for both female gametogenesis and embryogenesis. *Plant J.*, **69**, 227–240. Available at: http://doi.wiley.com/10.1111/j.1365-313X.2011.04785.x

Wang, Z.-P., Xing, H.-L., Dong, L., Zhang, H.-Y., Han, C.-Y., Wang, X.-C. and Chen, Q.-J. (2015) Egg cell-specific promoter-controlled CRISPR/Cas9 efficiently generates homozygous mutants for multiple target genes in Arabidopsis in a single generation. *Genome Biol.*, **16**, 144. Available at: http://genomebiology.biomedcentral.com/articles/10.1186/s13059-015-0715-0.

Won, C., Shen, X., Mashiguchi, K., et al. (2011) Conversion of tryptophan to indole-3-acetic acid by tryptophan aminotransferases in Arabidopsis and YUCCAs in Arabidopsis. *Proc. Natl. Acad. Sci.*, **108**, 18518–18523.

Wu, M.F., Yamaguchi, N., Xiao, J., Bargmann, B., Estelle, M., Sang, Y. and Wagner, D. (2015) Auxin-regulated chromatin switch directs acquisition of flower primordium founder fate. *Elife*, **4**.

Yamaguchi, N., Wu, M.F., Winter, C.M., Berns, M.C., Nole-Wilson, S., Yamaguchi, A., Coupland, G., Krizek, B.A. and Wagner, D. (2013) A Molecular Framework for Auxin-Mediated Initiation of Flower Primordia. *Dev. Cell*, **24**, 271–282. Available at: https://pubmed.ncbi.nlm.nih.gov/23375585/.

Yao, X., Tian, L., Yang, J., Zhao, Y.N., Zhu, Y.X., Dai, X., Zhao, Y. and Yang, Z.N. (2018) Auxin production in diploid microsporocytes is necessary and sufficient for early stages of pollen development. *PLoS Genet.*, **14**, 1–19.

Yu, Y., Qiao, L., Chen, J., Rong, Y., Zhao, Y., Cui, X., Xu, J., Hou, X. and Dong, C.H. (2020) Arabidopsis REM16 acts as a B3 domain transcription factor to promote flowering time via directly binding to the promoters of SOC1 and FT. *Plant J.* Available at: https://pubmed.ncbi.nlm.nih.gov/32391591/

Zhao, X., Bramsiepe, J., Durme, M. Van, et al. (2017) RETINOBLASTOMA RELATED1 mediates germline entry in Arabidopsis. *Science*, **356**, eaaf6532. Available at: http://www.ncbi.nlm.nih.gov/pubmed/28450583

VI. APPENDIX

REM34 and REM35 Control Female and Male Gametophyte Development in Arabidopsis thaliana.

Caselli F [1], Beretta VM [1], Mantegazza O [1], Petrella R [1], Leo G [1], Guazzotti A [1], Herrera-Ubaldo H [2], de Folter S [2], Mendes MA [1], Kater MM [1] and Gregis V [1]

[1] Dipartimento di Bioscienze, Università degli Studi di Milano, Milan, Italy

[2] Laboratorio Nacional de Genómica para la Biodiversidad, Unidad de Genómica Avanzada, Centro de Investigación y de Estudios Avanzados del Instituto Politécnico Nacional, Irapuato, Mexico

October 2019; Front. Plant Sci. 10:1351; doi: 10.3389/fpls.2019.01351

In this paper we investigated the role of *REM34*, *REM35*, and *REM36*, three closely related and linked genes, in both female and male gametophytes development. Simultaneous silencing by RNA interference (RNAi) caused about 50% of the ovules to remain unfertilized.

Careful evaluation of both ovule and pollen developments showed that this partial sterility of the transgenic RNAi lines was due to a post-meiotic block in both female and male gametophytes. Furthermore, protein interaction assays revealed that REM34 and REM35 interact, which suggests that they work together during the first stages of gametogenesis.

Finally, to confirm the phenotype observed in the *REM_RNAi* lines we generated transgenic lines overexpressing *REM34,* fused to the *EAR* repressive motif. Also these lines displayed the same post-meiotic block of both ovules and pollen, confirming that *REM34, REM35* and *REM36* are involved in the control of a very early step of female and male gametogenesis.

I contributed to this paper by performing most of the described experiments, with the exception of the Bimolecular Fluorescence Complementation analysis (BiFC) and the confocal laser scanning microscopy (CLSM) imaging, and by writing the manuscript.

frontiers in Plant Science

ORIGINAL RESEARCH
published: 24 October 2019
doi: 10.3389/fpls.2019.01351

REM34 and *REM35* Control Female and Male Gametophyte Development in *Arabidopsis thaliana*

*Francesca Caselli[1], Veronica Maria Beretta[1], Otho Mantegazza[1], Rosanna Petrella[1], Giulia Leo[1], Andrea Guazzotti[1], Humberto Herrera-Ubaldo[2], Stefan de Folter[2], Marta Adelina Mendes[1], Martin M. Kater[1] and Veronica Gregis[1]**

[1] *Dipartimento di Bioscienze, Università degli Studi di Milano, Milan, Italy,* [2] *Laboratorio Nacional de Genómica para la Biodiversidad, Unidad de Genómica Avanzada, Centro de Investigación y de Estudios Avanzados del Instituto Politécnico Nacional, Irapuato, Mexico*

The REproductive Meristem (REM) gene family encodes for transcription factors belonging to the B3 DNA binding domain superfamily. In *Arabidopsis thaliana*, the *REM* gene family is composed of 45 members, preferentially expressed during flower, ovule, and seed developments. Only a few members of this family have been functionally characterized: *VERNALIZATION1* (*VRN1*) and, most recently, *TARGET OF FLC AND SVP1* (*TFS1*) regulate flowering time and *VERDANDI* (*VDD*), together with *VALKYRIE* (*VAL*) that control the death of the receptive synergid cell in the female gametophyte. We investigated the role of *REM34, REM35*, and *REM36,* three closely related and linked genes similarly expressed in both female and male gametophytes. Simultaneous silencing by RNA interference (RNAi) caused about 50% of the ovules to remain unfertilized. Careful evaluation of both ovule and pollen developments showed that this partial sterility of the transgenic RNAi lines was due to a postmeiotic block in both female and male gametophytes. Furthermore, protein interaction assays revealed that REM34 and REM35 interact, which suggests that they work together during the first stages of gametogenesis.

Keywords: gametophyte development, REM, transcriptional regulation, ovule, pollen, post-meiotic division, *Arabidopsis thaliana*

OPEN ACCESS

Edited by:
Sergio Lanteri, University of Turin, Italy

Reviewed by:
Gabriela Carolina Pagnussat, National University of Mar del Plata, Argentina
Maria Beatrice Bitonti, University of Calabria, Italy

***Correspondence:**
Veronica Gregis
veronica.gregis@unimi.it

Specialty section:
This article was submitted to Plant Breeding, a section of the journal Frontiers in Plant Science

Received: *18 March 2019*
Accepted: *01 October 2019*
Published: *24 October 2019*

Citation:
Caselli F, Beretta VM, Mantegazza O, Petrella R, Leo G, Guazzotti A, Herrera-Ubaldo H, de Folter S, Mendes MA, Kater MM and Gregis V (2019) REM34 and REM35 Control Female and Male Gametophyte Development in Arabidopsis thaliana. Front. Plant Sci. 10:1351. doi: 10.3389/fpls.2019.01351

INTRODUCTION

In higher plants, the alternation between the diploid sporophytic generation and the haploid gametophytic generation is a fundamental characteristic of their life cycle. The formation of the gametophyte from the sporophyte is the result of two sequential processes, sporogenesis, and gametogenesis. Angiosperms are heterosporous plants, characterized by the production of two types of unisexual gametophytes, the megagametophyte (embryo sac), and microgametophyte (pollen). Developments of both female and male gametophytes can be divided into two main steps: sporogenesis, during which meiosis occurs giving rise to haploid spores, and gametogenesis, which leads to the formation of the gametes (Berger and Twell, 2011).

In Arabidopsis, the female gametophyte develops in the gynoecium. The first step of megasporogenesis consists in the formation of the ovule primordia, in which one cell differentiates into the megaspore mother cell (MMC) or megasporocyte; the MMC sustains one meiotic division, giving rise to four

haploid megaspores. Only one of them, the functional megaspore, continues its development and goes through three mitotic divisions forming a mature embryo sac composed of eight nuclei and seven cells: three antipodal cells, two medial polar nuclei, and one egg cell surrounded by two synergids (Mansfield and Briarty, 1991).

In the anthers, the microspore mother cell gives rise, through meiosis, to four microspores, which develop into mature pollen grains, containing two sperm cells surrounded by the vegetative cell (Hafidh et al., 2016).

The transition from sporogenesis to gametogenesis is directly correlated with the cell cycle transition from meiosis to mitosis. During gametogenesis, the number of mitotic divisions (two for the male and three for the female gametophyte) has to be tightly regulated and coordinated with cytokinesis. This cell division process is complex and requires the integration of different pathways such as those involved in cell cycle progression, chromatin modifications, and hormonal signaling. Moreover, mitotic progression during gametogenesis is also affected when interfering with basic biological processes like organelle and ribosome biogenesis (Shi et al., 2005; Li et al., 2009; Wang et al., 2012).

In both gametophytes, the retinoblastoma-related protein (RBR) plays a key role in the regulation of the cell cycle by inhibiting cell cycle entry through repressing E2F transcription factors. The *rbr* mutation results in an uncontrolled nuclear proliferation in both gametophytes (Ebel et al., 2004; Ingouff et al., 2006; Johnston et al., 2008). More recently, *RBR* was also associated with the meiosis activation, when the MMC is getting reduced by meiosis and forming subsequently the functional megaspore (Zhao et al., 2017).

In all eukaryotic organisms, cell cycle progression is tightly linked to the activation and degradation of different cyclin-dependent kinases (CDKs). During both female and male gametophyte developments, the activity of two homologous RING finger E3 ubiquitin ligases, RHF1 and RHF2, are required for the degradation of the CDK inhibitor ICK4/KRP6, which allows the correct progression of the cell cycle. In the *rhf1 rhf2* double mutant, both female and male gametophytes fail to complete their development and are arrested in FG1 and microspore stage respectively (Liu et al., 2008).

The transcriptional activity in different cell types during plant development is dependent on epigenetic modifications, such as chromatin remodeling and histone modifications. Failure in the establishment of such modifications can cause different defects throughout the plant's life cycle. During gametogenesis, silencing of the *CHROMATIN-REMODELLING PROTEIN 11* (*CHR11*) within the embryo sac causes an arrest of nuclear proliferation from stage FG1 to FG5 (Huanca-Mamani et al., 2005). Furthermore, mutations in the histone acetyl transferase genes *HAM1* and *HAM2* cause an arrest in the early stages of both megagametogenesis and microgametogenesis (Latrasse et al., 2008).

Genetic studies have identified a large number of loci that control gametophyte development. Molecular cloning and characterization of some of them have revealed insights in sporocyte formation, meiosis/mitosis, and gametophyte development. Detailed phenotypic and molecular characterization of mutants remains a big challenge also because of the complication to work with such mutants, which often are partially sterile or even lethal (Muralla et al., 2011).

In the context of finding new players involved in the control of this process, the *REM* gene transcription factor family promises to be a good candidate since two of the four REMs that were functionally chatacterized, *VERDANDI* (*VDD or REM20*) and *VALKYRIE* (*VAL or REM11*), have a function in gametophyte development (Matias-Hernandez et al., 2010; Mendes et al., 2016). The other two members, *VERNALIZATION1* (*VRN1* or *REM5*) and *TARGET OF FLC AND SVP1* (*TFS1* or *REM17*), were shown to be involved in the control of flowering time (Levy, 2002; Sung and Amasino, 2004; Richter et al., 2019).

The expression patterns of *REM* genes were analyzed by Mantegazza et al. (2014) showing that the majority of the members of this family are preferentially expressed during flower and seed developments. Through this analysis, we identified *REM34*, *REM35*, and *REM36*, which are mainly expressed in the reproductive meristems but also throughout different stages of flower development. *REM34*, *REM35*, and *REM36* are located in a cluster, containing in total nine *REM* genes on the fourth chromosome of *Arabidopsis*. *REM34*, *REM35*, and *REM36* are very similar, which might indicate a possible functional redundancy.

Insertional mutants already analyzed for *REM34* and *REM36* are not complete knock-outs and showed no visible phenotype whereas no insertional mutants are available for *REM35* (Mantegazza et al., 2014). Since these genes are located in linkage on the *Arabidopsis* genome, it is also practically impossible to obtain multiple mutant combinations by crossing the available mutant lines.

Therefore, in this study, we investigated the role of *REM34*, *REM35*, and *REM36* through their simultaneous downregulation by RNA interference. Plants in which at least *REM34* and *REM35* were down-regulated showed an early arrest in the development of both female and male gametophytes. The process of mega/micro sporogenesis was not affected, and meiosis was taking place. However, subsequent mitosis was not occurring after spore formation, suggesting that these genes play a role in gametogenesis progression.

MATERIALS AND METHODS

Plant Material and Growth Conditions

All experiments were performed in *Arabidopsis thaliana* ecotype Columbia-0 (Col-0). Plants were grown in a controlled environment at 20–22°C either under long day conditions (16 h light/8 h dark) or under short day (8 h light/16 h dark) conditions for 4 weeks after germination and then transferred to long day conditions. The *suf4-1 pSUF4*:*SUF4-GUS* seeds were donated by S.D. Michaels. Tobacco plants were germinated and grown at 20–22°C under long day conditions.

RNA Interference and *35S:EAR_REM34* Constructs

To obtain the *REM_RNAi* construct 252, 232 and 254 base pairs long DNA fragments specific for the coding sequence of

each of the genes *REM34, REM35,* and *REM36* were selected (the primers used to amplify the fragments are listed in the **Supplementary Table 1**). The fragments specificity was checked by BLAST against the Arabidopsis genome.

The three selected regions were PCR amplified, adding the *BsaI* sites to the primers, and cloned in a pENTR™ vector previously modified to function as a Golden Gate acceptor, with a single Golden Gate reaction, producing the pENTR-*RNAi_REM* vector. The Gateway LR reaction (Invitrogen™ Gateway™ recombination cloning system) was then performed to sub-clone the *RNAi_REMs* fragments into the pFGC5941 vector and used to transform Arabidopsis. Primers that were used are listed in **Supplementary Table 1.**

The EAR motif was added to the C terminus of the *REM34* coding sequence (see primer sequences in **Supplementary Table 1**). The fragment was cloned into the pB2GW7 plasmid (35S) passing through the pENTRY-D-TOPO vector (Invitrogen™ Gateway™ recombination cloning system). Arabidopsis plants were transformed using the floral-dip method (Clough and Bent, 1998).

Quantitative RT-PCR

Total RNA was extracted from whole inflorescences. RNA samples were treated with DNase (TURBO DNA-free®; Ambion, http://www.ambion.com/) and retrotranscribed employing the ImProm-IITM Reverse Transcription System (Promega). Diluted aliquots of the cDNAs or genomic DNA were used as templates in qRT-PCRs, using the iQ SYBR Green Supermix (Bio-Rad) to detect target synthesis. All the experiments were performed with three technical replicates for each of the three biological replicates, with the exception of the expression analysis of *REM34, REM35,* and *REM36* in the T1 *REM_RNAi*, in the T1 35S:*REM34_EAR* plants and for T-DNA abundancy evaluation. Primers employed for these analyses are listed in **Supplementary Table 1**.

Silique Length, Seed Number Evaluation, and Reciprocal Crosses

For each line, 10 siliques (dissected from three different plants) were measured, and seed, aborted seed, and non-fertilized ovule numbers were counted. For this purpose, a Leica® MZ 6 microscope was used.

For the reciprocal crosses between wild-type and *REM_RNAi* #1 plants, mature siliques as well as open flowers and buds in an advanced stage of development were removed from the inflorescence of the mother plant, along with the meristem and smallest buds. Remaining buds were emasculated by removal of all floral organs except for the ovary. Then, anthers in the correct stage of development were taken from other flowers and used to pollinate the stigma. The numbers of seeds and unfertilized ovules were assessed for at least five pistils for each cross, and three biological replicas of the experiment were performed.

In Situ Hybridization Analysis

In situ hybridization analysis for *REM34, REM35,* and *REM36* were performed following the same protocol and employing the same probes described by Mantegazza et al. (2014). Evaluation of the expression profile in the inflorescence and flower meristems was used as a positive control.

Protein–Protein Interaction Analysis

Yeast two-hybrid assays were performed in the yeast strains PJ69-4A and PJ69-4α (de Folter and Immink, 2011). The coding sequences of *REM34, REM35,* and *REM36* were cloned in the pDEST32 (bait vector, BD; Invitrogen) and pDEST22 (prey vector, AD; Invitrogen) Gateway vector. The bait constructs were tested for autoactivation on selective yeast synthetic dropout medium lacking Leu, Trp, and His supplemented with 1, 3, 5, 10, or 15 mM of 3-aminotriazole, in order to set the screening conditions. After mating, colonies were plated on the proper selective media and grown for 5 days at 20°C.

The same coding sequences were also cloned in the pYFPN43 and pYFPC43 vectors, to perform the BiFC assay. Agrobacterium, transformed with the vectors and the viral suppressor p19 construct, was used to infiltrate tobacco leaves. The abaxial surfaces of infiltrated leaves were imaged 3 days after inoculation. As positive control for the infiltration, the already published VAL-VDD interaction was tested (Mendes et al., 2016). As negative controls, the constructs containing the proteins of interest were co-transformed with the empty pYFN43 and pYFC43 vectors. Furthermore, REM34 homodimerization, which was not observed in the Y2H assays, was also employed as a negative control (**Supplementary Figure 5**).

Female Gametophyte Characterization

Female gametophytes were cleared and analyzed as previously described by Brambilla et al. (2007). Inflorescences were prepared for observation using the following protocol: flowers were emasculated and the next day harvested. The emasculated pistils were left O/N at 4°C in a 1:9 acetic acid:ethanol solution. Samples were rehydrated by subsequent washes with ethanol 90 and 70% and then incubated O/N at 4°C in clearing solution (160 g chloral hydrate, 50 g glycerol, and H_2O to a final volume of 250 ml). Pistils at different developing states were separated from the other floral organs and opened to evaluate the female gametophyte morphology. For these experiments, a Zeiss Axiophot® microscope equipped with differential interference contrast (DIC) optics was used.

In Vitro Pollen Germination

For this experiment, the protocol published by Bou Daher et al. (2009) was followed applying minor modifications.

Pollen grains were plated on small glass plates, containing 2.5 ml of pollen germination medium [PGM:18% sucrose, 0.01% boric acid, 1 mM $CaCl_2$, 1 mM $Ca(NO_3)_2$, 1 mM $MgSO_4$, 0.5% agarose pH = 7]. The plates were incubated overnight at 22°C, with wet paper to maintain humidity. The next day, pollen germination and growth were evaluated with a Zeiss Axiophot® microscope.

Aniline Blue Staining

Flowers were emasculated and, after 24 h, pollinated. The pollinated ovaries were collected at two different time points:

5 and 24 h after pollination. Samples were overnight fixed and stained in absolute ethanol/glacial acetic acid 9:1, as previously described by Mori et al. (2006). Subsequently, they were transferred into a 8M NaOH solution for 1 h at 50°C. Finally, the carpels were washed twice with ddH_2O for 10 min. The staining was performed with a modified aniline blue solution (aniline blue 2%, glycerol 1 M ddH_2O) (Takeuchi and Higashiyama, 2016). Samples were stored at 4°C for 3 h or overnight. The observation was done under UV light (350–400 nm) with a Zeiss Axiophot® microscope.

Pollen DAPI Staining

Pollen was stained according to Park et al. (1998). Mature pollen was obtained by placing 3–4 open flowers in a microcentrifuge tube containing 300 µl of 4′,6-diamidino-2-phenylindole (DAPI) staining solution (0.1 M sodium phosphate (pH 7), 1 mM EDTA, 0.1% Triton X-100, 0.4 µg/ml DAPI high grade, Sigma). After brief vortexing and centrifugation, the pollen pellet was transferred to a microscope slide and observed with a Zeiss Axiophot® microscope. Pollen at earlier stages of maturation was also analyzed by dissecting single anthers. Anthers were disrupted on microscope slides and squashed in DAPI staining solution (1 µg/ml) under a coverslip.

GUS Staining

β-Glucuronidase (GUS) assays were performed as described by Resentini et al. (2017). Pistils at different developmental stages were dissected and fixed in acetone 90% and incubated O/N at 37°C. After staining, they were cleared using the protocol described above.

Alexander Staining for Pollen Grains

Staining of pollen grains was performed as described by Peterson et al. (2010). After fixation (performed with 6 alcohol:3 chloroform:1 acetic acid), the anthers were placed on a microscope slide with a few drops of staining solution (10 ml 95% alcohol, 1 ml malachite green (1% solution in 95% alcohol), 50 ml distilled water, 25 ml glycerol, 5 ml acid fuchsin (1% solution in water), 0.5 ml orange G (1% solution in water), 4 ml glacial acetic acid, and distilled water (4.5 ml) to a total of 100 ml). Samples were analyzed with a Zeiss Axiophot® microscope.

CLSM Analysis

For confocal imaging, the Laser Scanning Confocal Microscope Nikon A1 was used. Inflorescences were fixed as described by Braselton et al. (1996). Samples were then excited using a laser (532 nm), and emission was detected between 570 and 740 nm.

RESULTS

RNAi Mediated Silencing of *REM34, REM35, and REM36*

Since *REM34, REM35,* and *REM36* are very similar and in linkage, an RNA interference approach was adopted to investigate their role during reproductive development in Arabidopsis.

Due to sequence divergency, even in the B3 DNA binding domain (Romanel et al., 2009), it was impossible to design a single artificial small interfering RNA fragment that was able to silence the three *REM* genes simultaneously. Therefore, a multiple RNA interference (RNAi) technology was used to express a single chimeric double stranded RNA that targeted the three REM genes under the control of CaMV35S (Miki et al., 2005; Bucher et al., 2006) (**Figure 1A**).

We selected three regions specific for the coding sequence of *REM34*, *REM35*, and *REM36*. The regions selected for *REM34* and *REM36* are highly specific for the genes of interest and were expected not to have any off target in the Arabidopsis genome. The RNAi fragment that targets *REM35* has a partial complementarity with *REM36*, and, at a lower level, with *REM37*, whose expression is almost undetectable in most Arabidopsis tissues (Mantegazza et al., 2014; Klepikova et al., 2016).

Forty *REM_RNAi* T1 transgenic *Arabidopsis* lines were obtained. We evaluated the down-regulation of the *REM* genes in nine different T1 lines (**Figure 1B**), which all showed defects in silique and gametophyte development.

Silencing of the three target genes was confirmed in the T2 generation by qRT-PCRs (**Supplementary Figure 1**). Furthermore, we showed that the RNAi construct was specific for their targets by testing the expression of *REM37* and *REM39*. The latter was chosen due to the fact that *REM39* is highly expressed in the tissues where *REM34, REM35*, and *REM36* are also active (Mantegazza et al., 2014; **Supplementary Figure 1**).

REM_RNAi Lines Have a Reduced Ovule Number and Seed Set Compared to Wild-Type Plants

We selected three *REM_RNAi* lines (#1, #4, and #5), with different levels of silencing of *REM36,* for further investigations in the

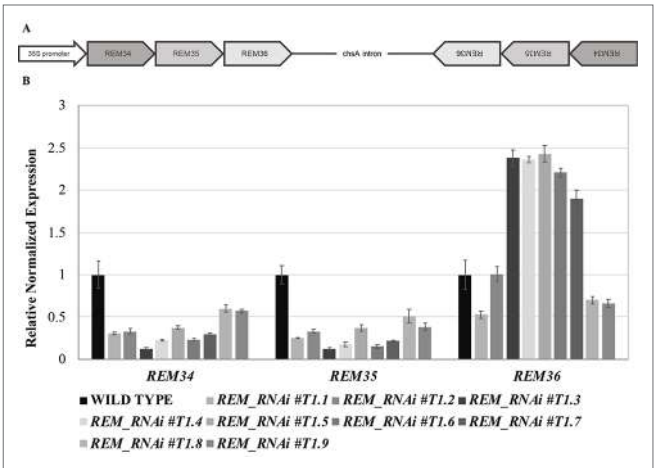

FIGURE 1 | Multiple RNA interference lines. **(A)** Schematic representation of the RNAi construct. The REM34-REM35-REM36 sense and antisense fragments are separated by the chsA intron, to allow the hairpin structure formation. **(B)** qRT-PCR on nine different *REM_RNAi* T1 inflorescences, showing a strong downregulation of *REM34* and *REM35* and different levels of *REM36* expression.

T2 generation. In line #1, *REM36* showed a downregulation of around 50%, while in lines #4 and #5, *REM36* was found to be slightly upregulated compared to the wild-type (**Figure 1B**).

In the T2 generation, silique length and seed number were evaluated for the three selected lines. The *REM_RNAi #T2.1* line showed a decrease of 35.3% in the silique length and a 19.4% reduction in total ovule number (**Figures 2A–C**). Furthermore, on average 66% of the ovules failed to be fertilized (**Figures 2C, D**). The other two *REM_RNAi* lines, *#T2*.4 and *#T2*.5, showed a similar phenotype even if the percentage of unfertilized ovules was lower, 35.3 and 45.4%, respectively (**Figure 2C**).

The *REM_RNAi #1* line was selected to further investigate the sterility phenotype caused by the downregulation of *REM34, REM35,* and *REM36.* This line was propagated to the T3 generation, where plants homozygous for the *REM_RNAi* construct were selected. Even if the RNAi construct has a dominant effect, we evaluated whether the sterility observed in the *REM_RNAi T2* segregating lines was exacerbated in plants homozygous for the construct. For this purpose, the seed set of the *REM_RNAi T3.1* homozygous line was evaluated.

Interestingly, comparing both the *REM_RNAi #T2.1* and the *REM_RNAi #T3.1*, we noticed that the percentage of ovule abortion was the same, suggesting that the silencing of REMs is probably acting both at the sporophytic and gametophytic levels.

Since the two lines in which *REM36* was not downregulated displayed a milder phenotype compared to the *REM_RNAi #T2.1 and REM_RNAi #T3.1* lines, in which all three genes were downregulated, it is possible that *REM36* is partially redundant to *REM34* and *REM35* during gametophyte development. On the contrary, the ovule number was the same in all three *REM_RNAi* lines (**Figures 2A**, **C**), indicating that *REM36* is not involved in the determination of the ovule primordia number.

To further confirm that no phenotypical differences were detectable between plants homozygous and heterozygous for the T-DNA insertion, we analyzed the silique content of 10 *REM_RNAi #T2.4* and 10 *REM_RNAi #T2.5* T2 plants in which the construct was still segregating, and we found no significant differences between all the herbicide resistant plants (**Supplementary Figures 2A, C**). For both *REM_RNAi #T2.4* and *#T2.5* lines, a relative evaluation of T-DNA copies in each of the nine plants considered was performed. The RT-PCR analyses showed a various amount of T-DNA amplicons which is clearly unrelated to the ovule abortions and the overall seed set observed in all the *REM_RNAi #T2.4* and *#T2.5* analyzed individuals (**Supplementary Figure 2**). The *ACTIN7* amplicon was used as normalizer and the herbicide resistance BAR gene used to estimate the abundancy of T-DNA copies.

These analyses allowed excluding the possibility that the reduced seed set was linked to the presence of a heterozygous T-DNA insertion (Curtis et al., 2009; Clark and Krysan, 2010) and suggests that either the sporphytic silencing of *REM34*, *REM35,* and *REM36* affects the gametophyte or that the mobile siRNA diffuses from the sporophyte to the gametes (Mlotshwa et al., 2002; Melnyk et al., 2011; Skopelitis et al., 2018).

To understand if the reduced seed set was due to problems in the female or the male gametophyte, we performed reciprocal crosses between *REM_RNAi #T3.1* and wild-type plants. As a control, both *REM_RNAi #T3.1* (homozygous for the T-DNA triggering the RNAi silencing) and wild-type plants were manually selfed, in order to evaluate if the manipulation of the flower was affecting the fertility of the analyzed plants (**Figure 2E**).

When *REM_RNAi #T3.1* pistils were pollinated with *REM_RNAi #T3.1* pollen, 73.3% of the ovules failed to be fertilized while wild-type lines manually pollinated with wild-type pollen resulted in 19.5% unfertilized ovules. When the *REM_RNAi #T3.1* line pistils were pollinated with wild-type pollen, the percentage of unfertilized ovules was 78.6%, indicating a strong contribution of the female reproductive organ defects to this phenotype. Interestingly, when wild-type pistils were pollinated with *REM_RNAi #T3.1* pollen, still 61.0% of the ovules were not fertilized (**Figure 2E**). Moreover, we observed a high variability in the number of unfertilized ovules using *REM_RNAi* pollen as shown in **Figure 2E**. Macroscopical inspection revealed a decrease in pollen grain number compared to wild-type anthers and a lack of adherence of the pollen to the wild-type stigma, both observations were further investigated (see below). All these considerations strongly suggest that both female and male reproductive organs are affected in the *REM_RNAi* lines.

REM34, REM35, and *REM36* Are Expressed in Both Female and Male Reproductive Organs in Adjacent Sporophytic and Gametophytic Cells

Previously, the expression pattern of the *REM* genes was characterized in the shoot apex by *in situ* hybridization analysis, showing that *REM34, REM35,* and *REM36* are expressed from the earliest stages of reproductive development of *Arabidopsis* in the inflorescence meristem and flower meristem and during the first stages of flower development with the exception of sepals (Franco-Zorrilla et al., 2002; Mantegazza et al., 2014).

In order to analyze the expression profiles in more detail during male and female sporophytic/gametophytic developments, we performed *in situ* hybridization analysis for *REM34, REM35,* and *REM36* in both female and male reproductive organs. The flower stages are described accordingly to Smyth et al. (1990) and Schneitz et al. (1995).

In Arabidopsis, pollen mother cells differentiate inside the young anther, ovule primordia arise from the placenta in stage 8 of flower development, and differentiation is completed at stage 13.

At stage 8/9 of flower development (Smyth et al., 1990), hybridization signals were detected for all three genes, in the anthers where the pollen mother cells differentiate and within the carpels, although in this case, the signal was stronger in the placenta and ovule primordia (**Figure 3A**).

At stage 10, a strong signal was always detected in developing ovules and pollen (**Figure 3B**). Our analysis revealed that the timing of expression of the three REM genes coincided with male and female sporogenesis.

During subsequent stages of flower development, stages 11–12, both female and male initiate gametophyte development. During these stages, a decrease in the signal was clearly observed

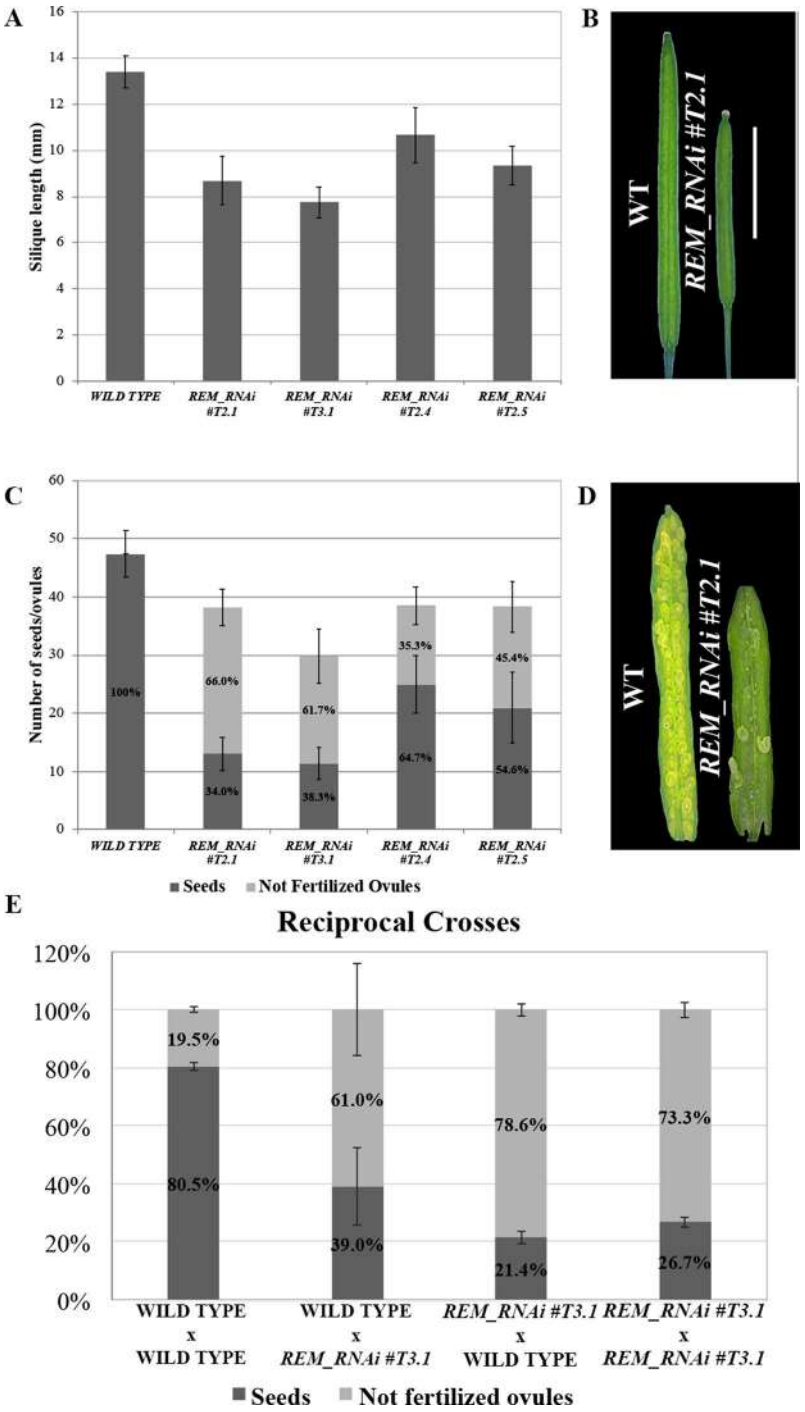

FIGURE 2 | *REM_RNAi* lines have shorter siliques and a reduced seed set compared to the wild-type. **(A)** Graph showing the mean length of 10 wild-type and 10 *REM_RNAi #T2.1, #T3.1, #T2.4,* and *#T2.5* siliques. A wild-type silique measures on average 13.4 mm, the siliques from the different *REM_RNAi* lines were found to measure on average between 7.8 and 10.7 mm. ($p < 0.01$ for all comparison with the wild-type, ANOVA and *post hoc* Tukey HSD test were used). **(B)** Example of wild-type and *REM_RNAi #T2.1* siliques (bar = 5 mm). **(C)** Graph showing the mean number of ovules/silique in the wild-type and *REM_RNAi #T2.1, #T3.1, #T2.4,* and *#T2.5* plants, divided in seeds and not fertilized ovules. Compared to the wild-type situation, in which each silique contains on average 47.4 ovules, the *REM_RNAi* siliques have on average 29.8 to 38.5 ovules ($p < 0.01$ for all comparison with the wild-type, ANOVA and *post hoc* Tukey HSD test were used). On average between 35.3 and 66.0% of ovules, depending from the analyzed line, failed to be fertilized, while no aborted ovules were detected in the wild type situation ($p < 0.01$ for all comparison with the wild type, ANOVA and *post hoc* Tukey HSD test were used). **(D)** Example of wild-type and *REM_RNAi #T2.1* seed sets (bar = 5 mm). **(E)** Reciprocal crosses analysis between wild-type and *REM_RNAi #T3.1* plants. As a control, both wild-type x wild-type and *REM_RNAi #T3.1* x *REM_RNAi #T3.1* crosses were performed. Crosses are indicated female x male. ($p < 0.01$ for all comparison with the wild type of the non-fertilized ovules number, ANOVA and post hoc Tukey HSD test were used).

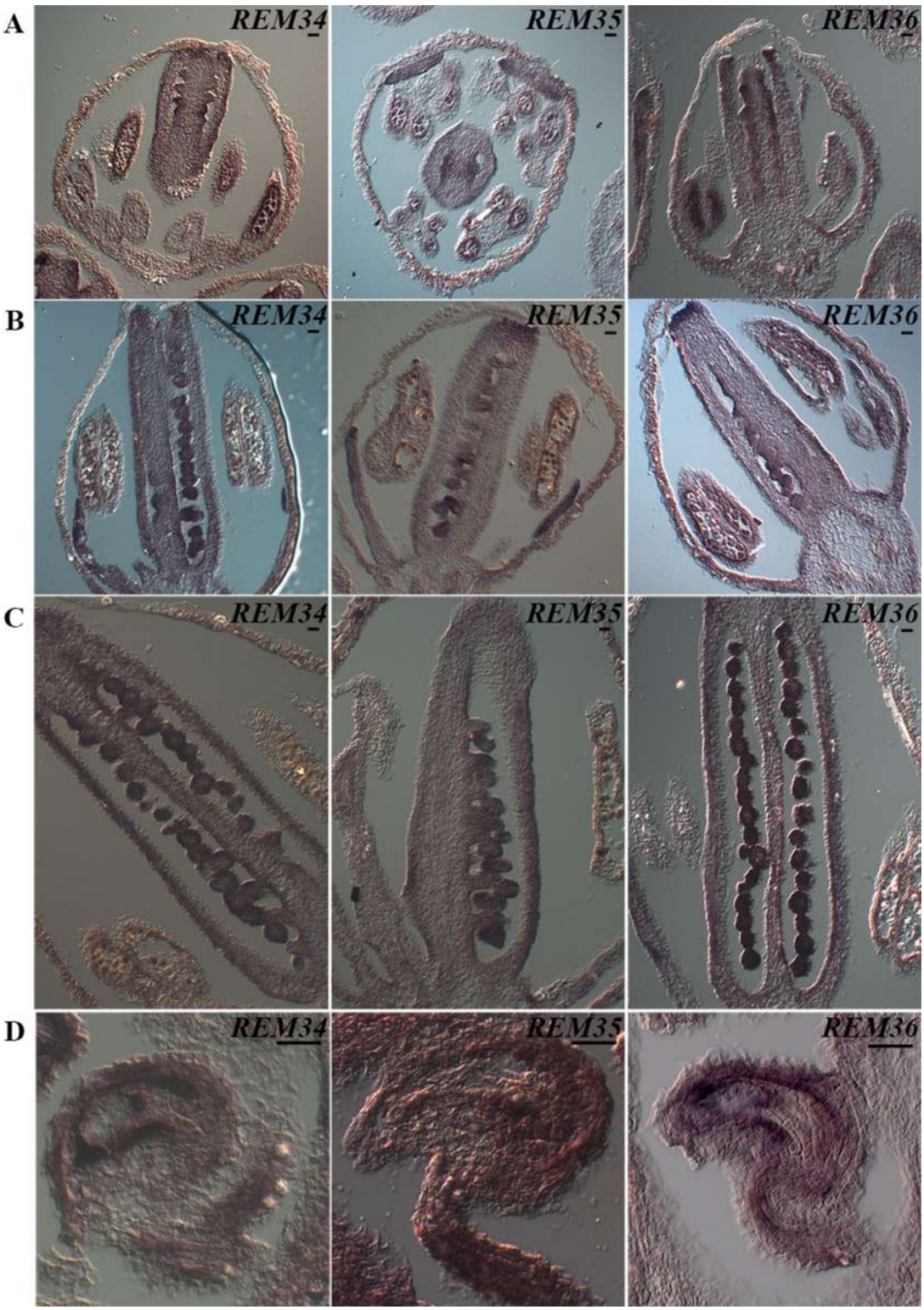

FIGURE 3 | *REM34*, *REM35,* and *REM36* expression patterns. **(A)** In flowers at ST8-9, the signal in the carpel is restricted in the tissue of the placenta and ovules primordia. At the same stage, a clear signal is also visible in the anthers. **(B)** At ST10-11, the signal is present in the ovules, which are completing megagametogenesis, and in the anthers, where the pollen grains are undergoing the first mitotic division. **(C)** At ST12, when pollen reaches maturity, the signal is no longer visible in the anthers. **(D)** In flowers at anthesis, the target genes are expressed in the mature female gametophytes, in particular in the funiculus, inner integuments, and central cell. Flower stages are described accordingly to Smyth et al., 1990 (bar = 20 μm).

in anthers (**Figure 3C**); during these stages, pollen reaches maturity, and the vegetative and generative cells are differentiated after mitosis (Park et al., 1998). In contrast, a strong signal was detected during ovule development when the surviving megaspore undergoes three rounds of mitosis and passes from stages 3I to 3V (Schneitz et al., 1995). Interestingly, when the ovule is at its very last stage of development 3-VI (Schneitz et al., 1995), a strong signal was detected in the funiculus, in the innermost integument and, inside the mature female gametophyte, in the central cell region (**Figure 3D**).

The expression analysis of *REM34, REM35,* and *REM36* highlighted the fact that, also during anther/pollen and carpel/ovule development, these three *REMs* have a similar pattern of expression.

The analysis of the expression patterns of *REM34, REM35*, and *REM36* combined with the phenotypes observed in the *REM_RNAi* lines denote an important role for these genes during the development and production of viable male and female structures and gametes.

In *REM-RNAi* Lines the Female Gametophyte Is Unable to Complete Its Development

The expression profile of *REM34, REM35,* and *REM36* suggests that these genes play a role during ovule development. Furthermore, the reciprocal crosses showed that between 73.3 and 78.6% of the ovules in the *REM_RNAi #T3.1*, which is homozygous for the RNAi cassette, were not fertilized (**Figure 2E**).

Based on this evidence, we hypothesized that the ovule defects in the *REM_RNAi* lines might be due to an arrest in their development. Therefore, a detailed evaluation of female gametophyte development was carried out in the *REM_RNAi #T3.1* homozygous line. In this line, 42.9% (227/529) of the ovules failed to complete their development and showed an arrest in the FG1 stage (**Figure 4A**). These ovules were characterized by an embryo sac containing one large cell, the functional megaspore, with a single nucleus; the rest of the ovules completed their development reaching the FG7 stage (**Figures 4B**, **C**). The same phenotype was observed in the *RNAi #T2.4* and *#T2.5* lines which both derived from hemizygous mothers (**Supplementary Figure 3**).

To confirm that, in the *REM_RNAi* lines, the defective female gametophytes were arrested in the FG1 stage, after meiosis, we crossed the *pSUF4:SUF4-GUS* marker line with the *REM_RNAi #T3.1* line. In the *pSUF4:SUF4-GUS* marker line, GUS expression is not detectable during megasporogenesis, but it becomes visible after meiosis, once the functional megaspore is formed, and marks all the nuclei of the embryo sac (Resentini et al., 2017). Observing *REM_RNAi #T3.1* pistils, both wild-type like ovules, with more than one nucleus and ovules arrested in the FG1 stage, with the nucleus of the functional megaspore, expressed the *GUS* reporter (**Figure 4D**) suggesting that the defect in female gametophyte development was post-meiotic.

To investigate in detail the arrest at the FG1 stage, we carried out confocal laser scanning microscopy (CLSM) on *REM_RNAi #T3.1* developing ovules. The feulgen staining perfectly marked the cell wall of the ovule integuments and the embryo sac dividing nuclei, allowing the recognition of the gametophytic developmental stages. In the same *REM_RNAi #T3.1* pistil, we observed ovules that normally developed until stage FG4 (**Figure 4E**) and those that were arrested in FG1 in which the embryo sac contains the functional megaspore and the three degenerating spores on top of it (**Figure 4F**).

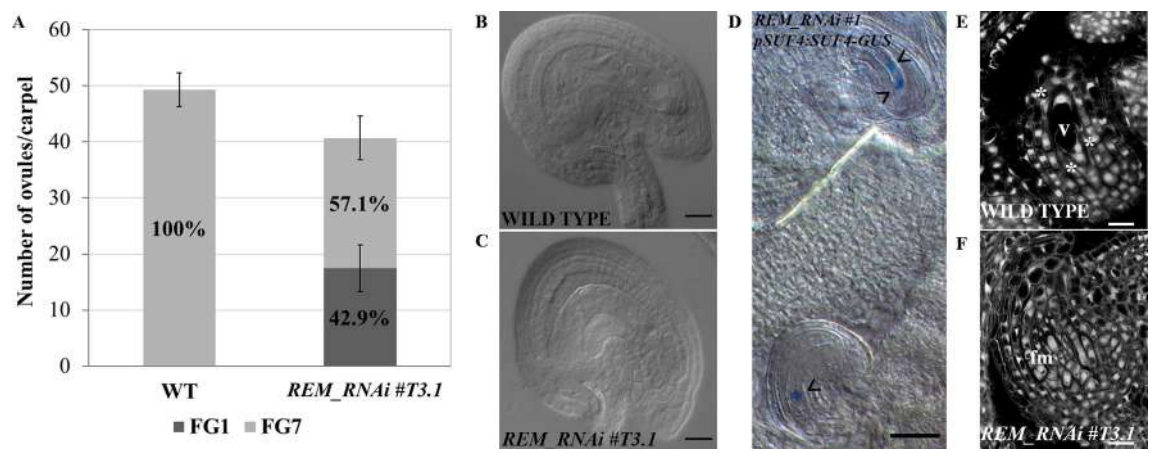

FIGURE 4 | *REM_RNAi #T3.1* female gametophyte characterization. **(A)** Analysis of cleared mature carpels of both wild-type (n = 11) and *REM_RNAi #T3.1* (n = 13). In wild-type mature carpels, all the ovules reach the FG7 stage (542/542 ovules), while in the *REM_RNAi* line, 227/529 ovules are arrested at the FG1 stage. **(B)**, **(C)** Cleared ovules collected from both wild-type **(B)** and *REM_RNAi #T3.1* **(C)** mature carpels. In the wild-type situation, 100% of the embryo sac reaches the FG7 stage, while in the RNAi line, almost 60% of embryo sacs show an arrest in the FG1 stage (bar = 20 µm). **(D)** *pSUF4:SUF4-GUS* in the *REM_RNAi* line. In the uppermost ovule, two nuclei are stained, indicating the progression of gametogenesis till FG4 stage. In the lowest ovule 1, nucleus is stained indicating an arrest in FG1 stage. The arrowheads marked nuclei (bar = 50 µm). **(E–F)** CLSM analysis of *REM_RNAi #T3.1* ovules. In the same carpel, it was possible to observe ovules progressing in their development **(E)** and ovules arrested at the FG1 stage **(F)**; asterisks indicate three out of the four nuclei. v, vacuole; fm, functional megaspore (bar = 10 µm).

The *REM-RNAi* Lines Showed a Post-Meiotic Defect of the Male Gametophyte

From the analysis of wild-type carpels pollinated with *REM_RNAi* pollen, we observed that 61.1% of the ovules were not fertilized, suggesting that the male gametophyte in these lines is also defective (**Figure 2E**). To understand the cause of this defect, we first carried out an *in vitro* pollen germination assay which showed a 30% decrease in the germination rate of the *REM_RNAi #T3.1* pollen compared to the wild type (**Figures 5A**, **B** and **Supplementary Figure 4**).

The growth rate of *REM_RNAi* pollen tubes and their ability to correctly target ovules were also evaluated *in vivo* by means of aniline blue staining (**Supplementary Figure 4**). The *REM_RNAi* pollen tubes did not show any growth defect, they reached the end of the pistil in the same time as the wild-type pollen tubes, and the mature ovules were correctly targeted (**Supplementary Figure 4**). We noticed that, as mentioned before, the *REM_RNAi* pollen number appeared to be lower, and it did not adhere well to the stigma papillae, which could explain the high variability observed in the backcrosses between wild-type pistils and *REM_RNAi* pollen (**Figure 2E**).

To try to understand the cause of the male sterility phenotype, pollen grains were collected from mature anthers and treated with Alexander's stain, which colors viable pollen red. While in the wild type, all the collected pollen was viable; in the *REM_RNAi #T3.1* anthers, 33.9% of the grains were not stained, indicating that those pollen grains were non-viable and did not appear to contain any cytoplasm (**Figures 5C–E**). Interestingly, the percentage of non-viable pollen grains in the *REM_RNAi* line corresponds to the decreased germination capability observed *in vitro,* suggesting that the grains which are unable to produce the pollen tube are the degenerated ones.

To investigate the pollen defect in more detail, confocal laser scanning microscopy (CLSM) was used. In **Figure 5F**, wild-type pollen from a mature anther is shown; intine and exine layers were very well distinguishable and inside the pollen grain, and the sperm cells and the vegetative cell nuclei were stained. On the contrary, in the *REM_RNAi #T3.1* mature anthers, a high percentage of pollen grains appeared shrunken and empty; neither sperm nor vegetative cells were identified, although the intine and exine layers looked intact (**Figure 5G**).

To understand when the pollen grains degenerated, we visualized their nuclei with DAPI staining at different developmental stages (**Figures 6A–F** and **Supplementary Figure 3**). At the microspore stage, all *REM_RNAi #T3.1* grains were characterized by the presence of a single bright nucleus localized at the center of the cell, indicating that the pollen, like wild-type, passed through meiosis correctly (**Figures 6A**, **D**). After meiosis, in wild-type, the microspores underwent a first mitotic division that produced one vegetative and one sperm nuclei (**Figure 6B**). Subsequently, the second round of mitosis led to the formation of the mature pollen grain, which contained two small sperm cells each with a bright and elongated nucleus and the vegetative cell (**Figure 6C**). Interestingly, in *REM_RNAi #T3.1* anthers, some grains were characterized by the lack of nuclei; this phenotype was detectable also at the tricellular stage (**Figures 6E**, **F** and **Supplementary Figure 3**).

Thus, after meiosis, *REM_RNAi* anthers displayed both viable pollen grains, with two sperm cell nuclei and a distinct vegetative nucleus, and not viable pollen grains, in which no DNA is detectable (**Figures 6E**, **F**). This is similar to what was observed with the CLSM analysis.

All this evidence suggests that the degeneration of pollen grains observed in the *REM_RNAi* lines could be due to a post-meiotic block in their development, a similar defect as the one observed in the female gametophytes.

REM35 Formed Homodimers and Heterodimers With REM34

REM transcription factors can form functional heterodimers (Mendes et al., 2016). To understand if also REM34, REM35, and REM36 could function *via* dimer formation, yeast two-hybrid assays were performed. This approach revealed that REM35 is able to interact strongly with itself and also with REM34, while no interactions were detected with REM36 (**Figure 7A** and **Supplementary Figure 5**).

All the interactions observed in the yeast two-hybrid assays were confirmed *in vivo* with a Bimolecular Fluorescence Complementation (BiFC) assay in *Nicotiana benthamiana* leaves (**Figures 7B**, **C** and **Supplementary Figure 5**). This finding suggests that REM34 and REM35 could act as heterodimers.

Downregulation of *REM34, REM35,* and *REM36* Altered Expression of Genes Involved in Post-Meiotic Divisions

As described above, the downregulation of *REM34, REM35,* and partially *REM36* resulted in a post-meiotic arrest in both female and male gametophytes, suggesting that these transcription factors could be involved in regulating mitosis progression during gametogenesis.

To elucidate the molecular mechanism causing this block, we measured the expression levels of genes that control gametogenesis by q-RTPCR. We focused on genes that, when mutated or overexpressed, cause similar defects to those observed in the *REM_RNAi* gametophytes. Those genes were divided into three categories based on the biological process in which they are involved in: ribosome biogenesis (*MDS, NLE*), cell cycle control (*RBR, KRP6*), and chromatin regulation (*HAM1, HAM2*).

MDS, which, together with *NLE,* is involved in the biogenesis of the 60S ribosomal subunit and is essential during megagametogenesis (Chantha et al., 2010), was downregulated in the *REM_RNAi #T3.1* lines. *KRP6*, a CDK inhibitor whose overexpression causes a block in mitosis progression during female and male gametophytic development, was also downregulated in the *REM_RNAi* lines.

Among the genes involved in chromatin modifications, two histone acetyltransferases (HATs), *HAM1* and *HAM2,* were selected. Only *HAM2* was downregulated in the *REM_RNAi #T3.1* line (**Figure 8**).

These results suggest an intricate interconnection among regulators and effectors, which end up in a correct gametogenesis program.

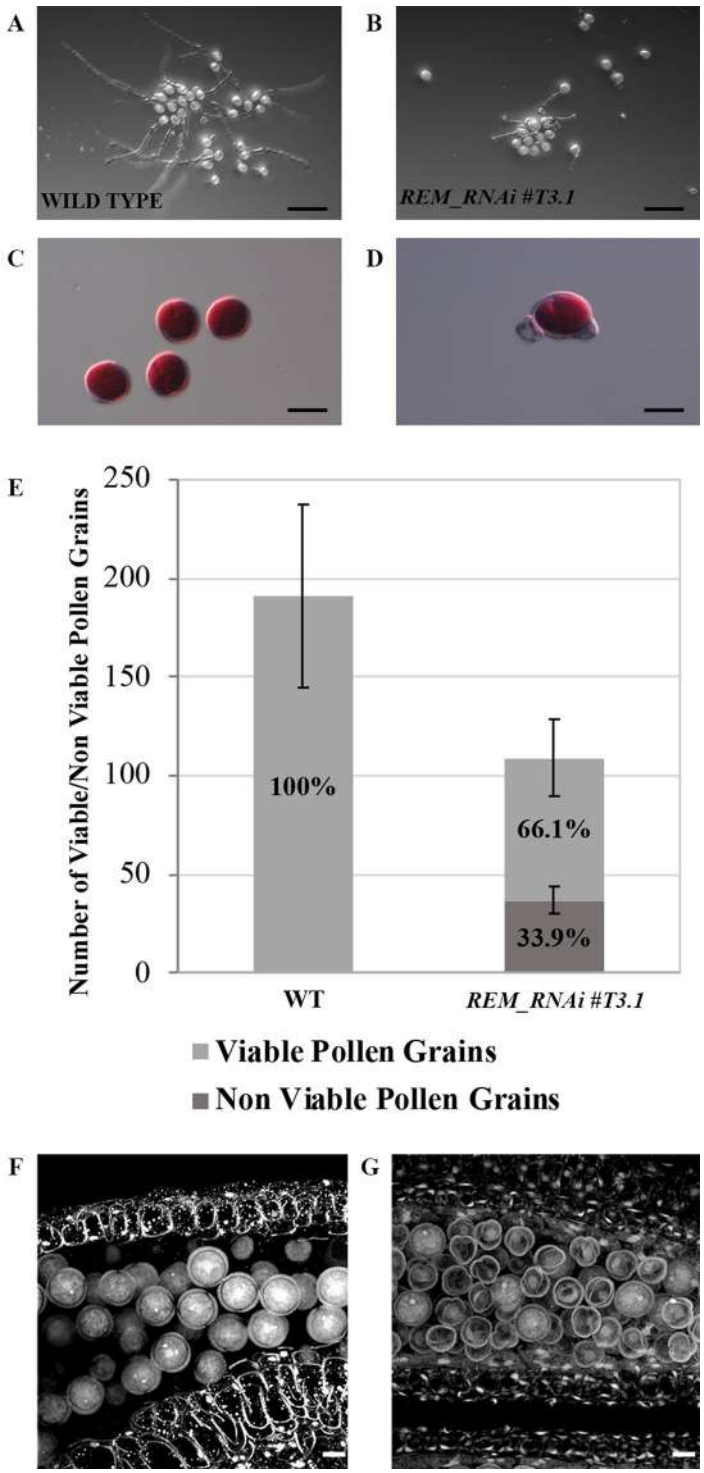

FIGURE 5 | *REM_RNAi #T3.1* male gametophyte characterization. **(A**–**B)** *In vitro* germination test of wild-type **(A)** and *REM_RNAi #T3.1* **(B)** pollen grains, plates were imaged 24 h after plating (bar = 100 μm). **(C**–**D)** Pollen grains, collected from mature anthers of both wild-type **(C)** and *REM_RNAi #T3.*1 anthers **(D)**, were stained with Alexander's staining to check pollen grain viability. While all the wild type grains were viable, some *REM_RNAi#T3.*1 pollen grains appeared shrunken and unable to be stained in red (bar = 20 μm). **(E)** Mature anthers from wild-type and *REM_RNAi#T3.1* flowers were dissected, the released pollen was collected and treated with Alexander's staining to discriminate between viable and non-viable pollen grains. In the wild type, 100% of the pollen grains resulted vital while 33.9% of *REM_RNAi#T3.*1 pollen was found to be non-vital. (wt n = 1,337, *REM_RNAi#T3.*1 = *874;* $p < 0.01$ for all comparison with the wild-type, ANOVA and *post hoc* Tukey HSD test were used). **(F**–**G)** CLSM analysis of wild-type **(F)** and *REM_RNAi#T3.*1 **(G)** mature anthers. All the wild-type grains are round and contain the vegetative nucleus and the two sperm cell nuclei; in the *REM_RNAi#T3.1* anthers, it is possible to visualize both pollen grains at two nuclei stage, as well as degenerate pollen grains, without any visible nucleus (bar = 10 μm).

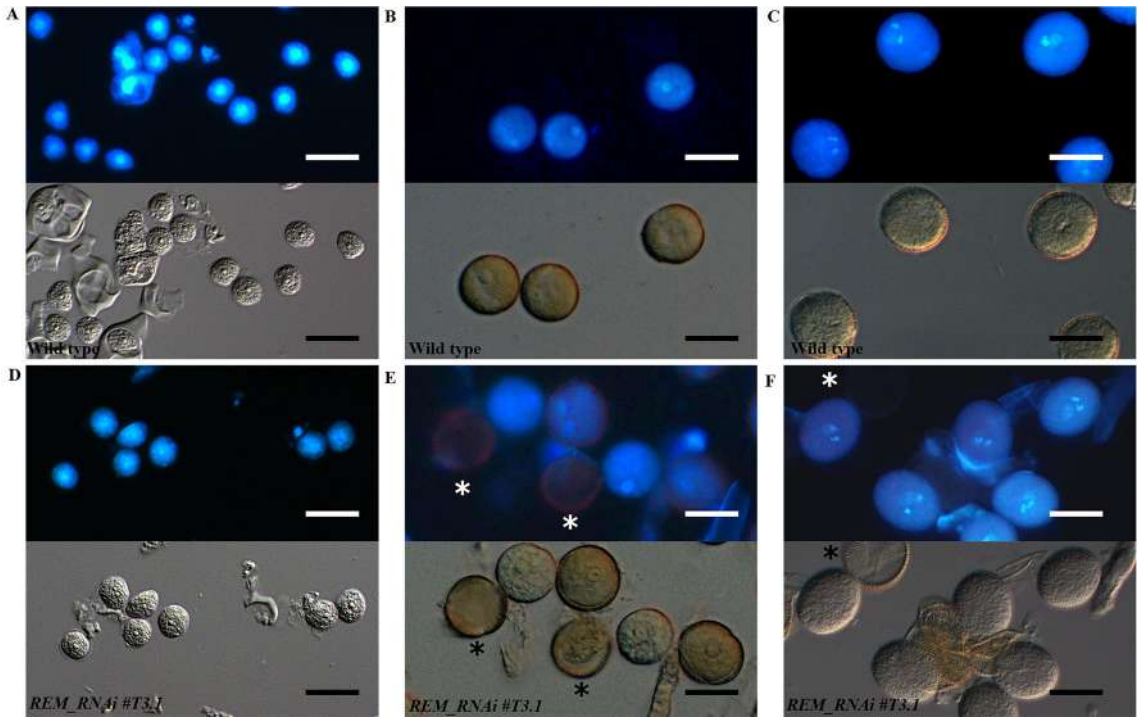

FIGURE 6 | Wild type and *REM_RNAi* pollen development. DAPI staining of wild-type and *REM_RNAi#T3.*1 pollen grains at different developmental stages. At the microspore stage **(A** and **D)**, all the grains contain a well-defined central nucleus. At the bicellular stage in all wild-type grains **(B)**, the spermatic and vegetative nuclei are distinguishable, while in the *REM_RNAi#T3.*1 lines **(E)**, some grains, marked with an asterisk, do not display any nucleus. Wild-type mature pollen grains **(C)**, characterized by the presence of two sperm cells and one vegetative nucleus. *REM_RNAi#T3.*1 mature pollen **(F)**, the asterisk marks a mutant pollen grain without nucleus (bar = 10 μm).

Overexpression of the REM34_EAR Chimeric Protein

The genes that were downregulated in the *REM_RNAi* lines might be targets of the REM transcription factors. This suggests that REM34 and REM35 might be transcriptional activators. To investigate whether REM transcription factors work as activators of transcription, we fused REM34 with the dominant EAR repressor domain (known as chimeric repressor silencing technology CRES-T) and transformed wild-type *Arabidopsis* plants with this construct. Five transgenic lines that overexpressed the *REM34_EAR* chimeric gene at different levels in the T1 generation were obtained (**Figure 9A**).

In the T2 generation, silique length and ovule number were measured in two independent lines (*REM34_EAR#*T2.1 and *REM34_EAR#*T2.7). In both the selected T2 *REM34_EAR* lines, we observed a decrease in the silique length of 23.1 and 25.0%, respectively, and the presence of 55.0 and 42.6% aborted ovules, similar to what was observed in the *REM_RNAi* lines (**Figures 9B–E**).

The phenotype of the aborted ovules was further evaluated in cleared mature carpels of the *REM34_EAR #T2.1* and *#T2.7* lines. We detected both ovules at FG7 stage, with the seven cells clearly distinguishable, and ovules at FG1 stage, characterized by a single cell embryo sac (**Figure 9F**).

To confirm also the post meiotic block in the male gametophyte, mature pollen of both *REM34_EAR #T2.1* and *#T2.7* lines were stained with DAPI. Similarly to what was observed in the *REM_RNAi* lines, some pollen grains were able to reach the tricellular stage while others appeared shrunken and degenerated, with no visible nuclei (**Figure 9G**).

The strong similarity between the *REM34_EAR* and the *REM_RNAi* phenotypes might suggest that the overexpression of the chimeric REM34_EAR protein was causing co-suppression of other *REM* genes. To exclude this possibility, we investigated the expression level of *REM35, REM36, REM37,* and *REM39* in the *REM34_EAR #T2.1* and *#T2.7* lines. The level of expression of the endogenous *REM34* was not taken into account, as the perturbation of *REM34* expression alone did not cause any evident phenotypical defects (**Supplementary Figure 6**) (Franco-Zorrilla et al., 2002; Mantegazza et al., 2014). The obtained results showed that the closely related *REMs* were not affected suggesting that the expression of the REM34_EAR chimeric protein caused the observed phenotypes.

DISCUSSION

Functional Analysis of *REM* Genes

The plant-specific REM family in Arabidopsis is composed of 45 genes, generated through multiple duplication events, which are mostly expressed during flower and ovule development (Romanel et al., 2009). Even if the expression pattern of these genes suggests that they could play an important role in regulating

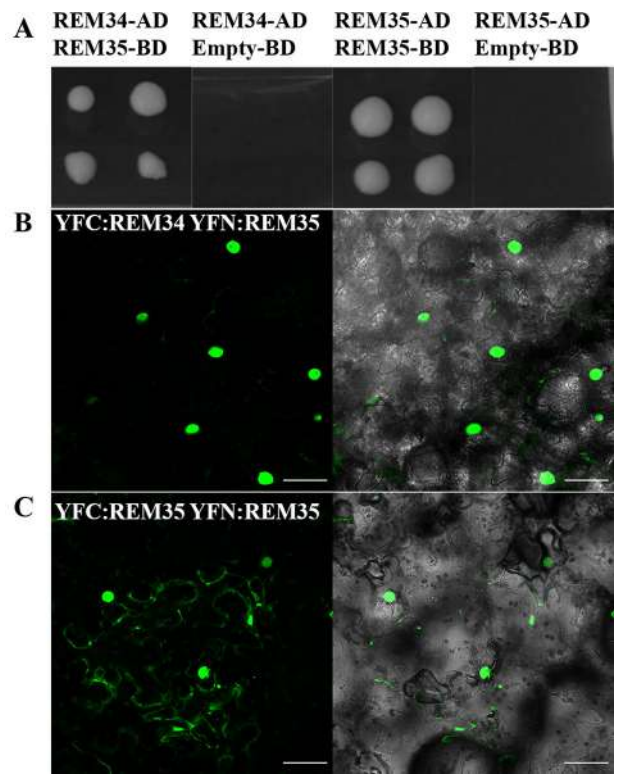

FIGURE 7 | REM34 and REM35 interaction. **(A)** Yeast two hybrid assays showing the interactions between REM34 and REM35 and REM35 and REM35, on –L-W-H + 2.5 3-AT selective media. Empty pDEST32 vector was employed as a negative control. **(B–C)** BiFC experiments in tobacco leaf cells showing the reconstitute YFP fluorescence (green) between **(B)** REM34 and REM35 fusions to the C- and N-terminal fragments of YFP, respectively. **(C)** REM35 fusions to the C- and N-terminal fragments of YFP (bar = 50 μm).

developmental processes such as shoot architecture and flower development, until now, only a few of them have been associated to a function (Levy, 2002; Matias-Hernandez et al., 2010; Mendes et al., 2016). This might be due to their functional redundancy but also because they are often in linkage on the genome.

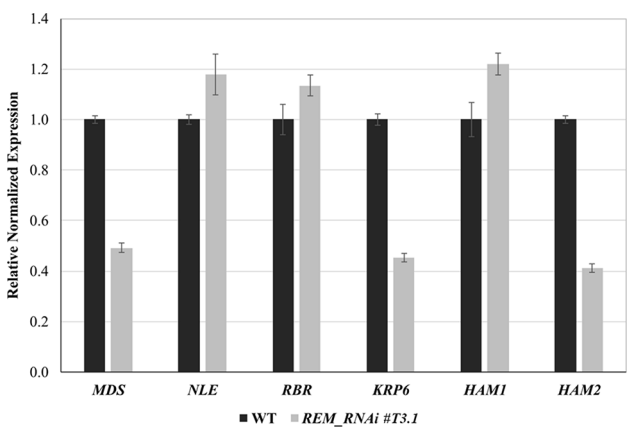

FIGURE 8 | Expression analysis of genes involved in gametophyte development by qRT-PCR. Selected gene expression in inflorescence of wild-type and *REM_RNAi #T3.1*. The expression of selected genes was normalized to that of UBI, and the expression level in Col was set to 1.

Here, we investigated the function of the linked duplicated *REM34, REM35,* and *REM36* genes by a multiple RNAi approach and showed that *REM34*, *REM35,* and partially *REM36,* are involved in male and female gametophytic developments during post-meiotic divisions. A similar multiple RNAi approach was previously employed to silence simultaneously up to six target genes in *Arabidopsis thaliana* (Czarnecki et al., 2016).

The *REM_RNAi* construct was found to be a very efficient tool: by selecting specific gene sequences, we were able to silence the three target genes with a single construct and a single transformation event. Importantly, the construct showed to be highly specific for the three genes of interest without any obvious off-target activity. Transgenic lines showing silencing of the *REM* genes under study were all characterized by a reduced seed set and an arrest in female gametophyte development at the earliest stages of gametogenesis. Since *REM34, REM35,* and *REM36* appeared to be mainly expressed in sporophytic tissues throughout Arabidopsis reproductive development, the CaMV35S promoter was chosen to drive the expression of the RNAi fragments. The activity of the CaMV35S promoter seems to be low during female and male gametophyte developments, but it has been shown that such promoter can be successfully employed to silence genes during gametophytic development (Acosta-García and Vielle-Calzada, 2004; Mendes et al., 2016). A valid hypothesis for the observed gametophyte phenotypes might be that it is caused indirectly by the silencing of *REM34, REM35,* and *REM36* in the female and male sporophytic cells. However, it is also important to consider that the RNAi construct is dominant and that it can trigger a non-cell autonomous and systemic silencing signal which might be maintained throughout the different phases of plant development (Mlotshwa et al., 2002; Melnyk et al., 2011; Skopelitis et al., 2018).

Since functional redundancy is a common phenomenon in plants (Briggs et al., 2006), this kind of RNAi approach will be helpful for the functional characterization of members of highly redundant families and especially that are in linkage. Furthermore, since silencing of genes by *RNAi* is often not complete, this approach could favor the analysis of genes for whom knock-out leads to lethality or complete sterility.

REM Protein Interactions

Protein interaction studies revealed that REM34 and REM35 were able to interact with each other; while no interaction was found with REM36, this supports the hypothesis that *REM36* might not be able to substitute completely *REM34* and *REM35* functions. Interactions between REM factors were found before. VDD and VAL, two functionally characterized REM factors involved in synergid degeneration upon fertilization (Mendes et al., 2016), also interact with each other. Furthermore, both *VAL* and *REM35* were also able to make homodimers. These characteristics might well be a common feature for the REM family and, in perspective of the guilt-by-association principle, it would be informative to analyze all possible REM protein interactions. The same approach was shown to be extremely useful for the characterization of MADS

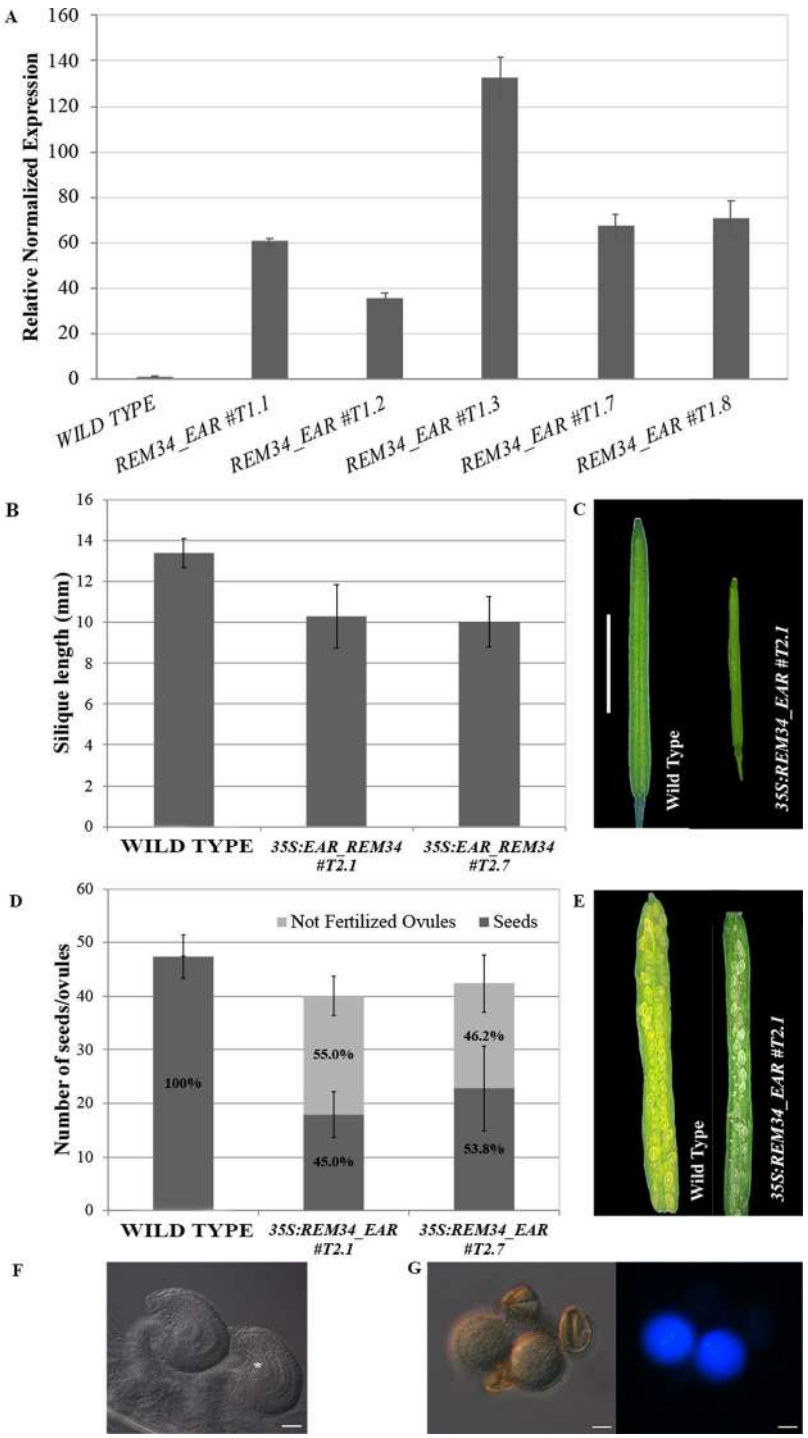

FIGURE 9 | Analysis of the *35S:REM34_EAR* lines. **(A)** qRT-PCR for the evaluation of the *REM34_EAR* overexpression in five T1 transgenic lines. **(B)** Graph showing the mean length of 10 *REM34_EAR #T2.1 #T2.7* siliques, compared to the wild-type, the two lines have a reduction in the silique length ($p < 0.01$ for all comparison with the wild type, ANOVA and *post hoc* Tukey HSD test were used). **(C)** Example of wild-type and *REM34_EAR #T2.1* siliques (bar = 5 mm). **(D)** Graph showing the mean number of ovules/silique in the wild-type and *REM34_EAR #T2.1 #T2.7* plants. Both lines were characterized by a reduction in the total seed set of around 10% compared to the wild-type ($p < 0.01$ for all comparison with the wild type, ANOVA and *post hoc* Tukey HSD test were used). On average between 55.0 and 46.2% of ovules, depending from the analyzed line, failed to be fertilized, while no aborted ovules were detected in the wild type situation ($p < 0.01$ for all comparison with the wild type, ANOVA and *post hoc* Tukey HSD test were used). **(E)** Example of wild-type and *REM34_EAR #T2.1* seed sets (bar = 5 mm). **(F)** Cleared ovules sampled from mature *REM34_EAR #T2.1* carpels, the asterisk marks the one blocked at the FG1 stage (bar = 20 μm). **(G)** DAPI stained pollen grains, sampled from mature *REM34_EAR #T2.1* anthers; some grains were able to reach the tricellular stage and showed fluorescent nuclei while others appeared degenerated and with no visible nucleus (bar = 20 μm).

domain transcription factor family, for which extensive protein–protein interaction studies effectively guided genetic studies and functional characterization of many of them (de Folter et al., 2005; Gregis et al., 2006; Fornara et al., 2008; Immink et al., 2009).

REM34 and *REM35* Control Female and Male Gametogenesis

We discovered that, in the *REM_RNAi* lines, both the male and female germ lines were able to go through meiosis correctly, but they were not able to pass the FG1 stage, suggesting a role for *REM34* and *REM35* in the control of gametogenesis in Arabidopsis.

Although the *REM* gene family was named after the specific meristematic expression of its first member *AtREM1,* which was named *REM34* (Franco-Zorrilla et al., 2002), our data showed that *REM34, REM35,* and *REM36* are also expressed during gametophytic development, and we discovered that they were expressed starting from both carpels and anther primordia specification throughout all the stages of anther and carpel developments. In the carpel, the signal is strongly localized in the placenta and ovule primordia and in the developing ovules.

Indeed, our deep morphological analysis of both female and male gametophytes of the *REM_RNAi* lines showed that from 35 to 65% of the female gametophytes were unable to undergo mitosis and were arrested at the FG1 stage when the MMC acquires functional megaspore identity.

REM36 seemed to be partially redundant with *REM34* and *REM35.* Indeed, in the two lines in which the level of *REM36* expression was higher compared to the wild-type, the penetrance of the embryo sac defect was less. However, in all *REM_RNAi* lines, we also observed a decrease of around 20% in the total ovules number irrespectively of the expression levels of *REM36.* Thus, *REM36* might be involved in embryo sac development together with *REM34* and *REM35* but is not controlling ovule primordia specification.

In these lines, also pollen development was affected showing the same post meiotic arrest of the embryo sac. Thus, in Arabidopsis, REM34, REM35, and partially REM36 transcription factors seem to be required post-meiotically for gametophytic development.

Further confirmation for their role during both female and male gametogenesis came from the analysis of different *35S:REM34_EAR* lines. These plants, in which *REM34* fused to the EAR repressor domain was overexpressed, showed the same postmeiotic arrest both in embryo sac and pollen development, suggesting that a complex formed by REM34 and REM35 could act as a positive transcriptional regulator of gametogenesis.

Because of the redundancy and position in linkage of the three genes of interest in the genome, most of this functional study was conducted using RNAi. This approach was found to be very effective in the silencing of *REM34, REM35,* and *REM36,* but the transgenic lines cannot be easily employed for genetic studies, due to the fact that it acts dominantly and because the level of silencing of the target genes can vary between different lines and throughout subsequent generations. Despite these difficulties, the analyses performed on both segregating and homozygous lines suggest that these three genes can influence gametogenesis acting mainly at the sporophytic level. This hypothesis is also supported by the expression pattern of these genes which, as shown by the *in situ* hybridization analysis, are present in the sporophytic tissues both in pistils and anthers when gametogenesis is taking place. The observation that *REM34, REM35,* and *REM36* appeared to be expressed throughout all stages of gametogenesis in the embryo sac leaves of course the possibility open that they directly play a function in the female gametophyte. The employment of an embryo sac specific promoter could be useful in order to validate this hypothesis and to be able to better distinguish between the sporophytic and gametophytic roles of *REM34, REM35,* and *REM36.*

To understand how the *REM* genes under study act, we tested whether the down-regulations of *REM34, REM35,* and *REM36* perturbed the expression of genes known to be involved in gametogenesis progression. These genes were classified accordingly to their biological function in three categories: cell cycle control, chromatin remodeling, and ribosome biogenesis. Interestingly, we observed that several genes involved in different biological pathways were downregulated in the *REM_RNAi* lines. This observation suggests that *REM34, REM35,* and, in some measures, *REM36* are involved in the control of a very early steps of gametogenesis. In particular, they regulate the expression of different targets both directly and indirectly along the genetic network that controls gametophytic development in *Arabidopsis*.

Among the downregulated genes, the one that stands out most is *HAM2*, a HAT that, together with its homolog *HAM1*, belongs to the MYST clade of the HAT family and was shown to be involved in post-meiotic control of female and male gametophytic development (Latrasse et al., 2008). In mammals, the MYST protein family was found to be involved in many fundamental cell functions such as cell cycle progression and DNA repair (Pillus, 2008; Sapountzi and Côté, 2011). Furthermore, the human MYST4 acetylase was found to be expressed and involved in the control of gametogenesis as well (McGraw et al., 2007). In *Arabidopsis*, the *ham1 ham2* double mutant is lethal, while keeping one of the two genes heterozygous for the mutant allele resulted in a post-meiotic arrest of both female and male gametophyte developments (Latrasse et al., 2008). This phenotype is similar to the one observed in the *REM_RNAi* as well as in the *35S:REM34_EAR* lines. Interestingly, *HAM1* and *HAM2* were also found to be involved in the control of flowering time *via* the epigenetic regulation of *FLOWERING LOCUS C* (*FLC*), which is also a target of VRN1, one of the four *REM* genes for which the function is known so far, suggesting a common mechanism throughout plant development. The artificial silencing of these two acetyltransferases causes an early flowering phenotype (Xiao et al., 2013) which was also noticed in the *REM_RNAi* lines (data not shown). The downregulation of *HAM2* and the phenotypical similarity between the *REM_RNAi* lines and the *HAM* downregulation suggest that these genes might be involved in the control of the same biological processes throughout *Arabidopsis* development. Further analysis will be needed to confirm the possible interaction between *REM34, REM35,* and the HATs HAM1 and HAM2. The observed downregulation of the other analyzed target genes could be due to the general deregulation of transcription caused by the reduced expression of the chromatin remodeling factor *HAM2.*

While not much is known about the *REM* gene family, substantial information is available for other transcription factor

families that are characterized by the presence of the B3 DNA binding domain. In particular, the well-characterized *auxin response factor* (*ARF*) family, known to play a crucial role in regulating auxin responses, and the *related to ABI3/VP1* (*RAV*) family, which was found to be involved in hormonal regulation during different stages of *Arabidopsis* development (Swaminathan et al., 2008). The plant hormone auxin was found to be involved in gametogenesis (Pagnussat et al., 2009; Panoli et al., 2015). Indeed, perturbation of auxin transport in the embryo sac causes an arrest in the earliest stages of megagametogenesis (Ceccato et al., 2013). Auxin biosynthesis in the male gametophyte was also recently shown to be essential for the transition from microsporogenesis to microgametogenesis (Yao et al., 2018). Because of the phenotypic similarities between the auxin defective mutant (Pagnussat et al., 2009; Panoli et al., 2015; Ceccato et al., 2013) and the *REM_RNAi* lines and because of the linkage between transcription factors containing the B3 DNA-binding domain and the regulation of hormonal responses, it is tempting to speculate that the role of *REM34, REM35,* and *REM36* play in gametogenesis is also based on the regulation of a hormonal related processes.

In summary, we gained new information about the expression pattern and function of *REM34, REM35,* and *REM36* during gametophyte development in *Arabidopsis*; those genes might control post-meiotic divisions in both embryo sac and pollen grains. These findings underline further the importance of *REM* genes during reproductive development in plants. Although these genes are often highly redundant and physically linked in the genome, slowly on, we start to get a better understanding about their functions in plant development. Of course, we just see the tip of the iceberg and still a huge amount of work has to be done to fully understand in detail the molecular and genetic mechanisms by which *REM* genes function.

DATA AVAILABILITY STATEMENT

All datasets generated for this study are included in the manuscript/**Supplementary Files**.

AUTHOR CONTRIBUTIONS

FC performed most of the experiments and wrote the manuscript. VB performed morphological analyses and contributed to writing the manuscript. OM and GL designed and employed the RNA interference and EAR constructs. MM designed and performed the CLS experiment and performed part of the back-crosses. RP made BiFC experiments. HH-U and SF designed the Y2H screening and helped FC with the experiment. AG designed the in-vitro pollen germination experiment and the Aniline blue analyses. MK contributed to the design of the experiments and helped writing the manuscript. VG designed the research, helped with the experiments and wrote the manuscript.

FUNDING

VG was supported by Ministero dell'Istruzione, dell'Università e della Ricerca MIUR, SIR2014 MADSMEC, Proposal number RBSI14BTZR. The post-doctoral fellowship of AG was supported by MIUR, SIR2014 MADSMEC, Proposal number RBSI14BTZR.

The PhD fellowship of FC and RP were supported by the Doctorate School in Molecular and Cellular Biology, Università degli Studi di Milano. FC was supported by PROCROP-H20MC_RISE15LCOLO_M. RP was supported by H2020-MSCA-RISE-2015 ExpoSEED Proposal Number: 691109.

Work in the SF laboratory was financed by the Mexican National Council of Science and Technology (CONACyT) grants CB-2012-177739 and FC-2015-2/1061, and SF acknowledges support of the Marcos Moshinsky Foundation and the European Union H2020-MSCA-RISE-2015 project ExpoSEED (grant no. 691109).

ACKNOWLEDGMENTS

We thank Simona Masiero, Francesca Resentini, Lucia Colombo for helpful suggestions and valuable discussions. We also thank Annamaria Piva, Radha Cighetti and Francesco Gozzo from University of Milan, Toshiaki MITSUI and Marouane BASLAM Department of Applied Biological Chemistry Graduate School of Science & Technology - Niigata University Ikarashi, Nishi-ku, Niigata, Japan and Ravishankar Palanivelu School of Plant Science-University of Arizona Tucson for their technical support.

Part of this work was carried out at NOLIMITS, an advanced imaging facility established by the Università degli Studi di Milano.

SUPPLEMENTARY MATERIAL

The Supplementary Material for this article can be found online at: https://www.frontiersin.org/articles/10.3389/fpls.2019.01351/full#supplementary-material

REFERENCES

Acosta-García, G., and Vielle-Calzada, J.-P. (2004). A classical arabinogalactan protein is essential for the initiation of female gametogenesis in *Arabidopsis*. *Plant Cell* 16, 2614–2628. doi: 10.1105/tpc.104.024588

Berger, F., and Twell, D. (2011). Germline Specification and Function in Plants. *Annu. Rev. Plant Biol.* 62, 461–484. doi: 10.1146/annurev-arplant-042110-103824

Bou Daher, F., Chebli, Y., and Geitmann, A. (2009). Optimization of conditions for germination of cold-stored *Arabidopsis thaliana* pollen. *Plant Cell Rep.* 28, 347–357. doi: 10.1007/s00299-008-0647-1

Brambilla, V., Battaglia, R., Colombo, M., Masiero, S., Bencivenga, S., Kater, M. M., et al. (2007). Genetic and Molecular Interactions between BELL1 and MADS Box Factors Support Ovule Development in *Arabidopsis*. *Plant Cell Online* 19, 2544–2556. doi: 10.1105/tpc.107.051797

Braselton, J. P., Wilkinson, M. J., and Clulow, S. A. (1996). Feulgen staining of intact plant tissues for confocal microscopy. *Biotech. Histochem.* 71, 84–87. doi: 10.3109/10520299609117139

Briggs, G., Osmont, K., Shindo, C., Sibout, R., and Hardtke, C. (2006). Unequal genetic redundancies in *Arabidopsis* – a neglected phenomenon? *Trends Plant Sci.* 11, 492–498. doi: 10.1016/j.tplants.2006.08.005

Bucher, E., Lohuis, D., van Poppel, P. M. J. A., Geerts-Dimitriadou, C., Goldbach, R., and Prins, M. (2006). Multiple virus resistance at a high frequency using a single transgene construct. *J. Gen. Virol.* 87, 3697–3701. doi: 10.1099/vir.0.82276-0

Ceccato, L., Masiero, S., Sinha Roy, D., Bencivenga, S., Roig-Villanova, I., Ditengou, F. A., et al. (2013). Maternal Control of PIN1 Is Required for Female Gametophyte Development in *Arabidopsis*. *PLoS One* 8, 2–8. doi: 10.1371/journal.pone.0066148

Chantha, S. C., Gray-Mitsumune, M., Houde, J., and Matton, D. P. (2010). The MIDASIN and NOTCHLESS genes are essential for female gametophyte development in *Arabidopsis thaliana*. *Physiol. Mol. Biol. Plants* 16, 3–18. doi: 10.1007/s12298-010-0005-y

Clark, K. A., and Krysan, P. J. (2010). Chromosomal translocations are a common phenomenon in *Arabidopsis thaliana* T-DNA insertion lines. *Plant J.* 64, 990–1001. doi: 10.1111/j.1365-313X.2010.04386.x

Clough, S. J., and Bent, A. F. (1998). Floral dip: a simplified method for Agrobacterium-mediated transformation of *Arabidopsis thaliana*. *Plant J.* 16, 735–743. doi: 10.1046/j.1365-313x.1998.00343.x

Curtis, M. J., Belcram, K., Bollmann, S. R., Tominey, C. M., Hoffman, P. D., Mercier, R., et al. (2009). Reciprocal chromosome translocation associated with TDNA-insertion mutation in *Arabidopsis*: genetic and cytological analyses of consequences for gametophyte development and for construction of doubly mutant lines. *Planta* 229, 731–745. doi: 10.1007/s00425-008-0868-0

Czarnecki, O., Bryan, A. C., Jawdy, S. S., Yang, X., Cheng, Z. M., Chen, J. G., et al. (2016). Simultaneous knockdown of six non-family genes using a single synthetic RNAi fragment in *Arabidopsis thaliana*. *Plant Methods* 12, 1–11. doi: 10.1186/s13007-016-0116-8

de Folter, S., and Immink, R. G. H. (2011). "Yeast Protein–Protein Interaction Assays and Screens," in *Methods in molecular biology*. *Methods Mol. Biol.* 754, 145–165. doi: 10.1007/978-1-61779-154-3_8

de Folter, S., Immink, R. G. H., Kieffer, M., Parenicová, L., Henz, S. R., Weigel, D., et al. (2005). Comprehensive Interaction Map of the *Arabidopsis* MADS Box Transcription Factors. *Plant Cell Online* 17, 1424–1433. doi: 10.1105/tpc.105.031831

Ebel, C., Mariconti, L., and Gruissem, W. (2004). Plant retinoblastoma homologues control nuclear proliferation in the female gametophyte. *Nature* 429, 776–780. doi: 10.1038/nature02637

Fornara, F., Gregis, V., Pelucchi, N., Colombo, L., and Kater, M. (2008). The rice StMADS11-like genes OsMADS22 and OsMADS47 cause floral reversions in *Arabidopsis* without complementing the svp and agl24 mutants. *J. Exp. Bot.* 59, 2181–2190. doi: 10.1093/jxb/ern083

Franco-Zorrilla, J. M., Cubas, P., Jarillo, J. A., Fernández-Calvín, B., Salinas, J., and Martínez-Zapater, J. M. (2002). AtREM1, a member of a new family of B3 domain-containing genes, is preferentially expressed in reproductive meristems. *Plant Physiol.* 128, 418–427. doi: 10.1104/pp.010323

Gregis, W. V., Sessa, A., Colombo, L., Kater, M. M., Gregis, V., Sessa, A., et al. (2006). AGL24, SHORT VEGETATIVE PHASE, and APETALA1 Redundantly Control AGAMOUS during Early Stages of Flower Development in *Arabidopsis*. *Plant Cell Online* 18, 1373–1382. doi: 10.1105/tpc.106.041798

Hafidh, S., Fíla, J., and Honys, D. (2016). Male gametophyte development and function in angiosperms: a general concept. *Plant Reprod.* 29, 31–51. doi: 10.1007/s00497-015-0272-4

Huanca-Mamani, W., Garcia-Aguilar, M., Leon-Martinez, G., Grossniklaus, U., and Vielle-Calzada, J.-P. (2005). CHR11, a chromatin-remodeling factor essential for nuclear proliferation during female gametogenesis in *Arabidopsis thaliana*. *Proc. Natl. Acad. Sci.* 102, 17231–17236. doi: 10.1073/pnas.0508186102

Immink, R. G., Tonaco, I. A., de Folter, S., Shchennikova, A., van Dijk, A. D., Busscher-Lange, J., et al. (2009). SEPALLATA3: the "glue" for MADS box transcription factor complex formation. *Genome Biol.* 10, R24. doi: 10.1186/gb-2009-10-2-r24

Ingouff, M., Jullien, P. E., and Berger, F. (2006). The female gametophyte and the endosperm control cell proliferation and differentiation of the seed coat in *Arabidopsis*. *Plant Cell* 18, 3491–3501. doi: 10.1105/tpc.106.047266

Johnston, A. J., Matveeva, E., Kirioukhova, O., Grossniklaus, U., and Gruissem, W. (2008). A Dynamic Reciprocal RBR-PRC2 Regulatory Circuit Controls *Arabidopsis* Gametophyte Development. *Curr. Biol.* 18, 1680–1686. doi: 10.1016/j.cub.2008.09.026

Klepikova, A. V., Kasianov, A. S., Gerasimov, E. S., Logacheva, M. D., and Penin, A. A. (2016). A high resolution map of the *Arabidopsis thaliana* developmental transcriptome based on RNA-seq profiling. *Plant J.* 88, 1058–1070. doi: 10.1111/tpj.13312

Latrasse, D., Benhamed, M., Henry, Y., Domenichini, S., Kim, W., Zhou, D. X., et al. (2008). The MYST histone acetyltransferases are essential for gametophyte development in *arabidopsis*. *BMC Plant Biol.* 8, 1–16. doi: 10.1186/1471-2229-8-121

Levy, Y. Y. (2002). Multiple Roles of *Arabidopsis* VRN1 in Vernalization and Flowering Time Control. *Science* (80-.). 297, 243–246. doi: 10.1126/science.1072147

Li, N., Yuan, L., Liu, N., Shi, D., Li, X., Tang, Z., et al. (2009). SLOW WALKER2, a NOC1/MAK21 Homologue, Is Essential for Coordinated Cell Cycle Progression during Female Gametophyte Development in *Arabidopsis*. *PLANT Physiol.* 151, 1486–1497. doi: 10.1104/pp.109.142414

Liu, J., Zhang, Y., Qin, G., Tsuge, T., Sakaguchi, N., Luo, G., et al. (2008). Targeted Degradation of the Cyclin-Dependent Kinase Inhibitor ICK4/KRP6 by RING-Type E3 Ligases Is Essential for Mitotic Cell Cycle Progression during *Arabidopsis* Gametogenesis. *Plant Cell Online* 20, 1538–1554. doi: 10.1105/tpc.108.059741

Mansfield, S. G., and Briarty, L. G. (1991). Early embryogenesis in *Arabidopsis thaliana*. II. The developing embryo. *Can. J. Bot.* 69, 461–476. doi: 10.1139/b91-063

Mantegazza, O., Gregis, V., Mendes, M. A., Morandini, P., Alves-Ferreira, M., Patreze, C. M., et al. (2014). Analysis of the *arabidopsis* REM gene family predicts functions during flower development. *Ann. Bot.* 114, 1507–1515. doi: 10.1093/aob/mcu124

Matias-Hernandez, L., Battaglia, R., Galbiati, F., Rubes, M., Eichenberger, C., Grossniklaus, U., et al. (2010). VERDANDI is a direct target of the MADS domain ovule identity complex and affects embryo sac differentiation in *Arabidopsis*. *Plant Cell* 22, 1702–1715. doi: 10.1105/tpc.109.068627

McGraw, S., Morin, G., Vigneault, C., Leclerc, P., and Sirard, M.-A. (2007). Investigation of MYST4 histone acetyltransferase and its involvement in mammalian gametogenesis. *BMC Dev. Biol.* 7, 123. doi: 10.1186/1471-213X-7-123

Melnyk, C. W., Molnar, , A., and Baulcombea, D. C. (2011). Intercellular and systemic movement of RNA silencing signals. *EMBO J.* 30 (17), 3553–3563. doi: 10.1038/emboj.2011.274

Mendes, M. A., Guerra, R. F., Castelnovo, B., Silva-Velazquez, Y., Morandini, P., Manrique, S., et al. (2016). Live and let die: a REM complex promotes fertilization through synergid cell death in *Arabidopsis*. *Development* 14, 2780–2790. doi: 10.1242/dev.134916

Miki, D., Itoh, R., and Shimamoto, K. (2005). RNA silencing of single and multiple members in a gene family of rice. *Plant Physiol.* 138, 1903–1913. doi: 10.1104/pp.105.063933

Mlotshwa, S., Voinnet, O., Mette, M. F., Matzke, M., Vaucheret, H., Ding, S. W., et al. (2002). RNA silencing and the mobile silencing signal. *Plant Cell.;14* Suppl, S289–S301. doi: 10.1105/tpc.001677

Mori, T., Kuroiwa, H., Higashiyama, T., and Kuroiwa, T. (2006). GENERATIVE CELL SPECIFIC 1 is essential for angiosperm fertilization. *Nat. Cell Biol.* 8, 64–71. doi: 10.1038/ncb1345

Muralla, R., Lloyd, J., and Meinke, D. (2011). Molecular Foundations of Reproductive Lethality in *Arabidopsis thaliana*. *PLoS One* 6, e28398. doi: 10.1371/journal.pone.0028398

Pagnussat, G. C., Alandete-Saez, M., Bowman, J. L., and Sundaresan, V. (2009). Auxin-Dependent Patterning and Gamete Specification in the *Arabidopsis* Female Gametophyte. *Science (80)* 324, 1684–1689. doi: 10.1126/science.1167324

Panoli, A., Martin, M. V., Alandete-Saez, M., Simon, M., Neff, C., Swarup, R., et al. (2015). Auxin Import and Local Auxin Biosynthesis Are Required for Mitotic Divisions, Cell Expansion and Cell Specification during Female Gametophyte Development in *Arabidopsis thaliana*. *PLoS One* 10, e0126164. doi: 10.1371/journal.pone.0126164

Park, S. K., Howden, R., and Twell, D. (1998). The *Arabidopsis thaliana* gametophytic mutation gemini pollen1 disrupts microspore polarity, division asymmetry and pollen cell fate. *Development* 125, 3789–3799.

Peterson, R., Slovin, J., and Cheng, C. (2010). A simplified method for differential staining of aborted and non-aborted pollen grains. *Int. J. Plant Biol.* 1, e13. doi: 10.4081/pb.2010.e13

Pillus, L. (2008). MYSTs mark chromatin for chromosomal functions. *Curr. Opin. Cell Biol.* 20, 326–333. doi: 10.1016/j.ceb.2008.04.009

Resentini, F., Cyprys, P., Steffen, J. G., Alter, S., Morandini, P., Mizzotti, C., et al. (2017). SUPPRESSOR OF FRIGIDA (SUF4) Supports Gamete Fusion via Regulating *Arabidopsis* EC1 Gene Expression. *Plant Physiol.* 173, 155–166. doi: 10.1104/pp.16.01024

Richter, R., Kinoshita, A., Vincent, C., Martinez-Gallegos, R., Gao, H., van Driel, A. D., et al. (2019). Floral regulators FLC and SOC1 directly regulate expression of the B3-type transcription factor TARGET OF FLC AND SVP 1 at the *Arabidopsis* shoot apex via antagonistic chromatin modifications. *PLoS Genet.* 15, e1008065. doi: 10.1371/journal.pgen.1008065

Romanel, E. A. C., Schrago, C. G., Couñago, R. M., Russo, C. A. M., and Alves-Ferreira, M. (2009). Evolution of the B3 DNA binding superfamily: New insights into REM family gene diversification. *PLoS One* 4, e5791. doi: 10.1371/journal.pone.0005791

Sapountzi, V., and Côté, J. (2011). MYST-family histone acetyltransferases: beyond chromatin. *Cell. Mol. Life Sci.* 68, 1147–1156. doi: 10.1007/s00018-010-0599-9

Schneitz, K., Hulskamp, M., and Pruitt, R. E. (1995). Wild-type ovule development in Arabidopsis thaliana: a light microscope study of cleared whole-mount tissue. *Plant J.* 7, 731–749. doi: 10.1046/j.1365-313X.1995.07050731.x

Skopelitis, D. S., Hill, K., Klesen, S., Marco, C. F., von Born, P., Chitwood, D. H., et al. (2018). Gating of miRNA movement at defined cell-cell interfaces governs their impact as positional signals. *Nat Commun. 2018;* 9, 3107. doi: 10.1038/s41467-018-05571-0

Shi, D.-Q., Liu, J., Xiang, Y.-H., Ye, D., Sundaresan, V., and Yang, W.-C. (2005). SLOW WALKER1, essential for gametogenesis in *Arabidopsis*, encodes a WD40 protein involved in 18S ribosomal RNA biogenesis. *Plant Cell* 17, 2340–2354. doi: 10.1105/tpc.105.033563

Smyth, D. R., Bowman, J. L., and Meyerowitz, E. M. (1990). Early flower development in *Arabidopsis*. *Plant Cell* 2, 755–767. doi: 10.1105/tpc.2.8.755

Sung, S., and Amasino, R. M. (2004). Vernalization in *Arabidopsis thaliana* is mediated by the PHD finger protein VIN3. *Nature* 427, 159–164. doi: 10.1038/nature02195

Swaminathan, K., Peterson, K., and Jack, T. (2008). The plant B3 superfamily. *Trends Plant Sci.* 13, 647–655. doi: 10.1016/j.tplants.2008.09.006

Takeuchi, H., and Higashiyama, T. (2016). Tip-localized receptors control pollen tube growth and LURE sensing in *Arabidopsis*. *Nature* 531, 245–248. doi: 10.1038/nature17413

Wang, S.-Q., Shi, D.-Q., Long, Y.-P., Liu, J., and Yang, W.-C. (2012). GAMETOPHYTE DEFECTIVE 1, a Putative Subunit of RNases P/MRP, Is Essential for Female Gametogenesis and Male Competence in *Arabidopsis*. *PLoS One* 7, e33595. doi: 10.1371/journal.pone.0033595

Xiao, J., Zhang, H., Xing, L., Xu, S., Liu, H., Chong, K., et al. (2013). Requirement of histone acetyltransferases HAM1 and HAM2 for epigenetic modification of FLC in regulating flowering in *Arabidopsis*. *J. Plant Physiol.* 170, 444–451. doi: 10.1016/j.jplph.2012.11.007

Yao, X., Tian, L., Yang, J., Zhao, Y. N., Zhu, Y. X., Dai, X., et al. (2018). Auxin production in diploid microsporocytes is necessary and sufficient for early stages of pollen development. *PLoS Genet.* 14, 1–19. doi: 10.1371/journal.pgen.1007397

Zhao, X., Bramsiepe, J., Van Durme, M., Komaki, S., Prusicki, M. A., Maruyama, D., et al. (2017). RETINOBLASTOMA RELATED1 mediates germline entry in *Arabidopsis*. *Science (80)* 356, eaaf6532. doi: 10.1126/science.aaf6532

Conflict of Interest: The authors declare that the research was conducted in the absence of any commercial or financial relationships that could be construed as a potential conflict of interest.

Crop reproductive meristems in the genomic era: a brief overview.

Caselli F [1]**,** Zanarello F [1], Kater MM [1], Battaglia R [2], Gregis V [1]

[1] Dipartimento di Bioscienze, Università degli Studi di Milano, Milan, Italy

[2] CREA Research Centre for Genomics and Bioinformatics, 29017 Fiorenzuola d'Arda (PC), Italy

June 2020; Biochem Soc Trans ; 48 (3): 853–865; doi: 10.1042/BST20190441

In this review, we summarized some of the knowledge acquired in recent years on the transcription factors involved in the regulation of meristem determinacy and identity in some of the staple cereal species. To do so, we compared the transcriptomic datasets generated from the reproductive meristems of *Oryza sativa, Zea mays, Hordeum vulgare* and *Triticum aestivum,* extrapolating the transcriptional factor families, whose members are differentially expressed in the transition from indeterminate to determinate meristem.

We included in the analysis also the transcriptomic data available for the model species *Arabidopsis thaliana*, because of the extensive data available for this plant.

We decided to focus on inflorescence architecture and organization, as it is a trait fundamental for the determination of fruit and seed yield. Understanding the regulatory networks underlying inflorescence development will thus facilitate crop improvement for traits like grain yield.

I contributed to this paper by helping with the production of the concept for the review, interpreting the comparison data and writing the manuscript.

Mini Review - *Biochemical Society Transactions*

"Crop reproductive meristems in the genomic era, a brief overview"

Francesca Caselli[1], Fabio Zanarello[1], Martin M. Kater[1], Raffaella Battaglia[2], Veronica Gregis[1*]

[1] Department of Biosciences, University of Milan, Via Celoria 26, 20133 Milan, Italy
[2] CREA Research Centre for Genomics and Bioinformatics, 29017, Fiorenzuola d'Arda (PC), Italy

Contact information: *Email of corresponding author Veronica Gregis: veronica.gregis@unimi.it
Keywords: inflorescence-architecture, meristem-determinacy, transcriptomes, crops-improvement, gene-families.

ABSTRACT

Modulation of traits beneficial for cultivation and yield is one of the main goals of crop improvement. One of the targets for enhancing productivity is changing the architecture of inflorescences since in many species it determines fruit and seed yield. Inflorescence shape and organization is genetically established during the early stages of reproductive development and depends on the number, arrangement, activities, and duration of meristems during the reproductive phase of the plant life cycle. Despite the variety of inflorescence architectures observable in nature, many key aspects of inflorescence development are conserved among different species. For instance, the genetic network in charge of specifying the identity of the different reproductive meristems, which can be indeterminate or determinate, seems to be similar among distantly related species. The availability of a large number of published transcriptomic datasets for plants with different inflorescence architectures, allowed us to identify transcription factor gene families that are differentially expressed in determinate and indeterminate reproductive meristems. The data that we review here for Arabidopsis, rice, barley, wheat, and maize, particularly deepens our knowledge of their involvement in meristem identity specification.

INTRODUCTION

Crops are characterized by a striking variety of inflorescence types, determined by the coordinated activity of niches of undifferentiated stem cells, called meristems (Fig.1).
A mathematical "transient model" predicts that the final architecture of the inflorescence is determined by the fine-tuning of the proliferative activity of the indeterminate meristems (IMe), and their ability to differentiate into a determinate meristem (DMe) (1).
Stem cells homeostasis within the reproductive meristems is crucial to tailor inflorescence architecture and ultimately depends on the balance between meristematic cell population versus daughter cell differentiation. A feedback signaling loop is responsible for this equilibrium, and despite being mainly studied in Arabidopsis, this pathway seems to be broadly conserved across species such as maize, rice, and tomato (reviewed in (2)). Master players are WUSCHEL (WUS) and WUSCHEL-RELATED HOMEOBOX (WOX) and KNOTTED-LIKE HOMEOBOX (KNOX) transcription factors and CLAVATA leucine-rich repeat receptor-like kinases and their ligands. These factors modulate the transcription of target genes which include many genes involved in biosynthesis or signaling of phytohormones (3).

The dicot model species *Arabidopsis thaliana* has a raceme inflorescence, in which the indeterminate inflorescence meristem (IM) grows indeterminately producing on its flanks several determinate flower meristems (FMs), whose destiny unequivocally leads to flower formation and the depletion of meristematic cells (Fig. 1A). Cymose inflorescences, such as those of Solanaceae, are characterized by IM that ends with a

flower meristem and eventually produces a new IM on the side which reiterates the same developmental pattern. In grasses, the IM produces different meristem types which ultimately differentiate into a spikelet meristem (SM), producing florets that can be directly attached to the main inflorescence axis, as in spikes, or developing on flower-bearing branch meristems (BMs), as in panicles (4). Figure 1 describes the development and the architectures of reproductive meristems in Arabidopsis, rice, wheat, maize, and barley.

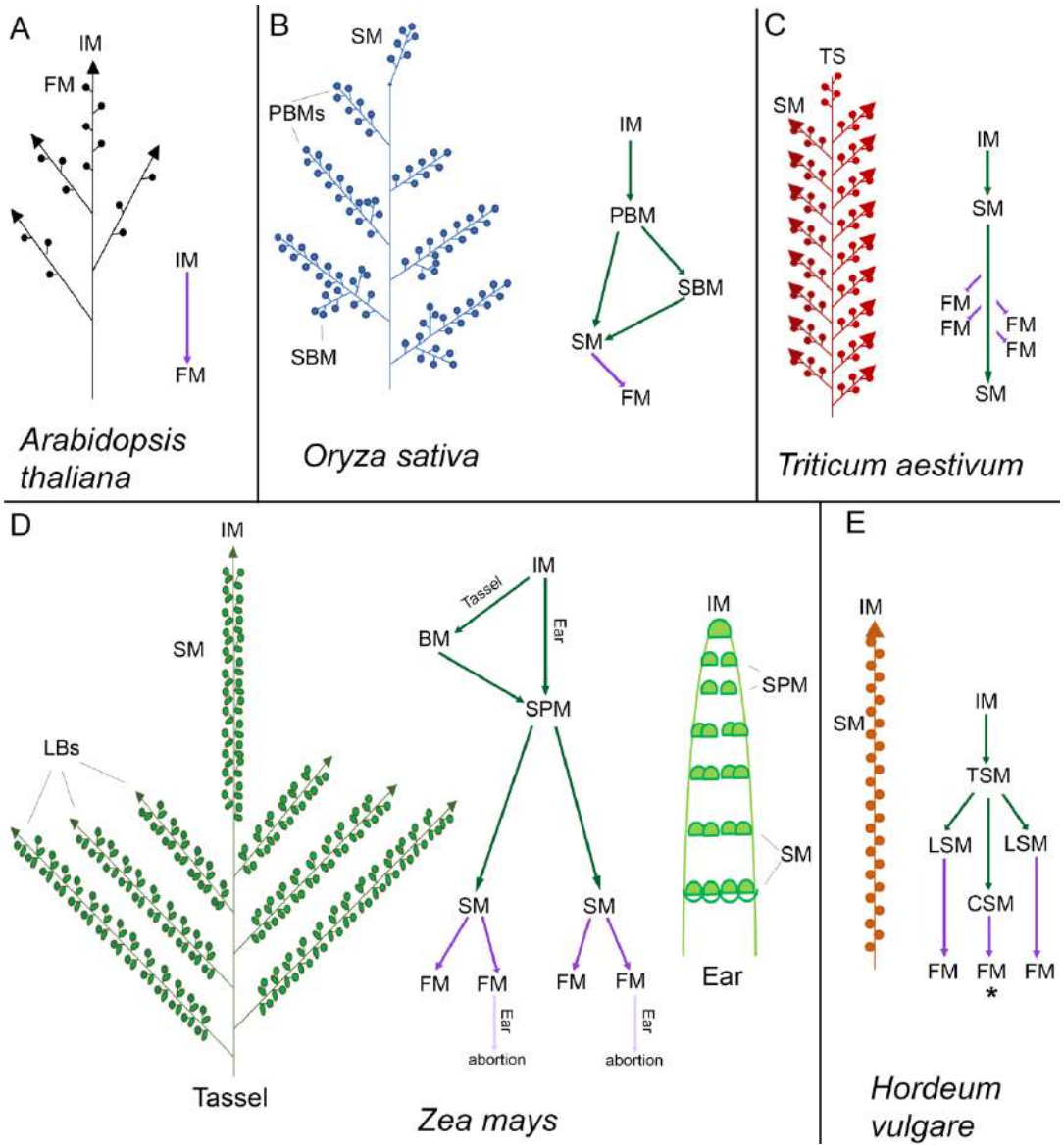

Figure 1. *Scheme of inflorescence architecture and meristem identity transition with a graphical configuration of reproductive meristems development in (A) Arabidopsis, (B) rice, (C) wheat, (D) maize, and (E) barley. Circles: Determinate Meristem (DMe), arrows: Indeterminate Meristems (IMe).*

(A) In Arabidopsis thaliana, the IMe lasts for the entire life of the plant and produces DMe which differentiates completely in FM.

(B) In the branched panicle of Oryza sativa, the IMe is called rachis meristem (RM). During inflorescence development, some cells of the IMe differentiate into the Primary Branch Meristems (PBMs) and Secondary BMs (SBMs) which produce and differentiate determinate SMs. IM elongates after the branches differentiation and aborts after producing a variable number of PBMs.

(C) In Triticum aestivum, the inflorescence is a determinate spike where the IMe differentiates into SMs which produce a variable number of FMs.

(D) In Zea mays two distinct inflorescences are produced, tassel and ear, which differentiate into male and female flowers, respectively. Both structures share a similar architecture in which an apical IMe develops a series of lateral meristems (LBs). The spikelet-pair meristem (SPM) initiates two spikelet meristems (SM), each of which develops two floral meristems (FMs); in ears, one FM undergoes a selective abortion. Contrary to the ear, the tassel is a branched inflorescence, in which the IM can differentiate both SPM and Branch Meristems (BM).
(E) In Hordeum vulgare, the Ie produces triple spikelet meristem (TSM) which differentiates in lateral spikelet meristems (LSM) and a central spikelet meristem (CSM). In two-rowed spikes, only the CSM produces a fertile flower (*) in six-rowed spikes LSMs, and CSM all differentiate fertile flowers.
*Green arrow: IMe (Indeterminate Meristem) formation, purple arrow: DMe (Determinate Meristem) formation), pink arrow: abortion of floral meristems. Abbreviations: LB: lateral branch meristem; FM: floral meristem; IM: inflorescence meristem; LSM: lateral spikelet meristem; PBM: primary branch meristem; SBM: secondary branch meristem; SM: spikelet meristem: SPM: spikelet pair meristem; TSM: triple spikelet meristem; * FM which develops in two-rowed spikes.*

The determination of meristem identity and the transition from indeterminate to determinate meristem activity are governed by a complex gene network of which some master regulators have been well characterized, but many others remain still unknown. Identifying new players in this complex process will provide a better understanding of the mechanisms through which the architecture of the inflorescence is determined and will facilitate crop improvement for traits like grain yield per hectare, which is closely linked to finding solutions to feed a fast-growing world population. Therefore, there is an increasing interest in understanding the regulatory networks underlying inflorescence development. The growing number of plant genomes that have been sequenced and annotated together with the huge number of transcriptome datasets, including meristem-specific ones, facilitate comparative analysis of meristem related datasets (5–13). Furthermore, inter-species comparative transcriptomic is rapidly gaining popularity, as it has been proven to be a useful tool both to discover common meristem regulators and to identify factors behind the divergences observed among different inflorescence architectures (9,11,12).

In this review, we summarize some of the knowledge acquired in the recent years on the master regulators of meristem determinacy and identity in some of the staple cereals species, focusing in particular on families of transcription factors, which are considered to be the major players in the evolution and domestication of crops. Because of their role in regulating gene expression, transcription factors are generally considered important targets of crop improvement, especially when dealing with multigenic traits (14,15).
To identify those families whose activity controls the specification of the different meristem types, we compared the transcriptomes generated from reproductive meristems of *Arabidopsis thaliana* (5), rice (multiple accessions) (9), maize (*Zea mays,* cv B73) (7), barley (*Hordeum vulgare,* cv Morex) (13) and bread wheat (*Triticum aestivum*, cv Chinese Spring) (8). In particular, since we wanted to specifically review the genetic pathway controlling the transition from indeterminate to determinate fate, we decided to prioritize the comparison between indeterminate meristem (IMe) and determinate meristem (DMe) transcriptomes (Fig. 2). We, therefore, selected datasets of Differentially Expressed Genes (DEGs), that were generated with a similar methodology: hand-dissection meristems with a morphological control to assess their developmental stage (Table 1). Because of the extensive knowledge available for *Arabidopsis thaliana*, the transcriptome generated from laser-dissected inflorescence meristems of this specie was also included in the analysis (5). We exploited the PLAZA database (16) to assign each DEG to a specific gene family and families coding for transcription factors (TF) were selected and grouped according to their functional domains. This strategy allowed us to extrapolate which TF families are differentially expressed during the transition from IMe to DMe.
The sets of families from the different species were then intersected, to extrapolate the number of families in common in all the possible comparisons between the selected species (Fig. 3). We were then able to visualize

common and species-specific gene families that might control meristem identity and determination during inflorescence differentiation.

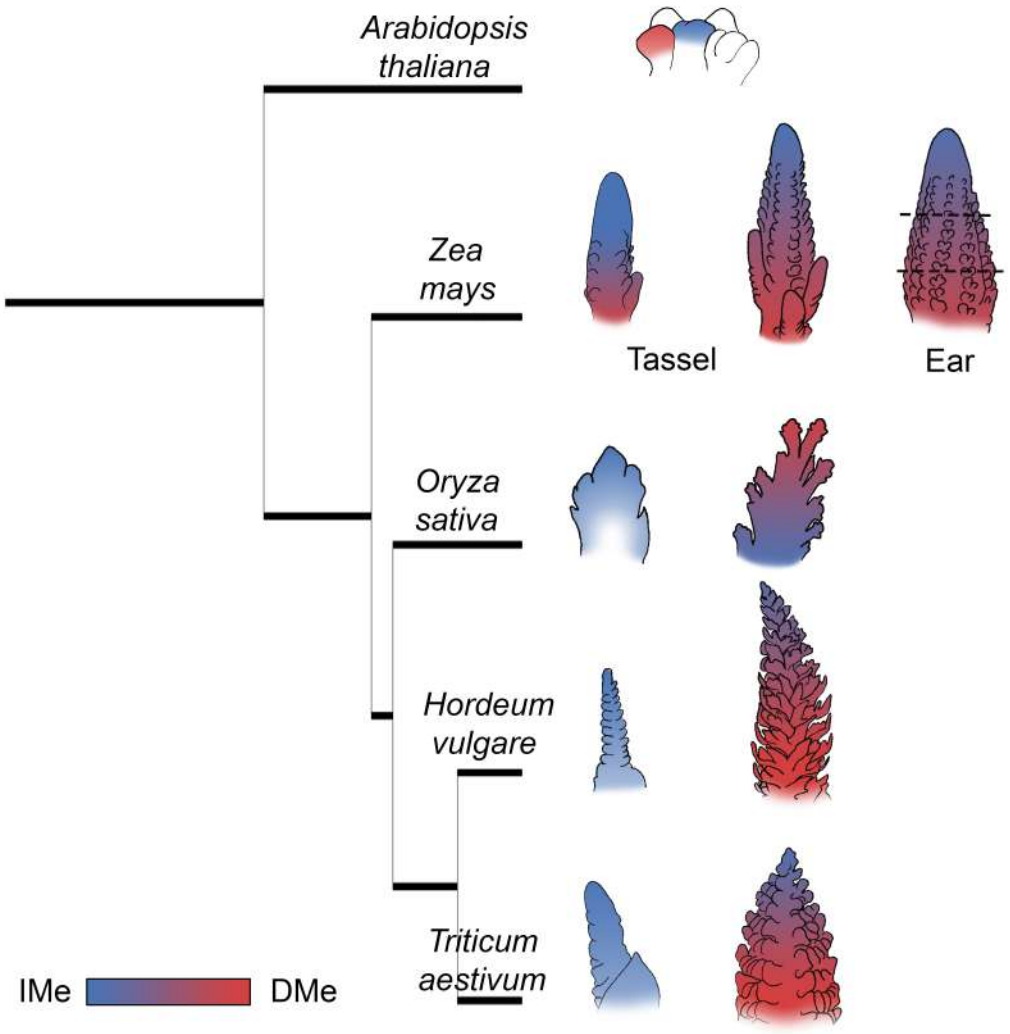

***Figure 2**. Schematic representation of the Indeterminate Meristems (IMe) and Determinate Meristems (DMe) sampled in Arabidopsis, rice, wheat, maize, and barley.*
The qualitative phylogenetic tree was produced and adapted from PhyloT (https://phylot.biobyte.de/) based on the NCBI taxonomy of the four species.
The draws represent the IMe-enriched samples (Blue) and DMe-enriched samples (Red) collected in the different experiments of RNAseq transcriptome analysis considered in this review.
In Arabidopsis, the IM (IMe) and FM (DMe) were sampled through laser-dissection, as indicated in the drawing. Zea mays tassels were hand dissected and separated, according to their dimensions, in IM/SPM (IMe enriched tissue) and SM (DMe enriched tissue). Ears were sectioned into different segments, as indicated by the dotted lines, into IM/SPM (IMe enriched tissue) and SM (DMe enriched tissue). Drawings were adapted from (6).
Oryza sativa meristems were hand dissected and classified according to their morphology, into indeterminate meristems (PBM and SBM) and determinate meristems (SM). Oryza sativa reproductive meristems were adapted from (9).
In Hordeum vulgare inflorescence meristems at double-ridge (DR) corresponding to the Waddington stage W2.0 (IMe) and awn primordium (AP), corresponding to W3.5(DMe), stages were collected. Drawings were adapted from (12).
Triticum aestivum meristems at Double Ridge (IMe) and FM (DMe) stages were collected. Drawings were modified from (7).

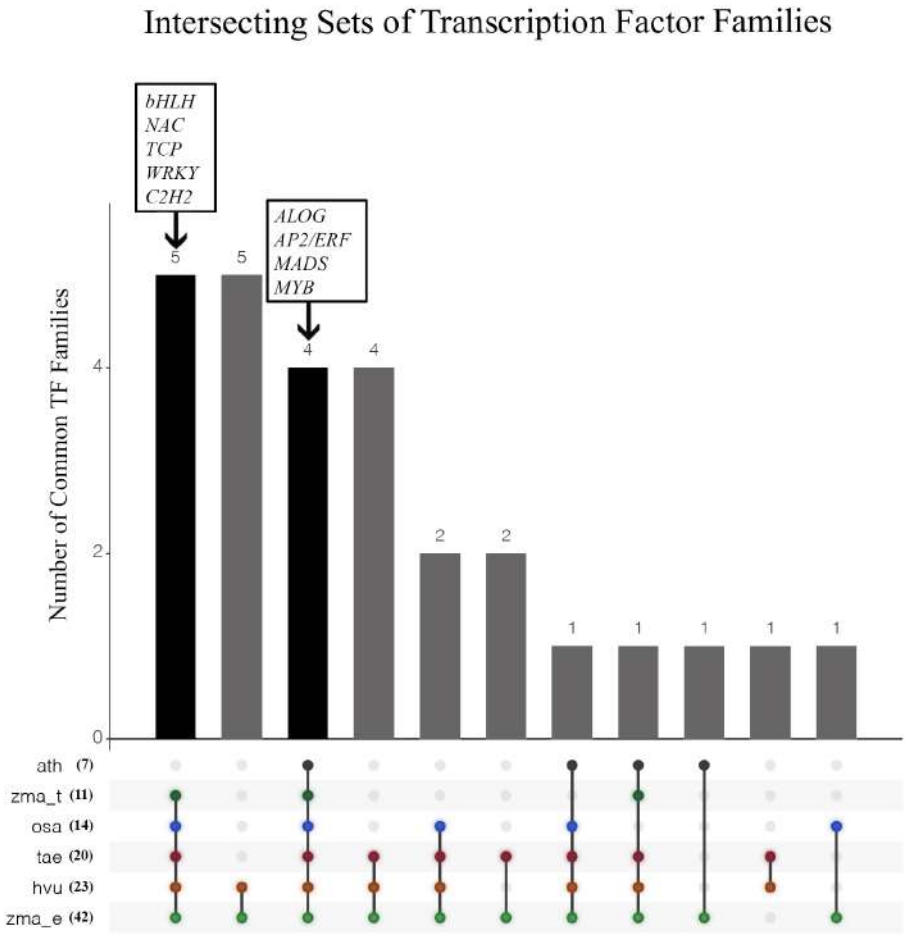

Figure 3. *Intersecting sets of TF families of Arabidopsis, rice, wheat, barley, and maize (tassel and ear).*
All the different comparisons are shown with dots on the x-axis, the number in brackets indicates the number of TF families differentially expressed in each species. The histogram shows the number of detected TF families in common between the different transcriptomic sets considered in this review, the number of families for each comparison is indicated on top of each bar. The two black bars represent the intersections between rice, maize, barley, and wheat (the crop-specific regulators: NAC, TCP, WRKY, C2H2, and bHLH) and between all the species considered (common regulators: MADS; ALOG, AP2/ERF, and MYB).
ath: Arabidopsis thaliana; osa: Oryza sativa; zma_t: Zea mays_tassel; tae: Triticum aestivum; hvu: Hordeum vulgare; zma_e: Zeam mays_ear. The plot was designed with the UpSetR package.

The GO enrichment analysis revealed that all the DEG lists are significantly enriched of terms as TF, expression regulation, DNA binding, RNA biosynthesis, and flower development. The list of DEG TF genes allowed us to identify four TF families, ALOG, AP2/ERF, MADS, and MYB, in the Arabidopsis, rice, wheat, barley, and maize transcriptomes (Fig 4A). The meristem transition from indeterminate to determinate is a crucial step in the life cycle of plants, as it strongly influences the final plant architecture. Despite the variety of inflorescence morphologies that characterize different species, this process is likely orchestrated by a conserved set of master regulators, which includes the TF families mentioned above.
From the analysis, we further defined a group of five cereal-specific TF families: *bHLH, NAC, TCP, WRKY*, and *C2H2* (Fig. 4B); we foresee that these factors could be putative targets for crop improvement.
Here, we reviewed the current knowledge on these two sets of conserved and cereal-specific TF families, deepening, in particular, their role in indeterminate vs determinate meristem development.

SPECIES (Ref)	IMe Indeterminate Meristem	DMe Determinate Meristem	Replicas	Sampling	SEQ technique	Cutoff (p value)	DEGs tot	% TF
Ath (5)	Inflorescence Meristem	Floral Meristem	3	laser dissection	Illumina 50-bp reads	0.05	46	26.09
Zma_t (7)	Inflorescence Meristem/ Spikelet Pair Meristem	Spikelet Meristem	2	hand dissection	Illumina 50-bp reads	0.05	144	13.89
Osa (9)	Primary Branch Meristem/ Axillary Meristem	Spikelet Meristem/ Floret Differentiation	3	hand dissection	Illumina 125-bp reads	0.05	130	27.69
Tae (8)	Double Ridge/ Spikelet Meristem	Floret Meristem	2	hand dissection	Illumina 50-bp reads	0.05	753	9.56
Hvu (13)	Double Ridge	Awn Primordium	3	hand dissection	Illumina 200-bp reads	0.05	702	16.38
Zma_e (7)	Inflorescence Meristem/ Spikelet Pair Meristem	Spikelet Meristem	2	hand dissection	Illumina 50-bp reads	0.05	8327	7.626

Table 1. *Sequencing information for the different datasets employed in this review.*
For each species, the tissues sampled in the Indeterminate Meristem (IMe) and Determinate Meristem (DMe) stages are briefly described. Sequencing information, DEGs number, and the percentage of TF in each DEG list are also indicated.

Conserved regulators among different species

A core of four transcription factor families, *MADS*, *ALOG*, *AP2/ERF*, and *MYB*, resulted differentially expressed in all the datasets that were reviewed in this work (Fig. 3 and Fig. 4A).

MADS-box transcription factors are implicated in several developmental processes in fungi, plants, and animals. The name of this family is an acronym of *MCM1* from *Saccharomyces cerevisiae*, *AG* from Arabidopsis, *DEFICIENS* from *Antirrhinum majus*, and *SRF* from *Homo sapiens,* the first MADS-box domain proteins to be discovered (17).
In the plant kingdom, these transcription factors are best known for their key role in the control of meristem identity specification and organ differentiation. Genome-wide analyses led to the characterization of this family in different plant model species, including crops (18–21). *MADS-box* genes are already well known as key regulators of inflorescence development and, for this reason, it was not surprising to find members of this family differentially expressed in all the meristems and species considered.
Since MADS-box gene functions and relevance in the context of inflorescence development and crop improvement have been recently reviewed (22–25), we will not further discuss this gene family.

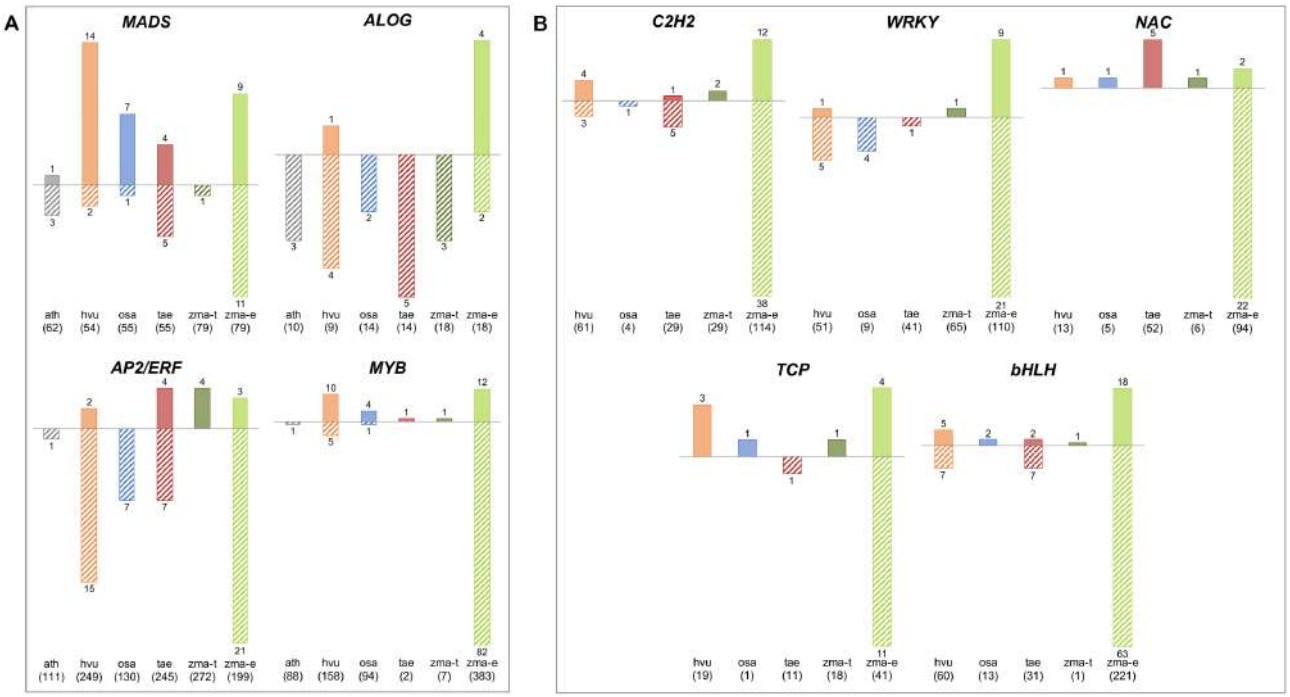

Figure 4. *Expression trend of the DEGs of the families described.*
The panels display the DEGs belonging to the different families here described, grouped in families with differentially expressed members in all the species considered (A) and only in monocots (B). The solid bars of each histogram shows the number of genes whose expression increases during the switch from indeterminate (IMe) to the determinate meristem (DMe), and the striped bars indicate the number of genes whose expression is higher in the indeterminate meristem (IMe). On the x-axis, the names of the species and the total number of genes belonging to the family are indicated. ath: Arabidopsis thaliana; osa: Oryza sativa; zma_t: Zea mays_tassel; tae: Triticum aestivum; hvu: Hordeum vulgare; zma_e: Zeam mays_ear

The *ALOG* genes encode plant-specific transcription factors named after the first two identified members of this family, *LHS1* in Arabidopsis and *G1* in rice. In Arabidopsis, *LSH1* was found to be involved in the light-dependent regulation of seedling growth (26). *LSH3* and *LSH4,* which are differentially expressed between the indeterminate and determinate meristems of Arabidopsis, are specifically expressed in the meristematic boundary cells. In these regions, they suppress organ differentiation and their expression is regulated by a boundary gene belonging to the *NAC* family, *CUC1* (*CUP-SHAPED COTYLEDON1*) (27,28).
Recently, in monocotyledons, genome-wide analyses led to the identification of several genes belonging to this family (29,30). Among these genes, the rice *TAWAWA1* (*TAW1*) is one of the few *ALOG* genes with a characterized role in inflorescence architecture determination. This transcription factor is expressed in the reproductive meristem and was proven to be necessary and sufficient to promote meristem indeterminacy, delaying its shift to SM. *TAW1* is a transcriptional activator, able to induce the expression of several *MADS-box* genes that are known to regulate BM maintenance. In the dominant *tawawa1-D* mutant, the BM can produce more branches before spikelet formation, leading to an increase in the total spikelet number and grain yield (31).
It is interesting to mention that, in the datasets considered for this review, the majority of the *ALOG* differentially expressed between IMe and DMe showed the same trend of expression, being downregulated as the meristem acquires a determinate identity (Fig. 4A). Although functional information is still missing for the maize, barley, and wheat *ALOG* gene family, it becomes tempting to speculate that these transcription factors share a similar role in the specification of the indeterminate reproductive meristems in distantly related species, thus being promising targets for crop improvement.

The APETALA2/Ethylene Response Factors belong to one of the largest superfamily of TFs in the plant kingdom. Based on the number of AP2/ERF domains and their sequence similarity, the members of this superfamily can be further divided into three groups: *AP2*, characterized by the presence of two AP2 domains, the *ERF*, with a single AP2 domain, and the *RAV*, which contains also a B3 DNA-binding domain. Members of this superfamily have been functionally studied in several species, including Arabidopsis, rice, and wheat (32–34).

In several plant species, a sub-group of AP2/ERF TFs has also been linked to the regulation of reproductive development (35). In Arabidopsis, for instance, *DORNRÖSCHEN, DORNRÖSCHEN-LIKE*, and *PUCHI* control floral meristem identity and organ number (36–38).

Recent transcriptomic data from wild and domesticated rice species revealed that the expression of several *AP2/ERF* genes strongly correlates with the domestication status and branching potential of the analyzed varieties, which indicates that the evolution of the ERF family was driven by artificial selection (9). Among the rice AP2/ERF transcription factors, the *PUCHI* homologous *FRIZZY PANICLE (FZP)/BRANCHED FLORETLESS1 (BFL1)* is considered one of the key regulators of SM determinacy (39–41). *FZP* expression is regulated by two AP2 genes, *SUPERNUMERARY BRACT* (*SNB*) and *OsINDETERMINATE SPIKELET1* (*OsIDS1*), which redundantly control the transition from SM to FM (42,43). Finally, *MULTI-FLORET SPIKELET1* (*MFS1*) was also found to be a regulator of spikelet meristem and flower development (44).

A similar role in the determinacy of SM branching and identity was also established for the maize AP2/ERF genes *BRANCHED SILKLESS1(BD1), INDETERMINATE SPIKELET1 (IDS1)* and *SISTER OF IDS1 (SID1)* (45,46). *IDS1* and *OsIDS1* activity is regulated with a similar mechanism, that involves the interaction with miR172 (47,48). Interestingly, an important role for AP2/miR172 in shaping the inflorescence structure has been described in different monocots and it is known that mutants in this pathway have been selected during crop domestication (49–52).

Even though the functional characterization of most of the AP2/ERF genes described suggests a role for these genes during later stages of spikelet meristem development, our comparative transcriptomic analysis highlighted the presence of a subset of AP2/ERF factors already active during the transition from indeterminate to determinate meristem. It would not be surprising to find that, overall, this gene family plays crucial roles throughout reproductive development, coordinating different steps that allow the progression of inflorescence differentiation.

The fourth family of common regulators is characterized by the presence of the MYB DNA-binding domain. MYB-containing proteins can be divided into four subfamilies, according to the type and number of repeats they contain. The R2R3-MYB subfamily is the most represented group in plants, with more than 100 identified in different species (53,54). This superfamily has been linked with the control of plant metabolism and to the response to biotic and abiotic stress in several species (55–59). A few members of this family were also found to be involved in the regulation of developmental processes such as flowering time (60,61), floral organ development (62) and shoot branching and axillary meristems formation (63).

Cereal-specific regulators

Interestingly, transcriptomic analysis of determinate and indeterminate meristems highlighted the presence of monocot-specific TF families differentially expressed between IMe and DMe. (Fig. 3 and 4B).-

Despite the knowledge that the activity of the maize RAMOSA genes is required to modulate branching (7,64), no C2H2 protein has yet been linked to this process in other species.

The C2H2 Zinc Finger proteins represent one of the largest family of transcriptional regulators in eukaryotic organisms and, in the plant kingdom, the majority of the characterized members of this family have been linked to abiotic stress response pathways (65–67).

An exception can be found in rice, where *STAMENLESS1 (SL1)* is known to be involved in flower development (68). Furthermore, two other members of this family, *EMBRYONIC FLOWER 2* (*OsEMF2)* and *ZINC FINGER PROTEIN 15* (*OsZFP15*) were shown to be specifically expressed during reproductive development, however, their function in these tissues is still unclear(69,70).
The observation that several members of this family are differentially expressed between indeterminate and determinate meristem in different cereal crops, in conjunction with the key role played by the RAMOSA3 factor in maize, suggests the possibility that a deeper analysis of the function of the C2H2 zinc finger transcription factors would uncover new mechanisms at the base of meristem identity determination and branching in these species.

From our transcriptome data analysis, a second family of zinc finger transcription factors, the *WRKY* family, was found to be differentially expressed in the comparison between indeterminate and determinate meristems in rice, maize, barley, and wheat even if the role of these genes in the regulation of plant reproductive development is still elusive.
The *WRKY* genes contain at least one repeat of the WRKY DNA-binding domain, which code for 60 highly conserved amino acidic residues, and a C2H2 or C2H2C zinc finger domain. Based on the number of WRKY domains and the structure of the zinc finger domain these proteins are divided into three different subgroups.
WRKY transcription factors have been extensively studied in the model species Arabidopsis, as well as in several agronomic relevant crops, since they are considered to be key regulators of plant immunity and biotic and abiotic stress responses, but also in developmental processes such as seed development and senescence (71–77). Until now, a restricted number of *WRKY* genes have been linked to the control of agronomical relevant traits, like yield, in rice and maize (78–81).

The *NAC* genes have been extensively analyzed in barley, wheat, maize, and rice (82–86) and are considered an important target for crop improvement, as they were found to control biotic stress responses and senescence. This large family of plant-specific transcription factors has been named after the first three members characterized: *NO APICAL MERISTEM (NAM), ACTIVATION FACTOR 1* (AF1), and *CUP-SHAPED COTYLEDON 2 (CUC2)*. Besides their role in stress-related pathways, the *NAC* genes are best known for their function in specifying organ boundaries. In Arabidopsis, *CUC1*, *CUC2*, and *CUC3* are expressed in the boundary regions between the SAM and leave primordia and between the IM and FM. Furthermore, they are also found in the regions between different floral organs and in the gynoecium. Multiple *cuc* mutants display organ fusion phenotypes, with different degrees of severity (87–89).
Moving to cereals, only for the maize *NAM1*, *NAM2,* and *NAM3* genes the expression profile was analyzed and resulted to be similar to the profiles of the homologous genes in Arabidopsis (90). Notably, in rice different members of the *NAC* family were shown to be involved in shoot branching and seed size control (91–93).

In Arabidopsis, *CUC* expression is under control of miR164, which is in turn regulated by members of the *TCP* transcription factor family (94,95). It was thus not a surprise to find that also the *TCPs* are among the genes differentially expressed in cereal meristems.
These transcription factors are plant-specific and share a conserved non-canonical basic helix-loop-helix DNA binding domain. *TPC* factors are divided into two classes, according to their sequence homology, and are suggested to work antagonistically to regulate cell proliferation throughout the life cycle of plants.
The maize *BRANCHING ANGLE DEFECTIVE 1 (BAD1)* is one of the few *TCP* transcription factors with a known function in regulating inflorescence architecture. It is expressed in the inflorescence axillary meristems, where it inhibits cell division and proliferation. *bad1* mutants are characterized by an up-right tassel, with acute branching angles (96).
The *TEOSINTE BRANCHED1 (TB1)* allele has been associated with inflorescence development in several crops. *TB1* was selected during maize domestication from teosinte as a major factor involved in axillary branch regulation (97,98). The rice orthologous *OsTB1* or *FINECULM* showed to have a similar function since this

gene is negatively regulating secondary branching (99,100). The orthologous of *TB1* in barley, *INTERMEDIUM*-C (*INT-C/HvTB1*), and wheat *taTB1* were found to be involved in regulating tillering and in determining the fertility of lateral spikelets (101,102).

The last group of cereal-specific TFs is characterized by the presence of the *bHLH* domain, which is composed of 60 aa with DNA-binding and a protein-protein dimerization function. The bHLH superfamily is widespread in the animal and plant kingdom, and its members have been genome-wide identified in several crops (53,103–105), but their role in plant reproductive development is still poorly characterized. In maize, *MALE STERILITY32 (MS32)* was found to be involved in the control of male fertility (106). In the same species, *BARREN STALK1* (BA1) controls the differentiation of the aerial lateral meristems, in connection with auxin signaling (107,108). Also in rice, a member of this family, *LAX PANICLE (LAX1)*, controls axillary meristem formation (109).

PERSPECTIVE

- *Highlight the importance of the field*

Future food security will require improved crops that provide increased grain yield under less favorable environmental conditions. Thanks to the development of high-tech genomics approaches and new breeding technologies, trait development for increased environmental resilience and productivity can count on the discovery of until now unexplored information about genetic variability and gene networks controlling key aspects of plant growth. Plant performance is greatly linked to plant development, which ultimately is decided at the meristematic level. It is then fundamental to comprehend the molecular mechanisms controlling plant meristem identity and the regulation of the meristem transition from indeterminacy to determinacy to further improve yield components as flower, fruit, and seed number.

- *A summary of the current thinking*

One of the possible targets that could help to overcome the plateau in crop yield is the possibility to extend the lifespan of indeterminate meristems, thus allowing the development of more flowers and seeds. Recently extensive molecular and genetic analyses have demonstrated that transcriptional regulators, which are the focus of this review, act as master players regulating discrete developmental programs, enforcing the concept that novel morphological differences may be modulated by changes in the action of these key regulators. Genome sequences, comparative genomics, and functional data are today the tools supporting the identification of molecular hubs at the base of inflorescence differentiation in distantly related species.

- *A comment on future directions*

We are convinced that using genome-wide data analysis for the identification of conserved and cereal-specific potential regulators governing inflorescence architecture, will allow making a careful selection of the best candidates. Further analyses using mutant alleles and/or screening for natural variants, will be required to confirm the role of candidate genes in controlling yield. An extremely powerful method to create novel allelic variation is through the use of genome editing approaches (110,111). CRISP/RCas9 has been used until now mainly to introduce mutations in coding sequences for the generation of null alleles for functional studies (112) but new CRISPR technologies becoming available, like Prime editing (113), which allow also the creation of amino acid substitutions to modulate transcription factor activity or inducing cis-regulatory mutations to inflect gene function by changing the expression profile of a gene.

COMPETING INTERESTS

The authors declare that there are no competing interests associated with the manuscript.

AUTHOR CONTRIBUTIONS

V.G., F.C., and R.B produced the concept for the review and authored the manuscript. F.Z. performed the comparison of the datasets. V.G., F.C., F.Z., R.B., and M.M.K interpreted data and wrote the manuscript. All authors discussed the results and commented on the manuscript. All authors read and approved the final manuscript.

ACKNOWLEDGMENTS

We thank M. Chiara and D.S. Horner (Università degli Studi di Milano) for helpful suggestions and valuable discussions.

FUNDING

This work was supported by the Ministero dell'Istruzione, dell'Università e della Ricerca MIUR, SIR2014 MADSMEC, Proposal number RBSI14BTZR. This work was also supported by MIPAAF (Ministry of Agricultural, Food and Forestry Policies, Ministero delle Politiche Agricole, Alimentari e Forestali), Project BIOTECH-WHEADIT. The PhD fellowships F.C was supported by the Doctorate School in Molecular and Cellular Biology, Università degli Studi di Milano.

REFERENCES

1. Prusinkiewicz P, Erasmus Y, Lane B, Harder LD, Coen E. Evolution and development of inflorescence architectures. Science (80-). 2007;316(5830):1452–6.
2. Somssich M, Je B Il, Simon R, Jackson D. CLAVATA-WUSCHEL signaling in the shoot meristem. Vol. 143, Development (Cambridge). 2016.
3. Busch W, Miotk A, Ariel FD, Zhao Z, Forner J, Daum G, et al. Transcriptional control of a plant stem cell niche. Dev Cell [Internet]. 2010 May 18 [cited 2020 Feb 28];18(5):841–53. Available from: http://www.ncbi.nlm.nih.gov/pubmed/20493817
4. Prusinkiewicz P, Erasmus Y, Lane B, Harder LD, Coen E. Evolution and development of inflorescence architectures. Science (80-). 2007 Jun 8;316(5830):1452–6.
5. Mantegazza O, Gregis V, Chiara M, Selva C, Leo G, Horner DS, et al. Gene coexpression patterns during early development of the native Arabidopsis reproductive meristem: Novel candidate developmental regulators and patterns of functional redundancy. Plant J. 2014;
6. Digel B, Pankin A, von Korff M. Global transcriptome profiling of developing leaf and shoot apices reveals distinct genetic and environmental control of floral transition and inflorescence development in barley. Plant Cell. 2015;27(9):2318–34.
7. Eveland AL, Goldshmidt A, Pautler M, Morohashi K, Liseron-Monfils C, Lewis MW, et al. Regulatory modules controlling maize inflorescence architecture. Genome Res. 2014;24(3):431–43.
8. Feng N, Song G, Guan J, Chen K, Jia M, Huang D, et al. Transcriptome profiling of wheat inflorescence development from spikelet initiation to floral patterning identified stage-specific regulatory Genes. Plant Physiol. 2017;174(3):1779–94.
9. Harrop TWR, Mantegazza O, Luong AM, Béthune K, Lorieux M, Jouannic S, et al. A set of AP2-like genes is associated with inflorescence branching and architecture in domesticated rice. J Exp Bot. 2019;(July).
10. Harrop TWR, Din IU, Gregis V, Osnato M, Jouannic S, El Ene Adam H, et al. Gene expression profiling of reproductive meristem types in early rice inflorescences by laser microdissection. 2016;
11. Leiboff S, Hake S. Reconstructing the Transcriptional Ontogeny of Maize and Sorghum Supports an Inverse Hourglass Model of Inflorescence Development. Curr Biol [Internet]. 2019;29(20):3410-3419.e3. Available from: https://doi.org/10.1016/j.cub.2019.08.044
12. Lemmon ZH, Park SJ, Jiang K, Van Eck J, Schatz MC, Lippman ZB. The evolution of inflorescence diversity in the nightshades and heterochrony during meristem maturation. Genome Res. 2016;26(12):1676–86.
13. Liu H, Li G, Yang X, Kuijer HNJ, Liang W, Zhang D. Transcriptome profiling reveals phase-specific gene expression in the developing barley inflorescence. Crop J [Internet]. 2020;8(1):71–86. Available

from: https://doi.org/10.1016/j.cj.2019.04.005
14. Anwar A, Kim JK. Transgenic Breeding Approaches for Improving Abiotic Stress Tolerance: Recent Progress and Future Perspectives. Vol. 21, International journal of molecular sciences. NLM (Medline); 2020.
15. Rabara RC, Tripathi P, Rushton PJ. The potential of transcription factor-based genetic engineering in improving crop tolerance to drought. Vol. 18, OMICS A Journal of Integrative Biology. Mary Ann Liebert Inc.; 2014. p. 601–14.
16. Van Bel M, Diels T, Vancaester E, Kreft L, Botzki A, Van De Peer Y, et al. PLAZA 4.0: An integrative resource for functional, evolutionary and comparative plant genomics. Nucleic Acids Res. 2018;46(D1):D1190–6.
17. Schwarz-Sommer Z, Huijser P, Nacken W, Saedler H, Sommer H. Genetic control of flower development by homeotic genes in Antirrhinum majus. Science (80-). 1990;250(4983):931–6.
18. Arora R, Agarwal P, Ray S, Singh AK, Singh VP, Tyagi AK, et al. MADS-box gene family in rice: Genome-wide identification, organization and expression profiling during reproductive development and stress. BMC Genomics. 2007;8.
19. Parenicová L, de Folter S, Kieffer M, Horner DS, Favalli C, Busscher J, et al. Molecular and Phylogenetic Analyses of the Complete MADS-Box Transcription Factor Family in Arabidopsis: New Openings to the MADS World. Plant Cell. 2003;15:1538–51.
20. Schilling S, Kennedy A, Pan S, Jermiin LS, Melzer R. Genome-wide analysis of MIKC-type MADS-box genes in wheat: pervasive duplications, functional conservation and putative neofunctionalization. New Phytol. 2020;225(1):511–29.
21. Qiong Zhao, Allison L. Weber, Michael D. McMullen, Katherine Guill J, Doebley. MADS-box genes of maize: frequent targets of selection during domestication. Genet Res. 2012;93(1):65–75.
22. Becker A, Theißen G. The major clades of MADS-box genes and their role in the development and evolution of flowering plants. Mol Phylogenet Evol. 2003;29(3):464–89.
23. Callens C, Tucker MR, Zhang D, Wilson ZA. Dissecting the role of MADS-box genes in monocot floral development and diversity. J Exp Bot. 2018;69(10):2435–59.
24. Castelán-Muñoz N, Herrera J, Cajero-Sánchez W, Arrizubieta M, Trejo C, García-Ponce B, et al. MADS-box genes are key components of genetic regulatory networks involved in abiotic stress and plastic developmental responses in plants. Front Plant Sci. 2019;10(July).
25. Schilling S, Pan S, Kennedy A, Melzer R. MADS-box genes and crop domestication: The jack of all traits. J Exp Bot. 2018;69(7):1447–69.
26. Zhao L, Nakazawa M, Takase T, Manabe K, Kobayashi M, Seki M, et al. Overexpression of LSH1, a member of an uncharacterised gene family, causes enhanced light regulation of seedling development. Plant J [Internet]. 2004 Mar [cited 2019 Sep 27];37(5):694–706. Available from: http://www.ncbi.nlm.nih.gov/pubmed/14871309
27. Cho E, Zambryski PC. ORGAN BOUNDARY1 defines a gene expressed at the junction between the shoot apical meristem and lateral organs. Proc Natl Acad Sci U S A. 2011;108(5):2154–9.
28. Takeda S, Hanano K, Kariya A, Shimizu S, Zhao L, Matsui M, et al. CUP-SHAPED COTYLEDON1 transcription factor activates the expression of LSH4 and LSH3, two members of the ALOG gene family, in shoot organ boundary cells. Plant J. 2011;66(6):1066–77.
29. Chen F, Zhou Q, Wu L, Li F, Liu B, Zhang S, et al. Genome-wide identification and characterization of the ALOG gene family in Petunia. BMC Plant Biol. 2019;19(1):1–15.
30. Nan W, Shi S, Jeewani DC, Quan L, Shi X, Wang Z. Genome-Wide Identification and Characterization of wALOG Family Genes Involved in Branch Meristem Development of Branching Head Wheat. Genes (Basel) [Internet]. 2018 Oct 19 [cited 2019 Sep 27];9(10):510. Available from: http://www.ncbi.nlm.nih.gov/pubmed/30347757
31. Yoshida A, Sasao M, Yasuno N, Takagi K, Daimon Y, Chen R, et al. TAWAWA1, a regulator of rice inflorescence architecture, functions through the suppression of meristem phase transition. Proc Natl Acad Sci U S A. 2013;110(2):767–72.
32. Nakano T, Suzuki K, Fujimura T, Shinshi H. Genome-Wide Analysis of the ERF Gene Family in Arabidopsis and Rice. 2006;140:411–32.
33. Rashid M, Guangyuan H, Guangxiao Y, Hussain J, Xu Y. AP2/ERF transcription factor in rice: Genome-wide canvas and syntenic relationships between monocots and eudicots. Evol Bioinforma. 2012;2012(8):321–55.
34. Zhao Y, Ma R, Xu D, Bi H, Xia Z, Peng H. Genome-Wide Identification and Analysis of the AP2

Transcription Factor Gene Family in Wheat (Triticum aestivum L.). Front Plant Sci. 2019;10(October):1–13.
35. Chandler JW. Class VIIIb APETALA2 Ethylene Response Factors in Plant Development. Trends Plant Sci [Internet]. 2018;23(2):151–62. Available from: http://dx.doi.org/10.1016/j.tplants.2017.09.016
36. Chandler JW, Werr W. A phylogenetically conserved APETALA2/ETHYLENE RESPONSE FACTOR, ERF12, regulates Arabidopsis floral development. Plant Mol Biol. 2020;102(1–2):39–54.
37. Chandler JW, Werr W. DORNRÖSCHEN, DORNRÖSCHEN-LIKE, and PUCHI redundantly control floral meristem identity and organ initiation in Arabidopsis. J Exp Bot. 2017;68(13):3457–72.
38. Karim MR, Hirota A, Kwiatkowska D, Tasaka M, Aida M. A role for arabidopsis PUCHI in floral meristem identity and bract suppression. Plant Cell. 2009;21(5):1360–72.
39. Bai X, Huang Y, Mao D, Wen M, Zhang L, Xing Y. Regulatory role of FZP in the determination of panicle branching and spikelet formation in rice. Sci Rep. 2016;6(August 2015):1–11.
40. Zhu QH, Hoque MS, Dennis ES, Upadhyaya NM. Ds tagging of BRANCHED FLORETLESS 1 (BFL1) that mediates the transition from spikelet to floret meristem in rice (Oryza sativa L). BMC Plant Biol. 2003;3:1–13.
41. Komatsu M, Chujo A, Nagato Y, Shimamoto K, Kyozuka J. Frizzy panicle is required to prevent the formation of axillary meristems and to establish floral meristem identity in rice spikelets. Development. 2003;130(16):3841–50.
42. Lee DY, Lee J, Moon S, Park SY, An G. The rice heterochronic gene SUPERNUMERARY BRACT regulates the transition from spikelet meristem to floral meristem. Plant J. 2007;49(1):64–78.
43. Lee DY, An G. Two AP2 family genes, SUPERNUMERARY BRACT (SNB) and OsINDETERMINATE SPIKELET 1 (OsIDS1), synergistically control inflorescence architecture and floral meristem establishment in rice. Plant J. 2012;69(3):445–61.
44. Ren D, Li Y, Zhao F, Sang X, Shi J, Wang N, et al. MULTI-FLORET SPIKELET1, which encodes an AP2/ERF protein, determines spikelet meristem fate and sterile lemma identity in rice. Plant Physiol. 2013;162(2):872–84.
45. Chuck G, Muszynski M, Kellogg E, Hake S, Schmidt RJ. The control of spikelet meristem identity by the branched silkless1 gene in maize. Science (80-). 2002;298(5596):1238–41.
46. Chuck G, Meeley R, Hake S. Floral meristem initiation and meristem cell fate are regulated by the maize AP2 genes ids1 and sid1. Development. 2008;135(18):3013–9.
47. Chuck G, Meeley R, Irish E, Sakai H, Hake S. The maize tasselseed4 microRNA controls sex determination and meristem cell fate by targeting Tasselseed6/indeterminate spikelet1. Nat Genet. 2007;39(12):1517–21.
48. Lee YS, Lee DY, Cho LH, An G. Rice miR172 induces flowering by suppressing OsIDS1 and SNB, two AP2 genes that negatively regulate expression of Ehd1 and florigens. Rice. 2014;7(1):1–13.
49. Debernardi JM, Lin H, Chuck G, Faris JD, Dubcovsky J. microRNA172 plays a crucial role in wheat spike morphogenesis and grain threshability. Dev. 2017;144(11):1966–75.
50. Dobrovolskaya O, Pont C, Sibout R, Martinek P, Badaeva E, Murat F, et al. Frizzy panicle drives supernumerary spikelets in bread wheat. Plant Physiol. 2015;167(1):189–99.
51. Poursarebani N, Seidensticker T, Koppolu R, Trautewig C, Gawroński P, Bini F, et al. The genetic basis of composite spike form in barley and 'miracle-wheat.' Genetics. 2015;201(1):155–65.
52. Simons KJ, Fellers JP, Trick HN, Zhang Z, Tai YS, Gill BS, et al. Molecular characterization of the major wheat domestication gene Q. Genetics. 2006;172(1):547–55.
53. Feller A, MacHemer K, Braun EL, Grotewold E. Evolutionary and comparative analysis of MYB and bHLH plant transcription factors. Plant J. 2011;66(1):94–116.
54. Stracke R, Werber M, Weisshaar B. The R2R3-MYB gene family in Arabidopsis thaliana. Vol. 4, Current Opinion in Plant Biology. Elsevier Ltd; 2001. p. 447–56.
55. Ambawat S, Sharma P, Yadav NR, Yadav RC. MYB transcription factor genes as regulators for plant responses: An overview. Vol. 19, Physiology and Molecular Biology of Plants. Springer; 2013. p. 307–21.
56. Baillo EH, Kimotho RN, Zhang Z, Xu P. Transcription factors associated with abiotic and biotic stress tolerance and their potential for crops improvement. Vol. 10, Genes. MDPI AG; 2019.
57. Chen YH, Cao YY, Wang LJ, Li LM, Yang J, Zou MX. Identification of MYB transcription factor genes and their expression during abiotic stresses in maize. Biol Plant. 2018 Jun 1;62(2):222–30.
58. Dubos C, Stracke R, Grotewold E, Weisshaar B, Martin C, Lepiniec L. MYB transcription factors in

Arabidopsis. Trends Plant Sci. 2010;15(10):573–81.
59. Li C, Ng CKY, Fan LM. MYB transcription factors; active players in abiotic stress signaling. Environ Exp Bot. 2015 Jun 1;114:80–91.
60. Shi Y, Zhao X, Guo S, Dong S, Wen Y, Han Z, et al. ZmCCA1a on Chromosome 10 of Maize Delays Flowering of Arabidopsis thaliana. Front Plant Sci. 2020;11(February):1–15.
61. Zhang L, Liu G, Jia J, Zhao G, Xia C, Zhang L, et al. The wheat MYB-related transcription factor TaMYB72 promotes flowering in rice. J Integr Plant Biol. 2016;58(8):701–4.
62. Ren D, Cui Y, Hu H, Xu Q, Rao Y, Yu X, et al. AH2 encodes a MYB domain protein that determines hull fate and affects grain yield and quality in rice. Plant J. 2019;100(4):813–24.
63. Müller D, Schmitz G, Theres K. Blind homologous R2R3 Myb genes control the pattern of lateral meristem initiation in Arabidopsis. Plant Cell. 2006 Mar 1;18(3):586–97.
64. Vollbrecht E, Springer PS, Goh L, Buckler IV ES, Martienssen R. Architecture of floral branch systems in maize and related grasses. Nature. 2005;436(7054):1119–26.
65. Agarwal P, Arora R, Ray S, Singh AK, Singh VP, Takatsuji H, et al. Genome-wide identification of C2H2 zinc-finger gene family in rice and their phylogeny and expression analysis. Plant Mol Biol. 2007;65(4):467–85.
66. Faraji S, Rasouli SH, Kazemitabar SK. Genome-wide exploration of C2H2 zinc finger family in durum wheat (Triticum turgidum ssp. Durum): insights into the roles in biological processes especially stress response. BioMetals [Internet]. 2018;31(6):1019–42. Available from: https://doi.org/10.1007/s10534-018-0146-y
67. Han G, Lu C, Guo J, Qiao Z, Sui N, Qiu N. C2H2 Zinc Finger Proteins : Master Regulators of Abiotic Stress Responses in Plants. 2020;11(February):1–13.
68. Xiao H, Tang J, Li Y, Wang W, Li X, Jin L, et al. STAMENLESS 1, encoding a single C2H2 zinc finger protein, regulates floral organ identity in rice. Plant J. 2009;59(5):789–801.
69. Huang J, Wang J, Zhang H. Rice ZFP15 gene encoding for a novel C2H2-type zinc finger protein lacking DLN box, is regulated by spike development but not by abiotic stresses. Mol Biol Rep. 2005;32(3):177–83.
70. Li K, Yang J, Liu J, Du X, Wei C, Su W, et al. Cloning, characterization and tissue-specific expression of a cDNA encoding a novel EMBRYONIC FLOWER 2 gene (OsEMF2) in Oryza sativa. DNA Seq - J DNA Seq Mapp. 2006;17(1):74–8.
71. Bakshi M, Oelmüller R. Wrky transcription factors jack of many trades in plants. Plant Signal Behav. 2014;9(FEB):1–18.
72. Gupta S, Mishra VK, Kumari S, Raavi, Chand R, Varadwaj PK. Deciphering genome-wide WRKY gene family of Triticum aestivum L. and their functional role in response to Abiotic stress. Genes and Genomics [Internet]. 2019;41(1):79–94. Available from: http://dx.doi.org/10.1007/s13258-018-0742-9
73. Jiang J, Ma S, Ye N, Jiang M, Cao J, Zhang J. WRKY transcription factors in plant responses to stresses. J Integr Plant Biol. 2017;59(2):86–101.
74. Ning P, Liu C, Kang J, Lv J. Genome-wide analysis of WRKY transcription factors in wheat (Triticum aestivum L.) and differential expression under water deficit condition. PeerJ. 2017;2017(5):1–24.
75. Rushton PJ, Somssich IE, Ringler P, Shen QJ. WRKY transcription factors. Trends Plant Sci [Internet]. 2010;15(5):247–58. Available from: http://dx.doi.org/10.1016/j.tplants.2010.02.006
76. Satapathy L, Kumar D, Kumar M, Mukhopadhyay K. Functional and DNA–protein binding studies of WRKY transcription factors and their expression analysis in response to biotic and abiotic stress in wheat (Triticum aestivum L.). 3 Biotech [Internet]. 2018;8(1). Available from: https://doi.org/10.1007/s13205-017-1064-3
77. Wei KF, Chen J, Chen YF, Wu LJ, Xie DX. Molecular phylogenetic and expression analysis of the complete WRKY transcription factor family in maize. DNA Res. 2012;19(2):153–64.
78. Jang S, Li HY. Overexpression of OsAP2 and OSWRKY24 in arabidopsis results in reduction of plant size. Plant Biotechnol. 2018;35(3):273–9.
79. Qin Z, Lv H, Zhu X, Meng C, Quan T, Wang M, et al. Ectopic Expression of a Wheat WRKY Transcription Factor Gene TaWRKY71-1 Results in Hyponastic Leaves in Arabidopsis thaliana. PLoS One. 2013;8(5).
80. Tian X, Li X, Zhou W, Ren Y, Wang Z, Liu Z, et al. Transcription factor OsWRKY53 positively regulates brassinosteroid signaling and plant architecture. Plant Physiol. 2017;175(3):1337–49.

81. Zhang CQ, Xu Y, Lu Y, Yu HX, Gu MH, Liu QQ. The WRKY transcription factor OsWRKY78 regulates stem elongation and seed development in rice. Planta. 2011;234(3):541–54.
82. Borrill P, Harrington SA, Uauy C. Genome-Wide sequence and expression analysis of the NAC transcription factor family in polyploid wheat. G3 Genes, Genomes, Genet. 2017;7(9):3019–29.
83. Murozuka E, Massange-Sánchez JA, Nielsen K, Gregersen PL, Braumann I. Genome wide characterization of barley NAC transcription factors enables the identification of grain-specific transcription factors exclusive for the Poaceae family of monocotyledonous plants. PLoS One. 2018;13(12):1–28.
84. Nuruzzaman M, Manimekalai R, Sharoni AM, Satoh K, Kondoh H, Ooka H, et al. Genome-wide analysis of NAC transcription factor family in rice. Gene [Internet]. 2010;465(1–2):30–44. Available from: http://dx.doi.org/10.1016/j.gene.2010.06.008
85. Ooka H, Satoh K, Doi K, Nagata T, Otomo Y, Murakami K, et al. Comprehensive Analysis of NAC Family Genes in Oryza sativa and Arabidopsis thaliana. DNA Res. 2003;10(6):239–47.
86. Shiriga K, Sharma R, Kumar K, Yadav SK, Hossain F, Thirunavukkarasu N. Genome-wide identification and expression pattern of drought-responsive members of the NAC family in maize. Meta Gene [Internet]. 2014;2(1):407–17. Available from: http://dx.doi.org/10.1016/j.mgene.2014.05.001
87. Cucinotta M, Manrique S, Cuesta C, Benkova E, Novak O, Colombo L. CUP-SHAPED COTYLEDON1 (CUC1) and CUC2 regulate cytokinin homeostasis to determine ovule number in Arabidopsis. J Exp Bot. 2018;69(21):5169–76.
88. Gonçalves B, Hasson A, Belcram K, Cortizo M, Morin H, Nikovics K, et al. A conserved role for CUP-SHAPED COTYLEDON genes during ovule development. Plant J. 2015;83(4):732–42.
89. Takada S, Hibara KI, Ishida T, Tasaka M. The CUP-SHAPED COTYLEDON1 gene of Arabidopsis regulates shoot apical meristem formation. Development. 2001;128(7):1127–35.
90. Zimmermann R, Werr W. Pattern formation in the monocot embryo as revealed by NAM and CUC3 orthologues from Zea mays L. Plant Mol Biol. 2005;58(5):669–85.
91. Chen X, Lu S, Wang Y, Zhang X, Lv B, Luo L, et al. OsNAC2 encoding a NAC transcription factor that affects plant height through mediating the gibberellic acid pathway in rice. Plant J. 2015;82(2):302–14.
92. Mao C, Ding W, Wu Y, Yu J, He X, Shou H, et al. Overexpression of a NAC-domain protein promotes shoot branching in rice. New Phytol. 2007;176(2):288–98.
93. Mathew IE, Das S, Mahto A, Agarwal P. Three rice NAC transcription factors heteromerize and are associated with seed size. Front Plant Sci. 2016;7(November 2016):1–16.
94. Koyama T, Mitsuda N, Seki M, Shinozaki K, Ohme-Takagi M. TCP transcription factors regulate the activities of ASYMMETRIC LEAVES1 and miR164, as well as the auxin response, during differentiation of leaves in Arabidopsis. Plant Cell. 2010;22(11):3574–88.
95. Uberti-Manassero NG, Lucero LE, Viola IL, Vegetti AC, Gonzalez DH. The class i protein AtTCP15 modulates plant development through a pathway that overlaps with the one affected by CIN-like TCP proteins. J Exp Bot. 2012;63(2):809–23.
96. Bai F, Reinheimer R, Durantini D, Kellogg EA, Schmidt RJ. TCP transcription factor, BRANCH ANGLE DEFECTIVE 1 (BAD1), is required for normal tassel branch angle formation in maize. Proc Natl Acad Sci U S A. 2012;109(30):12225–30.
97. Doebley J, Stec A, Hubbard L. The evolution of apical dominance in maize. Nature. 1997;386(6624):485–8.
98. Hubbard L, Mcsteen P, Doebley J, Hake S. Expression Patterns and Mutant Phenotype of. 2002;1(December):1927–35.
99. Takeda T, Suwa Y, Suzuki M, Kitano H, Ueguchi-Tanaka M, Ashikari M, et al. The OsTB1 gene negatively regulates lateral branching in rice. Plant J. 2003;33(3):513–20.
100. Yano K, Ookawa T, Aya K, Ochiai Y, Hirasawa T, Ebitani T, et al. Isolation of a novel lodging resistance QTL gene involved in strigolactone signaling and its pyramiding with a QTL gene involved in another mechanism. Mol Plant [Internet]. 2015;8(2):303–14. Available from: http://dx.doi.org/10.1016/j.molp.2014.10.009
101. Dixon LE, Greenwood JR, Bencivenga S, Zhang P, Cockram J, Mellers G, et al. TEOSINTE BRANCHED1 regulates inflorescence architecture and development in bread wheat (Triticum aestivum). Plant Cell. 2018;30(3).
102. Ramsay L, Comadran J, Druka A, Marshall DF, Thomas WTB, MacAulay M, et al.

INTERMEDIUM-C, a modifier of lateral spikelet fertility in barley, is an ortholog of the maize domestication gene TEOSINTE BRANCHED 1. Nat Genet. 2011;43(2):169–72.
103. Carretero-Paulet L, Galstyan A, Roig-Villanova I, Martínez-García JF, Bilbao-Castro JR, Robertson DL. Genome-wide classification and evolutionary analysis of the bHLH family of transcription factors in Arabidopsis, poplar, rice, moss, and algae. Plant Physiol. 2010;153(3):1398–412.
104. Li X, Duan X, Jiang H, Sun Y, Tang Y, Yuan Z, et al. Genome-wide analysis of basic/helix-loop-helix transcription factor family in rice and Arabidopsis. Plant Physiol. 2006 Aug;141(4):1167–84.
105. Wei K, Chen H. Comparative functional genomics analysis of bHLH gene family in rice, maize and wheat. BMC Plant Biol. 2018;18(1):1–21.
106. Moon J, Skibbe D, Timofejeva L, Wang CJR, Kelliher T, Kremling K, et al. Regulation of cell divisions and differentiation by MALE STERILITY32 is required for anther development in maize. Plant J. 2013 Nov 5;76(4):592–602.
107. Gallavotti A, Zhao Q, Kyozuka J, Meeley RB, Ritter MK, Doebley JF, et al. The role of barren stalk1 in the architecture of maize. Nature. 2004 Dec 2;432(7017):630–5.
108. Galli M, Gallavotti A. Expanding the Regulatory Network for Meristem Size in Plants. Trends Genet [Internet]. 2016;32(6):372–83. Available from: http://dx.doi.org/10.1016/j.tig.2016.04.001
109. Komatsu K, Maekawa M, Ujiie S, Satake Y, Furutani I, Okamoto H, et al. LAX and SPA: Major regulators of shoot branching in rice. Proc Natl Acad Sci U S A. 2003 Sep 30;100(20):11765–70.
110. Doudna JA, Charpentier E. The new frontier of genome engineering with CRISPR-Cas9. Vol. 346, Science. American Association for the Advancement of Science; 2014.
111. Hsu PD, Lander ES, Zhang F. Development and applications of CRISPR-Cas9 for genome engineering. Vol. 157, Cell. Cell Press; 2014. p. 1262–78.
112. Belhaj K, Chaparro-Garcia A, Kamoun S, Patron NJ, Nekrasov V. Editing plant genomes with CRISPR/Cas9. Vol. 32, Current Opinion in Biotechnology. Elsevier Ltd; 2015. p. 76–84.
113. Anzalone A V., Randolph PB, Davis JR, Sousa AA, Koblan LW, Levy JM, et al. Search-and-replace genome editing without double-strand breaks or donor DNA. Nature. 2019 Dec 5;576(7785):149–57.

***BPC* transcription factors and a Polycomb Group protein confine the expression of the ovule identity gene *SEEDSTICK* in Arabidopsis.**

Petrella R [1], **Caselli F** [1], Roig-Villanova I [2], Vignati V [1], Chiara M [1], Ezquer I [1], Tadini L [1], Kater, M M [1], and Gregis V [1]

[1] Dipartimento di Bioscienze, Università degli Studi di Milano, Milan, Italy

[2] Department of Agri-Food Engineering and Biotechnology, Barcelona School of Agricultural Engineering, UPC. Esteve Terrades 8, Building 4, 08860 Castelldefels, Spain.

January 2020; Plant J. 102(3):582-599; doi: https://doi.org/10.1111/tpj.14673

In this paper, the molecular mechanisms that drive transcription regulation of STK expression was investigated and, for the first time, the involvement of a super protein complex, in which BPCs, MADS domain factors and PRC factors can act for the regulation of STK, was described.

I contributed to this paper by performing the protein-protein yeast-two-hybrid analysis between the different BPCs classes and between BPCs and SVP.

BPC transcription factors and a Polycomb Group protein confine the expression of the ovule identity gene *SEEDSTICK* in *Arabidodpsis*

Rosanna Petrella[1], Francesca Caselli[1], Irma Roig-Villanova[1,2], Valentina Vignati[1], Matteo Chiara[1], Ignacio Ezquer[1], Luca Tadini[1], Martin M. Kater[1], Veronica Gregis[1*]

[1] Università Degli Studi di Milano, Dipartimento di Bioscienze. Via Celoria 26, 20133, Milan, Italy.

[2] Department of Agri-Food Engineering and Biotechnology, Barcelona School of Agricultural Engineering, UPC. Esteve Terrades 8, Building 4, 08860 Castelldefels, Spain.

Contact information: [*]Email of corresponding author Veronica Gregis: veronica.gregis@unimi.it

Running title: BPCs, SVP and LHP1 confine *STK* expression

Keywords: MADS-box, BPCs, homeotic genes, STK, LHP1, PRC, *Arabidopsis thaliana*, transcription factors

Summary

The BASIC PENTACYSTEINE (BPC) GAGA (C-box) binding proteins belong to a small plant transcription factor family. We previously reported that BPCs of class I bind directly to C-boxes in the *SEEDSTICK (STK)* promoter and the mutagenesis of these *cis*-elements affects *STK* expression in the flower. The MADS-domain factor SHORT VEGETATIVE PHASE (SVP) is another key regulator of *STK*. Direct binding of SVP to CArG-boxes in the *STK* promoter are required to repress its expression during the first stages of flower development. Here we show that BPCs of class II directly interact with SVP and that MADS-domain binding sites in the *STK* promoter region are important for the correct spatial and temporal expression of this homeotic gene. Furthermore, we show that BPCs of class I and II act redundantly to repress *STK* expression in the flower, most likely by recruiting TERMINAL FLOWER 2/LIKE HETEROCHROMATIN PROTEIN 1 (TFL2/LHP1) and mediating the establishment and the maintenance of H3K27me3 repressive marks on the DNA. We investigate the role of LHP1 in the regulation of *STK* expression. Besides providing a better understanding of the role of BPC transcription factors in the regulation of S*TK* expression, our results suggest the existence of a more general regulatory complex composed of BPCs, MADS-domain factors and PRCs, that cooperate to regulate gene expression in reproductive tissues. We believe that our data along with the molecular model herein described could provide significant insights for a more comprehensive understanding of gene regulation in plants.

Introduction

Transcription factors (TFs) are regulators of gene expression; they act at multiple levels to orchestrate developmental processes. TFs bind specific DNA sequences and they can cooperate through genetic and epigenetic mechanisms. TFs act in multimeric complexes that can include members of different TFs families and other proteins. The composition of these complexes determines their binding specificity and their activity on target gene regulation (Martinez and Rao, 2012). Although in the last decades different classes of plant TFs have been characterised, the molecular mechanisms by which they act and the complexes they are part of, are yet to be fully understood. Recently, a new class of transcription factors, named BASIC PENTACYSTEINE/ BARLEY B RECOMBINANT (BPC/BBR), has been identified (Santi et al., 2003). BPCs bind the RGARAGRRA consensus site, also called GAGA or C-box, to regulate their target genes (Meister et al., 2004; Kooiker et al., 2005; Simonini et al., 2012; Simonini and Kater, 2014; Hecker et al., 2015; Mu et al., 2017; Shanks et al., 2018; Theune et al., 2019; Roscoe et al., 2019; Wu et al., 2019). BPCs have been described in different plant species including monocots (*Oryza sativa* (rice) and *Hordeum vulgare* (barley)) and dicots (*Glycine max* (soy-bean) and *Arabidopsis thaliana)* (Sangwan and O'Brian, 2002; Santi et al., 2003; Kooiker et al., 2005; Monfared et al., 2011; Berger and Dubreucq, 2012; Simonini et al., 2012; Simonini and Kater, 2014; Hecker et al., 2015; Mu et al., 2017; Xiao et al., 2017; Shanks et al., 2018; Theune et al., 2019; Roscoe et al., 2019; Wu et al., 2019). In Arabidopsis, *BPCs* are divided into three subfamilies: class I (containing *BPC1* to *BPC3*), class II (containing *BPC4* to *BPC6*), and class III (containing only *BPC7*) (Meister et al., 2004; Monfared et al., 2011). Except for *BPC5*, which is a pseudogene, all the other *BPCs* are ubiquitously expressed. Combinations of multiple *bpc* mutants show strong phenotypes with a wide range of defects, addressing an important role during plant development (Monfared et al., 2011).

Previously, we have identified the MADS-box gene *SEEDSTICK (STK)* as a direct target of BPCs belonging to the class I (Kooiker et al., 2005; Simonini et al., 2012). *STK* is specifically expressed during ovule and seed development and has a wide range of functions in these tissues (Favaro et al., 2003; Pinyopich et al., 2003; Brambilla et al., 2007; Losa et al., 2010; Mizzotti et al., 2014; Mendes et al., 2016; Balanzà et al., 2016; Ezquer et al., 2016; Herrera-Ubaldo et al., 2019).

During carpel development, *STK* expression is confined to placental tissues and ovule primordia; in mature ovules, it is expressed strongly in the funiculus and in integuments that will later form the seed coat (Mizzotti et al., 2014). *STK* acts redundantly with two other MADS-box factors named

SHATTERPROOF 1 (*SHP1*) and *SHATTERPROOF 2* (*SHP2*) in the determination of ovule identity (Favaro et al., 2003; Pinyopich et al., 2003). BPCs of class I form homo- and hetero-dimers and bind C-boxes in the promoter of *STK* inducing DNA loop formation (Kooiker et al., 2005). C-boxes are important for *STK* regulation since mutations in these sequences result in the ectopic expression of the homeotic gene in the flower (Kooiker et al., 2005; Simonini and Kater, 2014). The MADS-domain factor SHORT VEGETATIVE PHASE (SVP) is another key regulator of *STK.* SVP acts redundantly with APELATA1 (AP1) and AGAMOUS-LIKE24 (AGL24) to repress *STK* expression during early stages of flower development, by binding directly to its promoter (Simonini et al., 2012; Gregis et al., 2013). Furthermore, BPCs of class I and SVP directly interact to repress *STK* expression in the floral meristem, and C-boxes are important to facilitate the binding of SVP to the *STK* promoter region (Simonini et al., 2012).

Recently, members of the BPCs family have been shown to be implicated in the recruitment of histone-modifying complexes that can inactivate gene expression, like the Polycomb Repressive Complexes (PRCs) (Hecker et al., 2015; Mu et al., 2017; Xiao et al., 2017; Roscoe et al., 2019; Wu et al., 2019). BPCs of class II directly interact with LHP1, a component of plant PRC1 that is associated with genes marked by trimethylation of histone H3 lysine 27 (H3K27me3) (Hecker et al., 2015). Furthermore, LHP1 also acts as a component of PRC2 to establish H3K27me3 and has a role in maintaining this mark at PRC2 target genes (Zhang et al., 2007b; Derkacheva et al., 2013; Wang et al., 2016). Interestingly, it was demonstrated that SVP can form heterodimers with LHP1 to modulate H3K27me3 deposition on the *SEPALLATA3* (*SEP3*) locus (Liu et al., 2009). Furthermore, BPCs can physically interact with the PRC2 subunit SWINGER (SWN) to repress the expression of their target *ABSCISIC ACID INSENSITIVE4 (ABI4)* during root development by the trimethylation of Histone H3 Lysine 27 (Mu et al., 2017); moreover a close proximity of BPC6 with VERNALIZATION2 (VRN2) has been reported (Hecker et al., 2015).

Here we clarify the molecular mechanisms by which BPCs of class II and SVP act in the regulation of *STK* expression. We show that MADS-domain binding sequences in the *STK* promoter region are important for the correct spatial and temporal expression of the ovule identity gene. Our data indicate that both BPCs of class I and II redundantly control the expression of *STK*, by modulating the deposition and/or the maintenance of H3K27me3 marks. Our results provide insights into the molecular mechanisms that drive transcription regulation in plants and investigate the involvement of a protein complex in which BPCs, MADS-domain factors and LHP1 can cooperate to orchestrate the expression of homeotic genes during plant development.

Results

STK is deregulated during flower development in the *bpc1-2 bpc2 bpc3 bpc4 bpc6* mutant

To gain more insights into the role of class I and class II BPCs in the regulation of *STK* expression during flower development we generated the *bpc1-2 bpc2 bpc3 bpc4 bpc6* quintuple mutant (henceforth called *bpcV*). In contrast with the previously published quintuple mutant, this mutant includes the *bpc1-2* allele which leads to a complete knock-out of the gene (Monfared et al., 2011; Simonini and Kater, 2014). The contribution of class I and II BPCs to the correct regulation of *STK* was analysed by *in-situ* hybridisation assays (Figure 1). In wild-type plants, *STK* expression was confined to ovules and the placenta and was never observed in flowers before stage 8 neither in inflorescences nor in floral meristems (Figure 1a, b). The knock-out of all the BPCs of class I (Figure 1c, d) or class II (Figure 1e, f) did not affect *STK* expression in the flower. In contrast, in the *bpcV* mutant the expression of *STK* was not only observed in ovules and placenta, but also in floral meristems, young flowers and developing petals (Figure 1h). *STK* expression was also detectable in flower organ primordia (Figure 1g). The *in-situ* hybridisation controls, using a H4 gene- specific probe (confirming the integrity of the tissue) and a *STK* sense probe (Figure S1; Fobert et al., 1994; Favaro et al., 2003), were performed to confirm the *in-situ* data. These results clearly demonstrated the redundant role that class I and II BPCs have in the regulation of *STK* expression during flower development.

Phenotypical characterization of the *bpcV* mutant and *35S:STK* lines

To further investigate the role of BPCs in plant development, we performed a phenotypical analysis of the *bpcV* mutant. The quintuple mutant plants were shorter when compared to wild-type plants and were characterized by both vegetative and reproductive defects (Figure 2a, b and Figure S2b and c). The knockout of the five BPC genes caused a drastic phenotype in the siliques. In wild-type, upon successful fertilization, from 3 to 12 days after pollination (dap), the siliques elongate to reach their maximum length. In contrast, in the *bpcV* mutant no silique elongation was registered (Figure 2b). As also pointed out in Monfared et al. (2011), these results suggest that BPCs are involved in different aspects of plant development.

To analyse the phenotypic effects of the deregulation of *STK* and to compare them with the phenotypes observed in the *bpcV* mutant, we transformed wild-type plants with a chimeric gene

construct in which the CDS of *STK* was fused to the Cauliflower mosaic virus (CaMV) 35S promoter (Favaro et al., 2003). *STK* expression was analysed by quantitative Real-Time PCR in three lines, where we could detect statistically significant upregulation of *STK* expression (Figure S2a). The line that showed the highest upregulation (henceforth called *35S:*STK) was propagated and in the next generations used for further analysis. Intriguingly, also this plant was shorter compared to the wild-type (Figure 2a) and showed defects that phenocopy the *bpcV* mutant, including the silique phenotype (Figure 2b) which is consistent with an upregulation of *STK* in the *BPCV* mutant.

The MADS-domain factor *STK* is a master player in ovules and seeds development (Favaro et al., 2003; Pinyopich et al., 2003; Mizzotti et al., 2014; Ezquer et al., 2016).

To determine whether the constitutive expression of *STK* affected seed development, seed area was analysed in *35S:STK* plants and *bpcV* mutants. As a control, wild-type, *stk* and *arf2-8* seeds were used. Our results confirmed that *stk* had smaller seeds, as previously reported by Pinyopich et al. (2003) whereas *arf2-8* seeds were larger (Schruff et al., 2006). Interestingly, both *bpcV* and *35S:*STK plants showed a wider seed area when compared to the wild-type and the *stk* mutant, even though *bpcV* mutant seeds were larger than those of *35S:STK* (Figure 2c). Our results support the hypothesis that BPCs regulate *STK* expression in the gynoecium and in seeds.

BPCs of class II interact with SVP

Previously, we have shown that class I BPCs act together with SVP in the control of *STK* expression (Simonini et al., 2012). The *in-situ* analysis (Figure 1) suggests that BPCs of class II have an important role in regulating *STK* expression. To understand whether BPCs of class II (BPC4 and BPC6) interact with SVP, different protein interaction assays were performed.

We confirmed by yeast two-hybrid assays and bimolecular fluorescence complementation assays (BiFC) in tobacco leaves (*Nicotiana benthamiana*) that BPC4 and BPC6 can form homo- and heterodimers (Wanke et al., 2011; Figure S3a, c). Furthermore. we showed, using yeast two-hybrid assays, that both BPC4 and BPC6 can interact with SVP (Figure 3a). To confirm the interactions between SVP and the BPC4 and BPC6 factors, a co-Immunoprecipitation (Co-IP) assay was performed, using SVP-GFP in combination with BPC4-RFP and BPC6-RFP fusion proteins, transiently co-expressed under the control of the Cauliflower mosaic virus (CaMV) promoter in *Nicotiana benthamiana* leaves. These Co-IP experiments all revealed co-precipitation of the BPC and SVP

proteins, respectively (Figures 3b and Figure S3b), suggesting that BPC4 and BPC6 are able to interact with SVP *in vivo*.

Further validation of these results *in planta* was obtained by BiFC assays in tobacco (*Nicotiana benthamiana*) leaves. The combination SVP-YFP^N BPC4-YFP^C showed a clear nuclear interaction between BPC4 and SVP (Figure 3c). All the other combinations that were tested (BPC4-YFP^N SVP-YFP^C, SVP-YFP^N BPC6-YFP^C, BPC6-YFP^N SVP-YFP^C) resulted in an interaction in the cytoplasm (Figure 3c, all the control experiments are reported in Figure S3-S5). Although this result was unexpected, Immink et al. (2002) previously showed that some MADS-domain proteins need to dimerise with another MADS-domain factor for their nuclear localisation. SVP interacts with the MADS-domain protein AP1 during floral development and therefore it might facilitate the nuclear location of SVP-BPC dimers (Pelaz et al., 2002; de Folter et al., 2005). To test this hypothesis, we co-expressed SVP-BPC4 and SVP-BPC6 dimers with an AP1-RFP fusion protein in tobacco leaves. As shown in Figure 3d, the presence of AP1 facilitates the nuclear localisation of the BPC4-SVP and BPC6-SVP dimers. To determine whether BPCs of class II could directly interact with AP1, a BIFC interaction assay was performed which showed no interaction between BPCs of class II and AP1, as reported in Figure S3c. Taken together these results clearly show that AP1 is sufficient for the translocation of class II BPCs-SVP heterodimers to the nucleus.

Finally, we also analysed the subcellular localization of BPC4/6-RFP, SVP-GFP and AP1-RFP in tobacco leaves (*Nicotiana benthamiana*). As shown in Figure S4b, BPC4, BPC6 and AP1 all localized in the nuclei whereas SVP localization was registered in the cytoplasm as well, suggesting that in the BiFC assays described above, SVP is in most combinations tested the critical factor for cytoplasmatic localization.

Molecular mechanism of SVP-class I BPCs binding to the regulatory region of *STK*

To clarify the mechanism by which BPCs and SVP interact with the *STK* regulatory region, we performed a series of Chromatin Immunoprecipitation (ChIP) experiments in different mutant backgrounds.

As shown in Figure 4a, SVP binds CArG-boxes that are surrounded by C-boxes in the regulatory region of *STK*. As previously shown, SVP, AP1 and AGL24 redundantly determine the identity of the floral meristem through direct repression of floral homeotic genes (Gregis et al., 2006; Gregis et al.,

2008; Gregis et al., 2009). In fact, in the *svp agl24 ap1-12* triple mutant, *STK* is ectopically expressed in floral meristems and young flowers (Simonini et al., 2012). To determine whether SVP, AP1 and AGL24 are required for BPCs binding to the promoter of *STK*, three independent ChIP assays using specific antibodies against class I BPCs were performed. The experiments were conducted using *svp agl24 ap1-12* triple mutant inflorescences. Furthermore, inflorescences from wild-type and *bpc1-2 bpc2 bpc3* triple mutant plants were used as a positive and negative control, respectively. In our ChIP experiments, no enrichment was detected in the *svp agl24 ap1-12* triple mutant in the region containing C-box 12 and the region containing C-box 4 and 5 (region B) (Figure 4b). These results demonstrate that SVP, AP1 and AGL24 are necessary for the binding of class I BPCs to the *STK* promoter.

Subsequently, the role of class I and class II BPCs in the binding of SVP to the promoter of *STK* was investigated by crossing the *bpcV* mutant, described above, with *pSVP*:SVP-GFP *svp* plants. In subsequent generations, plants homozygous for the *svp* and *bpc1-2 bpc2 bpc3 bpc4 bpc6* mutations containing the *pSVP:*SVP-GFP construct were selected. ChIP experiments using commercial antibodies against GFP were performed. Inflorescences from *pSVP*:SVP-GFP *svp* plants were used as a positive control, whereas wild-type was used as a negative control. An enrichment was detected when binding to the consensus regions for SVP was tested in the *bpcV* mutant background (Figure 4c). These results suggest that BPCs of class I and class II are not necessary for SVP binding to *STK* promoter.

Taken together, the results obtained by these ChIP assays are consistent with a model where SVP binds the *STK* promoter independently of BPCs, whereas BPCs of class I require MADS-domain factors for the correct binding to the *STK* regulatory region.

CArG-boxes drive the correct temporal and spatial expression of *STK* and are important for SVP and BPCs of class I binding to the promoter of *STK*

To further characterise the role of SVP in *STK* regulation, we decided to perform a functional characterisation of the CArG-boxes contained in *STK* regulatory region; these regions were identified based on the MADS-domain factor consensus binding sequences located in the *STK* locus where SVP binding was detected by ChIP-seq (Gregis et al., 2013). Considering our previous experiments using a *STK* promoter with mutated C-boxes or CArG-boxes (Simonini et al., 2012; Mendes et al., 2016), we suspected that the 12 CArG-boxes in the regulatory region of *STK* could be redundant. Therefore,

a mutated version of the *STK* promoter was used in which 11 out of the 12 CArG-boxes were altered, considering the following criteria: (i) preserving the DNA conformation, introducing only 4 to 5 transitions to each consensus; (ii) avoiding the mutation of C-boxes; (iii) preventing the formation of new CArG-boxes (see Table S1). The mutagenized *STK* promoter was fused to the *uidA* reporter gene that encodes for beta-glucuronidase (GUS) and the resulting *pSTK_CArGm*:GUS construct was used to transform Arabidopsis wild-type plants and *pSVP*:SVP-GFP *svp* plants. As a positive control, the wild-type *STK* promoter (*pSTK_CArGwt*:GUS), which drives specific expression in the placenta and all stages of ovule development, was used (Figure 5a). Out of the 39 plants transformed with the *pSTK_CArGwt*:GUS construct, 36 showed a correct spatial and temporal expression of the GUS reporter, reflecting the endogenous expression of *STK* (Figure 5b-d), whereas the other three plants did not show any GUS activity. In contrast, out of 41 plants transformed with the *pSTK_CArGm*:GUS construct, two plants did not show any GUS activity, whereas 14 (36%) showed strong deregulation of GUS expression while the remaining 64% showed a correct expression of the reporter. Interestingly, GUS expression was extended also in the inflorescence and floral meristems (Figure 5e, f) and in all the floral organs (Figure 5f). These results support the idea that the CArG-boxes in the *STK* promoter are important for the correct expression of this MADS-box gene, although the possibility that other transcription factor binding sites (cis-elements) might be involved in the regulation of STK cannot be excluded.

To assess whether MADS-domain binding sites on the *STK* promoter are necessary for SVP binding, we performed ChIP experiments using antibodies against GFP and inflorescences of *pSVP*:SVP-GFP *svp* plants with *pSTK_CArGm*:GUS that showed deregulation of the reporter. The wild-type endogenous *STK* promoter was used as a positive control, whereas inflorescences of *pSTK_CArGm*:GUS plants without SVP:GFP served as a negative control. Specific primers were designed to discriminate between the endogenous (wild-type) and the mutagenized promoter (see Experimental procedures and Table S2). These experiments showed that no enrichment was detected when binding to the mutated region was tested (Figure 5h), which suggests that CArG-boxes in the promoter of *STK* are important for the binding of SVP.

To clarify the partial penetrance of the GUS deregulation phenotype, we investigated the binding of SVP to the mutated *STK* promoter in the *pSTK_CArGm*:GUS lines that did not show deregulation of the reporter. Interestingly, in these plants binding of SVP-GFP was still observed (Figure 5i), providing clear evidence that the presence or absence of SVP binding determined the correct spatial expression profile of *STK*.

To further investigate the role of SVP and BPCs in the regulation of *STK* expression, binding of class I BPCs to the *pSTK* promoter with the mutated CArG-boxes was tested using the *pSTK_CArGm*:GUS lines that showed deregulation of the reporter and using antibodies against BPCs. As a positive control, the endogenous region of the *STK* promoter was used, whereas as negative control antibodies against HA were used. No enrichment was detected when BPCs binding to the mutated region was tested, suggesting that mutagenesis of CArG-boxes abolished BPCs of class I binding (Figure 5l). Collectively, these results indicate that CArG-boxes are important for the correct spatiotemporal regulation of *STK* expression. Moreover, these experiments confirm that SVP binding is necessary for the recruitment of BPCs of class I to the *STK* promoter.

The expression of *STK* is influenced by epigenetic modifications

Recently, a novel role for BPCs in the regulation of target gene expression by the recruitment of PRCs, has been reported (Hecker et al., 2015; Mu et al., 2017; Xiao et al., 2017; Shanks et al., 2018; Roscoe et al., 2019; Wu et al., 2019). The presence of H3K27me3 is mainly correlated with gene silencing. However, in Arabidopsis H3K27me3 marks are also found to be enriched in genes with tissue-specific expression patterns, suggesting that this epigenetic mark is modulated in response to developmental cues (Zhang et al., 2007a). Interestingly, the locus of *STK* shows strong coverage of H3K27me3 deposition at least in seedlings (Turck et al., 2007; Lafos et al., 2011; Li et al., 2015).

To understand whether the *STK* locus was also decorated with H3K27me3 marks in reproductive tissues, we performed ChIP experiments using wild-type inflorescences. We included in these experiments also the analysis of *bpcV* inflorescences to investigate a possible role for BPCs in the deposition of H3K27me3 marks on the *STK* locus. Two regions were tested: region 1, located in the first *STK* intron, and region 2 immediately after the stop codon of the gene, as illustrated in Figure 6a. ChIP experiments were performed using specific antibodies against H3K27me3 and analysed by quantitative Real-Time PCR. The *AT2G22560* and *AGAMOUS* loci were used as a negative and positive control for H3K27me3 marks, respectively (Li et al., 2015). Our results showed that the *STK* locus was also decorated with H3K27me3 in inflorescence tissue. Interestingly, in *bpcV* mutant inflorescences, a reduction of H3K27me3 deposition was detected in both the two selected *STK* regions (Figure 6b). These results were consistent with the observed ectopic

expression of *STK* in the *bpcV* background (Figure 1g, h) and suggest an active role of BPCs in the establishment of repressive epigenetic marks.

LHP1 is involved in *STK* regulation during flower development

It was shown that SVP and BPC6 are both able to interact with the PRC1 factor LHP1 (Liu et al., 2009; Hecker et al., 2015). Furthermore, BPC6 possesses an Alanine Zipper-Like Coiled-Coil domain at the N-terminal region, which was shown to be essential for homo- or hetero-dimerization with other members of the BPC class II family as well as for the interaction with LHP1. The Alanine Zipper-Like Coiled-Coil domain is not present in class I and class III BPCs (Berger and Dubreucq, 2012; Hecker et al., 2015).

LHP1 recognises loci marked by H3K27me3 *in vivo*, acting as part of a mechanism that represses the expression of PRC2 targets (Turck et al., 2007). Furthermore, it has been recently reported that LHP1 could directly interact with several members of the PRC2 protein family (Derkacheva et al., 2013; Wang et al., 2016) to facilitate their recruitment to target genes.

Mutation of the LHP1 locus resulted in pleiotropic effects due to the deregulation of several genes during plant development (Larsson et al., 1998). To address the role of LHP1 in the regulation of *STK* during flower development, its expression was analysed in the *lhp1* mutant background by *in-situ* hybridisation (Figure 7). In line with our hypothesis, the knock-out of *LHP1* deregulated *STK* expression in the flower, showing expression in floral and inflorescence meristems, as well as in young flowers (Figure 7c) whereas the expression of *STK* in mature flowers was not altered (Figure 7d). *STK* expression was also analysed in *lhp1* inflorescences by quantitative Real-Time PCR. The MADS-box gene *STK* is upregulated in the *lhp1* mutant background, as shown in Figure 7e.

ChIP-on-chip data presented by Turck et al. (2007) suggest that LHP1 is associated to the *STK* genomic region in seedlings. To validate the high throughput data and analyse the association to the *STK* locus in reproductive tissues we performed a ChIP assay, collecting inflorescences from *pLHP1*:LHP1-GFP *lhp1* plants (Kotake et al., 2003). As previously done for H3K27me3 ChIP experiments, we tested region 1 and region 2 since they have been previously reported to be associated to LHP1 in seedlings (Turck et al., 2007). We confirmed LHP1 association to the *STK* locus

in Region 2, close to the 3'UTR of the homeotic gene (Figure 7f). Collectively, these results support a role of LHP1 in the modulation of *STK* expression in the flower.

Genome-wide analysis of BPCs and MADS-domain factor binding site locations

DNA affinity purification sequencing (DAP-seq) is a transcription factor (TF)-binding site discovery assay which combines next-generation sequencing of a genomic DNA library with affinity-purified TFs (Bartlett et al., 2017). In publicly available repository of *A. thaliana* transcription factor binding profiles (http://neomorph.salk.edu/dap_web/pages/index.php; O'Malley et al., 2016) patterns of genome-wide co-enrichment of MADS-domain and BPCs transcription binding sites were investigated. Average profiles for the two families were reconstructed by using a simple consensus method (see Experimental procedures). Overlap of genomic regions associated with DAP-seq peaks of MADS-domain and BPCs TFs families was used as a proxy to investigate possible interactions.

A highly significant over-representation of overlapping peaks (p-value hypergeometric ≤ 3.5e-4) was observed which can be considered as an indication of a possible direct interaction between MADS-domain and BPC proteins. Of note, our analysis of the complete dataset of O'Malley et al. (2016), which provides DAP-seq data for more than 500 TFs, belonging to 41 distinct transcription factor families, suggests that overall only 4 additional families of transcription factors show significant levels of overlap with DAP-seq peaks of members of the BPC family (REM, C2C2gata, SRS and Trihelix, Data S1). As outlined in Figure S6, overlap with DAP-seq peaks associated with transcription factors of the MADS-domain family accounts for 19.6% of the total number of significantly overlapped peaks. All in all, we believe that these data are consistent with a model where BPCs can interact with a restricted set of TFs families, which is not limited to- but is very likely to include members of the MADS-domain family. *In silico* prediction of enriched sequence motifs is largely concordant with this model (Figure 8). In fact, when *de-novo* reconstruction of enriched motifs is performed we observe: i) a strong enrichment in CArG-box like motifs in genomic regions that are bound by MADS-domain factors; ii) a strong enrichment of C-boxes like motifs in genomic regions associated with BPC DAP-seq peaks; iii) a strong enrichment of both type of motifs (CArG-boxes and C-boxes) when regions containing coincident DAP-seq peaks are considered.

Consistent with this model, analyses of a carefully selected collection of publicly available genome-wide binding profiles *in vivo*, as determined by ChIP-sequencing, showed highly significant levels of overlap between BPCs (BPC1 and BPC6; Xiao et al., 2017; Shanks et al., 2018) and MADS-domain

factors (SVP, SOC1, FLC and FLM; Mateos et al., 2015; Immink et al., 2012; Posé et al., 2013) in vegetative tissues. Values of overlap were varying between 18% and 36% for BPC6, whereas percentages were between 3% and 10% for BPC1 (Data S2 and Supplementary Figure S7).

To further investigate possible biological pathways regulated by MADS-BPCs complexes, genomic regions associated with overlapped MADS-domain and BPCs DAP-seq peaks were annotated by the means of the "AnnotatePeaks" program from the Homer suite (Heinz et al., 2010). A total of 519 candidate target genes was obtained, which were subjected to functional enrichment analyses using the DAVID program (Huang et al., 2009; Data S3).

Coincident MADS-BPCs and DAP-seq peaks were subsequently cross-referenced with H3K27me3 ChIP-seq peaks (Lafos et al., 2011), to gain a better insight on potential MADS-BPCs target genes that are co-regulated *in vivo*. A list of 93 candidate genes was obtained (Data S3). Interestingly, functional enrichment analysis of this set of genes resulted in a significant enrichment of transcription factor encoding genes (GO term "DNA-binding transcription factor activity") for both lists: genes associated with MADS-BPCs peaks and/or with MADS-BPCs and H3K27me3. These results support the idea that MADS-BPC-PRC complexes play a pivotal role in the regulation of master players in development as shown in Data S3.

Discussion

Our knowledge on the molecular mechanisms controlling gene expression in plants is still fragmented and needs further study. Here we used the ovule identity gene *STK*, which is specifically expressed in Arabidopsis placenta, ovules and seeds, as a model system to investigate the regulation of homeotic genes expression. Previously, we showed that the MADS-domain factors SVP, AGL24 and AP1 and the class I BPC transcription factors repress *STK* expression during early stages of flower development (Kooiker et al., 2005; Simonini et al., 2012; Gregis et al., 2013). Information concerning the role of the MADS-domain factors in *STK* regulation were derived from the analysis of the *agl24 svp ap1-12* triple mutant, whereas the role of BPC factors in *STK* regulation was mainly investigated by mutagenesis of multiple BPCs binding sites (C-boxes) in the *STK* regulatory region. Mutation of those sites caused indeed strong deregulation of *STK* during flower development, suggesting that C-boxes and therefore BPC factors are important for *STK* regulation (Simonini et al., 2012). Even though these data are very interesting, mutating cis-elements still provides indirect evidence for the

role of BPCs in *STK* regulation. This study provides now deeper insights in the interplay between Class I and II BPC proteins and MADS-domain factors in the ovule specific regulation of *STK*.

The roles of BPCs and MADS-domain factors containing complexes in the regulation of STK

We investigated the role of BPC factors in the regulation of *STK* by generating the *bpc1-2 bpc2 bpc3 bpc4 bpc6* quintuple mutant (*bpcV)*. In this mutant *STK* expression was deregulated and its transcripts were detected by *in-situ* hybridisation in the floral meristem and floral organs, confirming the importance and redundant role of BPCs, belonging to both class I and class II, in *STK* regulation. Intriguingly, ChIP experiments showed that in the *bpcV* mutant background SVP could still bind the *STK* promoter, suggesting that SVP can bind DNA independently of BPC factors. Previously, we reported that the mutagenesis of BPC binding sites (C-boxes) in the *STK* promoter affected SVP binding to the DNA. This discrepancy could not be due to the fact that nearby C-box mutations influence CArG-box affinity since control experiments ruled this option out (Simonini et al., 2012). However, we cannot exclude the possibility that mutagenesis of C-box elements in the promoter of *STK* introduced structural changes that altered the binding affinity of regulatory elements causing loss of binding of SVP or of unknown co-factors important for SVP binding to the *STK* promoter.

The *in silico* analyses, using the open-access database Jaspar (Khan et al., 2018), of the regulatory region of *STK* revealed binding motifs for different transcription factors of Arabidopsis. Interestingly, motifs recognized by HD-ZIP homeobox domain factors, C2H2 zinc finger Dof domain factors, Basic helix-loop-helix factors (bHLH), Beta-Hairpin-Ribbon AP2 MBD_like and GATA-type zinc fingers were detected. All these TFs families could indeed be part of the regulatory machinery for the correct spatiotemporal expression of *STK*. This scenario might also explain why the deregulation phenotype of the lines with the mutated *STK* promoter (*pSTK_CArGm:*GUS) was not fully penetrant (36% of the plants showed GUS expression outside the normal *STK* expression domain). The binding of the *STK* repressive complex might not only be dependent on the association of SVP with the promoter but other cofactors are expected to be involved in recruiting the complex to the DNA. In the absence of SVP binding, the interaction of the complex with the mutated *STK* promoter could be less stable and influenced by for instance fluctuations in environmental conditions.

It remains important to underline that all our experiments demonstrate that BPC and MADS-domain factors are together essential for the correct expression of *STK* and that, binding of SVP alone is not *per se* sufficient to repress *STK* expression in the floral meristems.

We previously revealed that BPCs of class I can interact with each other (Simonini et al., 2012); moreover, BPCs of class II form homo and heterodimers with members of class I (Wanke et al., 2011; Simonini et al., 2012 and Figure S3). BPC protein-protein interactions studies suggest that BPC factors of class I and II can act synergistically and redundantly to regulate the expression of their targets as we demonstrated for *STK*. An example has been provided by Mu et al. (2017), who showed that mutations in BPCs of class I and II increased *ABI4* expression in roots.

To further investigate the molecular and functional relationships between the MADS-domain factor SVP and BPCs of class II, we tested their ability to form heterodimers *in planta*. We revealed that SVP interacts with BPC4 and BPC6, but the dimers are mainly retained in the cytoplasm. An interesting observation was that the MADS-domain protein AP1, an interactor of SVP, facilitated the co-localisation of SVP-BPC4 (and BPC6) to the nucleus. These data further clarify the role of AP1 in the regulation of *STK* (Simonini et al., 2012).

The Role of BPCs during seed development

Pinyopich et al. (2003) reported that *STK* has also a role during seed development since the *stk* mutant presented smaller seeds compared to the wild-type.

In this work we found that BPCs can restrict the expression of STK in certain spatiotemporal window since in the *bpcV* mutant the expression of *STK* was extended to other tissues in floral organs. The analysis of the *35S:*STK line here presented, further explored the effects of the deregulation of *STK* throughout reproductive development. The defects in seeds size registered in the *bpcV* and *35S:*STK suggest that BPCs might control *STK* expression later during development, in seeds. The observation that in the *bpcV* mutant seeds are bigger than in *35S*:STK lines, suggests an addictive role of BPCs during seed development. It will be interesting to further investigate the role of BPCs in such an important aspect of plant development which has enormous implications in agronomical species.

BPCs of class II and SVP recruit LHP1 for the regulation of *STK*

Farkas et al. (1994) have first characterised the GAGA Associated Factor of *Drosophila melanogaster* (dGAFs). Even though GAFs and BPCs are phylogenetically unrelated, they present several similarities. BPCs can bind to (GA)n sequences (Berger and Dubreucq, 2012) to control the expression of their targets (Meister et al., 2004; Berger et al., 2011; Simonini et al., 2012; Simonini and Kater, 2014; Mu et al., 2017; Theune et al., 2019; Roscoe et al., 2019; Wu et al., 2019). They also present a highly conserved zinc finger like DNA-binding domain, similar to *Trl* of Drosophila (Wanke et al., 2011). Interestingly, cooperative binding of BPC1 proteins to GA-rich motifs in the *STK* promoter region leads to condensation and looping of DNA (Kooiker et al., 2005), similar to what has been described for dGAF from Drosophila. Recent works in Arabidopsis revealed an intriguing interaction among BPCs and Polycomb group proteins, similar to those described in animals for dGAF, which can cooperate with Polycomb Group factors (PcG) to repress gene expression (Horard et al., 2000). PcG complexes have paramount roles in cell fate determination and differentiation both in plants and in animals. These proteins have been identified in Drosophila more than 40 years ago as key repressors of homeotic genes (Hox) throughout embryonic development (Lewis, 1978). Besides, the sequences and functions of PcG genes are highly conserved between animals and plants. Several publications recently showed that BPCs can interact with proteins belonging to PRC1 and PRC2, suggesting that it could be a mechanism to repress the expression of their target genes (Wanke et al., 2011; Mu et al., 2017; Xiao et al., 2017). Our results provide further insights into the connection between BPCs and PRC members for the regulation of target genes. We suggest that BPCs of class II and SVP recruit LHP1 and act redundantly with the class I members to establish and maintain H3K27me3 repressive mark on the regulatory region of *STK* in reproductive tissue. In fact, we registered a reduction of H3K27me3 in the *bpcV* mutant. In the *lhp1* background, we detected increased levels of *STK,* moreover its expression is localized also in the inflorescences and in the floral meristems as well as in the first floral buds. In contrast to our results in the *bpcV*, no signal was detected in other floral structures at maturity, thus suggesting that BPCs of class I and II might repress *STK* expression during flower development also via other mechanisms that do not involve LHP1 activity.

Recently, several BPC targets have been discovered. Most of them are also associated with PRC mediated silencing: the KNOX gene *BREVIPEDICELLUS (BP)* is repressed by BPCs throughout flower development (Simonini et al., 2012). The expression of *BP* is directly regulated by the recruitment of the EMBRYONIC FLOWER (EMF) complex by ASYMMETRIC LEAVES 1 and 2 (AS1 and AS2), which triggers H3K27me3 deposition (Lodha et al., 2013). *BP* was also identified in our computational

analysis of regions enriched in binding sites for MADS-domain and BPC family members and resulted decorated with H3K27me3 marks (Data S3). Also, *FUS3* has recently been characterised as a BPC target (Roscoe et al., 2019; Wu et al., 2019) and already reported to be a target of PRCs (Makarevich et al., 2006; Zhang et al., 2007a; Bouyer et al., 2011; Yang et al., 2013; Xiao et al., 2017). Interestingly, our computational analysis showed that its regulatory region could also be bound by MADS-domain factors, suggesting a possible conserved mechanism for target regulation.

The MADS-domain factor SVP interacts with LHP1 and is required to recruit the PRC1 factor to the promoter of *SEPALLATA3 (SEP3)*, acting as a pioneer factor (Liu et al., 2009). In accordance to this hypothesis, H3K27me3 deposition on the *SEP3* locus is reduced in *lhp1* background.

Our ChIP assays confirm binding of LHP1 to the 3' end of *STK*, indicating a direct regulation of the homeotic gene by this factor. Interestingly, we previously reported that SVP binds the 3'UTR of many of its targets, among which *STK* (Gregis et al., 2013). Therefore, it is likely that SVP recruits LHP1 on the *STK* locus and subsequently repress the expression of the ovule identity gene via PRC2 recruitment, as previously shown for *SEP3* (Liu et al., 2009).

PRC2 components are required for H3K27me3 deposition to the target locus (Wang et al., 2016). Three different PRC2 complexes regulate plant development by targeting a subset of genes. LHP1 has been reported to associate with several PRC2 members (Derkacheva et al., 2013; Wang et al., 2016), to mediate their recruitment to the target locus. Previously was shown that the EMF complex played a role in the repression of *AGAMOUS (AG)* and *SEP3* in the flower (Yoshida et al., 2001; Kinoshita et al., 2001; Chanvivattana et al., 2004; Calonje et al., 2008). Notably, Derkacheva et al. (2013) reported that LHP1 is directly associated with the EMF complex. We previously characterised *SEP3* and *AG,* as targets of BPCs and SVP (Gregis et al., 2009; Simonini et al., 2012); as matter of fact, the upregulation of *AG* registered in the *lhp1* single mutant is increased in the *lhp1 bpc4 bpc6* triple mutant, confirming a LHP1-class II BPCs interplay in seedlings (Hecker et al., 2015).

Considering all these observations it is tempting to speculate that BPCs and SVP might regulate *STK* expression by the recruitment of LHP1. Then LHP1 as PRC1 member could interact with the EMF complex to mediate the correct deposition of the H3K27me3. Furthermore, LHP1 could assure the maintenance and the spreading of the repressor marks on the *STK* locus throughout flower development (Figure 9).

A general regulatory mechanism in plants

Understanding the molecular mechanisms through which BPCs and SVP containing complexes act, is important, since it is likely that the mechanism by which these factors regulate *STK* can be extended to many other genes during plant development. This is based on the following observations: (i) many genes contain both C-boxes and CArG-boxes in their putative promoter regions; (ii) BPCs are ubiquitously expressed in plants while MADS-domain factors are specifically expressed in all the fundamental developmental stages; and (iii) combination of *bpc* alleles showed pleiotropic phenotypes (Monfared et al., 2011). Furthermore, Berger et al. (2011) identified three cis-elements required for *LEAFY COTYLEDON2* (*LEC2*) repression: C-boxes, CArG-boxes and PRE-like elements, corroborating the idea that the understanding of the synergistic interaction between MADS-domain factors and BPCs is an important key to decode gene regulation in plants. Several key developmental factors that are worth to be tested as putative direct targets of both MADS-domain and BPC factors are reported in Data S3. In fact, they were identified in our computational analysis of regions enriched in binding sites for both MADS and BPC family members. Notably, the analyses of ChIP-seq data available for selected MADS-domain and BPCs in vegetative tissues reveal an highly significant levels of overlap of their binding profiles in vivo, which suggest a cooperative role of BPCs-MADS factors also during vegetative stages that will be interesting to investigate.

The regulatory mechanism through which BPCs act is of course not restricted to Arabidopsis. Several GAGA binding proteins have been discovered in crops and several targets have already been characterised (Sangwan and O'Brian, 2002; Santi et al., 2003; Meister et al., 2004; Gong et al., 2018). Therefore, a better understanding of the mechanisms by which these factors act in Arabidopsis may provide knowledge to be used for future crop improvement.

Experimental procedures

Plant Material and Growth Conditions

Arabidopsis thaliana ecotype Columbia was used in this study; the plants were directly sown on soil and kept under short-day conditions for 2 weeks (22°C, 8 h light and 16 h dark) and then moved to long-day conditions (22°C, 16 h light and 8 h dark). The *agl24 svp ap1-12* triple mutant and the *pSVP*:SVP-GFP *svp* line were previously described by Gregis et al. (2008; 2009); genotyping of the *bpc1-2 bpc2 bpc3 bpc4 bpc6* mutants was done according to Simonini and Kater (2014) and Monfared et al. (2011). Seeds from the *lhp1* (previously named *tfl2-1* (Larsson et al., 1998)),

arf2-8 and *stk* mutant in Columbia background were obtained from the Nottingham Arabidopsis Stock Centre.

Generation of quintuple mutants and marker lines

The *bpc 1-2 bpc2 bpc3 bpc4 bpc6* quintuple mutant was obtained by crossing the *bpc 1-2 bpc2 bpc3* triple mutant (Simonini and Kater, 2014) and *bpc4 bpc6* double mutant (Monfared et al., 2011); the *pSVP*:SVP-GFP *svp bpc1-2 bpc2 bpc3 bpc4 bpc6* was obtained crossing the line previously described by Gregis et al. (2009) and the *bpcV*.

Generation of *35S:*STK line

Arabidopsis plants were transformed with the chimeric gene construct in which the CDS of *STK* was fused to the Cauliflower mosaic virus (CaMV) 35S promoter (Favaro et al., 2003) using the *Agrobacterium tumefaciens*–mediated floral dip method (Clough and Bent, 1998). Transformant plants were sown on MS medium and selected by hygromycin (20 mg/L) resistance; presence of the construct was assessed by genotyping and analysis of *STK* expression.

***STK* promoter constructs and plant transformation**

The mutated version of the *STK* promoter (*pSTK_CArGm*) was synthesised by Twin Helix. The synthetic DNA fragment, like the wild-type version of the *STK* promoter, were cloned in pUC57-Simple (GenScript). The two fragments were digested with AccI and KpnI and cloned in pDONR207 entry clone (Invitrogen), and successively into pGWB3 binary vector containing the GUS reporter gene. Arabidopsis plants were transformed with these constructs using the *Agrobacterium tumefaciens*–mediated floral dip method (Clough and Bent, 1998). Transformant plants were sown on MS plates and selected by hygromycin (20 mg/L) resistance; presence of the construct was assessed by PCR.

GUS staining

GUS assays were performed as described previously by Liljegren et al. (2000). The samples were mounted in lactic acid and subsequently observed using a Zeiss Axiophot D1 microscope equipped with differential interference contrast optics. Images were captured on an Axiocam MRc5 camera (Zeiss) using the Axiovision program (version 4.1).

***In-situ* hybridisation assay**

Arabidopsis flowers were collected, fixed and embedded in paraffin as described by Huijser et al. (1992). Plant tissue sections were probed with *STK* antisense RNA, described in Brambilla et al. (2007); *STK*-sense and H4 histone gene were used as controls (Fobert et al., 1994). Hybridisation and immunological detection were executed as described previously by Coen et al. (1990).

ChIP assay

ChIP assays were performed as described by Gregis et al. (2009) using for SVP-GFP the commercial antibody GFP:Living Colors full-length (Clontech), and for BPCs of class I a polyclonal antibody as described by Simonini et al. (2012); HA antibody Anti-HA (Roche) were used as negative control in one of the experiments. Quantitative Real-Time PCR assays were performed to determine the enrichment of the fragments. The detection was performed in triplicate using the iQ SYBR Green Supermix (Bio-Rad) and the Bio-Rad iCycler iQ Optical System (software version 3.0a), with the primers listed in Table S2. ChIP-quantitative Real-Time PCR experiments and relative enrichments were calculated as reported by (Matias-Hernandez et al. (2010). We employed the following formulas to calculate the fold enrichment: dCT.tg = CT.i-CT.tg and dCT.nc =CT.i-CT.nc. Ct.tg is target gene mean value, Ct.i is input DNA mean value, and Ct.nc is ACTIN 7 (negative control) mean value: dCT.tg = CT.i-CT.tg and dCT.nc =CT.i-CT.nc. The propagated error values of these CTs are calculated using dSD.tg = sqrt((SD.i)^2+ (SD.tg^2)/sqrt(n) and dSD.nc = sqrt((SD.i)^2+ (SD.nc^2)/sqrt(n), n = number of replicate per sample. Fold-change over negative control was calculated finding the “delta delta CT” of the target region as follows: ddCT = dCT.tg- dCT.nc and ddSD = sqrt((dSD.tg)^2+ (dSD.nc)^2. The transformation to linear “fold-change” values is obtained as follows: FC = 2^(ddCT) and FC.error = ln(2)*ddSD*FC. All the experiments were performed in three biological replicates.

ChIP-based analysis of H3K27me3 histone modification

For ChIP-based analysis of histone modifications, the following antibodies were used for immunoprecipitation: Anti-H3K27me3 Rabbit Polyclonal Antibody (Merck 07-449) and Rabbit anti-histone H3 (Sigma-Aldrich H0164). 0,8 mg of grinded and fixed material from unfertilized flowers from wild-type and *bpcV* mutant was collected. ChIP experiments were performed in a modified version of a previously reported protocol (Mizzotti et al., 2014). The quantitative Real-Time PCR assay was conducted in triplicate on four different biological replicates, with three technical

replicates for each sample, and was performed in a Bio-Rad iCycler iQ optical system (software version 3.0a). Quantitative Real-Time PCR assays were performed on input and immunoprecipitated samples and % of input was calculated. The signal obtained after precipitation with anti-H3K27me3 antibody (as indicated in Figure 6b) was normalized to actin levels. *AGAMOUS* region was used as a reference as it carries the H3K27me3 mark (Li et al., 2015). Relative enrichment of *AT2G22560* was included as negative control for the H3K27me3 mark (Li et al., 2015). Sequences of oligonucleotides used for ChIP analyses are listed in Table S2.

Yeast two-hybrid assay

The two-hybrid assays were performed at 28°C in the yeast strain AH109 (Clontech). The coding sequences of *BPC4*, *BPC6* and *SVP* were cloned into pDONR207 (Life Technologies) and successively transferred to the Gateway vector GAL4 system (pGADT7 and pGBKT7; Clontech). Yeast two-hybrid assays were performed on selective yeast synthetic dropout medium lacking Leu, Trp, Ade, and His supplemented with different concentrations of 3-aminotriazole (1, 2.5, and 5 mM of 3-AT).

BiFC assay

The *BPC4*, *BPC6* and *SVP* coding sequences were first cloned into pDONR207 (Life Technologies) and subsequently transferred to the pYFPN43 and pYFPC43 vectors by Gateway recombination; while the *AP1* coding sequence was cloned into pDONR207 (Invitrogen) and then transferred to pB7RWG2, purchased from the Flanders Interuniversity Institute for Biotechnology (Gent, Belgium); the previously described formation of VERDANDI-VALKYRIE heterodimers was used as positive control, whereas VERDANDI-VERDANDI combination was used as negative control (Figure S4A; Mendes et al. (2016); all the controls are reported in Figures S3, S4 and S5. BiFC assays were performed injecting Agrobacterium expressing viral suppressor p19/experimental constructs as described by Belda-Palazón et al. (2012). The abaxial surfaces of infiltrated tobacco (*Nicotiana benthamiana*) leaves were imaged 3 days after inoculation.

Co-Immunoprecipitation (Co-IP) Protocol

The coding sequences of *BPC4, BPC6* and *SVP* were cloned into pDONR221 and then transferred to pB7RWG2 and pB7FWG2, both purchased from the Flanders Interuniversity Institute for Biotechnology (Gent, Belgium). *Nicotiana benthamiana* leaves were infiltrated with *Agrobacterium tumefaciens*, as previously described. 4 days after infiltration, leaf disks (16 mm

diameter) were collected and homogenised in 1 ml of immunoprecipitation (IP) buffer (30 mM HEPES-KOH pH 8.0, 200 mM NaCl, 60 mM KOAc, 10 mM MgOAc, 0,5% [v/v] Nonidet P-40 and proteinase inhibitor cocktail [cOmplete™, COEDTAF-RO, Roche]). Samples were incubated in ice for 15 min to allow membrane solubilisation and subjected to a centrifugation step (10 min at 16,000 *g*). Supernatants were incubated (2 h, at 4°C) with 20 µl RFP-Trap®_MA (ChromoTek) or GFP-Trap®_MA (ChromoTek). Beads were then washed 3 times for 10 min with 1 ml of IP buffer and eluted with Laemmli sample buffer. Protein samples were fractionated on SDS–PAGE (10% [w/v] acrylamide (Schägger and von Jagow, 1987) and then transferred to polyvinylidene difluoride (PVDF) membranes. Filters were immuno-decorated with specific antibodies; the Coomassie Brilliant Blue (CBB) staining of the gel was performed as loading control. The anti-GFP antibody was purchased from Thermo Fisher Scientific while the anti-RFP antibody was obtained from ChromoTek.

Gene expression analysis

Quantitative Real-Time PCR experiments were performed using cDNA obtained from inflorescences. Total RNA was extracted using lithium chloride. The Ambion TURBO DNA-free DNase kit was used to remove genomic DNA contaminations, according to the manufacturer's instructions (http://www.ambion.com/). The ImProm-IITM reverse transcription system (Promega) was used to retrotranscribe the treated RNA. Transcripts were detected using a Sybr Green Assay (iQ SYBR Green Supermix; Bio-Rad) using *UBIQUITIN* as a reference gene. Assays were done in in triplicate using a Bio-Rad iCycler iQ Optical System (software version 3.0a). The enrichments were calculated normalising the amount of mRNA against housekeeping gene fragments. The expression of different genes was analysed using specific oligonucleotides primers (Table S2).

Microscopy and imaging

Images of plants, cauline and rosette leaves were acquired using a Canon EOS 6D camera whereas images of siliques were taken using a Leica® MZ 6 stereomicroscope. For in-situ experiments sections were analysed using a Zeiss Axiophot D1 microscope supplied with differential interface contrast (DIC) optics and Axiocam MRc5 camera (Zeiss) using the AXIOVISION program (version 4.4).

Scanning

Seed area size were analysed by using SMART-GRAIN software. ANOVA and post-hoc Tukey HSD (honestly significant difference) test were used for wild-type versus other genotypes comparison.

Computational analyses

DAP-seq peaks data were obtained in the form of narrowpeaks files from from http://neomorph.salk.edu/dap_web/pages/index.php. Narrow-peaks files were concatenated and overlapped genomic regions were merged by the means of the bedtools merge utility. Finally, candidate binding regions showing a positive hit for the majority (that is n/2+1, if profiles for n family members were available) of the members of a family were retained to form the "consensus" family profile. ChIP-seq peaks for BPC1 (GSE84483), BPC6, SVP (GSE54881), SOC1 (GSE45846), FLC (GSE54881) and FLM (GSE48082) were retrieved directly from their respective entries in the GEO database. Data of selected MADS-box ChIP-seq were chosen based on the tissue in which the experiments were performed: seedling or vegetative tissues as for ChIP-seqs available for both BPC1 and BPC6. Intersection of peaks coordinates were performed using the bedtools intersect program (Quinlan and Hall, 2010) using default parameters; peaks with an overlap of 1 bp were considered coincident. The "-u" option was used in order to collapse peaks showing multiple overlaps. Statistical significance of overlaps was assessed by using the hyper-geometric distribution. Annotation of selected DAP-seq peaks was performed by the means of the annotatePeaks program from the Homer suite (Heinz et al., 2010) using the reference TAIR10 annotation. Identification of enriched sequence motifs and identification of closely related motifs from publicly available dataset of were performed by the means of the findMotifsGenome utility in Homer. Functional enrichment analyses were performed by using the web interface of the DAVID suite (Huang et al., 2009).

Accession numbers

Sequence data from this article can be found in the Arabidopsis Genome Initiative or GenBank/EMBL databases under the following accession numbers: *STK* (AT4G09960), *BPC1* (AT2G01930), *BPC2* (AT1G14685), *BPC3* (AT1G68120), *BPC4* (AT 2G21240), *BPC6* (AT5G42520), *AGL24* (AT4G24540), *SVP* (AT2G22540), *AP1* (AT1G69120), *LHP1* (A T5G17690), *NETWORK*
2D (AT2G22560), *AGAMOUS* (AT4G18960), *VERDANDI* (AT5G18000), *VALKYRIE* (AT2G24690), *ACTI N7* (AT5G09810) and *UBIQUITIN* (AT4G36800).

Conflict of interest

The authors declare that they have no conflicts of interest.

Funding

This work was supported by the Ministero dell'Istruzione, dell'Università e della Ricerca MIUR, SIR2014 MADSMEC, Proposal number RBSI14BTZR. The PhD fellowships of R.P and F.C were supported by the Doctorate School in Molecular and Cellular Biology, Università degli Studi di Milano. R.P. and F.C. were supported by H2020-MSCA-RISE-2015 ExpoSEED Proposal Number: 691109.

Author contributions

V.G. designed the research strategy and the experiments. V.G. and R.P. performed most of the experiments. F.C. performed yeast two-hybrid analyses. T.L. designed and performed CoIP experiments. V.V. did the expression analysis on *lhp1* by quantitative Real-Time PCR and performed bioinformatics analyses, M.C. supervised and performed bioinformatics analyses. I.R.V. obtained the *bpcV* multiple mutant. I.E. performed ChIP experiments on chromatin modifications and analysis on seed size area. V.G., R.P. and M.M.K interpreted data and wrote the manuscript. All authors discussed the results and commented on the manuscript. All authors read and approved the final manuscript.

Acknowledgments

We thank V. Borrelli, A. Ravasio, A. Piva (Università degli Studi di Milano) and S.de Folter (Centro de Investigación y de Estudios Avanzados del Instituto Politécnico Nacional, Mexico) for technical support. S. Masiero, P. Pesaresi, L. Colombo, L. Conti, L. Gianfranceschi (Università degli Studi di Milano) and R. Battaglia (CREA-GB - Fiorenzuola d'Arda PC) for helpful suggestions and valuable discussions. Part of this work was carried out at NOLIMITS, an advanced imaging facility established by the Università degli Studi di Milano.

Supporting Information

Additional Supporting Information may be found in the online version of this article.

Figure S1. *In situ* hybridisation controls.

Figure S2. Selection of *35S:*STK T1 lines and morphological analyses on *35S:*STK and *bpcV* background.

Figure S3. Yeast two-hybrid assay between BPCs of class II, Co-immunoprecipitation assays using GFP-trap and Bi-molecular fluorescence complementation (BiFC) assay between BPCs of class II, between BPCs of class II and AP1 and between BPC2 and SVP.

Figure S4. Bi-molecular fluorescence complementation (BiFC) assay positive controls and cellular localization of BPC4-RFP, BPC6-RFP, AP1-RFP and SVP-GFP.

Figure S5. Bi-molecular fluorescence complementation (BiFC) assay, negative controls.

Figure S6. Proportion of significantly overlapped DAP-Seq Peaks by TF family.

Figure S7. Venn diagrams of common ChIP-seq peaks between BPC1, BPC6 and a selection of MADS-domain TFs

Table S1. MADS-domain consensus regions identified in *STK* promoter and the designed mutated versions.

Table S2. Sequences of oligonucleotides used in this manuscript.

Data S1. p-values for the intersection of DAP-seq peaks of TFs with DAP-seq peaks of the BPCs family of transcription factors.

Data S2. p-values for the intersection of ChIP-seq peaks of a selection of MADS-domain TFs with ChIP-seq peaks of BPC1 and BPC6.

Data S3. Lists of identified genome-wide binding locations for all the MADS-box and BPCs factors, coincident DAP-seq peaks and functional enrichment analyses of associated target genes.

References

Balanzà, V., Roig-Villanova, I., Di Marzo, M., Masiero, S., and Colombo, L. (2016). Seed abscission and fruit dehiscence required for seed dispersal rely on similar genetic networks. *Development* **143**:3372–3381.

Bartlett, A., O'Malley, R. C., Huang, S. C., Galli, M., Nery, J. R., Gallavotti, A., and Ecker, J. R. (2017). Mapping genome-wide transcription-factor binding sites using DAP-seq. *Nat. Protoc.* **12**:1659–1672.

Belda-Palazón, B., Ruiz, L., Martí, E., Tárraga, S., Tiburcio, A. F., Culiáñez, F., Farràs, R., Carrasco, P., and Ferrando, A. (2012). Aminopropyltransferases Involved in Polyamine Biosynthesis Localize Preferentially in the Nucleus of Plant Cells. *PLoS One* **7**:e46907.

Berger, N., and Dubreucq, B. (2012). Evolution goes GAGA: GAGA binding proteins across kingdoms. *Biochim. Biophys. Acta - Gene Regul. Mech.* **1819**:863–868.

Berger, N., Dubreucq, B., Roudier, F., Dubos, C., and Lepiniec, L. (2011). Transcriptional regulation of Arabidopsis LEAFY COTYLEDON2 involves RLE, a cis-element that regulates trimethylation of histone H3 at lysine-27. *Plant Cell* **23**:4065–78.

Bouyer, D., Roudier, F., Heese, M., Andersen, E. D., Gey, D., Nowack, M. K., Goodrich, J., Renou, J.-P., Grini, P. E., Colot, V., et al. (2011). Polycomb Repressive Complex 2 Controls the Embryo-to-Seedling Phase Transition. *PLoS Genet.* **7**:e1002014.

Brambilla, V., Battaglia, R., Colombo, M., Masiero, S., Bencivenga, S., Kater, M. M., and Colombo, L. (2007). Genetic and Molecular Interactions between BELL1 and MADS Box Factors Support Ovule Development in Arabidopsis. *Plant Cell Online* Advance Access published 2007, doi:10.1105/tpc.107.051797.

Calonje, M., Sanchez, R., Chen, L., and Sung, Z. R. (2008). EMBRYONIC FLOWER1 Participates in Polycomb Group–Mediated *AG* Gene Silencing in *Arabidopsis*. *Plant Cell* **20**:277–291.

Chanvivattana, Y., Bishopp, A., Schubert, D., Stock, C., Moon, Y.-H., Sung, Z. R., and Goodrich, J. (2004). Interaction of Polycomb-group proteins controlling flowering in Arabidopsis. *Development* **131**:5263–76.

Clough, S. J., and Bent, A. F. (1998). Floral dip: a simplified method for Agrobacterium-mediated transformation of Arabidopsis thaliana. *Plant J.* **16**:735–43.

Coen, E. S., Romero, J. M., Doyle, S., Elliott, R., Murphy, G., and Carpenter, R. (1990). floricaula: a homeotic gene required for flower development in antirrhinum majus. *Cell* **63**:1311–22.

de Folter, S., Immink, R. G. H., Kieffer, M., Parenicová, L., Henz, S. R., Weigel, D., Busscher, M., Kooiker, M., Colombo, L., Kater, M. M., et al. (2005). Comprehensive Interaction Map of the Arabidopsis MADS Box Transcription Factors. *PLANT CELL ONLINE* **17**:1424–1433.

Derkacheva, M., Steinbach, Y., Wildhaber, T., Mozgová, I., Mahrez, W., Nanni, P., Bischof, S., Gruissem, W., and Hennig, L. (2013a). Arabidopsis MSI1 connects LHP1 to PRC2 complexes. *EMBO J.* **32**:2073–2085.

Derkacheva, M., Steinbach, Y., Wildhaber, T., Mozgová, I., Mahrez, W., Nanni, P., Bischof, S., Gruissem, W., and Hennig, L. (2013b). Arabidopsis MSI1 connects LHP1 to PRC2 complexes. *EMBO J.* **32**:2073–85.

Doughty, J., Aljabri, M., and Scott, R. J. (2014). Flavonoids and the regulation of seed size in *Arabidopsis*. *Biochem. Soc. Trans.* **42**:364–369.

Ezquer, I., Mizzotti, C., Nguema-Ona, E., Gotté, M., Beauzamy, L., Viana, V. E., Dubrulle, N., Costa de Oliveira, A., Caporali, E., Koroney, A.-S., et al. (2016). The Developmental Regulator SEEDSTICK Controls Structural and Mechanical Properties of the Arabidopsis Seed Coat. *Plant Cell* **28**:2478–2492.

Farkas, G., Gausz, J., Galloni, M., Reuter, G., Gyurkovics, H., and Karch, F. (1994). The Trithorax-like gene encodes the Drosophila GAGA factor. *Nature* **371**:806–808.

Favaro, R., Pinyopich, A., Battaglia, R., Kooiker, M., and Borghi, L. (2003). MADS-Box Protein Complexes Control Carpel and Ovule Development in Arabidopsis. *Plant Cell* **15**.

Fobert, P. R., Coen, E. S., Murphy, G. J., and Doonan, J. H. (1994). Patterns of cell division revealed by transcriptional regulation of genes during the cell cycle in plants. *EMBO J.* **13**:616–24.

Gong, R., Cao, H., Zhang, J., Xie, K., Wang, D., and Yu, S. (2018). Divergent functions of the GAGA-binding transcription factor family in rice. *Plant J.* **94**:32–47.

Gregis, V., Sessa, A., Colombo, L., and Kater, M. M. (2006). AGL24, SHORT VEGETATIVE PHASE and APETALA1 Redundantly Control AGAMOUS during Early Stages of Flower Development in Arabidopsis. The Plant Cell. 18:1373–1382.

Gregis, V., Sessa, A., Colombo, L., and Kater, M. M. (2008). *AGAMOUS-LIKE24* and *SHORT VEGETATIVE PHASE* determine floral meristem identity in Arabidopsis. *Plant J.* **56**:891–902.

Gregis, V., Sessa, A., Dorca-Fornell, C., and Kater, M. M. (2009). The Arabidopsis floral meristem identity genes AP1, AGL24 and SVP directly repress class B and C floral homeotic genes. *Plant J.* **60**:626–637.

Gregis, V., Andrés, F., Sessa, A., Guerra, R. F., Simonini, S., Mateos, J. L., Torti, S., Zambelli, F., Prazzoli, G. M., Bjerkan, K. N., et al. (2013). Identification of pathways directly regulated by SHORT VEGETATIVE PHASE during vegetative and reproductive development in Arabidopsis. *Genome Biol.* **14**:R56.

Hecker, A., Brand, L. H., Peter, S., Simoncello, N., Kilian, J., Harter, K., Gaudin, V., and Wanke, D. (2015a). The Arabidopsis GAGA-Binding Factor BASIC PENTACYSTEINE6 Recruits the POLYCOMB-REPRESSIVE COMPLEX1 Component LIKE HETEROCHROMATIN PROTEIN1 to GAGA DNA Motifs. *Plant Physiol.* Advance Access published 2015, doi:10.1104/pp.15.00409.

Hecker, A., Brand, L. H., Peter, S., Simoncello, N., Kilian, J., Harter, K., Gaudin, V., and Wanke, D. (2015b). The Arabidopsis GAGA-Binding Factor BASIC PENTACYSTEINE6 Recruits the POLYCOMB-REPRESSIVE COMPLEX1 Component LIKE HETEROCHROMATIN PROTEIN1 to GAGA DNA Motifs. *Plant Physiol.*

168:1013–1024.

Heinz, S., Benner, C., Spann, N., Bertolino, E., Lin, Y. C., Laslo, P., Cheng, J. X., Murre, C., Singh, H., and Glass, C. K. (2010a). Simple Combinations of Lineage-Determining Transcription Factors Prime cis-Regulatory Elements Required for Macrophage and B Cell Identities. *Mol. Cell* **38**:576–589.

Heinz, S., Benner, C., Spann, N., Bertolino, E., Lin, Y. C., Laslo, P., Cheng, J. X., Murre, C., Singh, H., and Glass, C. K. (2010b). Simple Combinations of Lineage-Determining Transcription Factors Prime cis-Regulatory Elements Required for Macrophage and B Cell Identities. *Mol. Cell* **38**:576–589.

Herrera-Ubaldo, H., Lozano-Sotomayor, P., Ezquer, I., Di Marzo, M., Chávez Montes, R. A., Gómez-Felipe, A., Pablo-Villa, J., Diaz-Ramirez, D., Ballester, P., Ferrándiz, C., et al. (2019). New roles of NO TRANSMITTING TRACT and SEEDSTICK during medial domain development in Arabidopsis fruits. *Development* **146**:dev172395.

Horard, B., Tatout, C., Poux, S., and Pirrotta, V. (2000). Structure of a polycomb response element and in vitro binding of polycomb group complexes containing GAGA factor. *Mol. Cell. Biol.* **20**:3187–97.

Huang, D. W., Sherman, B. T., and Lempicki, R. A. (2009). Systematic and integrative analysis of large gene lists using DAVID bioinformatics resources. *Nat. Protoc.* **4**:44–57.

Immink, R. G. H., Gadella, T. W. J., Ferrario, S., Busscher, M., and Angenent, G. C. (2002). Analysis of MADS box protein-protein interactions in living plant cells. *Proc. Natl. Acad. Sci.* **99**:2416–2421.

Immink RG, Posé D, Ferrario S, Ott F Kaufmann K, Valentim FL, de Folter S, van der Wal F, van Dijk AD, Schmid M, Angenent GC. (2012) Characterization of SOC1's central role in flowering by the identification of its upstream and downstream regulators. Plant Physiol **160**(1):433-49.

Mateos JL, Madrigal P, Tsuda K, Rawat V Richter R, Romera-Branchat M, Fornara F, Schneeberger K, Krajewski P, Coupland G. (2015). Combinatorial activities of SHORT VEGETATIVE PHASE and FLOWERING LOCUS C define distinct modes of flowering regulation in Arabidopsis. Genome Biol. **16**:31.

Khan, A., Fornes, O., Stigliani, A., Gheorghe, M., Castro-Mondragon, J. A., van der Lee, R., Bessy, A., Chèneby, J., Kulkarni, S. R., Tan, G., Baranasic D, Arenillas DJ, Sandelin A, Vandepoele K, Lenhard B, Ballester B, Wasserman WW, Parcy F, Mathelier A. (2018). JASPAR 2018: update of the open-access database of transcription factor binding profiles and its web framework. *Nucleic Acids Res.* **46**:D260–D266.

Kinoshita, T., Harada, J. J., Goldberg, R. B., and Fischer, R. L. (2001). Polycomb repression of flowering during early plant development. *Proc. Natl. Acad. Sci. U. S. A.* **98**:14156–61.

Kooiker, M., CA, A., A, L., PS, M., L, F., MM, K., and L., C. (2005). BASIC PENTACYSTEINE1, a GA Binding Protein That Induces Conformational Changes in the Regulatory Region of the Homeotic Arabidopsis Gene SEEDSTICK. *PLANT CELL ONLINE* **17**:722–729.

Kotake, T., Takada, S., Nakahigashi, K., Ohto, M., and Goto, K. (2003). Arabidopsis TERMINAL FLOWER 2 Gene Encodes a Heterochromatin Protein 1 Homolog and Represses both FLOWERING LOCUS T to Regulate Flowering Time and Several Floral Homeotic Genes. *Plant Cell Physiol.* **44**:555–564.

Lafos, M., Kroll, P., Hohenstatt, M. L., Thorpe, F. L., Clarenz, O., and Schubert, D. (2011). Dynamic Regulation of H3K27 Trimethylation during Arabidopsis Differentiation. *PLoS Genet.* **7**:e1002040.

Larsson, A. S., Landberg, K., and Meeks-Wagner, D. R. (1998). The TERMINAL FLOWER2 (TFL2) gene controls the reproductive transition and meristem identity in Arabidopsis thaliana. *Genetics* **149**:597–605.

Lewis, E. B. (1978). A gene complex controlling segmentation in Drosophila. *Nature* **276**:565–570.

Li, C., Chen, C., Gao, L., Yang, S., Nguyen, V., Shi, X., Siminovitch, K., Kohalmi, S. E., Huang, S., Wu, K., et al. (2015). The Arabidopsis SWI2/SNF2 Chromatin Remodeler BRAHMA Regulates Polycomb Function during Vegetative Development and Directly Activates the Flowering Repressor Gene SVP. *PLOS Genet.* **11**:e1004944.

Liljegren, S. J., Ditta, G. S., Eshed, Y., Savidge, B., Bowman, J. L., and Yanofsky, M. F. (2000). SHATTERPROOF MADS-box genes control seed dispersal in Arabidopsis. *Nature* **404**:766–770.

Liu, C., Xi, W., Shen, L., Tan, C., and Yu, H. (2009). Regulation of Floral Patterning by Flowering Time Genes. *Dev. Cell* **16**:711–722.

Lodha, M., Marco, C. F., and Timmermans, M. C. P. (2013). The ASYMMETRIC LEAVES complex maintains repression of KNOX homeobox genes via direct recruitment of Polycomb-repressive complex2. *Genes Dev.* **27**:596–601.

Losa, A., Colombo, M., Brambilla, V., and Colombo, L. (2010). Genetic interaction between AINTEGUMENTA (ANT) and the ovule identity genes SEEDSTICK (STK), SHATTERPROOF1 (SHP1) and SHATTERPROOF2 (SHP2). *Sex. Plant Reprod.* **23**:115–121.

Makarevich, G., Leroy, O., Akinci, U., Schubert, D., Clarenz, O., Goodrich, J., Grossniklaus, U., and Köhler, C. (2006). Different Polycomb group complexes regulate common target genes in Arabidopsis. *EMBO Rep.* **7**:947–952.

Malley, R. C. O., Carol, S., Song, L., Galli, M., Ecker, J. R., Malley, R. C. O., Huang, S. C., Song, L., Lewsey, M. G., Bartlett, A., et al. (2016). Cistrome and Epicistrome Features Shape the Regulatory DNA Landscape Resource Cistrome and Epicistrome Features Shape the Regulatory DNA Landscape. *Cell* **165**:1280–1292.

Martinez, G. J., and Rao, A. (2012). Cooperative Transcription Factor Complexes in Control. *Science (80-.).* **338**:891–892.

Matias-Hernandez, L., Battaglia, R., Galbiati, F., Rubes, M., Eichenberger, C., Grossniklaus, U., Kater, M. M., and Colombo, L. (2010). VERDANDI Is a Direct Target of the MADS Domain Ovule Identity Complex and Affects Embryo Sac Differentiation in Arabidopsis. *Plant Cell* **22**:1702–1715.

Meister, R. J., Williams, L. A., Monfared, M. M., Gallagher, T. L., Kraft, E. A., Nelson, C. G., and Gasser, C. S. (2004). Definition and interactions of a positive regulatory element of the *Arabidopsis INNER NO OUTER* promoter. *Plant J.* **37**:426–438.

Mendes, M. A., Guerra, R. F., Castelnovo, B., Silva-Velazquez, Y., Morandini, P., Manrique, S., Baumann, N., Groß-Hardt, R., Dickinson, H., and Colombo, L. (2016). Live and let die: a REM complex promotes fertilization through synergid cell death in *Arabidopsis*. *Development* **143**:2780–2790.

Mizzotti, C., Ezquer, I., Paolo, D., Rueda-Romero, P., Guerra, R. F., Battaglia, R., Rogachev, I., Aharoni, A., Kater, M. M., Caporali, E., et al. (2014). SEEDSTICK is a Master Regulator of Development and Metabolism in the Arabidopsis Seed Coat. *PLoS Genet.* **10**:e1004856.

Monfared, M. M., Simon, M. K., Meister, R. J., Roig-Villanova, I., Kooiker, M., Colombo, L., Fletcher, J. C., and Gasser, C. S. (2011). Overlapping and antagonistic activities of BASIC PENTACYSTEINE genes affect a range of developmental processes in Arabidopsis. *Plant J.* **66**:1020–1031.

Mu, Y., Zou, M., Sun, X., He, B., Xu, X., Liu, Y., Zhang, L., and Chi, W. (2017a). BASIC PENTACYSTEINE proteins repress Abscisic Acid INSENSITIVE 4 expression via direct recruitment of the polycomb-repressive complex 2 in arabidopsis root development. *Plant Cell Physiol.* **58**:607–621.

Mu, Y., Zou, M., Sun, X., He, B., Xu, X., Liu, Y., Zhang, L., and Chi, W. (2017b). Basic Pentacysteine Proteins Repress *Abscisic Acid Insensitive4* Expression *via* Direct Recruitment of the Polycomb-Repressive Complex 2 in *Arabidopsis* Root Development. *Plant Cell Physiol.* **58**:pcx006.

O'Malley, R. C., Huang, S. C., Song, L., Lewsey, M. G., Bartlett, A., Nery, J. R., Galli, M., Gallavotti, A., and Ecker, J. R. (2016). Cistrome and Epicistrome Features Shape the Regulatory DNA Landscape. *Cell* **165**:1280–1292.

Pelaz, S., Gustafson-Brown, C., Kohalmi, S. E., Crosby, W. L., and Yanofsky, M. F. (2002). APETALA1 and SEPALLATA3 interact to promote flower development. *Plant J.* **26**:385–394.

Pinyopich, A., Ditta, G. S., Savidge, B., Liljegren, S. J., Baumann, E., Wisman, E., and Yanofsky, M. F. (2003). Assessing the redundancy of MADS-box genes during carpel and ovule development. *Nature* **424**:85–88.

Posé, D., Verhage, L., Ott, F., Yant L., Mathieu, J., Angenent G.C., Immink R.G., Schmid M. (2013). Temperature-dependent regulation of flowering by antagonistic FLM variants. Nature **21**;503(7476):414-7.

Quinlan, A. R., and Hall, I. M. (2010). BEDTools: a flexible suite of utilities for comparing genomic features. *Bioinformatics* **26**:841–842.

Roscoe, T. J., Vaissayre, V., Paszkiewicz, G., Clavijo, F., Kelemen, Z., Michaud, C., Lepiniec, L., Dubreucq, B., Zhou, D.-X., and Devic, M. (2019). Regulation of *FUSCA3* Expression During Seed Development in Arabidopsis. *Plant Cell Physiol.* **60**:476–487.

Sangwan, I., and O'Brian, M. R. (2002). Identification of a soybean protein that interacts with GAGA element dinucleotide repeat DNA. *Plant Physiol.* **129**:1788–94.

Santi, L., Wang, Y., Stile, M. R., Berendzen, K., Wanke, D., Roig, C., Pozzi, C., Müller, K., Müller, J., Rohde, W., et al. (2003). The GA octodinucleotide repeat binding factor BBR participates in the transcriptional regulation of the homeobox gene *Bkn3*. *Plant J.* **34**:813–826.

Schägger, H., and von Jagow, G. (1987). Tricine-sodium dodecyl sulfate-polyacrylamide gel electrophoresis for the separation of proteins in the range from 1 to 100 kDa. *Anal. Biochem.* **166**:368–79.

Schruff, M. C., Spielman, M., Tiwari, S., Adams, S., Fenby, N., and Scott, R. J. (2006). The AUXIN RESPONSE FACTOR 2 gene of Arabidopsis links auxin signalling, cell division, and the size of seeds and other organs. *Development* **133**:251–61.

Shanks, C. M., Hecker, A., Cheng, C.-Y., Brand, L., Collani, S., Schmid, M., Schaller, G. E., Wanke, D., Harter, K., and Kieber, J. J. (2018). Role of *BASIC PENTACYSTEINE* transcription factors in a subset of cytokinin signaling responses. *Plant J.* **95**:458–473.

Simonini, S., and Kater, M. M. (2014). Class I BASIC PENTACYSTEINE factors regulate HOMEOBOX genes involved in meristem size maintenance. *J. Exp. Bot.* **65**:1455–1465.

Simonini, S., Roig-Villanova, I., Gregis, V., Colombo, B., Colombo, L., and Kater, M. M. (2012). BASIC PENTACYSTEINE Proteins Mediate MADS Domain Complex Binding to the DNA for Tissue-Specific Expression of Target Genes in *Arabidopsis*. *Plant Cell* **24**:4163–4172.

Theune, M. L., Bloss, U., Brand, L. H., Ladwig, F., and Wanke, D. (2019). Phylogenetic Analyses and GAGA-Motif Binding Studies of BBR/BPC Proteins Lend to Clues in GAGA-Motif Recognition and a Regulatory Role in Brassinosteroid Signaling. *Front. Plant Sci.* **10**:466.

Turck, F., Roudier, F., Farrona, S., Martin-Magniette, M.-L., Guillaume, E., Buisine, N., Gagnot, S., Martienssen, R. A., Coupland, G., and Colot, V. (2007). Arabidopsis TFL2/LHP1 Specifically Associates with Genes Marked by Trimethylation of Histone H3 Lysine 27. *PLoS Genet.* **3**:e86.

Wang, H., Liu, C., Cheng, J., Liu, J., Zhang, L., and He, C. (2016). Arabidopsis Flower and Embryo Developmental Genes are Repressed in Seedlings by Different Combinations of Polycomb Group Proteins in Association with Distinct Sets of Cis-regulatory Elements Advance Access published 2016, doi:10.1371/journal.pgen.1005771.

Wanke, D., Hohenstatt, M. L., Dynowski, M., Bloss, U., Hecker, A., Elgass, K., Hummel, S., Hahn, A., Caesar, K., Schleifenbaum, F., et al. (2011). Alanine zipper-like coiled-coil domains are necessary for homotypic dimerization of plant GAGA-factors in the nucleus and nucleolus. *PLoS One* **6**:e16070.

Wu, J., Petrella, R., Dowhanik, S., Gregis, V., and Gazzarrini, S. (2019). Spatiotemporal restriction of FUSCA3 expression by class I BPC promotes ovule development and coordinates embryo and endosperm growth. *bioRxiv* Advance Access published April 19, 2019, doi:10.1101/612408.

Xiao, J., Jin, R., Yu, X., Shen, M., Wagner, J. D., Pai, A., Song, C., Zhuang, M., Klasfeld, S., He, C., et al. (2017). Cis and trans determinants of epigenetic silencing by Polycomb repressive complex 2 in Arabidopsis. *Nat. Genet.* **49**:1546–1552.

Yang, J., Lee, S., Hang, R., Kim, S.-R., Lee, Y.-S., Cao, X., Amasino, R., and An, G. (2013). OsVIL2 functions with PRC2 to induce flowering by repressing *O s LFL 1* in rice. *Plant J.* **73**:566–578.

Yoshida, N., Yanai, Y., Chen, L., Kato, Y., Hiratsuka, J., Miwa, T., Sung, Z. R., and Takahashi, S. (2001). EMBRYONIC FLOWER2, a novel polycomb group protein homolog, mediates shoot development and flowering in Arabidopsis. *Plant Cell* **13**:2471–81.

Zhang, X., Clarenz, O., Cokus, S., Bernatavichute, Y. V, Pellegrini, M., Goodrich, J., and Jacobsen, S. E. (2007a). Whole-Genome Analysis of Histone H3 Lysine 27 Trimethylation in Arabidopsis. *PLoS Biol.* **5**:e129.

Zhang, X., Germann, S., Blus, B. J., Khorasanizadeh, S., Gaudin, V., and Jacobsen, S. E. (2007b). The Arabidopsis LHP1 protein colocalizes with histone H3 Lys27 trimethylation. *Nat. Struct. &Amp; Mol. Biol.* **14**:869.

Figures legends.

Figure 1. Mutation of BPCs of class I and class II affects *STK* expression in the flower.

In-situ hybridisation on wild-type [(a) and (b)], *bpc1-2 bpc2 bpc3* [(c) and (d)]*, bpc4 bpc6* [(e) and (f)] and *bpcV* [(g) and (h)] inflorescences using a *STK*-specific antisense probe. IM: inflorescence meristem; P: petal; numbers represent flower stages. Scale bars=50 µm.

Figure 2. Overexpression of *STK* affects vegetative and reproductive development.

(a) From left to right: wild-type, *bpcV* and *35S:*STK plants; plants were photographed six weeks after sowing; scale bars=1 cm. (b) Fruit morphology and length in wild type, *bpcV* and *35S*:STK (from top to bottom); scale bars=1.5 mm. (c) Average seeds area size of wild-type, *arf2-8* (Schruff et al., 2006), *stk* (Pinyopich et al., 2001), *35S*:STK and *bpcV*; error bars represent the standard error mean of replicates; ANOVA and post-hoc Tukey HSD (honestly significant difference) test were used, **P <

0.01 for wild-type versus other genotypes comparison. In the lower row, seeds of the analysed genotypes are shown.

Figure 3. Class II BPCs interact with SVP *in vivo*.

(a) Yeast two-hybrid interaction assay for SVP and BPCs of class II: positive interactions on selective media –W-L-H +5mM 3-AT.
(b) Co-immunoprecipitation assays. *Nicotiana benthamiana* leaves were infiltrated with constructs carrying SVP-GFP together with BPC4-RFP and BPC6-RFP, as described in experimental procedures. Immunoprecipitation step was performed using RFP-trap on total protein leaf extract. Samples were probed with GFP and RFP antibodies. S/N: supernatant; IP: immunoprecipitation.
(c) Bi-molecular fluorescence complementation (BiFC) assay. *Nicotiana benthamiana* epidermis cells were transiently transformed with the indicated YN and YC fusions. In the first and the second column yellow fluorescence and the merging in the bright field were shown, respectively.
(d) Bi-molecular fluorescence complementation (BiFC) assay. *N.benthamiana* epidermis cells were transiently transformed with the indicated YN and YC fusions and AP1-RFP construct. In the first, the second and the third column yellow fluorescence, red fluorescence and the merging between the two channels in the bright field were shown, respectively. Scale bars=40 μm.

Figure 4. ChIP experiments on different mutant backgrounds.

ChIP experiments on different mutant backgrounds. (a) Schematic diagram of the *STK* locus indicating the regions analysed by chromatin immunoprecipitation (ChIP; black bars). Black boxes, exons; white boxes, promoters and introns; asterisks, C-boxes; grey boxes, CArG-boxes; scale bar=500 bp. (b) Quantitative Real-Time PCR analysis of ChIP assay using chromatin extracted from *svp ap1-12 agl24*, wild-type (as a positive control), and *bpc1-2 bpc2 bpc3* (as a negative control) testing the C-12, B and NC box regions. Antibodies against BPCs of class I were used. (c) Quantitative Real-time PCR analysis of ChIP assay using chromatin extracted from *pSVP*:SVP-GFP *svp bpcV*, *pSVP*:SVP-GFP *svp* (as a positive control) and wild-type (as a negative control), testing C-12, B and

NC box regions. For the IP, commercial antibodies against GFP were used. Error bars represent the propagated error value using three replicates. ChIP results of one representative experiment are shown. Positive binding site fragments were considered only if they were enriched compared with the controls in at least three independent experiments.

Figure 5. Mutation of CArG-boxes interferes with SVP and class I BPCs binding to *STK* promoter.

(a)Schematic representation of the *STK* promoter versions generated: dark grey squares represent CArG-boxes wild-type and mutated (crossed). (b)-(g) GUS staining on inflorescences from *pSTK:*GUSwt (b-d) and *pSTK_CArGm:*GUS (e-g): whole inflorescence [(b) and (e)]; mature flower [(c) and (f)]; inflorescence meristem (IM), floral meristems (FM) and young flowers [(d) and (g)]; scale bars in (c), (d), (f) and (g)=100 µm. (h) Quantitative Real-Time PCR analysis of ChIP assay using chromatin extracted from *pSVP:*SVP-GFP *pSTK_CArGm svp* showing deregulation of the reporter and *pSTK_CArGm* as a negative control, testing wild-type region, mutated region and NC box. For the IP, antibodies against GFP have been used. (i) Quantitative Real-Time PCR analysis of ChIP assay using chromatin extracted from *pSVP:SVP-GFP pSTK_CArGm svp* showing correct expression of the reporter and *pSTK_CArGm* as a negative control, testing wild-type region, mutated region and NC box. For the IP, antibodies against GFP have been used. (l) Quantitative Real-Time PCR analysis of ChIP assay using chromatin extracted from *pSVP:SVP-GFP pSTK_CArGm* testing wild-type region, mutated region and NC box. For the IP, antibodies against Class I BPCs have been used; for negative control commercial antibodies against HA was used. Error bars represent the propagated error value using three replicates. ChIP results of one representative experiment are shown. Positive binding site fragments were considered only if they were significantly enriched compared to the controls in at least three independent experiments.

Figure 6. Epigenetic regulation of *STK.*

(a) Schematic representation of the *STK* genomic region tested in ChIP assay. Black boxes indicate exonic regions. Black bars indicate the regions analysed by chromatin immunoprecipitation (ChIP); region1 is located in the H3k27me3 – enriched region published by (Li et al. 2015) spanning -2627 upstream *STK*-transcriptional start site to +2050 pb downstream *STK*-transcriptional start site, whereas region 2 is localized 3 pb downstream the stop codon of the

gene. Black arrow indicates the *STK*-transcription start site. Scale bar= 500 bp. (b) ChIP-quantitative Real-Time PCR determining the levels of H3K27me3 across the *STK* locus in inflorescence tissue. Quantitative Real-Time PCR quantification of *STK* sequences in precipitated chromatin was used to infer the methylation of histone H3 at lysine 27 (H3K27me3) and histone H3 density. Ct values were used to calculate the IP/IN signal. ChIP enrichments are presented as the percentage (%) of bound/input signal normalized to actin levels in the relative regions. We tested the efficiency of IP on histone modifications by quantifying the presence of the H3K27me3 mark in AG region which carries the mark H3k27me3, reported in Li et al. (2015). H3K27me3 mark in AT2G22560 was used as negative control for H3K27me3 mark (Li et al. 2015). The data were normalized to *actin*, with error bars indicating standard deviations based on three independent technical replicates. Four, independent ChIP experiments were performed and similar results were obtained.

Figure 7. LHP1 directly regulates *STK* during flower development.

(a)-(d) *In-situ* hybridisation on wild-type [(a) and (b)] and *lhp1* inflorescences [(c) and (d)] using a *STK*-specific antisense probe (Brambilla et al., 2007). IM: inflorescence meristem; FM: floral meristem; numbers represent flower stages; scale bars=50 μm.

(e) Expression analysis of *STK* by quantitative Real-Time PCR in *lhp1* and wild-type inflorescences. The expression of *STK* was normalized to that of ubiquitin and the expression level in wild-type was set to 1. Asterisk indicates $P < 0.05$ in a Student's t-test.

(f) Quantitative Real-Time PCR analysis of ChIP assay using chromatin extracted from *pLHP1:*LHP1-GFP (Kotake et al, 2003) and wild-type (as a negative control), testing the Region 1 and Region 2 (Figure 6a). For the IP, commercial antibodies against SVP were used. Error bars represent the propagated error value using three replicates. ChIP results of one representative experiment are shown. Positive binding site fragments were considered only if they were significantly enriched compared with the controls in at least three independent experiments.

Figure 8. Analysis of BPC and MADS-box transcription factor families binding sites.

Venn diagram displaying the number of DAP-seq peaks and the common number of peaks associated to the BPC and MADS transcription factor families according to our analysis of the data by O'Malley et al (see Experimental procedures). Enriched motifs, as recovered by Homer (p-value ≤ 1e-30), are displayed underneath.

Figure 9. Model of the protein complex formed to represses gene expression during flower development.

BPCs and SVP bind C-boxes (in dark purple) and CArG-boxes (in light purple) respectively, and recruit LHP1 to a subset of gene loci.

Figures.

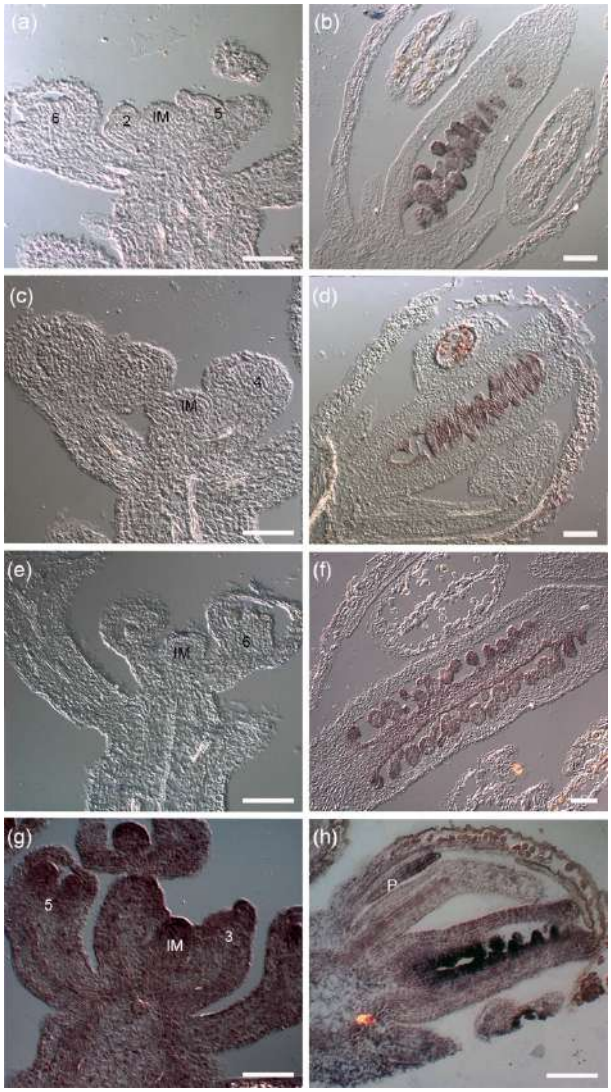

Figure 1. Mutation of BPCs of class I and class II affects *STK* expression in the flower.

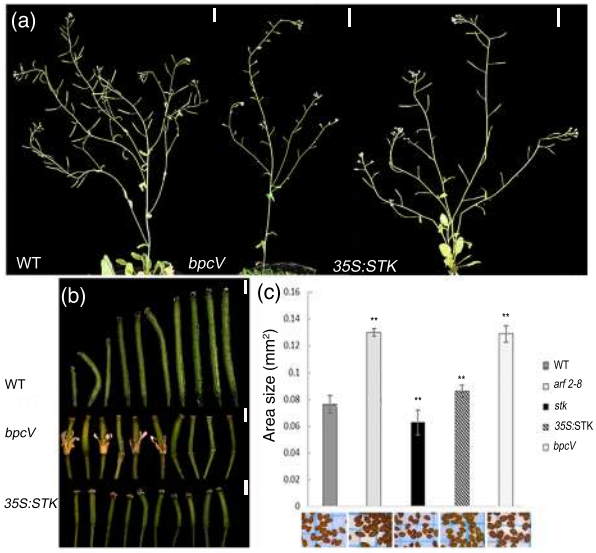

Figure 2. Overexpression of *STK* affects vegetative and reproductive development.

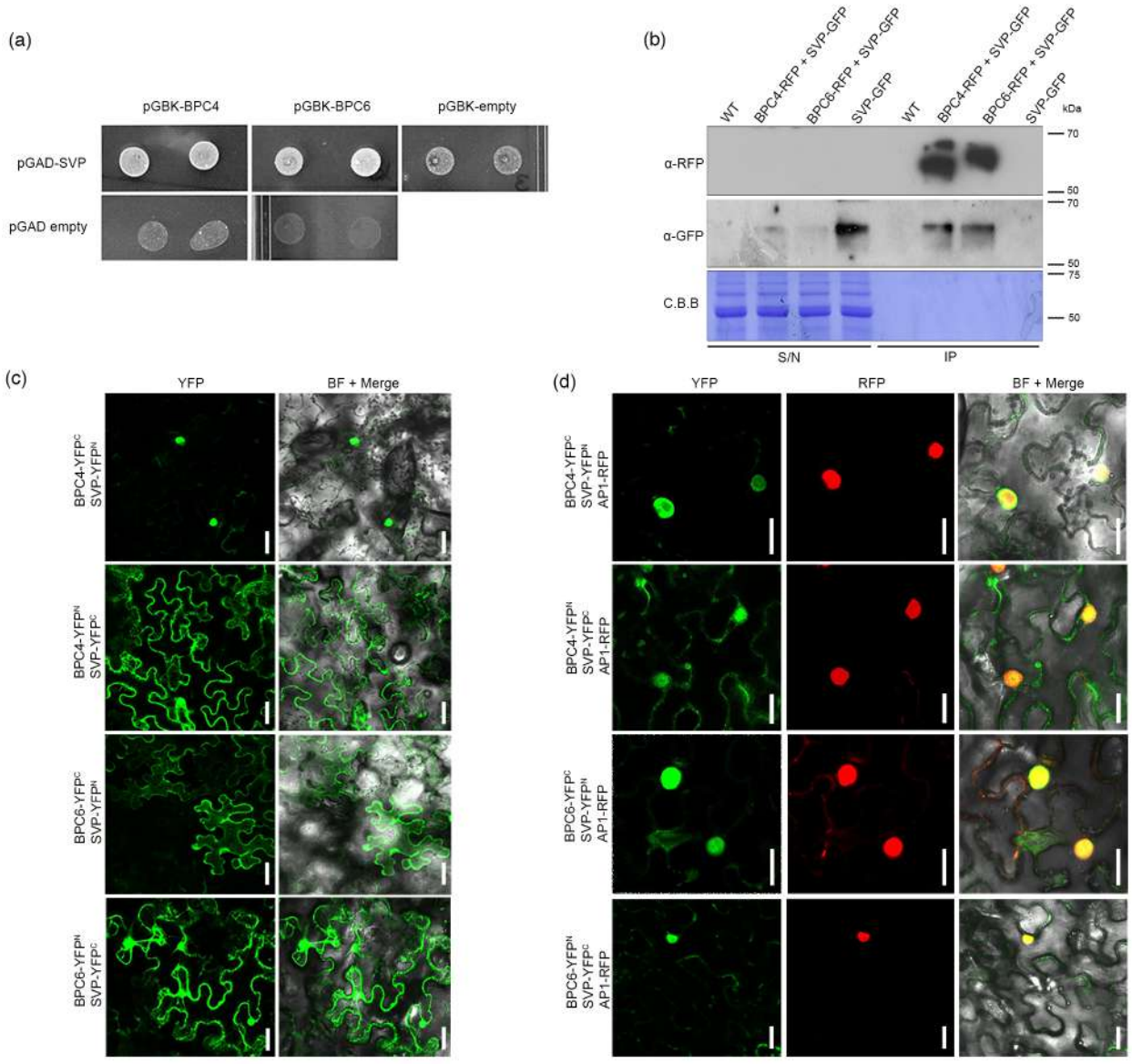

Figure 3. Class II BPCs interact with SVP *in vivo*.

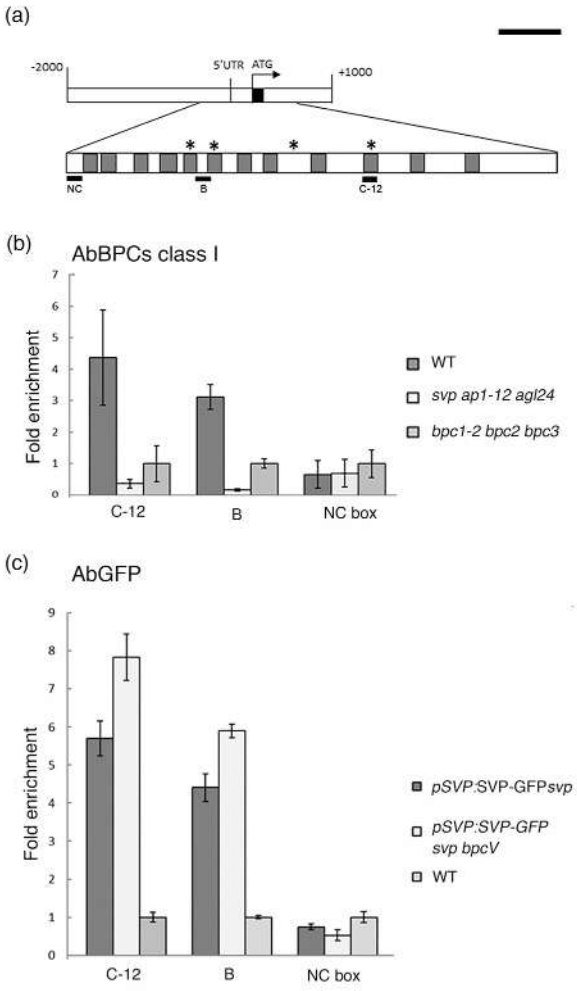

Figure 4. ChIP experiments on different mutant backgrounds.

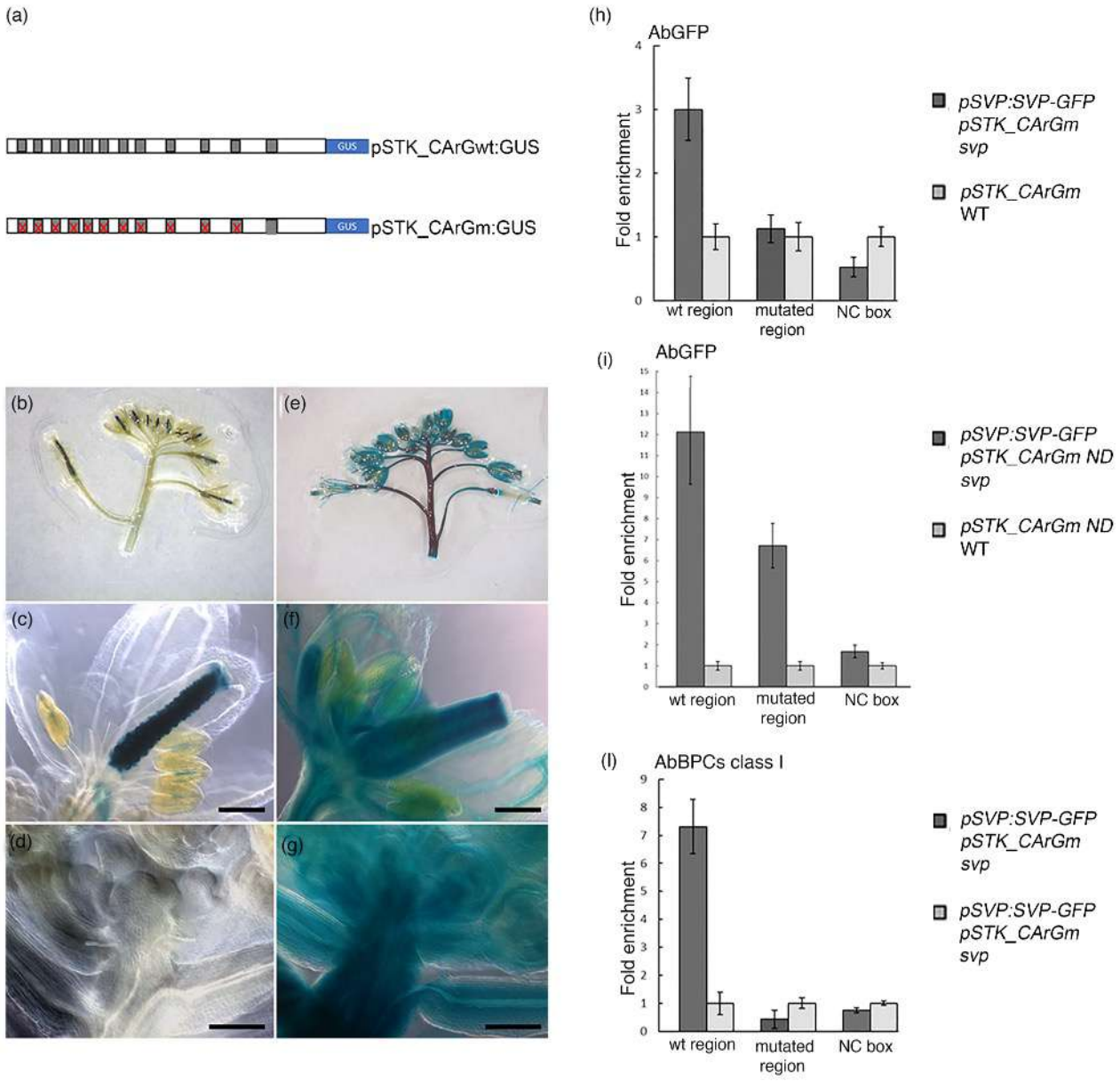

Figure 5. Mutation of CArG-boxes interferes with SVP and class I BPCs binding to *STK* promoter.

(a)

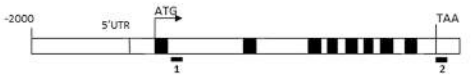

(b)

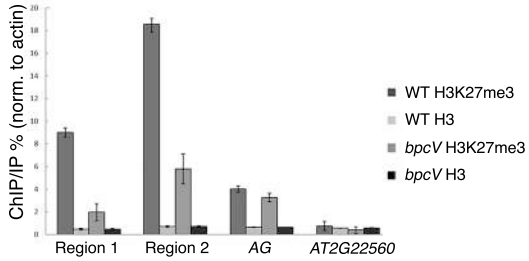

Figure 6. Epigenetic regulation of *STK*.

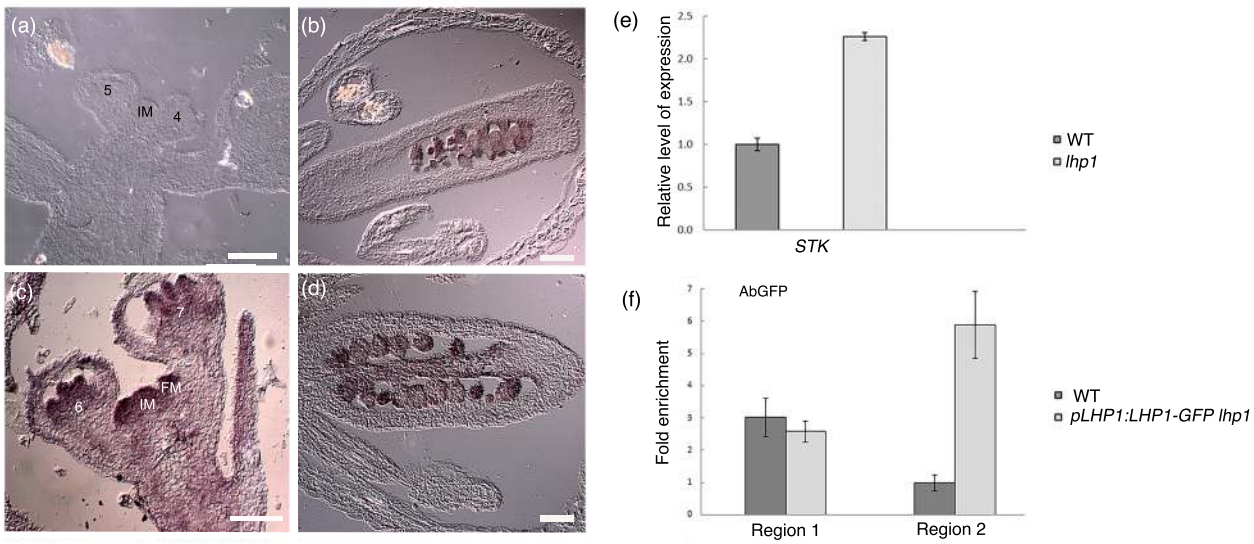

Figure 7. LHP1 directly regulates *STK* during flower development.

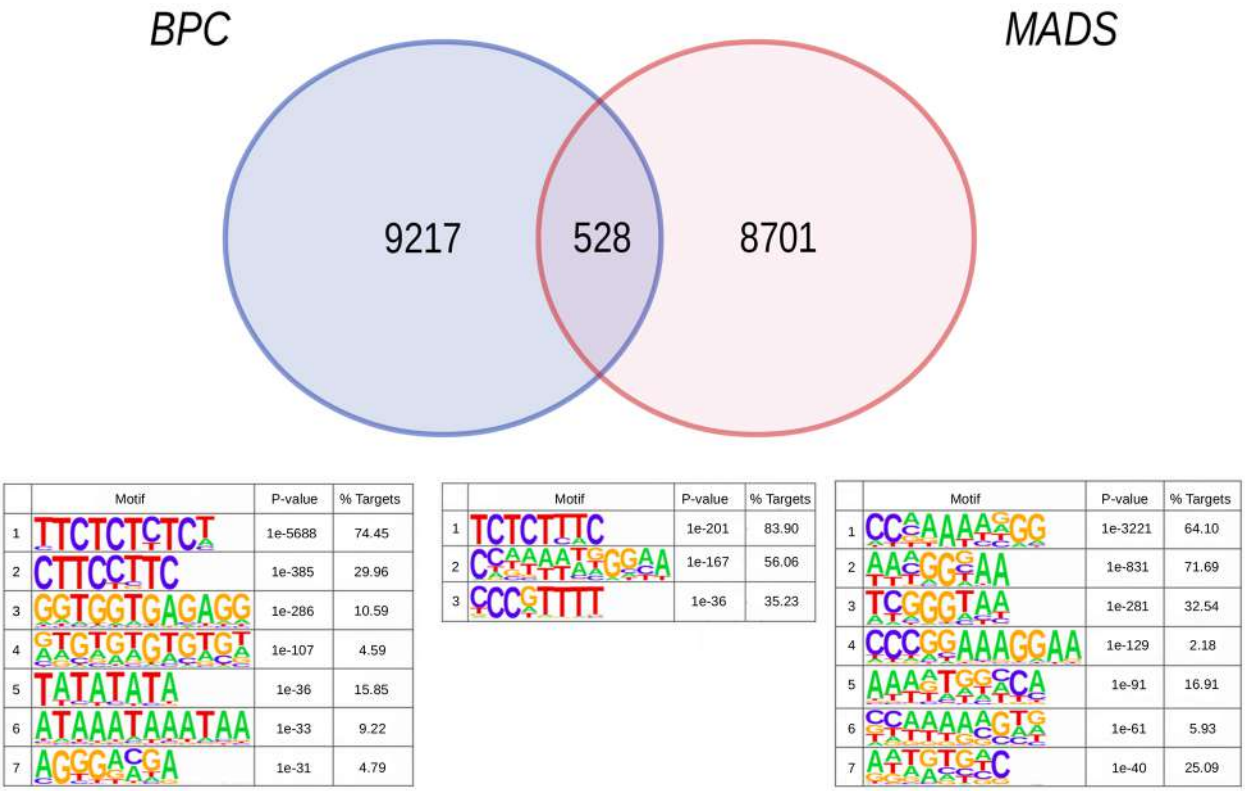

	Motif	P-value	% Targets
1	TTCTCTCTCT	1e-5688	74.45
2	CTTCCTTC	1e-385	29.96
3	GGTGGTGAGAGG	1e-286	10.59
4	GTGTGTGTGTGT	1e-107	4.59
5	TATATATA	1e-36	15.85
6	ATAAATAAATAA	1e-33	9.22
7	AGGGACGA	1e-31	4.79

	Motif	P-value	% Targets
1	TCTCTTTC	1e-201	83.90
2	CCAAAAATGGGAA	1e-167	56.06
3	CCCGTTTT	1e-36	35.23

	Motif	P-value	% Targets
1	CCAAAAAAGG	1e-3221	64.10
2	AAAGGGAA	1e-831	71.69
3	TCGGGTAA	1e-281	32.54
4	CCCGGAAAGGAA	1e-129	2.18
5	AAAATGGCCA	1e-91	16.91
6	CCAAAAAAGTG	1e-61	5.93
7	AATGTGAC	1e-40	25.09

Figure 8. Analysis of BPC and MADS-box transcription factor families binding sites.

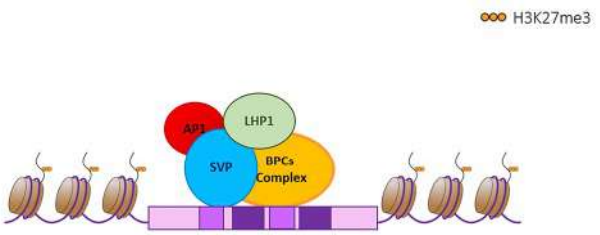

Figure 9. Model of the protein complex formed to represses gene expression during flower development.

Supplementary Figures.

Figure S1.

In-situ hybridisation on wild-type [(a) and (b); (e) and (f)] and *bpcV* [(c) and (d); (g) and (h)] inflorescences using a histone H4 probe (Fobert et al., 1994) [(a)-(d)] and *STK* sense probe [(e)-(h)] (Brambilla et al., 2007). Scale bars=50 μm.

Figure S2.

(a) Expression analysis of *STK* by quantitative Real-Time PCR in three different *35S:*STK T1 lines and wild-type inflorescences. The expression of *STK* was normalized to that of ubiquitin and the expression level in wild-type was set to 1. Asterisk indicates $P < 0.05$ in a Student's t-test. (b) Rosette leaves morphology and length: rosette leaves in wild-type, *bpcV* and *35S:*STK (from left to right); (c) Cauline morphology and length: cauline leaves in wild-type, *bpcV* and *35S:*STK (from left to right); scale bars= 0.5 cm.

Figure S3.

(a) Yeast two-hybrid assay between BPCs of class II: positive interactions on selective media –W-L-H +5mM 3-AT. (b) Co-immunoprecipitation assays. *Nicotiana benthamiana* leaves were infiltrated with constructs carrying SVP-GFP together with BPC4-RFP and BPC6-RFP, as described in experimental procedures. Immunoprecipitation step was performed using GFP-trap on total protein leaf extract. Samples were probed with GFP and RFP antibody. S/N: supernatant; IP: immunoprecipitation. (c) Bi-molecular fluorescence complementation (BiFC) assay. *Nicotiana benthamiana* epidermis cells were transiently transformed with the indicated YN and YC fusions; in the first and the second rows yellow fluorescence and merging in the bright field were shown, respectively. SVP-YFP^N BPC2-YFP^C and BPC2-YFP^N SVP -YFP^C were tested as negative control to prove the specificity of all the other BPCs-SVP heterodimers. Scale bars=50 μm.

Figure S4.

(a) Bi-molecular fluorescence complementation (BiFC) assay. *N.benthamiana* epidermis cells were transiently transformed with the indicated YN and YC fusions; VDD-VAL and VDD-VDD were tested as positive and negative control, respectively (Mendes et al., 2016). In the first and the second column yellow fluorescence

and merging in the bright field were shown, respectively. Scale bars=40 µm. (b) *N.benthamiana* epidermis cells were transiently transformed with the indicated constructs to assess cellular localization of BPC4-RFP, BPC6-RFP, AP1-RFP and SVP-GFP. In the first and the second row yellow/red fluorescence and merging in the bright field were shown, respectively. Scale bars=40 µm.

Figure S5.

(a) Bi-molecular fluorescence complementation (BiFC) assay, negative controls. *N.benthamiana* epidermis cells were transiently transformed with the indicated YN and YC fusions. In the first and the second column yellow fluorescence and merging in the bright field were shown, respectively. Scale bars=40 µm. (b) Bi-molecular fluorescence complementation (BiFC) assay, negative controls. *N.benthamiana* epidermis cells were transiently transformed with the indicated YN and YC fusions and AP1-RFP construct. In the first, the second and the third column yellow fluorescence, red fluorescence and the merging between the two channels in the bright field were shown, respectively. Scale bars=40 µm.

Figure S6.

Proportion of significantly overlapped DAP-Seq Peaks by TF family. Proportion, with respect to the total number of significantly overlapped peaks, of significantly overlapped DAP-seq peaks associated to each TF-family.

Figure S7. Venn diagrams of common ChIP seq peaks between BPC1, BPC6 and a selection of MADS-domain TFs. Venn diagrams displaying the total number of ChIP-seq peaks and the number of common of peaks between BPC1, BPC6 and a selection of MADS-domain transcription factors, including SVP, FLC, FLM and SOC1. Pairwise comparison are displayed. Left (A) intersection with BPC6. Right (B) intersection with BPC1.

Table S1. MADS-domain consensus regions identified in *STK* promoter and the designed mutated versions.

Table S2. Sequences of oligonucleotides used in this manuscript.

Data S1. p-values for the intersection of DAP-seq peaks of TFs families as defined by (Malley et al., 2016) with DAP-seq peaks of the BPCs family of transcription factors. Column1: transcription factor family. Column 2: p-

value for the overlap with DAP-seq peaks of BPC family transcription factors. Column 3: Bonferroni adjusted p-value.

Data S2. p-values for the intersection of ChIP-seq peaks of a selection of MADS-domain TFs with ChIP-seq peaks of BPC1 and BPC6. Column 1: gene symbol of the TF. Column 2: Number of peaks overlapped with BPC6 peaks. Column 3: number of peaks overlapped with BPC1 peaks. Column 4: Total number of peaks. Column 5: proportion of peaks overlapped with BPC6. Column 6: p-value for the statistical significance of the overlap with BPC6. Column 7: proportion of peaks overlapped with BPC1. Column 8: p-value for the statistical significance of the overlap with BPC1.

Data S3. Lists of identified genome-wide binding locations for all the MADS-box and BPCs factors, coincident DAP-seq peaks and functional enrichment analyses of associated target genes.

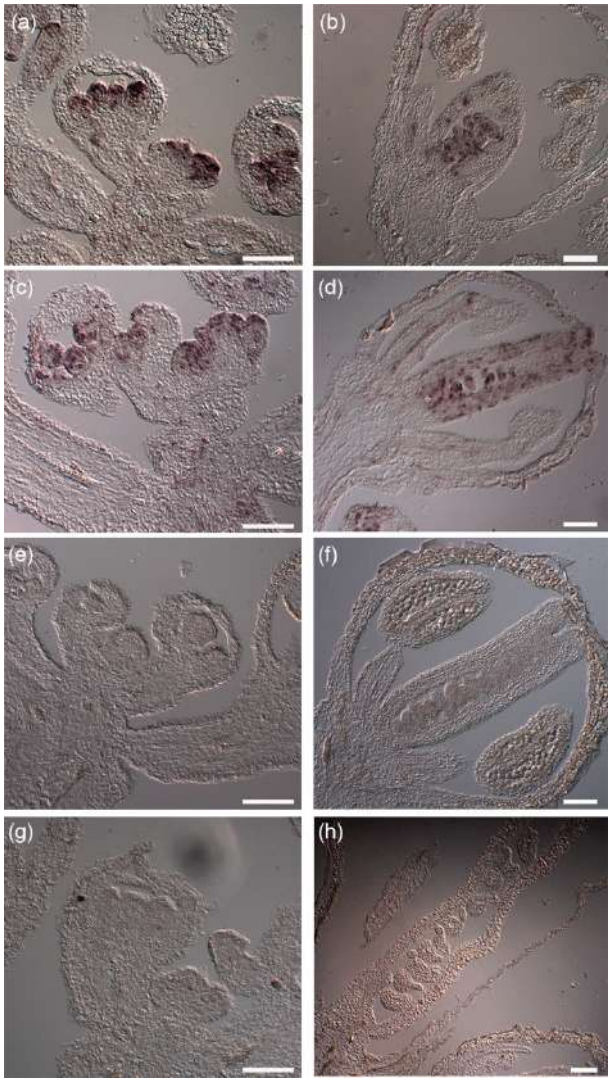

Figure S1. In situ hybridization controls.

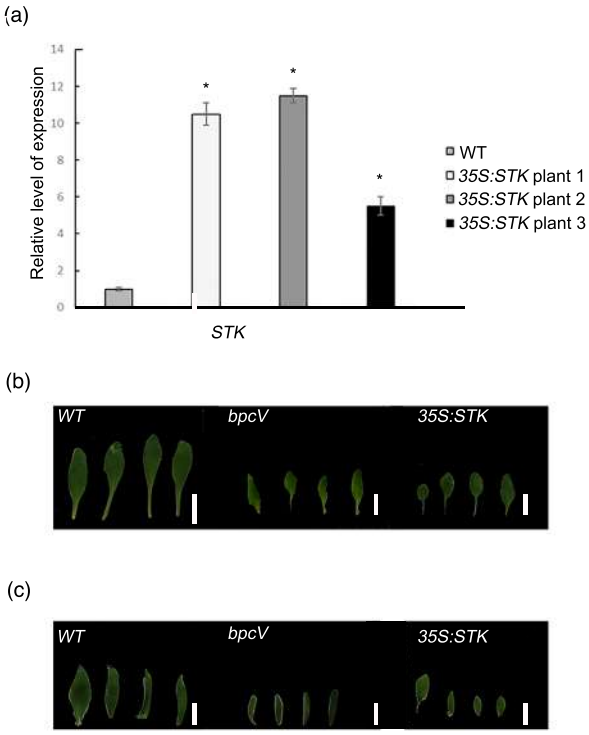

Figure S2. Selection of 35S:STK T1 lines and morphological analyses on 35S:STK and bpcV background.

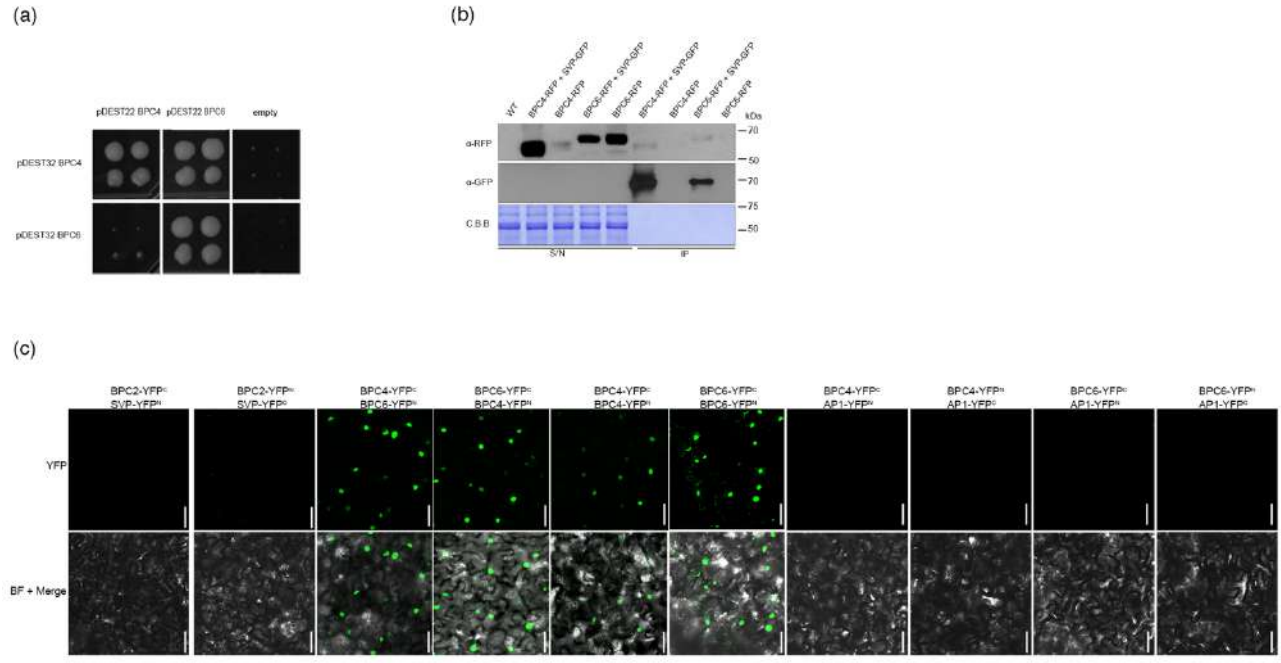

Figure S3. Yeast two-hybrid assay between BPCs of class II, Co-immunoprecipitation assays using GFP-trap and Bi-molecular fluorescence complementation (BiFC) assay between BPCs of class II, between BPCs of class II and AP1 and between BPC2 and SVP.

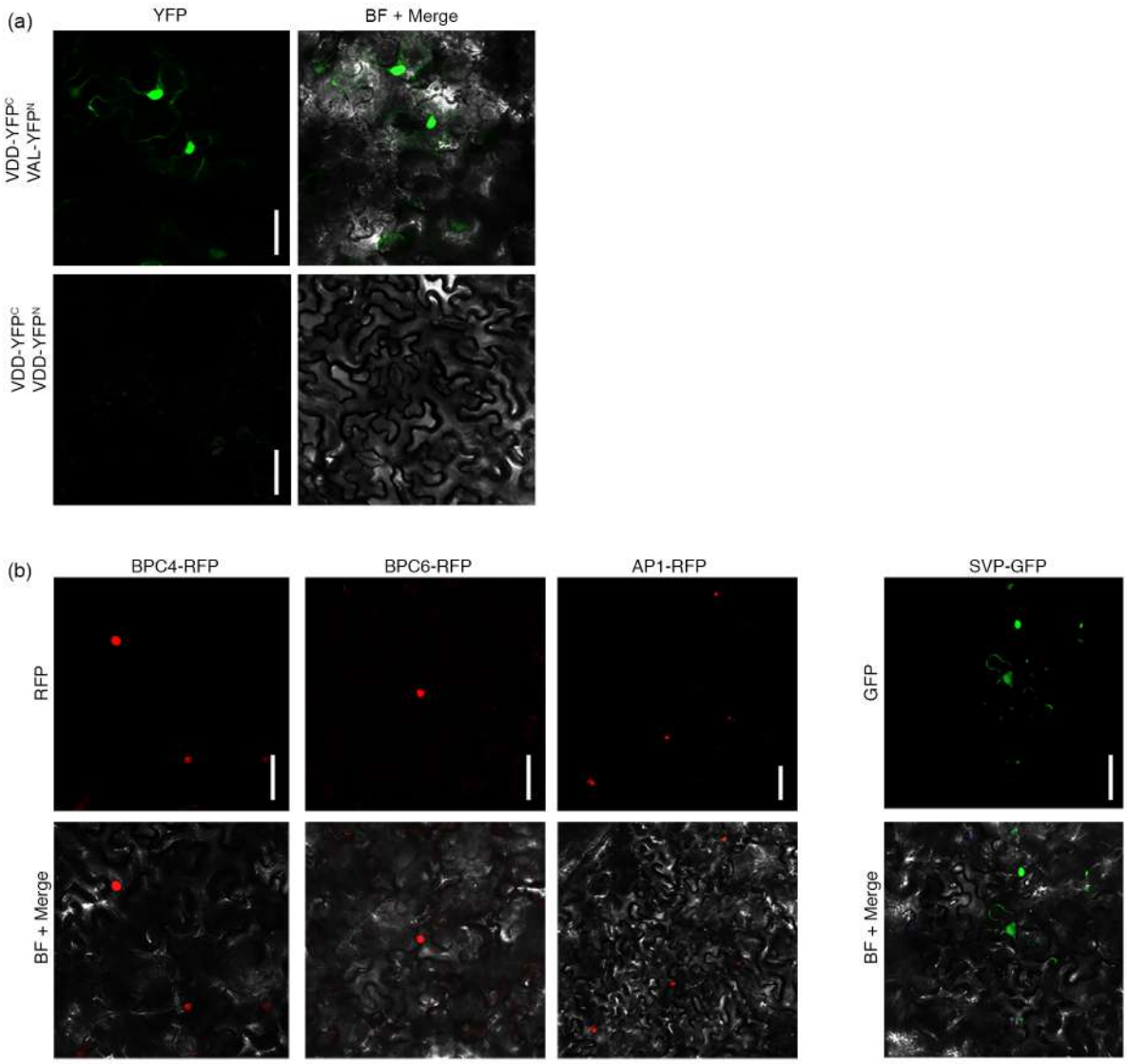

Figure S4. Bi-molecular fluorescence complementation (BiFC) assay positive controls and cellular localization of BPC4-RFP, BPC6-RFP, AP1-RFP and SVP-GFP.

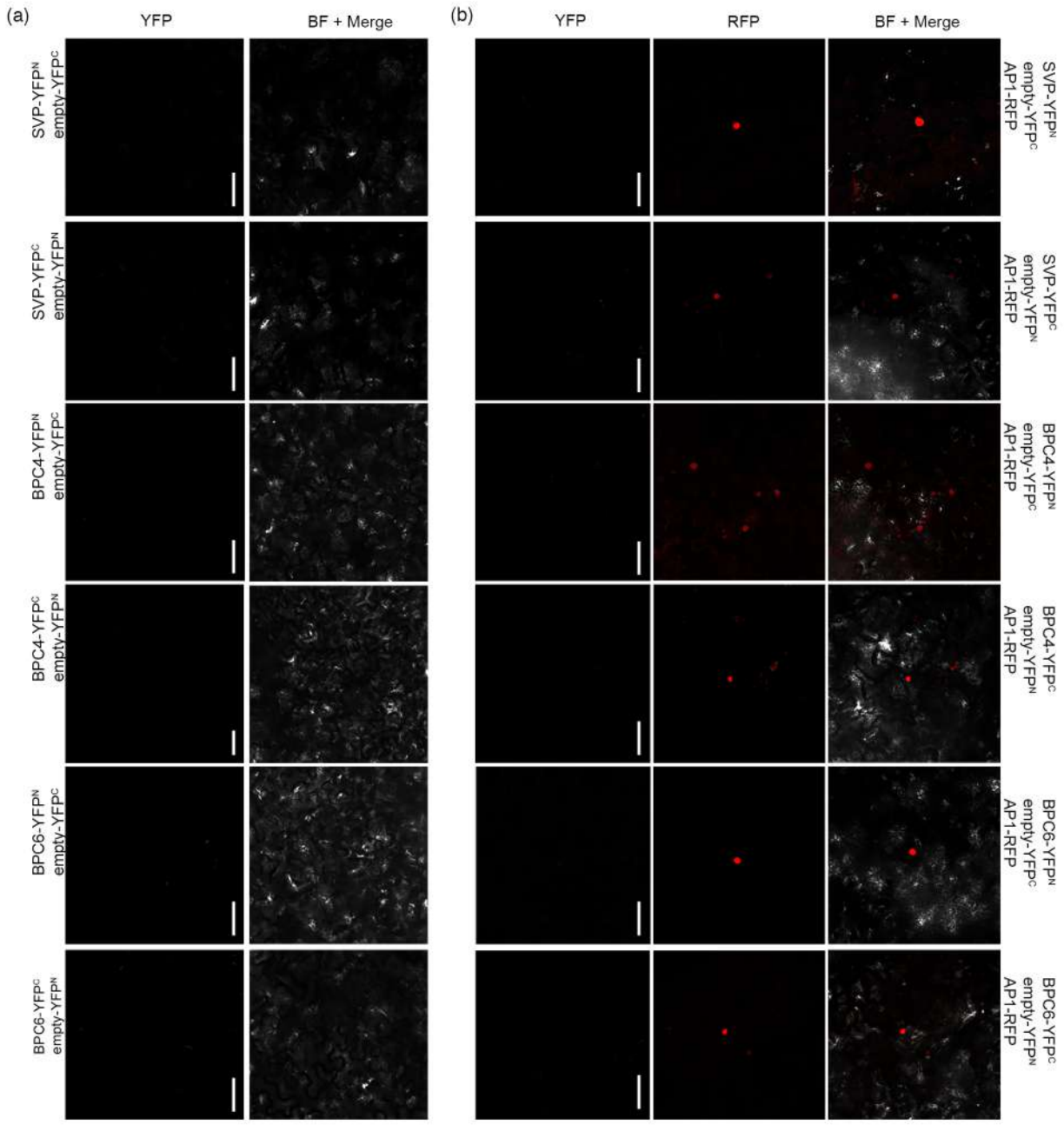

Figure S5. Bi-molecular fluorescence complementation (BiFC) assay, negative controls.

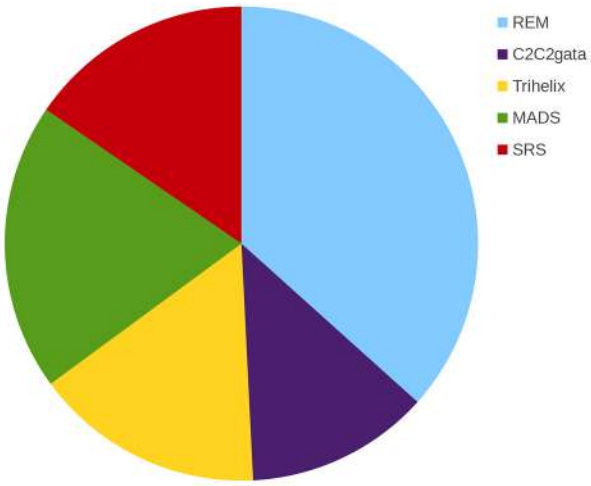

Figure S6. Proportion of significantly overlapped DAP-Seq Peaks by TF family.

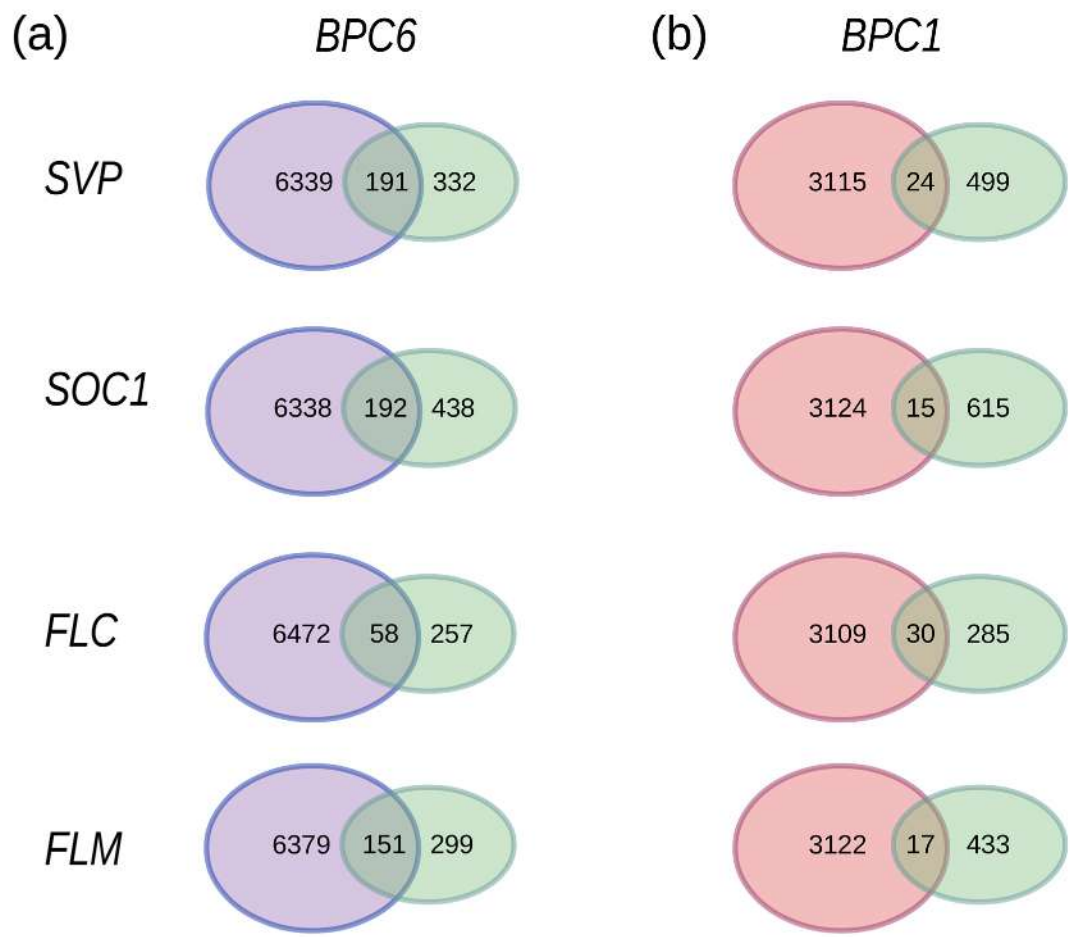

Figure S7. Venn diagrams of common ChIP-seq peaks between BPC1, BPC6 and a selection of MADS-domain TFs

Supporting Tables

CArG-box 1	Wild-type version	CCATCTTTGT
	Mutated version	CTGCGCTTGT
CArG-box 2	Wild-type version	CTATATATGC
	Mutated version	CTATGCGCAC
CArG-box 3	Wild-type version	ACAATTATGA
	Mutated version	ACAGCCACAA
CArG-box 4	Wild-type version	CCTTATTTTT
	Mutated version	CTCCGCTTTT
CArG-box 5	Wild-type version	CCATGAAAGA
	Mutated version	CTGCAGAAGA
CArG-box 6	Wild-type version	CCTTTCTTGT
	Mutated version	CCTTTTCCGT
CArG-box 7	Wild-type version	GCTAAAGTGG
	Mutated version	GCTAGGACAG
CArG-box 8	Wild-type version	CCAAATCTGT
	Mutated version	CCAAGCTCAT
CArG-box 9	Wild-type version	GTAATAATGT
	Mutated version	GTAACGGCAT
CArG-box 10	Wild-type version	CCATATTTCC
	Mutated version	CCATATGGTT
CArG-box 11	Wild-type version	CCAATTTTTT
	Mutated version	TTGGTTTTTT

Table S1. MADS-domain consensus regions identified in *STK* promoter and the designed mutated versions.

Genotyping	
BPC1 fw	TAGCGATCTTCTCATCGAAGC
BPC1 rv	AGTCGTACAACAAGCGGATTG
bpc 1-2 fw	TAGCGATCTTCTCATCGAAGC
bpc 1-2 rv	AGTCGTACAACAAGCGGATTG
BPC2 fw	AGCCCGGGCATGGATGACGATGGGTTTCG
BPC2 rv	AGTCGTACAACAAGCGGATTG
bpc2 fw	AGCCCGGGCATGGATGACGATGGGTTTCG
bpc2 rv	TAGCGATCTTCTCATCGAAGC
BPC3 fw	GGGGACCACTTTGTACAAGAAAGCTGGGTTTATCTGATGGTGACGAACTTATTGG
BPC3 rv	GAGTACAAAGAGAGAGAAGTCC
BPC4 fw	CCCCAGCATCAGATTAAGGA
BPC4 rv	CGTGCCTAGCCCAATAGTCT

bpc4 fw	CCCCAGCATCAGATTAAGGA
bpc4 rv	TAGCATCTGAATTTCATAACCAATCTCGATACAC
BPC6 fw	ATCTCAAATGGATGATGGTGG
BPC6 rv	TTCCCCATTTGTAGCACTGTC
bpc6 fw	ATCTCAAATGGATGATGGTGG
bpc6 rv	GCGTGGACCGCTTGCTGCAACT
SVP fw	GACCCACTAGTTATCAGCTCAG
SVP rv	AAGTTATGCCTCTCTAGGAC
svp-41 fw	GACCCACTAGTTATCAGCTCAG
svp-41 rv	AAGTTATGCCTCTCTAGGTT
AP1 fw	GGAGAGGGAAAAAATTCTTAGGGCTCCAC
AP1 rv	ATCATGACATCATGTAACCATCACTAACAGC
ap1-12 fw	TGGTTCTGCTGATCCCACTGCTCATA
ap1-12 rv	CCATACAGGAGCAAAACAGCATG
AGL24 fw	GATCCACCTTCTACTCATCTCC
AGL24 rv	CCACACACATGAAATAGATGATC
agl24-2 fw	GATCCACCTTCTACTCATCTCC
agl24-2 rv	GAGCGTCGGTCCCCACACTTCTATAC
Expression analysis by qRT-PCR	
UBI fw	CTGTTCACGGAACCCAATTC
UBI rv	GGAAAAAGGTCTGACCGACA
STK fw	ACGCGCAGAAAAGGGAGATTGAGC
STK rv	TGTCGGGATCAGAGTAAGAACCTCC
qRT-PCR ChIP assay	
ACTIN7 fw	CGTTTCGCTTTCCTTAGTGTTAGCT
ACTIN7 rv	AGCGAACGGATCTAGAGACTCACCTTG
gSTK region B fw	CTTTATAAAGGAGAAAGAAAGAGA
gSTK region B rv	CAAAGATGGGAACTTGATGAG
gSTK C-12 fw	TATCAATTTGATTTGTTTTCTCTCT
gSTK C-12 rv	CAAAGATGGGAACTTGATGAG
pSTK-CArGwt fw	TCTCTGCTAGATTCTCTTTC
pSTK-CArGwt rv	GGGAAACACAAGAAACATTA
pSTK-CArGm fw	TCTCTGCTAGATTCTCTTTC
pSTK-CArGm rv	GGGAAACACAAGAAATGCCG
gSTK region 1 fw	TCTCTGCTAGATTCTCTTTC
gSTK region 1 rv	GGGAAACACAAGAAACATTA
gSTK region 2 fw	CGTCTGCGAAAAACCGAGCT
gSTK region 2 rv	GGACCAATACCTTCATTGTACTTTGAA
AGAMOUS fw	ATGCTGAAGTCGCACTCATCGTCT
AGAMOUS rv	GAGCACGAGAAGAAGAAGAAACCTG
AT2G22560 fw	TAATGTCCCTAATGTTCCCAAA
AT2G22560 fw	CTCAGGCTTACTCAAACCCGA
NC box fw	CCTTATTTTGTTTCTTTTTACC
NC box rv	CTAAGATTGCGAGCAGTAG
Cloning yeast hybrid, BiFC and CoIP constructs	
BPC4 AttB1 fw	GGGGACAAGTTTGTACAAAAAAGCAGGCTTCATGGAGAATGGTGGTCAGTA
BPC4 AttB2 rv	GGGGACCACTTTGTACAAGAAAGCTGGGTCCTACTTGATAGTGATGTAGCGG
BPC6 AttB1 fw	GGGGACAAGTTTGTACAAAAAAGCAGGCTTCATGGATGATGGTGGGCA
BPC6 AttB2 rv	GGGGACCACTTTGTACAAGAAAGCTGGGTCTCATTTAATCGTAATGTAGCGG
SVP AttB1 fw	GGGGACAAGTTTGTACAAAAAAGCAGGCTTCATGGCGAGAGAAAAGATTC
SVP AttB2 rv	GGGGACCACTTTGTACAAGAAAGCTGGGTCCTAACCACCATACGGTAAGC

AP1 AttB1 fw	GGGGACAAGTTTGTACAAAAAAGCAGGCTTCATGGGAGGGGTAGGGTTCA
AP1 NO STOP AttB2 rv	GGGGACCACTTTGTACAAGAAAGCTGGGTTCATGCGGCGAAGCAGCCAAGG
BPC4 NO STOP AttB2 rv	GGGGACCACTTTGTACAAGAAAGCTGGGTCCTTGATAGTGATGTAGCGG
BPC6 NO STOP AttB2 rv	GGGGACCACTTTGTACAAGAAAGCTGGGTCTTTAATCGTAATGTAGCGG
SVP NO STOP AttB2 rv	GGGGACCACTTTGTACAAGAAAGCTGGGTCACCACCATACGGTAAGCCG

Table S2. Sequences of oligonucleotides used in this manuscript.

MADS-Box and bHLH Transcription Factors Coordinate Transmitting Tract Development in *Arabidopsis thaliana*.

Di Marzo M [1], Roig-Villanova I [2], Zanchetti E, **Caselli F** [1], Gregis V [1], Bardetti P [3], Chiara M [1], Guazzotti A [1], Caporali E [1], Mendes MA [1], Colombo L [1] and Kater MM [1]

[1] Dipartimento di Bioscienze, Università degli Studi di Milano, Milan, Italy

[2] Department of Agri-Food Engineering and Biotechnology, Barcelona School of Agricultural Engineering, UPC, Castelldefels, Spain.

[3] Department of Biology, Center for Genomics & Systems Biology, New York University, New York, NY, United States

May 2020; Front. Plant Sci. 11:526; doi:10.3389/fpls.2020.00526

In this paper, the role of a MADS-Box and bHLH transcription factor complex during transmitting tract development was investigated. Molecular and genetic evidences presented here revealed that the interactions between the AGAMOUS family members *STK*, *SHP1*, and *SHP2*, the bHLH gene *CES* and the closely related genes *BEE1* and *BEE3* controls transmitting tract development in Arabidopsis. Transcriptomic analysis of the *bee1 bee3 stk ces-4* quadruple mutant uncovering new downstream players, involved in transmitting tract differentiation.

I contributed to this work by performing yeast-two hybrid protein-protein interaction analysis between CST, STK and BEE1, which showed that CST and STK are able to interact.

frontiers in Plant Science

ORIGINAL RESEARCH
published: 06 May 2020
doi: 10.3389/fpls.2020.00526

MADS-Box and bHLH Transcription Factors Coordinate Transmitting Tract Development in *Arabidopsis thaliana*

*Maurizio Di Marzo†, Irma Roig-Villanova†‡, Eva Zanchetti, Francesca Caselli, Veronica Gregis, Paola Bardetti‡, Matteo Chiara, Andrea Guazzotti, Elisabetta Caporali, Marta Adelina Mendes, Lucia Colombo and Martin M. Kater**

Dipartimento di Bioscienze, Università degli Studi di Milano, Milan, Italy

The MADS-domain transcription factor *SEEDSTICK* (*STK*) controls several aspects of plant reproduction. *STK* is co-expressed with *CESTA* (*CES*), a basic Helix-Loop-Helix (bHLH) transcription factor-encoding gene. *CES* was reported to control redundantly with the brassinosteroid positive signaling factors BRASSINOSTEROID ENHANCED EXPRESSION1 (BEE1) and BEE3 the development of the transmitting tract. Combining the *stk ces-4* mutants led to a reduction in ovule fertilization due to a defect in carpel fusion which, caused the formation of holes at the center of the septum where the transmitting tract differentiates. Combining the *stk* mutant with the *bee1 bee3 ces-4* triple mutant showed an increased number of unfertilized ovules and septum defects. The transcriptome profile of this quadruple mutant revealed a small subset of differentially expressed genes which are mainly involved in cell death, extracellular matrix and cell wall development. Our data evidence a regulatory gene network controlling transmitting tract development regulated directly or indirectly by a STK-CES containing complex and reveal new insights in the regulation of transmitting tract development by bHLH and MADS-domain transcription factors.

Keywords: bHLH, cell death, cell wall, extracellular matrix, MADS-box, transmitting tract

OPEN ACCESS

Edited by:
Marc Libault,
University of Nebraska-Lincoln,
United States

Reviewed by:
Brigitte Poppenberger,
Technical University of Munich,
Germany
Natalia Pabón-Mora,
University of Antioquia, Colombia

***Correspondence:**
Martin M. Kater
martin.kater@unimi.it

†These authors have contributed equally to this work

‡Present address:
Irma Roig-Villanova,
Department of Agri-Food Engineering and Biotechnology, Barcelona School of Agricultural Engineering, UPC, Castelldefels, Spain
Paola Bardetti,
Department of Biology, Center for Genomics & Systems Biology, New York University, New York, NY, United States

Specialty section:
This article was submitted to Plant Cell Biology, a section of the journal Frontiers in Plant Science

Received: *19 December 2019*
Accepted: *07 April 2020*
Published: *06 May 2020*

Citation:
Di Marzo M, Roig-Villanova I, Zanchetti E, Caselli F, Gregis V, Bardetti P, Chiara M, Guazzotti A, Caporali E, Mendes MA, Colombo L and Kater MM (2020) MADS-Box and bHLH Transcription Factors Coordinate Transmitting Tract Development in Arabidopsis thaliana. Front. Plant Sci. 11:526. doi: 10.3389/fpls.2020.00526

INTRODUCTION

The plant life cycle in Angiosperms is characterized by the alternation of diploid sporophyte and haploid gametophyte generations. The sporophyte produces spores, which then develop into gametophytes. The gametophytes produce either the male or the female gametes. Sexual reproduction requires the delivery of sperm nuclei, via the pollen tube, to the embryo sac, where fertilization occurs, and the new diploid sporophyte is formed.

The growing of the pollen tube through the female reproductive organ tissues in Angiosperms is a crucial step in plant sexual reproduction. In *Arabidopsis thaliana*, the pistil or gynoecium results from the fusion of two carpels. The apical part of the pistil is formed by the stigma and the stigma papillae, which are needed to attach the pollen. The stigma is connected by the style to the ovary, in

which lodge the ovules. The septum divides the Arabidopsis ovary into two locules. At the center of the septum, as in the style, the transmitting tract tissue develops. Pollen tubes must travel through several distinct tissues before reaching ovules, including the stigma and the transmitting tract both in the style and in the septum (Lord and Russell, 2002; Roeder and Yanofsky, 2006).

The transmitting tract differentiates from the carpel margin meristem (CMM), a meristematic tissue that develops as two internal crests that, fuse when they reach each other in the middle of the young pistil at developmental stage 9. The transmitting tract is fully developed at stage 12 of pistil development (Bowman et al., 1999; Roeder and Yanofsky, 2006; Reyes-Olalde et al., 2013). The cells composing the transmitting tract secrete an extracellular matrix (ECM), a complex mixture of polysaccharides, glycoproteins, and glycolipids that accompany the growing pollen tubes (Lennon et al., 1998). Indeed, the pollen tubes grow faster, longer and more precisely *in vivo* than *in vitro*, suggesting the importance of the ECM for pollen tube growth in response to female signal factors (Johnson and Preuss, 2002; Johnson and Lord, 2006; Kim et al., 2006). Moreover, programmed cell death (PCD) in the transmitting tract is critical for pollen tube growth as well. The PCD of the transmitting tract starts before anthesis and can be accelerated by pollination (Crawford et al., 2007).

A complex genetic network controls the development of the transmitting tract. The zinc-finger transcription factor NO TRANSMITTING TRACT (NTT) has pivotal roles in this process. In the *ntt* mutant, the PCD of the cells composing the transmitting tract during fertilization, which is also influenced by the ECM composing cell wall, is severely compromised (Crawford et al., 2007). The changes in PCD and ECM in the *ntt* mutant cause a partial failure in pollen tube growth, with a high percentage of unfertilized ovules from the middle to the bottom part of the siliques (Crawford et al., 2007). NTT acts upstream of three genes that work redundantly in the control of the style and transmitting tract development, that are *CESTA* (*CES*), also named *HALF FILLED* (*HAF*), a bHLH-encoding transcription factor, and two phylogenetically related genes *BRASSINOSTEROID ENHANCED EXPRESSION1* (*BEE1*) and *BEE3* (Crawford and Yanofsky, 2011; Poppenberger et al., 2011).

*BEE*s expression and activity are induced in response to brassinosteroids (Friedrichsen et al., 2002). BRASSINOSTEROID INSENSITIVE 2 (BIN2) directly represses CES activity by phosphorylating it and thus promoting its degradation, restricting its subcellular localization and inhibiting the DNA binding activity of this transcription factor (Vert et al., 2005; Kim and Wang, 2010; Poppenberger et al., 2011). In response to brassinosteroids, phosphorylation of CES is inhibited and the unphosphorylated isoform accumulates promoting its SUMOylation (Khan et al., 2014). It is hypothesized that the brassinosteroid-induced SUMOylation of CES may facilitate the activation of some target genes involved in plant resistance to freezing stress (Eremina et al., 2016).

The triple mutant *ces* (*haf*) *bee1 bee3* shows similar defects in transmitting tract development as Crawford and collaborators previously observed in the *ntt* mutant (Crawford and Yanofsky, 2011). Furthermore, ectopic expression of *CES* (*HAF*) increases the diameter of the transmitting tract allowing more pollen tubes to pass through it simultaneously (Crawford and Yanofsky, 2011).

Recently, NTT was found to interact with the MADS-domain transcription factor SEEDSTICK (STK) to control transmitting tract development (Herrera-Ubaldo et al., 2019). STK was previously identified for its role in ovule development and acts redundantly with other two MADS-box transcription factors SHATTERPROOF1 (SHP1) and SHP2 (Pinyopich et al., 2003).

NTT and *STK* have similar expression patterns in the medial domain of the pistil (Herrera-Ubaldo et al., 2019). At anthesis, the *ntt stk* double mutant presents a number of cells composing the septum similar to wild type (Herrera-Ubaldo et al., 2019). However, in the *ntt stk* mutant siliques, there is a partial failure in septum fusion, and it appears to have holes. The fact that the cell number composing the septum has not changed suggests that the abnormal fusion is not related to early stages of development but rather to later defects during epidermis formation (Herrera-Ubaldo et al., 2019). The partial failure of pollen tube growth in the *ntt stk* mutant is also caused by the absence of degeneration and collapse of the cells composing the septum and consequently the transmitting tract (Herrera-Ubaldo et al., 2019).

Mendes et al. (2016) performed a bioinformatic analysis to identify genes with expression patterns similar to *STK*, using Arabidopsis Affymetrix microarray data from 2000 independent experiments. From this experiment *CES* was identified as one of the best candidates to participate in the same processes as STK.

Here we report a genetic and molecular analysis which revealed interactions between the AGAMOUS family members *STK*, *SHP1,* and *SHP2*, the bHLH gene *CES* and the closely related genes *BEE1* and *BEE3* in the control of transmitting tract development in Arabidopsis. We further performed a transcriptome analysis of the *bee1 bee3 stk ces-4* quadruple mutant uncovering new downstream players, involved in transmitting tract differentiation.

MATERIALS AND METHODS

Plant Material and Growth Conditions

All plants used in this study were in the Columbia (Col-0) ecotype. For all analyses, *Arabidopsis thaliana* seeds were incubated for 2 days at 4°C after sowing. Plants were grown at 22°C under long day conditions (LD). The *ces-4* mutant was obtained from NASC (SAIL_674_A01 lines). This line phenocopy the *ces-3* (*haf*), *ces-1* and *ces-2* mutant alleles that have been previously characterized (Crawford and Yanofsky, 2011; Eremina et al., 2016). The *stk*, *shp1,* and *shp2* mutants were provided by M. Yanofsky (Pinyopich et al., 2003), the *bee1 bee2 bee3* triple mutant was provided by J. Chory (Friedrichsen et al., 2002). The other mutant combinations analyzed were obtained by crossing. The *pCES::GUS* line was provided by Prof. B. Poppenberger (Poppenberger et al., 2011).

Mutant Genotyping

Genotyping of the mutants was done by PCR analysis. All the primers used in this study are listed in **Supplementary Table S11**.

In situ Hybridization Analysis

Arabidopsis flowers and siliques were fixed and embedded in paraffin as previously described in Dreni et al. (2011). Tissue sections (8 μm) were hybridized with a *CES* specific antisense RNA probe and observed with a Zeiss Axiophot D1 microscope. Images were captured on an Axiocam MRc5 camera (Zeiss) using the Axiovision program (version 4.1).

Gus-Staining Analysis

GUS staining of *pCES::GUS* was performed as described in Balanzà et al. (2016).

Silique Analysis

The percentage of unfertilized ovules per fruit was determined by opening at least 20 mature siliques for each genotype, counting the number of unfertilized ovules and the total number of developed seeds per silique under a stereomicroscope. The statistical significance of the differences in unfertilized ovules was analyzed using an Anova test followed by the Tukey HSD test ($^{**}p < 0.01$). All the experiments were repeated four times. For each experiment 5 siliques were collected from 4 independent plant lines of the same genotype.

Scanning Electron Microscope (SEM) Pictures

Biological samples were collected and fixed overnight at 4°C in FAA solution (3.7% formaldehyde, 5% acetic acid and 50% ethanol). Fixed tissues were washed with water and post-fixed with aqueous 2% osmium tetroxide for 2 h at room temperature. Tissues were rinsed several times in deionized water and dehydrated in a graded series of ethanol for 15 min per rinse. This step was followed by critical point drying with liquid CO_2 and sputter-coating with gold in a Nanotech sputter coater. Specimens were analyzed using a LEO 1430 Scanning Electron Microscope.

Pollen Tube Guidance Analysis

Experiments of pollen tube guidance were performed as previously described by Mendes et al. (2016) and images were captured on an Axiocam MRc5 camera (Zeiss) using the Axiovision program (version 4.1).

Bimolecular Fluorescence Complementation Assay (BiFC)

Coding Sequences (CDS) of *CES* and *STK* were amplified by PCR with the primers indicated in **Supplementary Table S11** and first cloned into pDONOR207 (Life Technologies) and subsequently into the pYFPN43 and pYFPC43 vectors.[1] BiFC experiments were conducted as previously described in Balanzà et al. (2016). Essentially, the abaxial surfaces of tobacco leaves were observed 2–5 days after agroinfiltration and the interactions were monitored using a Leica TCS confocal microscope.

Yeast Two-Hybrid Assays

The two-hybrid assays were performed at 22°C in the yeast strain AH109 (Clontech), using the cotransformation technique (Egea-Cortines et al., 1999). The coding sequences of *CESTA*, *STK*, and *BEE1* were cloned in the Gateway vector GAL4 system (pGADT7 and pGBKT7; Clontech) passing through pDONOR207 (Life Technologies). Yeast two-hybrid interaction assays were performed on selective yeast synthetic dropout medium lacking Leu, Trp, Adenine, and His supplemented with different concentrations of 3-aminotriazole (1, 2.5, 5, 10, and 15 mM of 3-AT).

RNA Extraction and qRT-PCR Analysis

For the qRT-PCR experiment of *ces-4* (knockout validation) total RNA was extracted from whole inflorescences using the LiCl method as previously described (Verwoerd et al., 1989). First-strand cDNA was synthesized using an IMProm-II ™ Reverse Transcription System (Promega). Enrichments fold were detected using a SYBER Green assay (Bio-Rad).[2] The qRT-PCR assay was performed in triplicate using a Bio-Rad iCycler iQ optical system (software version 3.0a). The qRT-PCR assay was repeated three times. For each experiment the RNA was extracted from three independent plant lines.

RNA Sequencing

Total RNA was extracted from three biological replicates (1 gr, obtained from a pool of 5 plants for each replicate) from both wild-type and *bee1 bee3 stk ces-4* mutant inflorescences till stage 12, using the Macherey Nagel "Nucleospin RNA Plant" according to the manufacturer's instructions. RNA concentrations and integrity were determined using Qubit Fluorometer and the Qubit™ RNA XR Assay Kit (Thermo Fisher Scientific). Sequencing libraries were prepared using the NEBNext Ultra II Directional RNA library Prep Kit for Illumina (NEB) according to the manufacture's instruction and sequenced on the HiSeq Illumina platform. Reads were mapped on the reference *Arabidopsis thaliana* genome (TAIR, version 10) using the bowtie2 program (Langmead and Steven, 2012; **Supplementary Table S4**). Estimation of gene expression levels was performed using RSEM (Li and Dewey, 2011). Identification of differentially expressed genes was performed by the quasi-likelihood *F*-test as implemented by edgeR (Robinson et al., 2009). A False Discovery Rate (FDR) cut-off value of 0.05 was applied for the identification of significantly differentially expressed genes. Graphical representation of the data was performed by means of the gplots R library. To validate the data obtained from the RNAseq experiment, we extracted total RNA from wild type and *bee1 bee3 stk ces-4* mutant inflorescences till stage 12, using the Macherey Nagel "Nucleospin RNA Plant" according to the manufacturer's instructions. The cDNA and qRT-PCR were performed as described in the previous paragraph "RNA extraction and qRT-PCR analysis." The qRT-PCR assay to validate RNAseq experiment was repeated three times. For each experiment the RNA was extracted from three independent plant lines that were used for RT-PCR analysis.

[1] http://www.ibmcp.upv.es/FerrandoLabVectors.php

[2] http://www.bio-rad.com

TFBS Analysis

Enrichment analysis of Transcription Factor Binding Sites (TFBS) was performed by means of the Pscan tool, using the "non-redundant" set of Jaspar TFBS matrices (Fornes et al., 2019) and considering a region spanning from the TSS to 500 bp upstream (default settings). Archetype consensus sites for the W-box, MADS-box and G-box elements were established as the Jaspar TFBS matrix showing the highest enrichment in our dataset according to Pscan. To identify genes with high confidence W-box, MADS-box and G-box elements in their promoters, the complete set of 33239 Arabidopsis transcripts according to the TAIR10 annotation were scanned using the highly significantly enriched TFBS matrices as defined above. Distribution of scores were established for each element, and an Expectation-Maximization algorithm as implemented in the R EM-cluster package was used to fit a 2 Gaussian mixture model. Based on the EM model promoters were partitioned in "high" and "low" scoring. Only promoters that were confidently assigned to high scoring clusters (confidence > 95%) were considered to have a bona fide TFBS element. Similarly, to our previous analyses promoters were defined as regions spanning 500 bp upstream of the TSS. *P*-values for the enrichment of genes with W-box, MADS-box and G-box elements in their promoters were performed by means of the hypergeometric distribution test as implemented in the R stats package.

Accession Numbers of the Genes

The GenBank/EMBL accession numbers for the genes shown in this study are the following: *BEE1*, At1g18400; *BEE2*, At4g36540; *BEE3*, At1g73830; *CES*, At1g25330; *SHP1*, At3g58780; *SHP2*, At2g42830; *STK*, At4g09960. The accession number of the genes identified in the transcriptomic analysis are indicated in **Supplementary Tables S5, S6**.

RESULTS

SEEDSTICK and CESTA Are Co-expressed

In order to identify new targets, partners and/or regulators of *STK*, a bioinformatic analysis was previously performed in the laboratory to discover genes co-expressed with *STK* (Mendes et al., 2016). This kind of analysis assumes that correlation between the patterns of gene expression in a large range of different experimental conditions could indicate a functional relationship (Aoki et al., 2007). As already described, the procedure to identify genes that have expression profiles that correlate with *STK* was proven successful since among the top listed genes *SHP1* and *SHP2* were found, which act redundantly with STK in the control of ovule identity (Pinyopich et al., 2003). Furthermore, top rated were *VERDANDI* (*VDD*) and *VALKYRIE* (*VAL*), targets of the STK-SEPALLATA3 (SEP3) complex, which both act in the control of the death of the synergid cell that is receptive of the pollen tube (Mendes et al., 2016). *CES* (At1g25330) rated in position 14 of the correlators, having an expression correlation with *STK* of p(LIN) 0.759 and p(LOG) 0.505 (Mendes et al., 2016).

Previously, it has been reported that *CES* is expressed from stage 8 to 15 of flower development, first in CMM and later in the stigma, septum and funiculi (Crawford and Yanofsky, 2011; Poppenberger et al., 2011). Since *STK* is expressed during female reproductive organ development (mainly septum, transmitting tract, replum, funiculus and ovule/seed) (Pinyopich et al., 2003; Mizzotti et al., 2014; Herrera-Ubaldo et al., 2019; Di Marzo et al., 2020), we investigated in more detail the spatio-temporal expression pattern of *CES* during pistil, ovule and seed development. We performed both RNA *in situ* hybridization and the analysis of the *pCES::GUS* reporter gene construct (**Figure 1**). The RNA *in situ* analysis experiments showed that *CES* was expressed in ovules during early stages of development until mature ovule formation and its transcripts were also present in the transmitting tract before fertilization (**Figures 1A–C**). In mature ovules, a high expression was detected in the funiculus (**Figure 1C**). After fertilization and during embryo development *CES* mRNA was present at high levels in the early globular stage, and at heart and torpedo stages mRNA levels were lower (**Figures 1D–F**). Analysis of the *pCES::GUS* plants confirmed the *in situ* data (**Figures 1G–I**) and these experiments showed that *STK* and *CES* partially overlap in their expression patterns during ovule and transmitting tract development (Pinyopich et al., 2003; Crawford and Yanofsky, 2011; Poppenberger et al., 2011; Herrera-Ubaldo et al., 2019).

Arabidopsis Plants With *stk, shp, ces,* and *bee* Mutant Combinations Are Partially Sterile

To further analyze the role of CES, we characterized a CES loss-of-function allele that we obtained from the SAIL collection (Alonso and Stepanova, 2003). This allele, that we called *ces-4*, has a T-DNA insertion in the second exon, differently from *ces-1, ces-2,* and *ces-3* (*haf*), previously published T-DNA knockout insertion alleles (Crawford and Yanofsky, 2011; Poppenberger et al., 2011; Eremina et al., 2016). The qRT-PCR analysis performed to check *CES* expression in the *ces-4* mutant indicated that this is also a null allele (**Supplementary Figure S1**). Analysis of *ces-4* homozygous plants did not reveal any general phenotype at the level of the entire plant, which was consistent with previous reports for the *ces* (*haf*) mutant alleles (Crawford and Yanofsky, 2011; Poppenberger et al., 2011; Eremina et al., 2016). We crossed the *ces-4* mutant with *stk* to obtain the *stk ces-4* double mutant. The double mutant was indistinguishable from wild type plants apart from a large number of unfertilized ovules at the lower part of the siliques. In wild type plants on average 1.0% of the ovules in a silique remained unfertilized. In the *stk* mutant we observed on average 6.2% unfertilized ovules, and in the *ces-4* single mutant 11.6% ($^{**}p < 0.01$ in respect to wild type; **Figure 2** and **Supplementary Table S1**). In the *stk ces-4* double mutant this phenotype was further increased to 28.1% of unfertilized ovules (**Figure 2** and **Supplementary Table S1**). Like in the *ces-4* single mutant, also

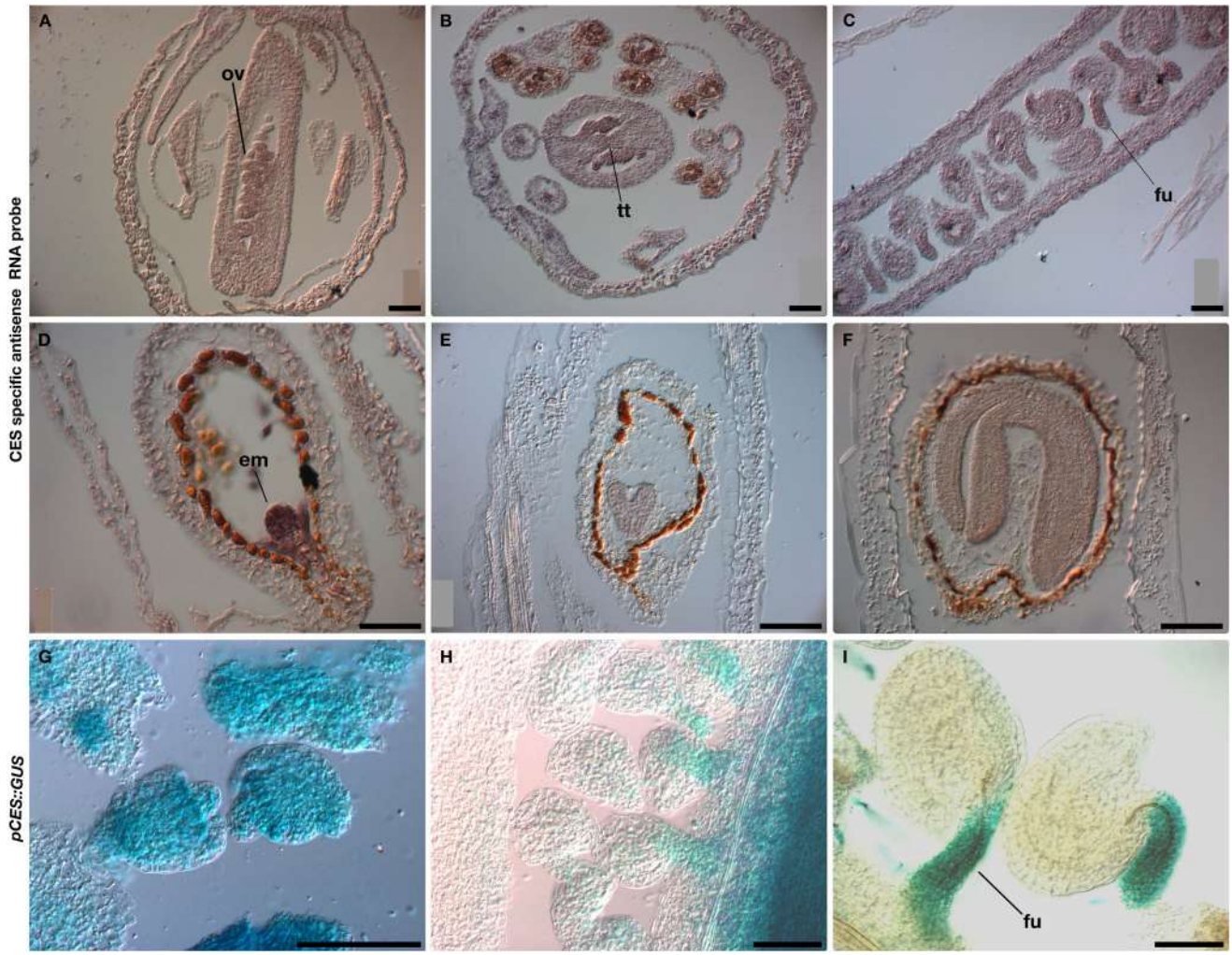

FIGURE 1 | Analysis of *CES* expression. *In situ* hybridization **(A–F)** and GUS activity of the *pCES::GUS* marker line **(G–I)** showed *CES* expression in ovules **(A–C,G–I)**, transmitting tract **(B)**, and in the embryos of the developing seeds **(D–F)**. Em, embryo; fu, funiculus; ov, ovule; tt, transmitting tract. Scale bars: 50 μm.

in the *stk ces-4* double mutant the unfertilized ovules were located always at the lower part of the siliques (**Figure 2** and **Supplementary Table S1**).

Since SHP1 and SHP2 are closely related to STK and have shown to control together with STK ovule identity redundantly (Pinyopich et al., 2003), we investigated whether they also play a role together with CES in the control of ovule fertilization. Therefore, the *shp1 shp2* double mutant was crossed with the *ces-4* mutant to obtain the *shp1 shp2 ces-4* triple mutant. The *shp1 shp2* double mutant showed on average 7.0% unfertilized ovules (**Figure 2** and **Supplementary Table S1**). The *shp1 shp2 ces-4* triple mutant showed a clear increase to 16.2%, also in this case the unfertilized ovules were localized at the lower part of the siliques ($^{**}p < 0.01$ in respect to wild type and *shp1 shp2*; **Figure 2** and **Supplementary Table S1**). Unfortunately we could not analyze the *stk shp1 shp2* triple mutant, because the triple mutant does not develop normal ovules (Pinyopich et al., 2003). These results suggest that the MADS-domain transcription factor STK, SHP1 and SHP2 have a role together with CES in the control of ovule fertilization.

The contribution of the *BEE* genes to this process was also investigated (**Figure 3** and **Supplementary Table S2**). *CES* is phylogenetically related to *BEE1* and *BEE3*, which have been described as redundant with *BEE2* (Friedrichsen et al., 2002). Moreover, it has been shown that CES together with BEE1 and BEE3 redundantly control the development of the transmitting tract in the pistil (Crawford and Yanofsky, 2011; Poppenberger et al., 2011). The single mutants *bee1* and *bee3* and the multiple mutant combinations *bee1 bee3* and *bee1 bee2 bee3* did not show any obvious phenotype (**Figure 3** and **Supplementary Table S2**). To investigate redundancy between *BEE* genes and *STK*, we obtained the *bee1 bee2 bee3 stk* quadruple mutant, that presented 9.2% of unfertilized ovules, with $^{**}p < 0.01$ when compared to wild type and the triple mutant *bee1 bee2 bee3*, which again were preferentially positioned at the lower part of the siliques (**Figure 3** and **Supplementary Table S2**). This percentage is

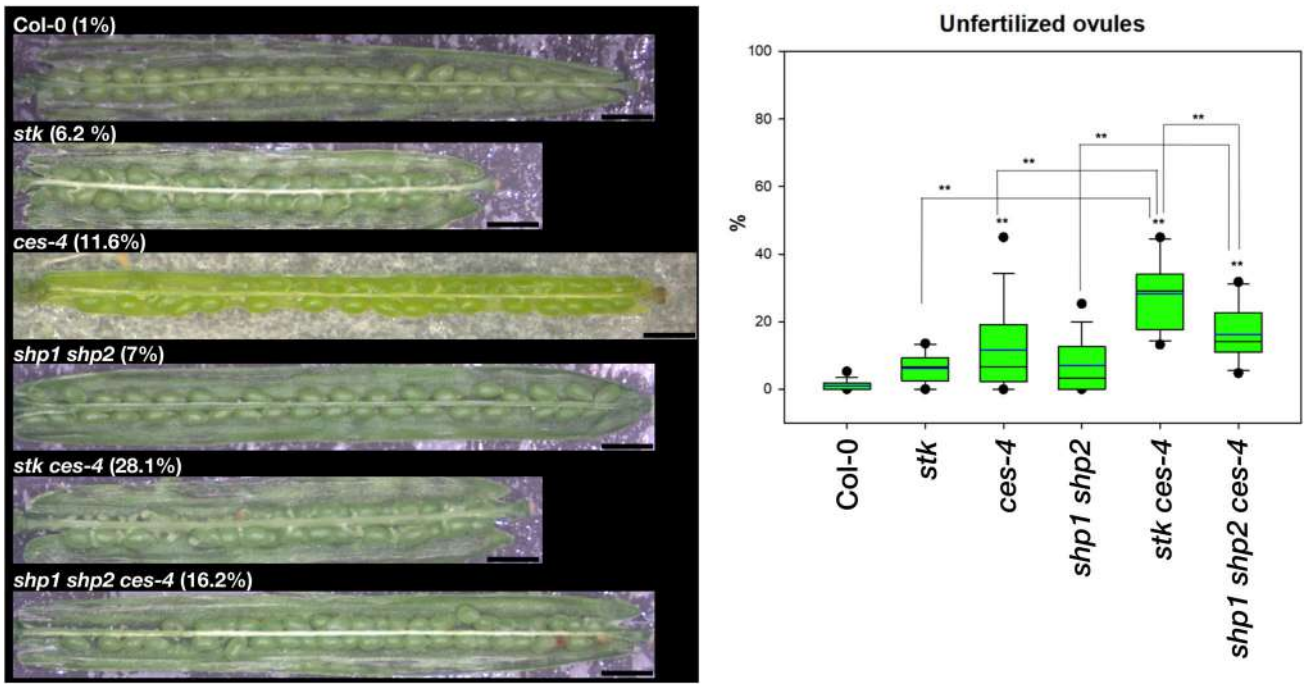

FIGURE 2 | Unfertilized ovules analysis in multiple mutant combination of *stk*, *ces-4,* and *shp1 shp2*. **(A)** Stereomicroscope images of opened siliques of the *stk and ces-4* single mutants, the *stk ces-4* and the *shp1 shp2* double mutants, the *shp1 shp2 ces-4* triple mutant and the wild type Col-0; Scale bars: 1 mm. **(B)** Box plots of all the mutants analyzed in comparison to wild type Col-0. Statistical analysis was performed using Anova followed by Tukey HSD test (**$p < 0.01$). The experiment was repeated four times. For each experiment 5 siliques were collected from 4 independent plant lines of the same genotype to obtain a total of 20 analyzed siliques.

lower than the *bee1 bee2 bee3 ces-4* quadruple mutant, which presented in average 28.7% of unfertilized ovules (**Figure 3** and **Supplementary Table S2**). Despite the weaker phenotype, our results demonstrated that STK and BEEs also have a role together in ovule fertilization. To investigate if combining the *ces-4* mutant could further enhance the unfertilized ovule phenotype, we generated the *bee1 bee3 stk ces-4* quadruple and the *bee1 bee2 bee3 stk ces-4* quintuple mutants. The results of this analysis showed that *bee1 bee3 stk ces-4* had on average 46.6% unfertilized ovules, and a similar result was obtained in the *bee1 bee2 bee3 stk ces-4* (44.0%) (**Figure 3** and **Supplementary Table S2**), showing that the addition of the *bee2* allele did not further enhance the phenotype. The unfertilized ovules in these cases are localized from the middle to the bottom part of the siliques. Altogether, these results indicated that the MADS-domain transcription factors function not only together with CES, but also with the BEEs in the control of the fertilization of all the ovules within the Arabidopsis fruit.

STK and CES Regulate Transmitting Tract Development

To better understand the defect that caused the presence of a high percentage of unfertilized ovules at the lower part of the siliques in the different mutant combinations, we performed reciprocal crosses between wild type and *stk ces-4* or *shp1 shp2 ces-4* mutant plants, to analyze if the female, male or both parts were defective. The outcome of the reciprocal crosses shown in **Supplementary Figure S2**, suggested that the unfertilized-ovules phenotype was only present when the mutant genotypes were used as mothers. This result indicates that the defects resides only in the female reproductive organ.

To further investigate the defect present in the female reproductive organs, which caused the high number of unfertilized ovules at the lower part of the siliques in the multiple mutant combinations, we analyzed the septum morphology by Scanning Electron Microscope (SEM), at stage 17-B of fruit development, when the siliques reach their maximum size (Roeder and Yanofsky, 2006).

The *stk* and *ces-4* single mutants presented a septum similar to wild type, while the double mutant *stk ces-4* disclosed a defect in septum morphology (**Figure 4A**). The double mutant was characterized by a partial failure of septum fusion in the central portion of the septum in conjunction with the medium portion of the ovary (**Figure 4A**). The quadruple mutant combinations *bee1 bee2 bee3 stk* and *bee1 bee2 bee3 ces-4* did not display defects in septum morphology when compared to wild type (**Figure 4A**). However, the damage of the septum appears stronger in the quadruple mutant *bee1 bee3 stk ces-4* and in the quintuple mutant *bee1 bee2 bee3 stk ces-4* where a hole in the central portion of the septum was seen in conjunction with the medium region of the ovary (**Figure 4A**).

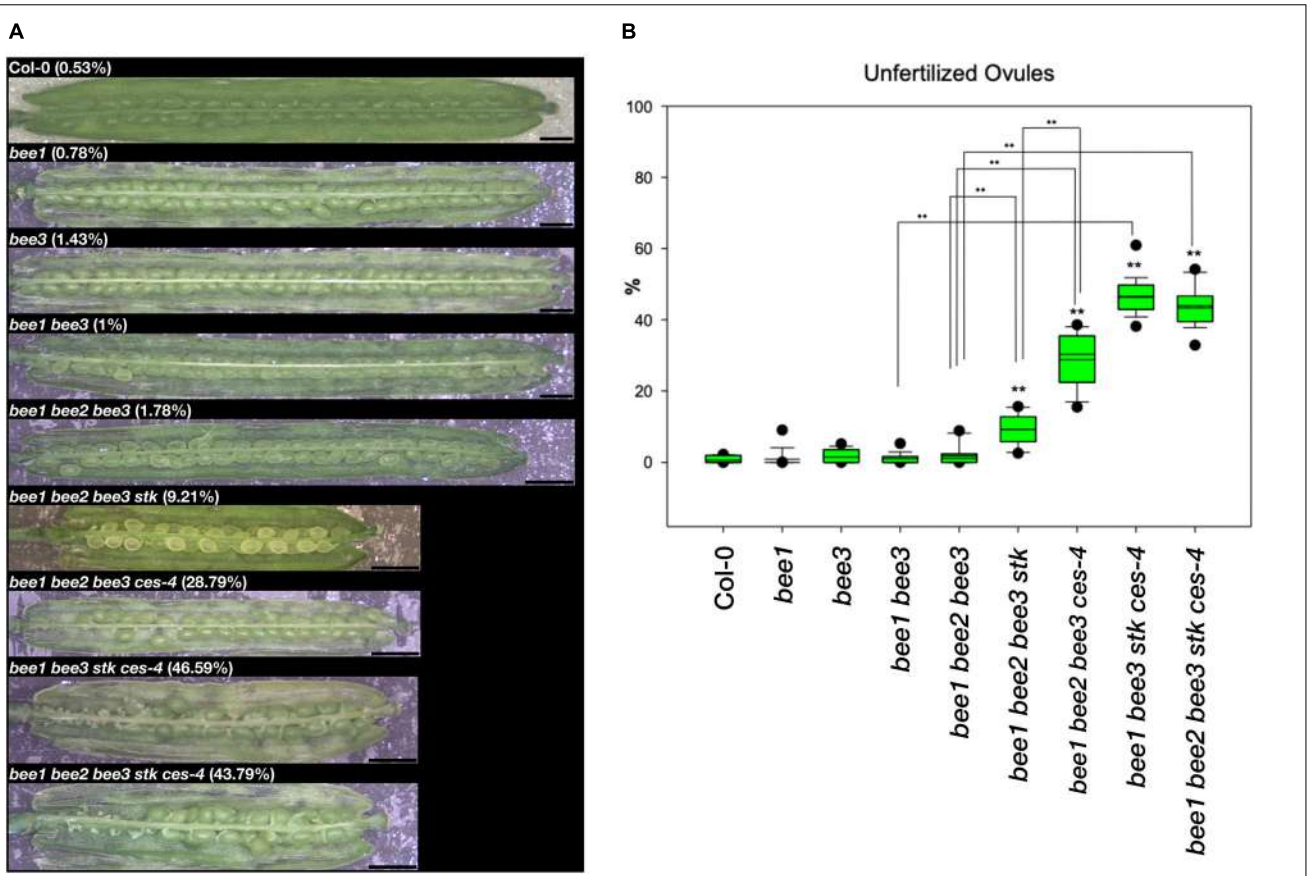

FIGURE 3 | Unfertilized ovules analysis in multiple mutant combination of *bee1*, *bee2*, *bee3*, *stk,* and *ces-4*. **(A)** Stereomicroscope images of opened siliques of the *bee1* and *bee3* single mutants, the *bee1 bee3* double mutant, the *bee1 bee2 bee3* triple mutant, the *bee1 bee2 bee3 stk,* the *bee1 bee2 bee3 ces-4,* and *bee1 bee3 stk ces-4* quadruple mutants, the *bee1 bee2 bee3 stk ces-4* quintuple mutants and the wild type Col-0; Scale bars: 1 mm. **(B)** Box plots of all the mutants analyzed in comparison to wild type Col-0. Statistical analysis was performed using Anova followed by Tukey HSD test (**$p < 0.01$). The experiment was repeated four times. For each experiment 5 siliques were collected from 4 independent plant lines of the same genotype to obtain a total of 20 analyzed siliques.

The septum morphological analysis at stage 17-B suggests a transmitting tract defect caused by a failure of the carpel fusion which happens from stage 9 to 12 (Roeder and Yanofsky, 2006). At these stages, fusion occurs within the two crests of the CMM leading to septum and transmitting tract formation (Bowman et al., 1999; Roeder and Yanofsky, 2006; Reyes-Olalde et al., 2013).

To confirm that the defects found in the septum and transmitting tract formation, described for *stk ces-4*, *bee1 bee3 stk ces-4,* and *bee1 bee2 bee3 stk ces-4* caused a defective growth of the pollen tubes through the ovary transmitting tract, pistils were hand pollinated with wild type pollen and an aniline blue staining was performed after 36 h (**Figure 4B**). In the wild-type-hand-pollinated control pistils all the pollen tubes reached the bottom part of the ovary. However, pollen tube growth was compromised in the three mutant combinations. In the *stk ces-4* double mutant the pollen tubes did not grow further than the middle region of ovary length (**Figure 4B**). A stronger phenotype was observed in *bee1 bee3 stk ces-4* quadruple and in the *bee1 bee2 bee3 stk ces-4* quintuple mutants, where the pollen tubes stopped growing at the upper part of the ovary (**Figure 4B**).

The differences in septum morphology and in pollen tube growth in the double mutant *stk ces-4*, in the quadruple mutant *bee1 bee3 stk ces-4* and in the quintuple mutant *bee1 bee2 bee3 stk ces-4* clearly indicate that the fusion of the carpels, that permits the correct development of the septum and consequently of the transmitting tract, was partially disturbed in these mutants and the cause that the ovules at the lower part of the siliques remained unfertilized.

SEEDSTICK and CESTA Interact in Yeast and *Planta*

The experiments described above showed a genetic interaction between *STK* and *CES*. To investigate if there is also a physical interaction between these proteins, Bimolecular Fluorescence Complementation (BiFC) was performed. As a positive control, cells were co-transformed with CES (YC-CES) and (YN-CES), as CES was shown to homodimerize in yeast (Poppenberger et al., 2011; **Figure 5A**). Reconstitution of YFP fluorescence in the nuclei of co-transformed cells confirmed that CES is able to interact with STK *in vivo* (**Figure 5A**), supporting our idea

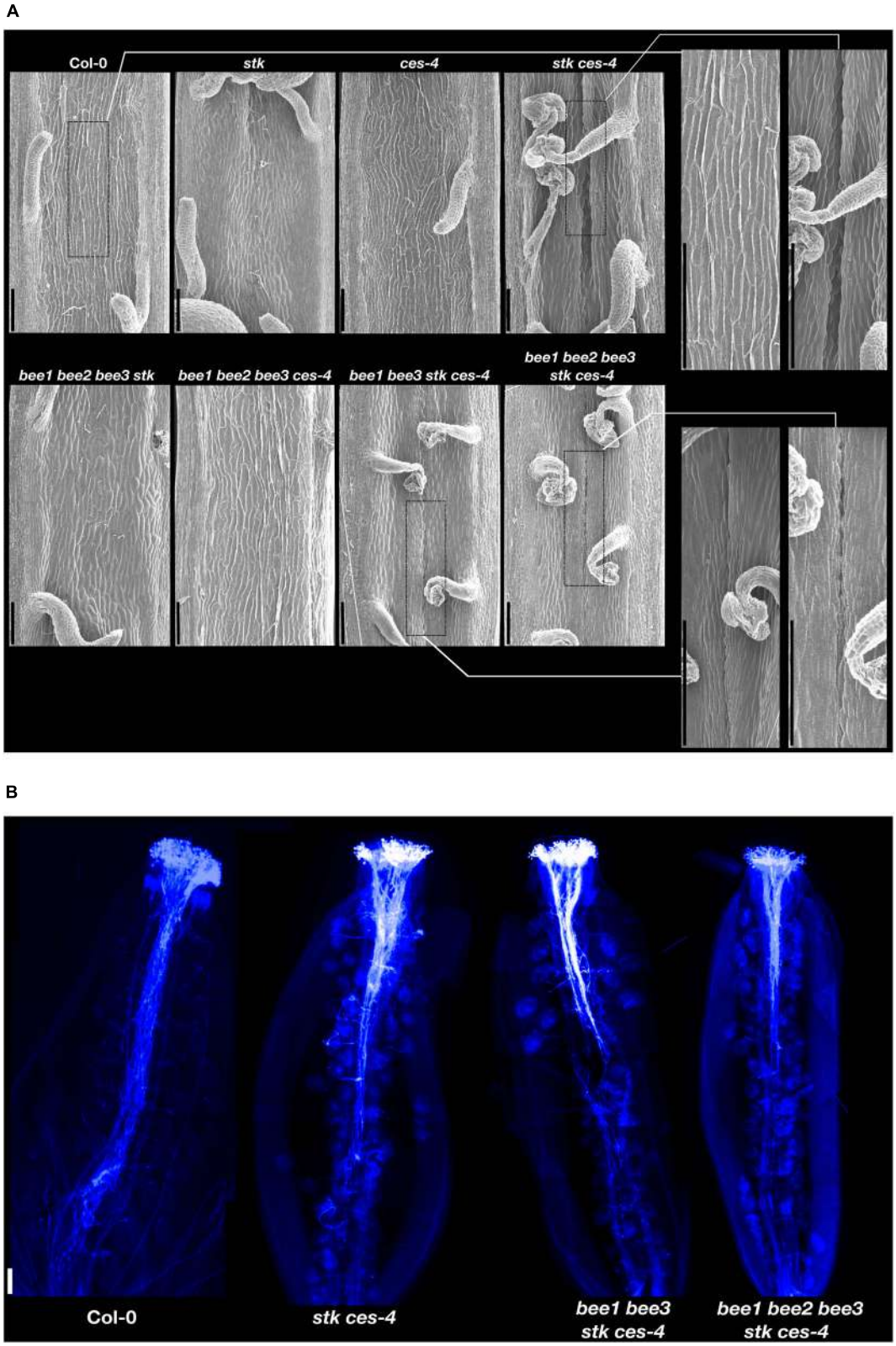

FIGURE 4 | Septum analysis and pollen tube growth. **(A)** Scanning Electron Microscope pictures of the septum of opened siliques of *stk*, *ces-4*, *stk ces-4*, *bee1 bee2 bee3 stk*, *bee1 bee2 bee3 ces-4*, *bee1 bee3 stk ces-4* and *bee1 bee2 bee3 stk ces-4* and wild type Col-0; Scale bars: 100 μm. **(B)** Aniline blue staining of *stk ces-4, bee1 bee3 stk ces-4* and *bee1 bee2 bee3 stk ces-4* and wild type Col-0; Scale bar: 50 μm.

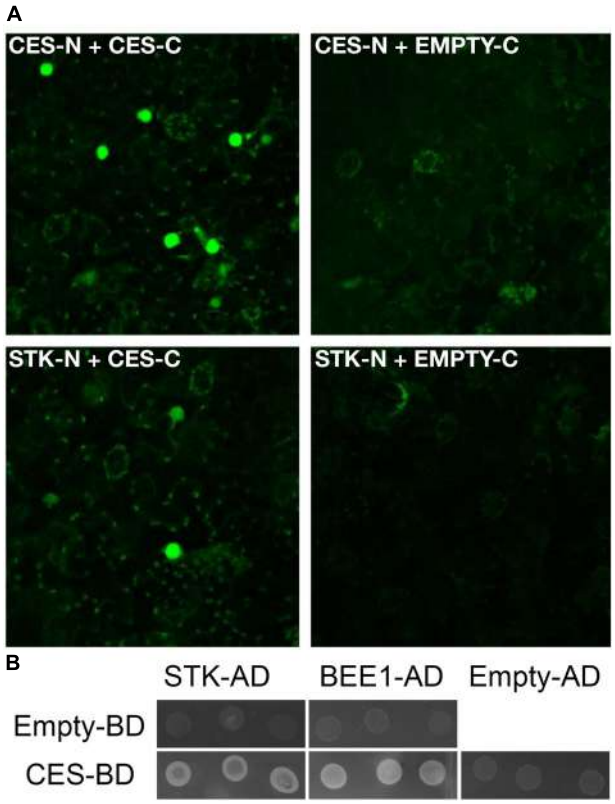

FIGURE 5 | STK, CES and BEE1 interaction assays in yeast and *in planta*. **(A)** BiFC assays showing the interaction of STK with CES. STK-N or CES-N: STK or CES fusion with the N-terminal part of the split YFP; STK-C or CES-C: STK or CES fusion with the C-terminal part of the split YFP. CES-N CES-C interaction was used as positive control. STK-N EMPTY-C and CES-N EMPTY-C were used as negative control. **(B)** Yeast two-hybrid assays testing interactions between STK-AD, BEE1-AD, and CES-BD; interactions were considered positive when growth on -W-L-H +15 mM of 3-AT selective media was observed. The experiments were performed at 22°C. The CES-BEE1 interaction was chosen as a positive control (Poppenberger et al., 2011), the growth of transformants carrying empty AD or BD vectors were used as negative controls of the experiments.

that CES and STK form a complex that controls transmitting tract formation. The interaction between STK and CES was also confirmed by Y2H experiments (**Figure 5B**). As positive control in these experiments we used the previously published interaction between BEE1 and CES (Poppenberger et al., 2011; **Figure 5B**). Furthermore, we observed that STK and BEE1 were not able to interact. The complete list of vector combinations, interactions and growth media used in this Y2H assay are described in **Supplementary Table S3**.

Transcriptome Analysis of the *bee1 bee3 stk ces-4* Quadruple Mutant Reveals Target Genes Involved in Transmitting Tract Development

To obtain a snapshot of the regulatory network controlled by STK, CES, and BEE proteins, in the development of the septum/transmitting tract, transcriptional profiles of the quadruple mutant *bee1 bee3 stk ces-4,* which displayed the most severe phenotype, were studied by RNA sequencing. RNA was extracted from the quadruple mutant and wild type inflorescences until stage 12 of pistil development, before fertilization since the transmitting tract is fully developed at this stage (Bowman et al., 1999; Roeder and Yanofsky, 2006; Reyes-Olalde et al., 2013).

For the identification of significantly differentially expressed genes, a FDR cut-off value of 0.05 was applied and a total of 202 differentially expressed genes were identified. A total of 31 genes were upregulated in the mutant (**Supplementary Table S5**) while 171 genes were downregulated (**Supplementary Table S6**). Furthermore, functional enrichment analyses revealed that gene ontology categories such as glycosinolate, glycoside and carbohydrate biosynthetic and metabolic processes were enriched for the upregulated genes (**Supplementary Table S7**), while the downregulated genes were involved in the cell death, cell wall, plant-type cell wall biosynthesis components and response to hormone stimulus (**Supplementary Table S8**).

Remarkably, among the downregulated genes, three genes were previously described as direct targets of STK (Herrera-Ubaldo et al., 2019): *AT3G26140*, *AT1G28710,* and *AT1G06080*. The *AT3G26140* gene which encodes a glycosyl hydrolase (GH5_11) is expressed in CMM during pistil development (Aspeborg et al., 2012; Herrera-Ubaldo et al., 2019). The GH5 enzymes are all mannan endo-beta-1,4-mannosidases which are known to be involved in cell wall remodeling processes (Aspeborg et al., 2012; Lombard et al., 2014; Herrera-Ubaldo et al., 2019). *AT1G28710* encodes for a nucleotide diphospho-sugar transferase protein which is involving in the biosynthesis of polysaccharides, that are fundamental components of the ECM (Lennon et al., 1998; Tung et al., 2005; Herrera-Ubaldo and de Folter, 2018). *AT1G06080* [*DELTA 9 DESATURASE1* (*ADS1*)], encodes for a fatty acid desaturase which is involved in lipid biosynthesis, expressed in flowers (Fukuchi-Mizutani et al., 1998; Yao et al., 2003; Heilmann et al., 2004; **Table 1**, see also **Figure 6** for heatmap description). Downregulation of these three genes was also confirmed by qRT-PCR (**Supplementary Figure S3**).

PCD is a key process in the transmitting tract for ovule fertilization (Crawford et al., 2007). Interestingly, several genes involved in the regulation of cell death were downregulated in the quadruple mutant (**Table 1** and **Figure 6**). One of the most important is *GRIM REAPER* (*GRI*, *AT1G53130*) that encodes for a small protein with an extracellular localization that is able to positively regulate cell death (Wrzaczek et al., 2009, 2015; **Table 1** and **Figure 6**). Moreover, we observe that *ACCELERATED CELL DEATH 6* (*ACD6*, *AT4G14400*) another positive regulator of cell death is also downregulated (Rate et al., 2007; **Table 1** and **Figure 6**).

Additionally, we notice the downregulation of three genes encoding for the Arabinogalactan proteins (AGPs) *ARABINOGALACTAN PROTEIN 5* (*AGP5*, *AT1G35230*), *AGP7* (*AT5G65390*), and *AGP14* (*AT5G56540*). AGPs are structurally complex plasma membrane and cell wall proteoglycans that are implicated in diverse developmental processes, including plant sexual reproduction (Lennon et al., 1998; Coimbra et al.,

TABLE 1 | RNAseq data of candidate genes regulated by STK-CES protein complex and involved in transmitting tract development.

TAIR ID	Gene name	log FC	FDR	Gene function
AT4G14400	*ACD6*	−4.0117	2.33E-05	Cell death
AT1G06080	*ADS1*	−1.0338	2.17E-05	Cell wall and ECM biosynthesis
AT1G35230	*AGP5*	−2.1455	0.0145	Cell death and ECM biosynthesis
AT5G65390	*AGP7*	−1.3013	0.0024	Cell death and ECM biosynthesis
AT5G56540	*AGP14*	−0.7840	0.0473	Cell death and ECM biosynthesis
AT1G72290	*ATWSCP*	−6.5142	1.42E-07	Cell death and pollen tube growth
AT5G09730	*BXL3*	−2.0805	1.71E-06	Cell wall
AT1G75890	GDSL family of serine esterases/lipases	0.8845	0.0038	Cell wall and lipid metabolic process
AT4G28780	GDSL family of serine esterases/lipases	0.6227	0.0393	Cell wall and lipid metabolic process
AT4G16230	GDSL family of serine esterases/lipases	1.0662	0.0127	Cell wall and lipid metabolic process
AT3G26140	Glycosyl hydrolase family 5	−2.7099	3.13E-06	Cell wall and ECM biosynthesis
AT1G53130	*GRI*	−7.9981	4.16E-09	Cell death
AT4G14560	*IAA1*	−0.7727	0.0387	AUX signaling
AT3G23030	*IAA2*	−0.6711	0.0393	AUX signaling
AT4G14550	*IAA14*	−0.9381	0.0265	AUX signaling
AT1G04250	*IAA17*	−1.2215	0.0037	AUX signaling
AT2G38530	*LTP2*	−0.8702	0.0257	Lipid transport, cell death, cuticle biosynthesis
AT1G28710	Nucleotide diphospho-sugar transferase protein	−1.2338	0.00008	Cell wall and ECM biosynthesis
AT5G49180	*PME58*	−0.6750	0.0459	Cell wall
AT4G36110	*SAUR9*	−1.2233	0.0447	Auxin response
AT2G21220	*SAUR12*	−0.7960	0.0239	Auxin response

Column 1, Gene ID according to the TAIR10 annotation of the A. thaliana genome; Column 2, Gene name; Column 3, Log Fold Change of expression between bee1 bee3 stk ces-4 and wild type plants; Column 4, FDR: Benjamini Hochberg adjusted P-value for differential expression. A Significance cut-off of 0.05 is applied; Column 5, Brief description of the gene according to TAIR10 (if available). Total RNA was extracted from three biological replicates (1 gr, obtained from a pool of 5 plants for each replicate) from both wild-type and bee1 bee3 stk ces-4 mutant inflorescences.

2007, 2009). Importantly, these protein are able to regulate cell death in Arabidopsis cell culture (Gao and Showalter, 1999; Guan and Nothnagel, 2004). Intriguingly, we also detect a significant downregulation of *ATWSCP* (*AT1G72290*), which encodes for a Kunitz-type protease inhibitor, member of a small family of proteins, that are water-soluble chlorophyll proteins, and *LIPID TRANSFER PROTEIN 2* (*LTP2, AT2G38530*) (**Table 1** and **Figure 6**). *ATWSCP* is expressed in the septum and transmitting tract during its development, and after fertilization the protein is located in the medial domain of the silique where is able to regulate cell death and pollen tube growth (Bektas et al., 2012; Boex-Fontvieille et al., 2015). The *LTP2* gene encodes for a lipid transfer protein necessary for the movement of hydrophobic wax components through the hydrophilic cell wall matrix to reach the cuticle (Kunst and Samuels, 2003). LTP2 mediates cell wall loosening *in vitro* (Nieuwland et al., 2005).

Numerous genes involved in cell wall biosynthesis processes are mis-regulated in the quadruple mutant, these include *BETA-XYLOSIDASE 3* (*BXL3*, *AT5G09730*), which encodes for an enzyme involved in arabinan and xylan catabolic process (Minic et al., 2006), and *PECTIN METHYLESTERASE 58* (*PME58*, *AT5G49180*), encoding for a pectin methylesterases that contributes to cell wall modification (Turbant et al., 2016; **Table 1** and **Figure 6**); both genes were downregulated. Among the upregulated genes, there are three genes of the GDSL family of serine esterases/lipases, *AT1G75890*, *AT4G28780,* and *AT4G16230* (**Table 1** and **Figure 6**). These genes are involved in numerous aspect of plant development, but in particular the acetylxylan esterase activity of these enzymes could contribute in the degradation of cell walls in association with xylanases, cellulases, and mannanases (Akoh et al., 2004).

Moreover, some genes involved in the auxin signaling pathway were downregulated. These include genes encoding for Aux/IAAs proteins, *INDOLE-3-ACETIC ACID INDUCIBLE 1* (*IAA1*) (*AT4G14560*), *IAA2* (*AT3G23030*), *IAA14* (*AT4G14550*), and *IAA17* (*AT1G04250*) (**Table 1** and **Figure 6**). The Aux/IAA proteins are the early auxin response proteins and participate in auxin signaling through interacting, as repressors, with AUXIN RESPONSE FACTOR (ARF) proteins (Lavy and Estelle, 2016). In addition, the *SMALL AUXIN UPREGULATED RNA 9* (*SAUR9*) and *SAUR12* were also downregulated. The SAURs are small transcripts induced by auxin, that are localized in elongated tissues (McClure and Guilfoyle, 1987; Knauss et al., 2003). *SAUR9* and *SAUR12* are part of the *SAUR10*-clade (van Mourik et al., 2017).

Finally, we decided to explore the enriched binding sites from our RNAseq data of the quadruple mutant in order to find possible direct target genes of the complex formed by STK, CES, BEE1, and BEE3. The binding sites used by the MADS-domain and bHLH transcription factors have been characterized: MADS factors bind to CArG boxes (Egea-Cortines et al., 1999; de Folter and Angenent, 2006) while bHLHs recognize E-boxes, being G-boxes the most common form (Quail, 2000; Toledo-Ortiz et al., 2003), in order to regulate the activity of their target genes. On the other hand, W-box is the binding site used by the WRKY transcription factors (Ciolkowski et al., 2008).

Transcription factor binding sites enrichment analyses, performed by means of the Pscan tool (Zambelli et al., 2009) suggest a strong enrichment of G-box and G-box like elements in the upregulated genes (**Supplementary Table S9**), while a significant enrichment of W-box and MADS-box elements is observed in the downregulated genes (**Supplementary Table S10**). Notably, according to our analyses G-box elements are identified in 35% (p = 4E-05) of the upregulated genes, while W-box elements and MADS box elements are identified in 17 and 19 downregulated genes (p-values 9.3E-04 and 0.035), respectively. Unsurprisingly, considering the limited number

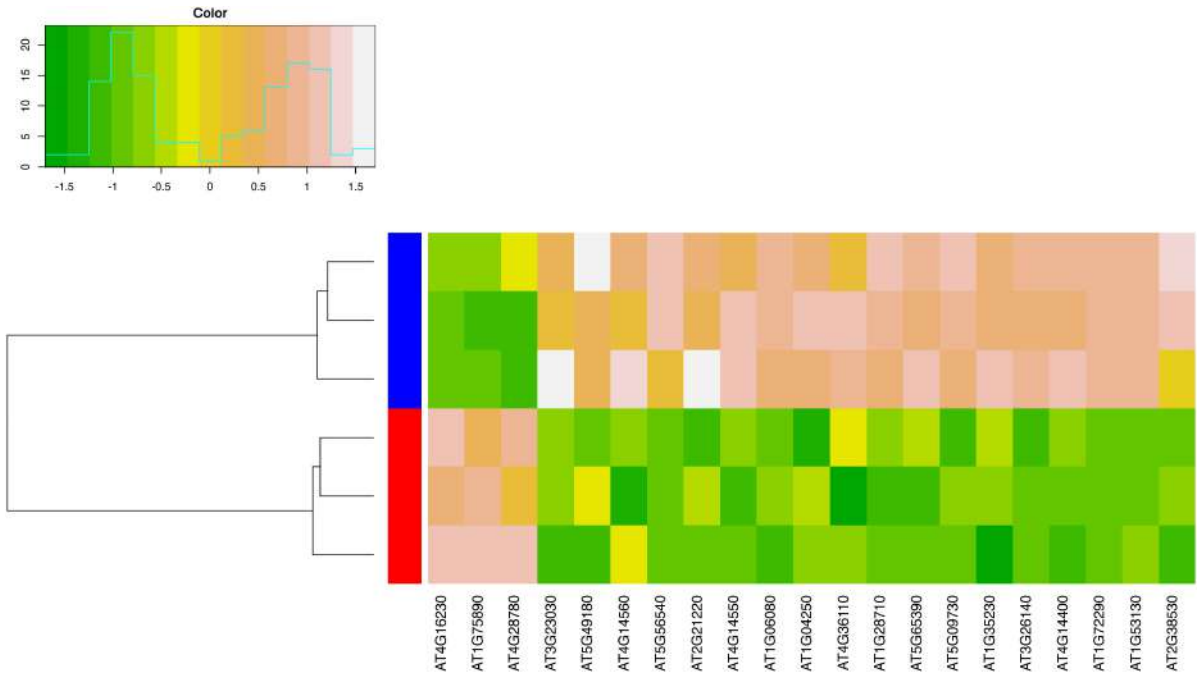

FIGURE 6 | Heatmap of differentially expressed genes described in **Table 1**. Expression levels are shown for each of the 6 independent biological replicates analyzed in this study. Genes are represented in the columns and the biological replicates in the rows. To facilitate comparison, the expression values were standardized with respect to the average expression of each gene. Dark green indicates low expression, light brown indicates high expression. In the columns, red is used to mark biological replicates for the quadruple mutant, blue is used to indicate biological replicates for wild type plants.

of genes that are differentially expressed in our experimental settings, we observe that only one gene has both a G-box and a CArG-box element in its promoter (*AT3G49270*, upregulated), only one gene has both a W-box and a MADS-box element (*AT1G05450*, downregulated), and none of the differentially expressed genes have a W-box and a G-box.

DISCUSSION

Genetic Redundancy Between MADS-Domain and bHLH Transcription Factors in Transmitting Tract Development

In Arabidopsis, the gynoecium is formed by the fusion of two carpels, which fuse vertically at their margins and give rise to the CMM. From this meristem the transmitting tract develops, an essential tissue to facilitate the growing pollen tubes to reach the ovules and fertilize them.

Recently, a role for STK in relation with NTT was shown during the development of transmitting tract (Herrera-Ubaldo et al., 2019). Here we reveal that STK may also act in the downstream pathway of NTT in a protein complex with CES. Our genetic analysis evidence the role and redundancies between the MADS-box genes *STK*, *SHP1,* and *SHP2*, the bHLH transcription factor gene *CES* and the closely related bHLH transcription factors *BEE1* and *BEE3* in the development of the transmitting tract in *Arabidopsis thaliana*. The *CES* gene was selected based on high correlation of its expression pattern with *STK* (Mendes et al., 2016) but also because this gene was shown to play a role in transmitting tract development (Crawford and Yanofsky, 2011; Poppenberger et al., 2011). *CES*, *BEE1,* and *BEE3* were shown to be expressed with distinct but overlapping patterns within the reproductive tract (Crawford and Yanofsky, 2011; Poppenberger et al., 2011). In the *ces* (*haf*) *bee1 bee3* triple mutant ECM biosynthesis and PCD fail to occur within this tissue (Crawford and Yanofsky, 2011).

The *stk* mutant did not present any type of reproductive defect (no statistical differences when the number of unfertilized ovules was compared with wild type), while the single mutant *ces-4* is characterized by a small but significative percentage of unfertilized ovules (**Figure 2**). However, the *stk ces-4* double mutant had 28.1% of unfertilized ovules, which were almost exclusively found at the basal part of the silique (**Figure 2**). This phenotype suggests, similar to the *ces bee1 bee3* triple mutant (Crawford and Yanofsky, 2011; Poppenberger et al., 2011), a defect in transmitting tract development.

Interestingly, we also observed a genetic interaction between *STK* and *BEE1* and *BEE3* in transmitting tract development since the *bee1 bee2 bee3 stk* quadruple mutant showed 9.21% unfertilized ovules at the lower part of the silique, while *stk* had only 6.2% and the triple mutant *bee1 bee2 bee3* displayed 1.8% of unfertilized ovules (**Figure 3**). In the light of the fact that this phenotype was weaker than that observed for *stk ces-4* (**Figure 2**), we suggest that CES plays a more predominant

role in transmitting tract formation together with STK. To understand a possible role of *SHP1* and *SHP2* in the formation of the transmitting tract, the triple mutant *shp1 shp2 ces-4* was obtained. This triple mutant showed 16.2% of unfertilized ovules which is also a milder phenotype when compared to *stk ces-4* (**Figure 2**). This suggests that STK is important for transmitting tract development, although is not able to cover for 100% *SHP*s function since the *shp1 shp2 ces-4* triple mutant presents a considerable percentage of unfertilized ovules.

Recently, it has been reported that in *Arabidopsis thaliana* the correct accomplishment of ovule fertilization directly influences the final length of the fruit. In the *ntt* mutant, in which the seeds only develop in the upper part of the fruit (Crawford et al., 2007), the authors described by using a fruit live imaging platform (FLIP) that in the upper part of the *ntt* siliques (where fertilization happens) the cells composing the valves elongate properly like in the wild type control while in the bottom part (where no fertilization occurs) the cells do not elongate properly (Ripoll et al., 2019). The quadruple mutant *bee1 bee3 stk ces-4*, which, similarly, to the *ntt* mutant displayed the highest percentage of unfertilized ovules from the middle to the bottom part of the fruit (Crawford et al., 2007), was characterized by a clear decrease in fruit length as can be seen in **Figure 3**, confirming the importance of ovule fertilization for fruit size.

The different degree of unfertilized ovule phenotypes obtained in the different mutant combinations points to redundancy between MADS-box, bHLH, and the BEEs transcription factor encoding genes in a dosage-dependent manner. The unfertilized ovules phenotype was only observed when different mutant alleles were combined and was more pronounced in the quadruple and quintuple mutants, suggesting an additive effect. Such a dosage dependent effect was already described for other MADS-box genes, like *FLOWERING LOCUS C* (*FLC*) that acts, in a dosage-dependent manner, as a potent repressor of the floral transition (Bastow et al., 2004; Michaels and Amasino, 2007; Sheldon et al., 2007).

Y2H and BIFC experiments showed that STK is able to interact with CES, but not with BEE1 (**Figure 5** and **Supplementary Table S3**). This result suggests that CES might bridge the interaction between MADS and BEE proteins to form a hypothetical multimeric complex that controls correct transmitting tract formation. Cooperative action of MADS-domain and bHLH transcription factors has been previously described in mice. Molkentin et al. (1995) showed that MEF2 factors, a family of MADS-domain proteins expressed in muscle cells and other cell types, acted as coregulators of myogenic bHLH proteins to activate muscle genes (Molkentin et al., 1995). Moreover, the authors show that these two types of transcription factors physically interact, and that either factor can interact with the other when one is bound to DNA (Molkentin et al., 1995). Interestingly, the authors present this as a general mechanism for the regulation of transcription in specific cell types (Molkentin et al., 1995). This might also be a mechanism for the combinatorial control of MADS-box (with STK as a main player) and bHLH (CES as principal component) transcription factors for the formation of the transmitting tract tissue in Arabidopsis. Studies to understand the nature of a multimeric complex formed by MADS-box and bHLH proteins would really be a very interesting field for future studies.

STK and CES Play a Role in Carpels Fusion

When we discovered, by backcrossing, that the male part was not compromised in the *stk ces-4* and *shp1 shp2 ces-4* multiple mutants (**Supplementary Figure S2**), we decided to perform a detailed analysis of the septum morphology of the mutants displaying the most stronger phenotype related to the percentage of unfertilized ovules. The single mutants *stk* and *ces-4* possess a similar septum respect to the wild type (**Figure 4**). However, when *STK* was mutated together with *CES* the fruits showed a septum fusion defect in the lower middle part in concomitance with the medial region of the ovary. The defective septum was found in the double mutant *stk ces-4*, in the quadruple mutant *bee1 bee3 stk ces-4* and in the quintuple mutant *bee1 bee2 bee3 stk ces-4*. Notably, no defective carpel fusion was revealed for the quadruple mutants *bee1 bee2 bee3 stk* and *bee1 bee2 bee3 ces-4* (**Figure 4**) which have a significant percentage of unfertilized ovules (**Figure 3**), confirming the hypothesis that only when *STK* and *CES* are mutated simultaneously the fusion of the carpels was in part compromised. Gynoecium defects were previously described only in the *ntt stk* double mutant, where there is a failure of the fusion with a septum that has a hole (Herrera-Ubaldo et al., 2019). The organ fusion defects were not disclosed for the single mutants *stk* and *ntt* and for the triple mutant *ces bee1 bee3* (Crawford and Yanofsky, 2011; Herrera-Ubaldo et al., 2019). In the *ces bee1 bee3* and probably in our quadruple mutant *bee1 bee2 bee3 ces-4* the unfertilized ovule phenotype is due to defects, as previously described by Crawford and Yanofsky (2011), in ECM components synthases and PCD failure in transmitting tract. In conclusion, only when the dimer STK-CES is not formed, the carpels fusion is compromised.

These phenotypes could be explained by mis-regulation of the genes involved in cuticle formation. The cuticle is a lipidic alteration of the cell wall (Yeats and Rose, 2013). The alteration in cuticle biosynthesis, deposition and wax component transports could cause organ fusion defects in plants, but in particular in flowers and carpels (Nawrath, 2006; Sieber et al., 2007; Panikashvili et al., 2010). Intriguingly transcriptional profiles of the quadruple mutant suggest a strong downregulation of *LTP2* (**Table 1** and **Figure 6**), a gene involved in lipid transport and/or wax transport to form the cuticle (Kunst and Samuels, 2003). Notably, the *LTP5* gene, expressed in the transmitting tract, which belongs to the same gene family as *LTP2*, and which did not show significantly altered expression in the quadruple mutant according to our analysis, has previously been shown to be involved in pollen tube guidance (Kunst and Samuels, 2003; Chae et al., 2009). We believe that also *LTP2* might be involved in the correct fertilization of the ovules influencing not just the pollen tube growth but also the correct fusion of the two carpels that permits to form the septum and transmitting tract. Moreover, in the *bee1 bee3 stk ces-4* quadruple mutant we detected the overexpression of three genes encoding for GDSL esterase/lipase involved in lipid catabolism (**Table 1** and

Figure 6). The overexpression of a GDSL named, *CUTICLE DESTRUCTING FACTOR 1* (*CDEF1*), causes abnormal organ fusion in leaves, stems and flowers (Takahashi et al., 2010). This gene codes for a protein which is considered a cutinase (Takahashi et al., 2010). It is possible that like for the *CDEF1* overexpression, the excess of cutinase in the quadruple mutant respect to wild type caused abnormal organ fusion.

STK and CES Influence Programmed Cell Death in Transmitting Tract

Cell death and tissue degeneration are required for pollen tube growth in the transmitting tract of Arabidopsis (Crawford et al., 2007). The phenotype described for combined *ces* and *bee* mutants showed that they fail to form the ECM and to accomplish PCD within the transmitting tract (Crawford and Yanofsky, 2011). Interestingly, STK has already been shown to control PCD in transmitting tract with NTT (Herrera-Ubaldo et al., 2019) but also in the receptive synergid cell through regulation of its direct target genes, *VDD* and *VAL*, two Reproductive Meristem (REM) transcription factors (Matias-Hernandez et al., 2010; Mendes et al., 2016).

As we show in the **Table 1**, in the quadruple mutant *bee1 bee3 stk ces-4* several genes involved in cell death are downregulated. The *ATWSCP* gene encodes for a Kunitz-type protease inhibitor localized preferentially in the transmitting tract and septum, which is involved in ECM and PCD but also in the exit of pollen tubes from the septum to reach the ovules during the fertilization phase (Bektas et al., 2012; Boex-Fontvieille et al., 2015). Also, *ACD6* is downregulated (**Table 1** and **Figure 6**), this gene encodes for a protein that promotes cell death in Arabidopsis (Rate et al., 2007). Furthermore, three Arabinogalactan genes (*AGPs*) resulted downregulated in the quadruple mutant (**Table 1** and **Figure 6**). The AGPs have been associated with ECM composition of the transmitting tract in different plant species (Hoggart and Clarke, 1984; Webb and Williams, 1988; Gane et al., 1995) and they have been shown to play a role in the regulation of PCD during pollen tube growth (Coimbra et al., 2009).

Does Auxin-Brassinosteroid Crosstalk Influence Transmitting Tract Development?

It was recently suggested that the auxin pathway plays an important role in the specification and formation of the tissues along the pistil axis (Larsson et al., 2013; Robert et al., 2015). However, the role of auxin signaling in transmitting tract development is still not fully understood. ARF6 and ARF8 regulate *CES* expression in the medial domain of the pistil during transmitting tract development (Crawford and Yanofsky, 2011). The double mutant *arf6 arf8* displayed reduced alcian blue staining, that detects acidic polysaccharides, the major components of the ECM (Crawford and Yanofsky, 2011). According to our RNAseq data, four *Aux*/*IAA*s and two *SAUR*s genes were downregulated in the quadruple mutant in respect to wild type (**Table 1** and **Figure 6**). Aux/IAA proteins and SAURs might be activated in presence of brassinosteroids since evidences of a crosstalk between auxin and brassinosteroid have already been described (Nakamura et al., 2006). Moreover, *SAUR9* expression is induced by a combination of auxin and brassinosteroids (van Mourik et al., 2017). Probably a STK-CES-BEE1-BEE3 complex is able to connect the auxin-brassinosteroid crosstalk in transmitting tract tissue, however, the precise role is of this crosstalk in the regulation of transmitting tract development remains unclear.

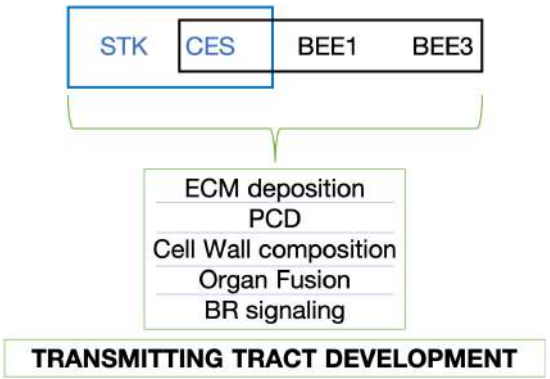

FIGURE 7 | Proposed model of transmitting tract development controlled by STK, CES, BEE1, and BEE3. The blue box symbolizes the interaction (STK-CES) that we found in this research project; The black box represents the interaction (CES-BEE1-BEE3) that has been previously described (Crawford and Yanofsky, 2011; Poppenberger et al., 2011). ECM, extracellular matrix; PCD, programmed cell death; BR, brassinosteroid.

Finally, from the analysis of the enriched binding sites an interestingly candidate was found to be a possible direct target of the complex composed by the MADS and bHLH transcription factors described in this work. The *AT3G49270* gene (upregulated, see **Supplementary Table S5**) has both CArG and G boxes binding sites. It encodes for an extensin-like protein that has been suggested to have a possible role in postpollination responses such as cell wall protein modification or degradation associated with pistil receptivity (Boavida et al., 2011).

In summary, the data presented here suggest that a MADS-box-bHLH protein complex mastered by the physical interaction of STK-CES, plays a role in the regulation of genes involved in the PCD, ECM and cell wall biosynthesis pathways and by that controlling correct carpel fusion and transmitting tract development to guarantee efficient ovule fertilization (**Figure 7**).

DATA AVAILABILITY STATEMENT

The datasets generated for this study can be found in the Gene Expression Omnibus (GEO) database under the accession number GSE135559 (https://www.ncbi.nlm.nih.gov/geo/query/acc.cgi?acc=GSE135559).

AUTHOR CONTRIBUTIONS

MD and IR-V designed, performed, analyzed experiments, and wrote the manuscript. EZ, PB, AG, FC, EC, and VG

performed experiments. MC performed bio-informatics analyses. MM performed aniline blue staining, analyzed all the results and, contributed writing the manuscript. LC and MK designed experiments, research strategies, and contributed to the writing of the manuscript. All the authors contributed to manuscript revision, read and approved the submitted version.

FUNDING

MD and LC were funded by the SEXSEED project-Horizon2020-MSCA RISE 2016 (690946). IR-V was funded by an EMBO Post-doctoral fellowship and by Fondo per gli Investimenti della Ricerca di Base-Futuro in Ricerca. EZ was funded by EVOCODE. VG was supported by Ministero dell'Istruzione, dell'Universitá e della Ricerca MIUR, SIR2014 MADSMEC, Proposal number RBSI14BTZR. The Ph.D. fellowship of FC was supported by the Doctorate School in Molecular and Cellular Biology, Universitá degli Studi di Milano. MM was funded by SEXSEED and Foundation for Science and technology (FCT), Portugal (SFRH/BPD/99936).

ACKNOWLEDGMENTS

We thank Drs. J. Chory and B. Poppenberger for seed sharing. Prof. J. Martínez for assistance in the genotyping of the *bee* mutants. We are grateful to I. Latorre for help with *in situ* hybridizations and general laboratory assistance. We also thank Domenico Loperfido for help with quadruple mutant genotyping and for the collection of the material for RNAseq experiment.

SUPPLEMENTARY MATERIAL

The Supplementary Material for this article can be found online at: https://www.frontiersin.org/articles/10.3389/fpls.2020.00526/full#supplementary-material

REFERENCES

Akoh, C. C., Lee, G. C., Liaw, Y. C., Huang, T. H., and Shaw, J. F. (2004). GDSL family of serine esterases/lipases. *Prog. Lipid Res.* 43, 534–552. doi: 10.1016/j.plipres.2004.09.002

Alonso, J. M., and Stepanova, A. N. (2003). "T-DNA mutagenesis in *Arabidopsis* BT - plant functional genomics," in *Plant Molecular Biology*, ed. E. Grotewold, (Totowa, NJ: Humana Press), 177–187.

Aoki, K., Ogata, Y., and Shibata, D. (2007). Approaches for extracting practical information from gene co-expression networks in plant biology. *Plant Cell Physiol.* 48, 381–390. doi: 10.1093/pcp/pcm013

Aspeborg, H., Coutinho, P. M., Wang, Y., Brumer, H., and Henrissat, B. (2012). Evolution, substrate specificity and subfamily classification of glycoside hydrolase family 5 (GH5). *BMC Evol. Biol.* 12:186. doi: 10.1186/1471-2148-12-186

Balanzà, V., Roig-Villanova, I., Di Marzo, M., Masiero, S., and Colombo, L. (2016). Seed abscission and fruit dehiscence required for seed dispersal rely on similar genetic networks. *Development* 143, 3372–3381. doi: 10.1242/dev.135202

Bastow, R., Mylne, J. S., Lister, C., Lippman, Z., Martienssen, R. A., and Dean, C. (2004). Vernalization requires epigenetic silencing of FLC by histone methylation. *Nature* 427, 164–167. doi: 10.1038/nature02269

Bektas, I., Fellenberg, C., and Paulsen, H. (2012). Water-soluble chlorophyll protein (WSCP) of Arabidopsis is expressed in the gynoecium and developing silique. *Planta* 236, 251–259. doi: 10.1007/s00425-012-1609-y

Boavida, L. C., Borges, F., Becker, J. D., and Feijó, J. A. (2011). Whole genome analysis of gene expression reveals coordinated activation of signaling and metabolic pathways during pollen-pistil interactions in Arabidopsis. *Plant Physiol.* 155, 2066–2080. doi: 10.1104/pp.110.169813

Boex-Fontvieille, E., Rustgi, S., von Wettstein, D., Reinbothe, S., and Reinbothe, C. (2015). Water-soluble chlorophyll protein is involved in herbivore resistance activation during greening of *Arabidopsis thaliana*. *J. Exp. Bot.* 66, 6119–6135. doi: 10.1073/pnas.1507714112

Bowman, J. L., Baum, S. F., Eshed, Y., Putterill, J., and Alvarez, J. (1999). "Molecular genetics of gynoecium development in *Arabidopsis*," in *Current Topics in Developmental Biology*, eds R. A. Pedersen, and G. P. Schatten, (Cambridge, MA: Academic Press), 155–205. doi: 10.1016/s0070-2153(08)60316-6

Chae, K., Kieslich, C. A., Morikis, D., Kim, S. C., and Lord, E. M. (2009). A gain-of-function mutation of *Arabidopsis* lipid transfer protein 5 disturbs pollen tube tip growth and fertilization. *Plant Cell* 21, 3902–3914. doi: 10.1105/tpc.109.070854

Ciolkowski, I., Wanke, D., Birkenbihl, R. P., and Somssich, I. E. (2008). Studies on DNA-binding selectivity of WRKY transcription factors lend structural clues into WRKY-domain function. *Plant Mol. Biol.* 68, 81–92. doi: 10.1007/s11103-008-9353-1

Coimbra, S., Almeida, J., Junqueira, V., Costa, M. L., and Pereira, L. G. (2007). Arabinogalactan proteins as molecular markers in *Arabidopsis thaliana* sexual reproduction. *J. Exp. Bot.* 58, 4027–4035. doi: 10.1093/jxb/erm259

Coimbra, S., Costa, M., Jones, B., Mendes, M. A., and Pereira, L. G. (2009). Pollen grain development is compromised in *Arabidopsis agp6 agp11* null mutants. *J. Exp. Bot.* 60, 3133–3142. doi: 10.1093/jxb/erp148

Crawford, B. C. W., Ditta, G., and Yanofsky, M. F. (2007). The NTT gene is required for transmitting-tract development in carpels of *Arabidopsis thaliana*. *Curr. Biol.* 17, 1101–1108. doi: 10.1016/j.cub.2007.05.079

Crawford, B. C. W., and Yanofsky, M. F. (2011). HALF FILLED promotes reproductive tract development and fertilization efficiency in *Arabidopsis thaliana*. *Development* 138, 2999–3009. doi: 10.1242/dev.067793

de Folter, S., and Angenent, G. C. (2006). trans meets cis in MADS science. *Trends Plant Sci.* 11, 224–231. doi: 10.1016/j.tplants.2006.03.008

Di Marzo, M., Herrera-Ubaldo, H., Caporali, E., Novák, O., Strnad, M., Balanzà, V., et al. (2020). SEEDSTICK controls *Arabidopsis* fruit size by regulating cytokinin levels and *FRUITFULL*. *Cell Rep.* 30, 2846–2857.e3. doi: 10.1016/j.celrep.2020.01.101

Dreni, L., Pilatone, A., Yun, D., Erreni, S., Pajoro, A., Caporali, E., et al. (2011). Functional analysis of all AGAMOUS subfamily members in rice reveals their roles in reproductive organ identity determination and meristem determinacy. *Plant Cell* 23, 2850–2863. doi: 10.1105/tpc.111.087007

Egea-Cortines, M., Saedler, H., and Sommer, H. (1999). Ternary complex formation between the MADS-box proteins SQUAMOSA, DEFICIENS and GLOBOSA is involved in the control of floral architecture in *Antirrhinum majus*. *EMBO J.* 18, 5370–5379. doi: 10.1093/emboj/18.19.5370

Eremina, M., Unterholzner, S. J., Rathnayake, A. I., Castellanos, M., Khan, M., Kugler, K. G., et al. (2016). Brassinosteroids participate in the control of basal and acquired freezing tolerance of plants. *Proc. Natl. Acad. Sci. U.S.A.* 113, E5982–E5991. doi: 10.1073/pnas.1611477113

Fornes, O., Castro-Mondragon, J. A., Khan, A., van der Lee, R., Zhang, X., Richmond, P. A., et al. (2019). JASPAR 2020: update of the open-access database of transcription factor binding profiles. *Nucleic Acids Res.* 48, D87–D92. doi: 10.1093/nar/gkz1001

Friedrichsen, D. M., Nemhauser, J., Muramitsu, T., Maloof, J. N., Alonso, J., Ecker, J. R., et al. (2002). Three redundant brassinosteroid early response genes encode putative bHLH transcription factors required for normal growth. *Genetics* 162, 1445–1456.

Fukuchi-Mizutani, M., Tasaka, Y., Tanaka, Y., Ashikari, T., Kusumi, T., and Murata, N. (1998). Characterization of Δ9 acyl-lipid desaturase homologues

from *Arabidopsis thaliana*. *Plant Cell Physiol.* 39, 247–253. doi: 10.1093/oxfordjournals.pcp.a029364

Gane, A. M., Clarke, A. E., and Bacic, A. (1995). Localisation and expression of arabinogalactan-proteins in the ovaries of *Nicotiana alata* Link and Otto. *Sex. Plant Reprod.* 8, 278–282. doi: 10.1007/BF00229384

Gao, M., and Showalter, A. M. (1999). Yariv reagent treatment induces programmed cell death in *Arabidopsis* cell cultures and implicates arabinogalactan protein involvement. *Plant J.* 19, 321–331. doi: 10.1046/j.1365-313X.1999.00544.x

Guan, Y., and Nothnagel, E. A. (2004). Binding of arabinogalactan proteins by yariv phenylglycoside triggers wound-like responses in Arabidopsis cell cultures. *Plant Physiol.* 135, 1346–1366. doi: 10.1104/pp.104.039370

Heilmann, I., Pidkowich, M. S., Girke, T., and Shanklin, J. (2004). Switching desaturase enzyme specificity by alternate subcellular targeting. *Proc. Natl. Acad. Sci. U.S.A.* 101, 10266–10271. doi: 10.1073/pnas.0402200101

Herrera-Ubaldo, H., and de Folter, S. (2018). Exploring cell wall composition and modifications during the development of the gynoecium medial domain in *Arabidopsis*. *Front. Plant Sci.* 9:454. doi: 10.3389/fpls.2018.00454

Herrera-Ubaldo, H., Lozano-Sotomayor, P., Ezquer, I., Di Marzo, M., Chávez Montes, R. A., Gómez-Felipe, A., et al. (2019). New roles of NO TRANSMITTING TRACT and SEEDSTICK during medial domain development in *Arabidopsis* fruits. *Development* 146:dev172395. doi: 10.1242/dev.172395

Hoggart, R. M., and Clarke, A. E. (1984). Arabinogalactans are common components of angiosperm styles. *Phytochemistry* 23, 1571–1573.

Johnson, M. A., and Lord, E. (2006). "Extracellular guidance cues and intracellular signaling pathways that direct pollen tube growth," in *The Pollen Tube: A Cellular and Molecular Perspective*, ed. R. Malhó, (Berlin: Springer), 223–242. doi: 10.1007/7089_051

Johnson, M. A., and Preuss, D. (2002). Plotting a course: multiple signals guide pollen tubes to their targets. *Dev. Cell* 2, 273–281. doi: 10.1016/s1534-5807(02)00130-2

Khan, M., Rozhon, W., Unterholzner, S. J., Chen, T., Eremina, M., Wurzinger, B., et al. (2014). Interplay between phosphorylation and SUMOylation events determines CESTA protein fate in brassinosteroid signalling. *Nat. Commun.* 5:4687. doi: 10.1038/ncomms5687

Kim, S. T., Zhang, K., Dong, J., and Lord, E. M. (2006). Exogenous free ubiquitin enhances lily pollen tube adhesion to an in vitro stylar matrix and may facilitate endocytosis of SCA. *Plant Physiol.* 142, 1397–1411. doi: 10.1104/pp.106.086801

Kim, T.-W., and Wang, Z. Y. (2010). Brassinosteroid signal transduction from receptor kinases to transcription factors. *Annu. Rev. Plant Biol.* 61, 681–704. doi: 10.1146/annurev.arplant.043008.092057

Knauss, S., Rohrmeier, T., and Lehle, L. (2003). The auxin-induced maize gene ZmSAUR2 encodes a short-lived nuclear protein expressed in elongating tissues. *J. Biol. Chem.* 278, 23936–23943. doi: 10.1074/jbc.M212585200

Kunst, L., and Samuels, A. L. (2003). Biosynthesis and secretion of plant cuticular wax. *Prog. Lipid Res.* 42, 51–80. doi: 10.1016/s0163-7827(02)00045-0

Langmead, B., and Steven, S. (2012). Fast gapped-read alignment with Bowtie 2. *Nat. Methods* 9, 357–359. doi: 10.1038/nmeth.1923.Fast

Larsson, E., Franks, R. G., and Sundberg, E. (2013). Auxin and the *Arabidopsis thaliana* gynoecium. *J. Exp. Bot.* 64, 2619–2627. doi: 10.1093/jxb/ert099

Lavy, M., and Estelle, M. (2016). Mechanisms of auxin signaling. *Development* 143, 3226–3229. doi: 10.1242/dev.131870

Lennon, K. A., Stéphane, R., Peter, H. K., and Lord, E. M. (1998). The structure of the transmitting tissue of *Arabidopsis thaliana* (L.) and the path of pollen tube growth. *Sex. Plant Reprod.* 11, 49–59.

Li, B., and Dewey, C. N. (2011). RSEM: accurate transcript quantification from RNA-seq data with or without a reference genome. *BMC Bionformatics* 12:323. doi: 10.1186/1471-2105-12-323

Lombard, V., Golaconda Ramulu, H., Drula, E., Coutinho, P. M., and Henrissat, B. (2014). The carbohydrate-active enzymes database (CAZy) in 2013. *Nucleic Acids Res.* 42, 490–495. doi: 10.1093/nar/gkt1178

Lord, E. M., and Russell, S. D. (2002). The mechanisms of pollination and fertilization in plants. *Annu. Rev. Cell Dev. Biol.* 18, 81–105. doi: 10.1146/annurev.cellbio.18.012502.083438

Matias-Hernandez, L., Battaglia, R., Galbiati, F., Rubes, M., Eichenberger, C., Grossniklaus, U., et al. (2010). *VERDANDI* is a direct target of the MADS domain ovule identity complex and affects embryo sac differentiation in *Arabidopsis*. *Plant Cell* 22, 1702–1715. doi: 10.1105/tpc.109.068627

McClure, B. A., and Guilfoyle, T. (1987). Characterization of a class of small auxin-inducible soybean polyadenylated RNAs. *Plant Mol. Biol.* 9, 611–623. doi: 10.1007/BF00020537

Mendes, M. A., Guerra, R. F., Castelnovo, B., Silva-Velazquez, Y., Morandini, P., Manrique, S., et al. (2016). Live and let die: a REM complex promotes fertilization through synergid cell death in *Arabidopsis*. *Development* 143, 2780–2790. doi: 10.1242/dev.134916

Michaels, S. D., and Amasino, R. M. (2007). FLOWERING LOCUS C encodes a novel MADS domain protein that acts as a repressor of flowering. *Plant Cell* 11, 949–956. doi: 10.2307/3870827

Minic, Z., Do, C. T., Rihouey, C., Morin, H., Lerouge, P., and Jouanin, L. (2006). Purification, functional characterization, cloning, and identification of mutants of a seed-specific arabinan hydrolase in *Arabidopsis*. *J. Exp. Bot.* 57, 2339–2351. doi: 10.1093/jxb/erj205

Mizzotti, C., Ezquer, I., Paolo, D., Rueda-Romero, P., Guerra, R. F., Battaglia, R., et al. (2014). SEEDSTICK is a Master Regulator of Development and Metabolism in the Arabidopsis Seed Coat. *PLoS Genet.* 10:e1004856. doi: 10.1371/journal.pgen.1004856

Molkentin, J. D., Black, B. L., Martin, J. F., and Olson, E. N. (1995). Cooperative activation of muscle gene expression by MEF2 and myogenic bHLH proteins. *Cell* 83, 1125–1136. doi: 10.1016/0092-8674(95)90139-6

Nakamura, A., Nakajima, N., Goda, H., Shimada, Y., Hayashi, K. I., Nozaki, H., et al. (2006). Arabidopsis *Aux/IAA* genes are involved in brassinosteroid-mediated growth responses in a manner dependent on organ type. *Plant J.* 45, 193–205. doi: 10.1111/j.1365-313X.2005.02582.x

Nawrath, C. (2006). Unraveling the complex network of cuticular structure and function. *Curr. Opin. Plant Biol.* 9, 281–287. doi: 10.1016/j.pbi.2006.03.001

Nieuwland, J., Feron, R., Huisman, B. A. H., Fasolino, A., Hilbers, C. W., Derksen, J., et al. (2005). Lipid transfer proteins enhance cell wall extension in tobacco. *Plant Cell* 17, 2009–2019. doi: 10.1105/tpc.105.032094

Panikashvili, D., Shi, J. X., Bocobza, S., Franke, R. B., Schreiber, L., and Aharoni, A. (2010). The *Arabidopsis* DSO/ABCG11 transporter affects cutin metabolism in reproductive organs and suberin in roots. *Mol. Plant* 3, 563–575. doi: 10.1093/mp/ssp103

Pinyopich, A., Ditta, G. S., Savidge, B., Liljegren, S. J., Baumann, E., Wisman, E., et al. (2003). Assessing the redundancy of MADS-box genes during carpel and ovule development. *Nature* 424, 85–88. doi: 10.1038/nature01741

Poppenberger, B., Rozhon, W., Khan, M., Husar, S., Adam, G., Luschnig, C., et al. (2011). CESTA, a positive regulator of brassinosteroid biosynthesis. *EMBO J.* 30, 1149–1161. doi: 10.1038/emboj.2011.35

Quail, P. H. (2000). Phytochrome-interacting factors. *Semin. Cell Dev. Biol.* 11, 457–466.

Rate, D. N., Cuenca, J. V., Bowman, G. R., Guttman, D. S., and Greenberg, J. T. (2007). The gain-of-function Arabidopsis *acd6* mutant reveals novel regulation and function of the salicylic acid signaling pathway in controlling cell death, defenses, and cell growth. *Plant Cell* 11, 1695–1708. doi: 10.2307/3871047

Reyes-Olalde, J. I., Zuñiga-Mayo, V. M., Chávez Montes, R. A., Marsch-Martínez, N., and de Folter, S. (2013). Inside the gynoecium: at the carpel margin. *Trends Plant Sci.* 18, 644–655. doi: 10.1016/j.tplants.2013.08.002

Ripoll, J. J., Zhu, M., Brocke, S., Hon, C. T., Yanofsky, M. F., Boudaoud, A., et al. (2019). Growth dynamics of the *Arabidopsis* fruit is mediated by cell expansion. *Proc. Natl. Acad. Sci. U.S.A.* 116, 25333–25342. doi: 10.1073/pnas.1914096116

Robert, H. S., Crhak Khaitova, L., Mroue, S., and Benková, E. (2015). The importance of localized auxin production for morphogenesis of reproductive organs and embryos in *Arabidopsis*. *J. Exp. Bot.* 66, 5029–5042. doi: 10.1093/jxb/erv256

Robinson, M. D., McCarthy, D. J., and Smyth, G. K. (2009). edgeR: a bioconductor package for differential expression analysis of digital gene expression data. *Bioinformatics* 26, 139–140. doi: 10.1093/bioinformatics/btp616

Roeder, A. H. K., and Yanofsky, M. F. (2006). Fruit Development in *Arabidopsis*. *Arabidopsis Book* 4:e0075. doi: 10.1199/tab.0075

Sheldon, C. C., Burn, J. E., Perez, P. P., Metzger, J., Edwards, J. A., Peacock, W. J., et al. (2007). The *FLF* MADS box gene: a repressor of flowering in Arabidopsis regulated by vernalization and methylation. *Plant Cell* 11, 445–458. doi: 10.2307/3870872

Sieber, P., Schorderet, M., Ryser, U., Buchala, A., Kolattukudy, P., Metraux, J.-P., et al. (2007). Transgenic Arabidopsis plants expressing a fungal cutinase show alterations in the structure and properties of the cuticle and postgenital organ fusions. *Plant Cell* 12, 721–738. doi: 10.2307/3870997

Takahashi, K., Shimada, T., Kondo, M., Tamai, A., Mori, M., Nishimura, M., et al. (2010). Ectopic expression of an esterase, which is a candidate for the unidentified plant cutinase, causes cuticular defects in *Arabidopsis thaliana*. *Plant Cell Physiol.* 51, 123–131. doi: 10.1093/pcp/pcp173

Toledo-Ortiz, G., Huq, E., and Quail, P. H. (2003). The Arabidopsis basic/helix-loop-helix transcription factor family. *Plant Cell* 15, 1749–1770. doi: 10.1105/tpc.013839.et

Tung, C. W., Dwyer, K. G., Nasrallah, M. E., and Nasrallah, J. B. (2005). Genome-wide identification of genes expressed in Arabidopsis pistils specifically along the path of pollen tube growth. *Plant Physiol.* 138, 977–989. doi: 10.1104/pp.105.060558

Turbant, A., Fournet, F., Lequart, M., Zabijak, L., Pageau, K., Bouton, S., et al. (2016). PME58 plays a role in pectin distribution during seed coat mucilage extrusion through homogalacturonan modification. *J. Exp. Bot.* 67, 2177–2190. doi: 10.1093/jxb/erw025

van Mourik, H., van Dijk, A. D. J., Stortenbeker, N., Angenent, G. C., and Bemer, M. (2017). Divergent regulation of Arabidopsis *SAUR* genes: a focus on the *SAUR10*-clade. *BMC Plant Biol.* 17:245. doi: 10.1186/s12870-017-1210-4

Vert, G., Nemhauser, J. L., Geldner, N., Hong, F., and Chory, J. (2005). Molecular mechanisms of steroid hormone signaling in plants. *Annu. Rev. Cell Dev. Biol.* 21, 177–201. doi: 10.1146/annurev.cellbio.21.090704.151241

Verwoerd, T. C., Dekker, B. M., and Hoekema, A. (1989). A small scale procedure for the rapid isolation of plant RNAs. *Nucleic Acid Res.* 17:2362.

Webb, M. C., and Williams, E. G. (1988). The pollen tube pathway in the pistil of *Lycopersicon peruvianum*. *Ann. Bot.* 61, 415–423. doi: 10.1093/oxfordjournals.aob.a087573

Wrzaczek, M., Brosche, M., Kollist, H., and Kangasjarvi, J. (2009). *Arabidopsis* GRI is involved in the regulation of cell death induced by extracellular ROS. *Proc. Natl. Acad. Sci. U.S.A.* 106, 5412–5417. doi: 10.1073/pnas.0808980106

Wrzaczek, M., Vainonen, J. P., Stael, S., Tsiatsiani, L., Help-Rinta-Rahko, H., Gauthier, A., et al. (2015). GRIM REAPER peptide binds to receptor kinase PRK5 to trigger cell death in *Arabidopsis*. *EMBO J.* 34, 55–66. doi: 10.15252/embj.201488582

Yao, K., Bacchetto, R. G., Lockhart, K. M., Friesen, L. J., Potts, D. A., Covello, P. S., et al. (2003). Expression of the *Arabidopsis ADS1* gene in *Brassica juncea* results in a decreased level of total saturated fatty acids. *Plant Biotechnol. J.* 1, 221–229. doi: 10.1046/j.1467-7652.2003.00021.x

Yeats, T. H., and Rose, J. K. C. (2013). The formation and function of plant cuticles. *Plant Physiol.* 163, 5–20. doi: 10.1104/pp.113.222737

Zambelli, F., Pesole, G., and Pavesi, G. (2009). Pscan: finding over-represented transcription factor binding site motifs in sequences from co-regulated or co-expressed genes. *Nucleic Acids Res.* 37, 247–252. doi: 10.1093/nar/gkp464

Conflict of Interest: The authors declare that the research was conducted in the absence of any commercial or financial relationships that could be construed as a potential conflict of interest.

Functionally Divergent Splicing Variants of the Rice *AGAMOUS* Ortholog *OsMADS3* Are Evolutionary Conserved in Grasses.

Dreni L [1], Ravasio A [1], Gonzalez-Schain N [1], Jacchia S, da Silva GJ [2], Ricagno S [1], Russo R [3], **Caselli F** [1], Gregis V [1] and Kater MM [1]

[1] Dipartimento di Bioscienze, Università degli Studi di Milano, Milan, Italy

[2] Plant Genomics and Breeding Center, Federal University of Pelotas, Pelotas, Brazil

[3] Department of Pathophysiology and Transplantation, Università degli Studi di Milano, Milan, Italy

May 2020; Front. Plant Sci. 11:637; doi: 10.3389/fpls.2020.00637

In this paper, an alternative splicing in *Oryza sativa,* which leads to the production of two variants of the AG ortholog *OsMADS3,* was described. These two splicing variants differ in one serine residue (S109), which is retained in the *OsMADS3*^{S109} variant, conserved and specific only to the grass family.

The functionality of these two variants was tested in *Arabidopsis thaliana,* where it was demonstrated that the eudicot-like OsMADS3 isoform, lacking the serine residue, had ability to specify stamens and carpels in ag mutant flowers, suggesting an important functional role for the serine residue at position 109 in AG proteins of grasses.

I contributed to this work by performing the yeast-two-hybrid screening, in which we tested the interaction of AtAG, OsMADS3^{S109} and OsMADS3 with Arabidopsis AtSEP1, AtSEP2 and AtSEP3 homeotic proteins.

frontiers in Plant Science

ORIGINAL RESEARCH
published: 25 May 2020
doi: 10.3389/fpls.2020.00637

Functionally Divergent Splicing Variants of the Rice AGAMOUS Ortholog OsMADS3 Are Evolutionary Conserved in Grasses

Ludovico Dreni[1]†, Andrea Ravasio[1], Nahuel Gonzalez-Schain[1†], Sara Jacchia[1†], Glacy Jaqueline da Silva[2†], Stefano Ricagno[1], Rosaria Russo[3], Francesca Caselli[1], Veronica Gregis[1] and Martin M. Kater[1]**

[1] Department of Biosciences, Università degli Studi di Milano, Milan, Italy, [2] Plant Genomics and Breeding Center, Federal University of Pelotas, Pelotas, Brazil, [3] Department of Pathophysiology and Transplantation, Università degli Studi di Milano, Milan, Italy

Within the MADS-box gene family, the *AGAMOUS*-subfamily genes are particularly important for plant reproduction, because they control stamen and carpel identity. A number of studies in the last three decades have demonstrated that the *AGAMOUS* (*AG*) function has been conserved during land plant evolution. However, gene duplication events have led to subfunctionalization and neofunctionalization of *AG*-like genes in many species. Here we show that alternative splicing in *Oryza sativa* produces two variants of the AG ortholog OsMADS3 which differ in just one serine residue, S109. Interestingly, this alternative splicing variant is conserved and specific to the grass family. Since in eudicots the S109 residue is absent in AG proteins, stamen and carpel identity determination activity of the two rice isoforms was tested in *Arabidopsis thaliana*. These experiments revealed that only the eudicot-like OsMADS3 isoform, lacking the serine residue, had ability to specify stamens and carpels in *ag* mutant flowers, suggesting an important functional role for the serine residue at position 109 in AG proteins of grasses.

Keywords: AGAMOUS, alternative splicing, OsMADS3, floral organ identity, protein structure, rice, transcription factor, homeotic

OPEN ACCESS

Edited by:
Amy Litt,
University of California, Riverside, United States

Reviewed by:
David Smyth,
Monash University, Australia
Juan José Ripoll,
University of California, San Diego, United States

***Correspondence:**
Ludovico Dreni
ludovico.dreni@gmail.com
Martin M. Kater
martin.kater@unimi.it

†Present address:
Ludovico Dreni, Instituto de Biología Molecular y Celular de Plantas, Consejo Superior de Investigaciones Científicas-Universidad Politécnica de Valencia, Valencia, Spain
Nahuel Gonzalez-Schain, Instituto de Biología Molecular y Celular de Rosario (IBR), Universidad Nacional de Rosario, CONICET, Ocampo y Esmeralda, Rosario, Argentina
Sara Jacchia, Food and Feed Compliance, Directorate F - Health, Consumers and Reference Materials, European Commission, Joint Research Centre (JRC), Ispra, Italy
Glacy Jaqueline da Silva, Department of Molecular Biology, Paranaense University, Mascarenhas de Moraes Square, Umuarama, Brazil

Specialty section:
This article was submitted to Plant Development and EvoDevo, a section of the journal Frontiers in Plant Science

Received: *28 December 2019*
Accepted: *24 April 2020*
Published: *25 May 2020*

INTRODUCTION

The evolution of flowers as reproductive structures is the most remarkable feature of angiosperms (flowering plants), which currently are by far the most dominating group of plants on Earth, counting over 350,000 species[1]. In its basic model, the flower is a bisexual structure composed of perianth organs surrounding the reproductive organs, the male stamens and the female gynoecium, which are located in the center of the flower. All organs are arranged either in a spiral phyllotaxy or in whorls, depending on the angiosperm lineage. The gynoecium can be composed of one or more pistils made by one carpel each, or by one pistil formed by multiple fused carpels. The pistil consists of a stigma, style and ovary which contains the ovules. The pistil upon pollination eventually becomes a fruit, and the ovules develop into seeds (Bowman, 1997).

[1]http://www.theplantlist.org/

The two most evolved and successful angiosperm *taxa* are referred to as eudicots and monocots, comprising *ca*. 75% and 20% of the living plant species, respectively. It is estimated that divergence between eudicot and monocot species occurred about 150 million years ago (MYA) (Magallon et al., 2015). Plants belonging to the two lineages evolved inflorescences and flowers that show an enormous variation in complexity and shapes, evidencing the forces of natural selection. Examples of structural diversity can be noticed by comparing the morphologies of two model species representing each lineage, the core eudicotyledon *Arabidopsis thaliana* (L.) Heynh. and the monocotyledon *Oryza sativa* L. However, if we compare the basic floral structure of these two species, a conserved organization emerges, in which four different types of floral organs are arranged into four concentric whorls. The two most outer whorls bear so-called perianth organs: (1) four sepals in Arabidopsis and the lemma and palea in rice (Lombardo and Yoshida, 2015), and (2) the petals or lodicules in Arabidopsis and rice, respectively. The male and female reproductive organs are located in the most inner two whorls. Both Arabidopsis and rice flowers develop six stamens in the third whorl, and in the innermost fourth whorl of Arabidopsis a bicarpellate pistil develops, whereas in rice the pistil is tricarpellate (Smyth et al., 1990; Yoshida and Nagato, 2011).

AGAMOUS (AtAG), a member of the MADS-box TF family (Dreni and Kater, 2014), is essential for stamen and carpel development in Arabidopsis (Bowman et al., 1989, 1991; Yanofsky et al., 1990). The *ag* loss-of-function mutant completely lacks reproductive organs; petals replace stamens in the third whorl and a new *ag* flower replaces the carpel in the fourth whorl, resulting in a complete loss of floral meristem determinacy (FMD) (Yanofsky et al., 1990). AGAMOUS acquires its reproductive organ identity function through the formation of a complex with SEPALLATA (AtSEP) MADS-domain proteins (Pelaz et al., 2000). Complexes formed by AtAG and AtSEP proteins direct carpel development, whereas in the third whorl AtSEP transcription factors mediate the interaction between AtAG, APETALA3 (AtAP3) and PISTILLATA (AtPI) to form the MADS-domain stamen identity complex (Theissen, 2001; Theissen and Saedler, 2001).

The *AGAMOUS* subfamily is typically represented by two or more genes in each angiosperm species, having various degrees of functional redundancy and sub-functionalization, and is further divided into many paraphyletic lineages. The main division which is important to mention here is the one between the *AG* and *AGL11* lineages (Kramer et al., 2004; Zahn et al., 2006), which diverged before the most recent common ancestor of extant angiosperms. All members of the *AGAMOUS* subfamily cluster into one of these two groups. Generally speaking, the genes providing carpel and stamen identity and FMD function belong to the *AG* lineage, whereas the *AGL11*-like genes provide ovule identity (Kramer et al., 2004; Zahn et al., 2006; Dreni and Kater, 2014). However, despite their ancestral origin, functional redundancy between the two clades is common (Pinyopich et al., 2003; Brambilla et al., 2007; Dreni et al., 2011; Heijmans et al., 2012).

Interestingly, in monocot grasses (Poaceae), the *AG* and *AGL11* lineages are further duplicated to form four conserved clades which are named after their representative genes of rice. Among them, the *OsMADS3* and *OsMADS58* clades belong to the *AG* lineage whereas the *OsMADS13* and *OsMADS21* clades belong to the *AGL11* lineage (Kramer et al., 2004; Yamaguchi et al., 2006; Zahn et al., 2006; Dreni and Kater, 2014). Therefore, the rice genes *OsMADS3* and *OsMADS58* are both direct orthologous of Arabidopsis *AtAG* with a similar expression domain, and they redundantly control the reproductive organ identity function in rice. Like the Arabidopsis *ag* mutant, the *osmads3 osmads58* double mutant shows a complete loss of reproductive organ identity; stamens are replaced by lodicules and an small ectopic palea emerges in place of the carpel. Moreover, FMD is also lost and the flower continues to produce ectopic lodicules from its center (Dreni et al., 2011). The phenotypes of the single mutants suggest that *OsMADS3* has an important role in stamen development, whereas the two genes seem to be almost completely redundant for pistil development (Dreni et al., 2011; Hu et al., 2011).

Like the eudicot AG proteins, rice OsMADS3 and OsMADS58 form complexes with rice SEP-like factors (Favaro et al., 2002; Cooper et al., 2003; Hu et al., 2015; Wu et al., 2018).

Ectopic *AtAG* expression in Arabidopsis results in a homeotic conversion of sepals into carpel-like organs and of petals into stamens (Mizukami and Ma, 1992). Several functional studies, using *AG* orthologous genes from other eudicot, monocot or even gymnosperm species, showed that when ectopically expressed in Arabidopsis, they mimic the ectopic expression of *AtAG,* or in some cases they even rescue the *ag* loss of function mutants (Rutledge et al., 1998; Kitahara and Matsumoto, 2000; Zhang et al., 2004; Martin et al., 2006; Airoldi et al., 2010; Heijmans et al., 2012). Stunningly, the *AGAMOUS* subfamily gene from the gymnosperm *Cycas edentata* de Laub. was able to rescue the Arabidopsis *ag* mutant, despite the two species likely diverged about 300 MYA (Zhang et al., 2004). Another study shows very clearly the importance of the conservation of the domains required for protein complex formation. The ectopic expression of the snapdragon *AG* lineage genes *PLENA (AmPLE)* and *FARINELLI (AmFAR)* either in Arabidopsis or snapdragon revealed that the two genes have different abilities in organ specification: *AmPLE* can convert petals into stamens and induces carpelloid features on the sepals, similar to *AtAG* ectopic expression, while *AmFAR* only affects petal identity (Davies et al., 1999; Causier et al., 2005; Airoldi et al., 2010). Airoldi and colleagues showed that this different ability of AmPLE and AmFAR is due to a different affinity to interact with SEP proteins (Airoldi et al., 2010). Indeed AmFAR is only able to interact with Arabidopsis AtSEP3, which is not expressed in sepals, but not with the other Arabidopsis AtSEPs. Hence, when AmFAR is expressed in Arabidopsis sepals it can't find any SEP interaction partner and remains therefore inactive. The restricted interaction ability of AmFAR is the result of a single glutamine insertion, Q173, near the end of the K domain. Q173 is the result of a three-base duplication of the splice acceptor site (CAG) at the 5′ end of AmFAR exon seven (Airoldi et al., 2010).

Extensive duplications of homeotic genes have likely contributed to the evolution of floral structures and their diversification in angiosperms. Besides gene duplication, variants of proteins can also arise via alternative splicing of transcripts from the same gene. For MADS-box genes of plants, a few cases of alternative splicing have been reported. Considering only the *AGAMOUS* subfamily, exon skipping gives rise to the double-flowered mutant of *Prunus lannesiana* (Carrière) E.H. Wilson (Rosaceae)(Liu et al., 2013). Alternative splicing of *AG* genes has also been reported in a few other angiosperms (Kitahara and Matsumoto, 2000; Tsaftaris et al., 2005; Lightfoot et al., 2008; Zhang et al., 2015), but the functional significance of these events is unknown. To date, a complete functional characterization of splicing variants has only been carried out for the *AG* lineage gene *PapsAG* from opium poppy (*Papaver somniferum* L.) (Hands et al., 2011). *PapsAG* undergoes alternative splicing generating two different transcripts, *PapsAG-1* and *PapsAG-2,* which are co-expressed in stamens and carpels and only differ in the last part of the *C*-terminal region. Even though they redundantly share the conserved functions of *AG*, *PapsAG-2* has distinctive roles in gynoecium development, particularly in the septum, ovule and stigma (Hands et al., 2011).

Here, we describe the identification of two alternative splicing isoforms of the rice *OsMADS3* gene, which differ for only three nucleotides in length, resulting from a three-base pair duplication of a splice acceptor site. The longer transcript encodes for an additional serine residue (S109) within the first predicted α-helix of the K-box, a domain whose length and amino acidic composition are highly conserved among angiosperms (Kaufmann et al., 2005). Search on public databases hints that the two splicing variants are broadly expressed in reproductive tissues, and probably ubiquitously within the whole *OsMADS3* clade of the grass family. Functional analysis revealed differences in their ability to rescue the *ag* mutant phenotype in Arabidopsis, which might be due to different affinities of the splice variants for the AtSEP1 protein.

MATERIALS AND METHODS

Plant Materials

Mature wild-type (WT) inflorescences of *Arabidopsis thaliana* and *Oryza sativa ssp. japonica* cv. Nipponbare were used for total RNA isolation and gene cloning. The *ag-3* mutant in the Arabidopsis L*er* background (Bowman et al., 1991) was already available in our lab. Inflorescences from *A. thaliana* transgenic lines were used for total RNA isolation and Real Time PCR analysis.

Bioinformatic Analysis of *AGAMOUS* Subfamily Member Splice Variants

To find suitable RNA-Seq samples from grasses and other Poales, we first interrogated the SRA database of Genebank[2], with the names of species of interest, and we eventually selected the most suitable samples (i.e., reproductive stages, when available). Then, for each gene/species, we used the nucleotide BLAST tool (settings: optimize for somewhat similar sequences), to screen those data with a query cDNA sequence of 37-47 nucleotides, comprising the exon4-exon5 splicing region of *OsMADS3* and of its grass homologs, and downloaded all the homologous reads. Control query and read homologous sequences where then aligned with MAFFT, and edited manually with Genedoc. After removing the dubious or low quality reads (i.e., those too short or with more than one or two different bases) the alternative splicing events were counted, in order to calculate their relative abundance. The accession codes and available references of the RNA-Seq samples are listed in **Table 1**. All the selected reads are available in **Supplementary Dataset 2** as Fasta format alignments. The monocot *AG*-lineage genes included in this work have been defined by sequence and phylogenetic analysis (Dreni et al., 2013; Dreni and Kater, 2014; data not shown) and their accession codes are available in **Supplementary Table 3**. The complete ORFs and protein products of *OsMADS3*$^{+S109}$ and *OsMADS3* are also provided in **Supplementary Dataset 1**.

Open reading frames were controlled by Gene Runner. Images were processed with Gimp and Paint.NET. Structures were analyzed and **Figure 1E** were generated using COOT and CCP4mg software (Emsley and Cowtan, 2004; McNicholas et al., 2011).

RNA Isolation

Total RNA was isolated using the LiCl precipitation method as previously described (Gregis et al., 2008). Total RNAs were converted into first-strand cDNA by using the ImProm-II Reverse Transcription System (Promega, Madison, WI, United States).

Gene Cloning and Arabidopsis Transformation

The CDS of *OsMADS3*$^{+S109}$, *OsMADS3* and *OsMADS58* were amplified in a thermocycler (MasterCycler EPGradient S, Eppendorf, Hamburg, Germany) using Phusion High-Fidelity DNA Polymerase (ThermoFisher Scientific, Waltham, MA, United States) using primers OsP337/OsP79 (for both *OsMADS3* isoforms) and OsP119/OsP120, respectively. The PCR products were isolated by gel electrophoresis, purified using NucleoSpin Gel Purification Kit (Macherey-Nagel, Duren, Germany) and cloned into pENTR/D-TOPO vector (Invitrogen). The recombination products were used to transform electrocompetent *E. coli* cells (DH10B strain) and colonies positive for the desired plasmids were isolated on LB-agar plates containing gentamycin (30 mg/L). Colony PCR was performed to confirm the presence of the constructs; in particular, colony PCR was performed to discriminate between colonies carrying *OsMADS3*$^{+S109}$ and colonies carrying *OsMADS3*, using the reverse primers OsP428 and OsP429 with the forward primer OsP17. The different constructs have been sent for sequencing to the StarSEQ facility (Mainz, Germany). Suitable clones of *AtAG* in pDONR207 entry vector were already available in the laboratory.

[2]https://www.ncbi.nlm.nih.gov/genbank/

TABLE 1 | Summary of the number of reads mapping on the exon 4-exon 5 junction of the *OsMADS3*-like genes from various grasses and from other families of the order Poales.

NCBI SRA Experiment	Species	Query sequence	Total high quality reads	Long splicing + S109		TAG deletion No S109	
SRX1332256; SRX507920; DRX000335; DRX000334; DRX000333 SRX100746 (Davidson et al., 2012)	***Oryza sativa ssp. japonica***	TAGCTTACAGAACGCAAACAG/TAG/GA CCATAGTGGGGGATTC	2021	**1238**	**61.3%**	**783**	**38.7%**
SRX472914	***Leersia perrieri***	CAGTAGCTTACAGAACGCAAACAA/GA CCATAGTGGGGGATTC	1205	**562**	**46.6%**	**643**	**53.4%**
SRX2342718; SRX2342716; SRX1583837; SRX1583838; SRX1583839 SRX100693; SRX100694; SRX100691 (Davidson et al., 2012)	***Brachypodium distachyon***	AGCCTGCAGAACTCAAACAG/TAG/GT CCTTAGTGAAGG	391	**324**	**82.9%**	**67**	**17.1%**
SRX375649; SRX378862 (Chen et al., 2014)	***Hordeum vulgare***	CTTGCAAAACTCAAACAG/TAG/GTCACTGG TGAGAGATT	39	**23**	**59%**	**16**	**41%**
SRX099185; SRX099141; SRX099021 (Davidson et al., 2012)	***Sorghum bicolor***	GCTTGCAAAACGCAAACAG/TAG/GACCATA GTGGGAGAT	223	**40**	**17.9%**	**183**	**83.1%**
SRX058598; SRX058600; SRX058607; SRX058605; SRX058604; SRX058601; SRX058599; SRX058597	***Zea mays***	ZMM2: CAGCTTGCAAAACGCAAACAC/TAG/GAAC ATAGTGGGAGATTC	496	**372**	**75%**	**124**	**25%**
		ZMM23: TAGCTTGCAAAACGCAAACAG/TAG/GACCA TAGTGGGAGATTC	118	**23**	**19.5%**	**95**	**80.5%**
SRX2375352; SRX2375353; SRX2375354 (Wang et al., 2017) SRX567871	***Phyllostachys edulis***	TAGCTTGCAGAACTCAAACAG/TAG/GAACT TAGTGGGGGATTC	83	**22**	**26.5%**	**61**	**73.5%**
SRX1639030	***Streptochaeta angustifolia***	TTACCACCTTGCAGAACAACAACAG/GACCA TAATGGGGGATTCTGTA	11	**1**	**9.1%**	**10**	**90.9%**
SRX1639019	***Ecdeiocolea monostachya (Ecdeiocoleaceae)***	TCACCAACTTGCAGAACTCCAATAG/CAG/GA CTATACAGGCAGGGGA	100	**24**	**24%**	**76**	**76%**
-	***Joinvillea ascendens (Joinvilleaceae)***	NO DATA AVAILABLE					
SRX1639020	***Flagellaria indica (Flagellariaceae)***	TACCAACTTGCAGAACTCAAATAG/GACTCTAC TGGGGGATTCA	23	**0**	**0%**	**23**	**100%**
ERX2099848; SRX1639024	***Elegia tectorum* and *E. fenestrata (Restionaceae)***	ACCAACCTACAGAACTCCAACAGTAGGATTT TTTTGGGGGAGTCT CTACAGAACTCCATCAGGATTTTGTTGGGGG AATGCCTTAGC	15	**2**	**13%**	**13**	**87%**

(Continued)

TABLE 1 | Continued

NCBI SRA Experiment	Species	Query sequence	Total high quality reads	Long splicing + S109		TAG deletion No S109	
ERX1349704	***Luzula elegans (Juncaceae)***	AGCACATTAAATAACAGTAATAG/GAATTTGTT GGGCGAG	1921	**0**	**0%**	**1921**	**100%**
SRX1465570; SRX1465595	***Ananas comosus (Bromeliaceae)***	CAACCTCCAGAATTCAAACAG/GAATTTACT GGGTGAGTCTCT	232	**0**	**0%**	**232**	**100%**

*The percentage of reads indicating the presence or absence of the second TAG at the splicing acceptor site of intron 4 is reported. In each query sequence, the exon 4-exon 5 junction is indicated by a slash. All reads are available in Fasta format (**Supplementary Dataset 1**).*

Clones were transferred, using the Gateway LR Clonase II Enzyme (ThermoFisher Scientific, Waltham, MA, United States), into the pB2GW7 Gateway destination vector (VIB-Gent University) for expression under the control of the CaMV 35S promoter. The recombination products were used to transform electrocompetent *E. coli* cells (DH10B strain) and positive colonies were isolated on LB agar plates containing spectinomycin (100 mg/L). Colony PCR was performed to confirm the presence of the constructs. Plasmids were re-extracted using NucleoSpin Plasmid Isolation kit (Macherey-Nagel, Duren, Germany) and used to transform electrocompetent *A. tumefaciens* cells (EHA105 strain). Positive colonies were selected on LB-agar plates containing rifampicin and spectinomycin (100 mg/L). Colony PCR was performed to confirm the presence of the constructs.

Agrobacterium strains carrying *pB2GW7-AtAG, pB2GW7-OsMADS3*$^{+S109}$*, pB2GW7-OsMADS3* and *pB2GW7-OsMADS58* were used to transform *ag-3/* + heterozygous plants in the *A. thaliana* L*er.* background (T_0) with the floral dip method (Clough and Bent, 1998). The T_1 of these plants was harvested and transformed plants were isolated through multiple rounds of BASTA selection. DNA extraction and PCR were performed on selected plants to confirm the presence of the transgene.

Primer sequences are available in **Supplementary Table 1**.

Real-Time PCR

Inflorescences of *A. thaliana* were pooled by construct and background (WT, *ag-3*) and total RNA was extracted as described above.

The expression levels of *35S:AtAG, 35S:OsMADS3*$^{+S109}$, *35S:OsMADS3* and *35S:OsMADS58* were evaluated by Real Time PCR using StoS Quantitative Master Mix (GeneSpin, Milano, Italy) and primers RT1898/RT1899, RT973/RT974 (for both *OsMADS3* isoforms) and RT975/RT976, respectively. For each construct, at least two independent lines were used (**Supplementary Figure 4**).

The expression levels of *SPOROCYTELESS (At4g27330), REM22 (At3g17010)* and *SHATTERPROOF1 (At3g58780)* were evaluated using primers RT1674/RT1675, RT1672/RT1673 and AtP650/AtP651, respectively.

For each experiment, three biological replicates were used and for each of these three technical replicates were done. Arabidopsis reference genes ubiquitin (*At4g36800*) and *ACT2-8* were used as an internal reference during the experiments. Primer sequences are listed in **Supplementary Table 1**.

Yeast-2-Hybrid Assay

The analysis focused on the M, I, K and C domains of all proteins, therefore the putative *N-terminus* preceding the MADS domain in AtAG and OsMADS3 was not included in the clones. The CDS of the candidate MADS-box genes were amplified using the primers SEP1f/SEP1r (*AtSEP1*), AtP4929/AtP4930 (*AtSEP3*), and Atp7069/Atp7070 (*AtAG*) and cloned into the Gateway entry vectors pDONR201 and pDONR207 by BP reaction. Both *OsMADS3* splicing variants were amplified by the primers LD264/LD265 and cloned into pCR8/GW/TOPO TA Cloning Kit (Invitrogen); *AtSEP2* CDS was amplified by the primers AtP3141/AtP3142 and cloned into pENTR/D-TOPO vector (Invitrogen). All the primer sequences are available in **Supplementary Table 1**. After sequencing, the clones were transferred by LR reaction in the Gateway destination vectors *pGADT7* and *pGBKT7* plasmids for C-terminal fusion to the GAL4 activation domain (AD) and binding domain (BD), respectively. The recombination product was used to transform electrocompetent *E. coli* cells (DH10B strain) and positive colonies were isolated on LB agar plates containing ampicillin (100 mg/L) for *pGADT7* or kanamycin (50 mg/L) for *pGBKT7*.

Combinations of *pGADT7* and *pGBKT7* constructs (see **Table 2**) have been simultaneously used to transform chemo-competent *S. cerevisiae* cells (AH109 strain). Positive colonies for both plasmids were isolated on YSD-agar plates lacking leucine and tryptophan (YSD-L-W). Interaction assays were performed on YSD-agar plates lacking leucine, tryptophan and histidine and containing increasing concentrations of 3-amino-1,2,4-triazole (YSD-L-W-H + 3AT 1mM/2,5mM/5mM/10mM) or on YSD-agar plates lacking leucine, tryptophan and adenine (YSD-L-W-A). Growth for interaction assay was performed at 28°C for one week. As a positive control for interaction, *pGADT7-AtAG* and *pGBKT7-AtSEP3* constructs were used.

RESULTS

OsMADS3 Encodes Two Protein Isoforms Differing Only for One Serine Residue in the K-Box

OsMADS3 (*LOC_Os01g10504*) is located on the short arm of rice chromosome 1, and is in the current MSU annotation represented by three gene models (**Figure 1A**), whose predicted protein products differ only for the few *C* terminal amino acidic residues after the conserved AG motif II (Kramer et al., 2004).

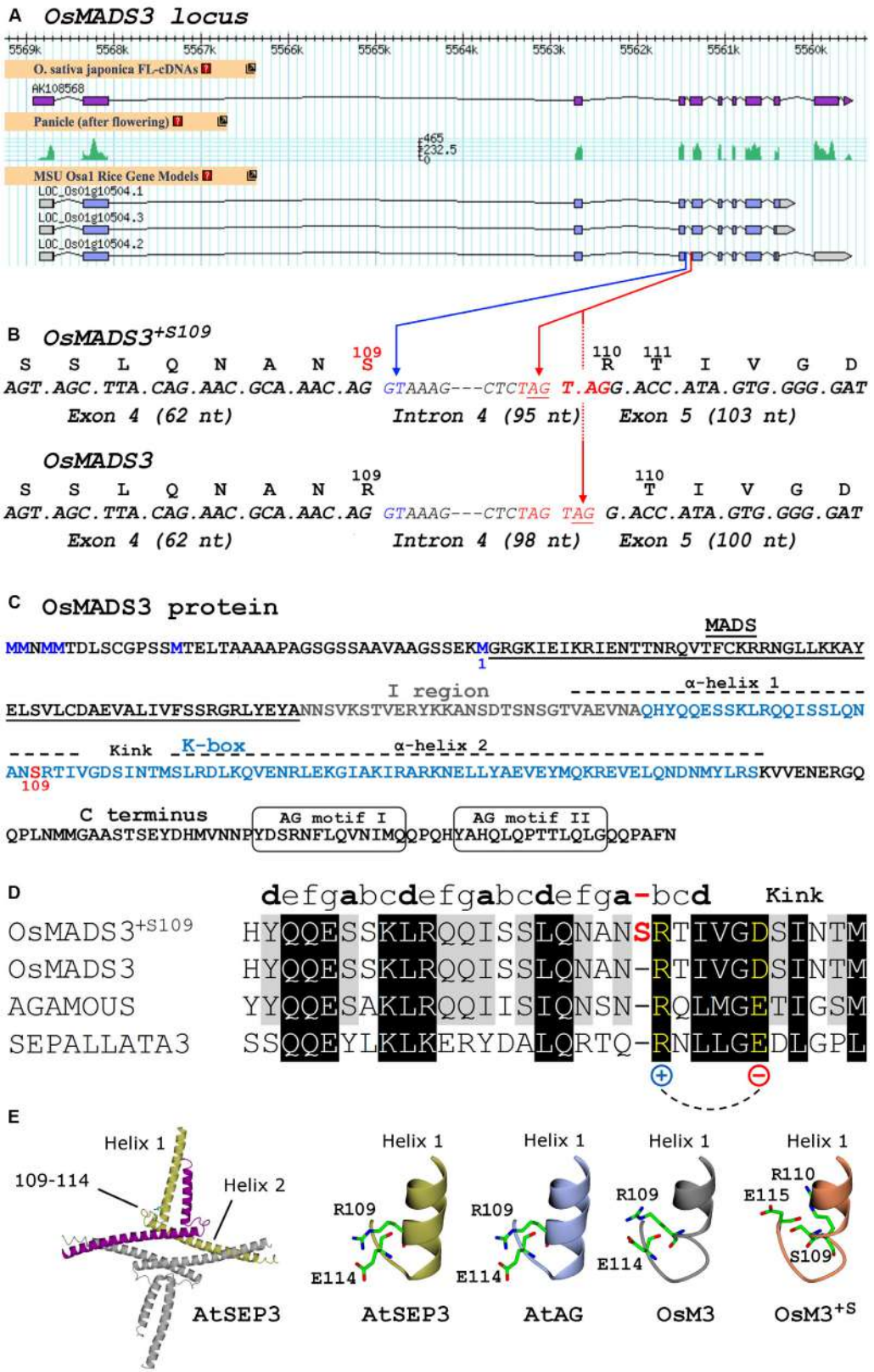

FIGURE 1 | Continued

FIGURE 1 | (A) Current gene models, mRNA-Seq and cDNA data of rice *OsMADS3* (*LOC_Os01g10504)* from the Rice Annotation Project Database (http://rapdb.dna.affrc.go.jp). **(B)** Detail of the *OsMADS3* locus around the fourth intron, including codons and translated protein isoforms of the two splicing variants. The blue arrow indicates the splicing donor site at the 5′ end of intron 4; the red arrows indicate the two alternative acceptor sites at the 3′ end of intron 4. **(C)** OsMADS3 protein sequence. The methionine residue preceding the MADS-domain (M1, blue), the serine at position 109 (red) and the main conserved motifs are highlighted. **(D)** Alignment of the region forming the first α-helix and the kink region, based on the crystal structure of AtSEP3 (Puranik et al., 2014), of AtSEP3 (bottom), AtAG, and the two isoforms of OsMADS3 (top). The partially conserved heptad repeats (abcdefg) of the first α-helix are indicated. The extra residue in OsMADS3^{+S109} (in red color) breaks the last partial heptad repeat between the positions 'a' and 'b', where 'b' is occupied by a conserved residue (in yellow) with positively charged side chain, which forms a salt bridge with a downstream conserved residue with negatively charged side chain (in yellow). This salt bridge contributes to the stabilization of the kink between the two α-helices (Puranik et al., 2014). **(E)** From the left to the right: cartoon presentation of the tetrameric structure of AtSEP3 K box; stick representation of the C-terminal region of helix 1 and the neighboring loop (kink) in the K box in AtSEP3, the position of R109, E110 and D115 side chains is shown. Structural models based on the AtSEP3 structure of the C-terminal region of helix 1 and the neighboring loop for AtAG, OsMADS3 and OsMADS3^{+S109}. Putative conformations of residues 109, 110, 114, and 115 side chains are shown in sticks.

The variants no. 2 and no. 3 have the same predicted protein product (**Figure 1C**), however no. 2 has at least one additional intron in the 3′UTR sequence, in addition to the eight conserved introns which are typical for *AG* lineage genes (Johansen et al., 2002; **Figure 1A**). The analysis of peaks of mRNA-seq reads and cDNA clones from public databases suggests that *LOC_Os01g10504.2* is the only correct and transcribed gene model (**Figure 1A**). We confirmed this by cloning the *OsMADS3* cDNA, but we noticed that some clones just lacked 3 nucleotides (TAG) when compared to the annotated transcript. These variants differed not for the C terminal region, but at the intron 4 – exon 5 splice junction which caused the loss of a serine (S) residue in the predicted OsMADS3 peptide (**Figure 1B**). Since the length of the N terminal region of AG lineage proteins has only been experimentally determined for Arabidopsis AtAG (Riechmann et al., 1999), we refer to this serine amino acidic position as S109, counting from the more conserved methionine residue just preceding the MADS domain (M1, **Figure 1C**). Based on known plant homologs, the lack of S109 is indeed the ancestral form of AG proteins. Therefore, we named the two protein variants OsMADS3^{+S109} (having S109) and OsMADS3 (lacking S109).

A deeper analysis revealed that in the *OsMADS3* locus residue S109 is encoded by an AGT codon which, in the pre-mRNA, is interrupted by the fourth intron (**Figure 1B**). The 3' acceptor site of the fourth intron is duplicated into a TAGTAG repetition (**Figure 1B**). We found that the splicing machinery often recognizes the first AG-base pairs as acceptor site (*OsMADS3*$^{+S109}$), confirming online annotations, but in a significant fraction of the transcripts the second AG-sequence is used instead, thus removing a TAG from the mature transcript and resulting in the absence of the serine residue in the encoded peptide (*OsMADS3*; **Figure 1B**). The existence of such two transcript variants was also confirmed by analyzing several mRNA-seq datasets from rice reproductive tissues which are available on the NCBI Sequence Read Archive (SRA). These data clearly show that wherever *OsMADS3* is expressed, roughly 39% of the transcripts carry this 3-nt deletion (**Table 1**). This amount varied substantially between different samples (range approx. 29–47%), but we could not find any obvious correlation with tissue type nor developmental stage, as the two transcripts were both present in young and mature whole panicles, stamens, ovaries and stigmas (not shown).

TABLE 2 | Summary of yeast-2-hybrid assays.

pGAD/pGBK	-L-W-H	+ 1mM 3aT	+2.5mM 3aT	+ 5mM 3aT	+10mM 3aT	-L-W-A
1. Empty/OsMADS3 + S	+++	+	–	–	–	–
2. Empty/OsMADS3	++	+	–	–	–	–
3. Empty/AtAG	++	+	+	–	–	–
4. AtSEP1/Empty	++	+	–	–	–	–
5. AtSEP2/Empty	++	+	–	–	–	–
6. AtSEP3/Empty	+++	+	–	–	–	–
7. AtSEP1/OsMADS3 + S	**+++**	**+**	**–**	**–**	**–**	**–**
8. AtSEP2/OsMADS3 + S	**++**	**–**	**–**	**–**	**–**	**–**
9. AtSEP3/OsMADS3 + S	**+++**	**+++**	**+++**	**+++**	**++**	**++**
10. AtSEP1/OsMADS3	**+++**	**+++**	**+++**	**+++**	**++**	**++**
11. AtSEP2/OsMADS3	**+++**	**–**	**–**	**–**	**–**	**–**
12. AtSEP3/OsMADS3	**+++**	**+++**	**+++**	**+++**	**++**	**+++**
13. AtSEP1/AtAG	**+++**	**+++**	**+++**	**+++**	**+++**	**+**
14. AtSEP2/AtAG	**+++**	**+++**	**+**	**–**	**–**	**–**
15. AtSEP3/AtAG	**+++**	**+++**	**+++**	**+++**	**+++**	**+++**

In each pair, the first protein is fused to GAL4 activation domain (AD) and the second protein is fused to GAL4 binding domain (BD). The symbols indicate strong growth (++ and +++), mild growth (+) or no growth (–) of yeast colonies on the different media.

To better understand the role of residue S109 on the structural properties of OsMADS3, we analyzed the structure of the AtSEP3 K-domain, which is the only available crystal structure of a plant MADS-dimerization domain to date available (Puranik et al., 2014). In the AtSEP3 structure, which lacks S109, R109 is located at the C-terminal end of helix 1 close to a loop region which orientates perpendicularly to the two helices of the K-box (**Figures 1D,E**). In the AtSEP3 structure, R109 establishes a salt bridge with E114 stabilizing the orientation of helix 1 and the adjacent loop: this region is strongly involved in the AtSEP3 dimerization interface (Puranik et al., 2014). Given the high level of conservation in position 109 and 114, this salt bridge is likely present also in OsMADS3 and AtAG (**Figures 1D,E**). Conversely, the insertion of a S residue in position 109 should slide all residues one position forward and, consequently, R110 and E115 are not well positioned as in the absence of the S residue (**Figure 1E**). This likely results in a re-organization of the end of helix 1 and of the neighboring loop region. The overall high level of conservation of the adjacent residues (**Figure 1D**) suggests that such conformational change is local: it may involve only the loop region and likely allows the formation of the R110 – E115 salt bridge. Hence, the presence of S109 is expected to trigger a loop reorganization and this results in a minor modification of the dimerization interface compared to the one present in MADS-domain proteins devoid of S109 as AtAG and AtSEP3. These considerations suggest that the formation of mixed dimers between floral homeotic MADS-domain proteins carrying S109 could well be unfavored.

The S109 Isoform Seems to Be Ubiquitously Present in Grass OsMADS3-Like Proteins

To trace the origin of the *OsMADS3* alternative splicing, we did alignments of AGAMOUS subfamily protein sequences from several different angiosperms and gymnosperms. In angiosperms, the AGAMOUS subfamily divides into the AG and AGL11 lineages, which in the grass family are further duplicated into the OsMADS3 (AG), OsMADS58 (AG), OsMADS13 (AGL11) and OsMADS21 (AGL11) clades (Kramer et al., 2004; Zahn et al., 2006; Dreni and Kater, 2014). The alignments suggested that residue S109 is conserved in many OsMADS3 homologs from grass species, but it is absent in the other AGAMOUS subfamily proteins within the same grass species, including those from the OsMADS58 subgroup, which is sister to the OsMADS3 clade (Kramer et al., 2004; Yamaguchi et al., 2006; Zahn et al., 2006). The S109 residue was found to be absent outside the grass family, in all the flowering plants and gymnosperms that we analyzed (**Figure 2** and **Supplementary Figure 2**).

Within the grass *OsMADS3* clade, a search in the Phytozome and Gramene databases revealed that both splicing variants are currently annotated for rice *OsMADS3*, and for the *OsMADS3*-like genes of *Brachypodium distachyon* (L.) P.Beauv., barley (*Hordeum vulgare* L.), and maize (*Zea mays* L.) *ZMM2*. Both the variants of rice and *Brachypodium* are also reported on NCBI (XM_015777004, XM_015777012, XM_010232289 and XM_010232291). Furthermore, we noticed that this alternative

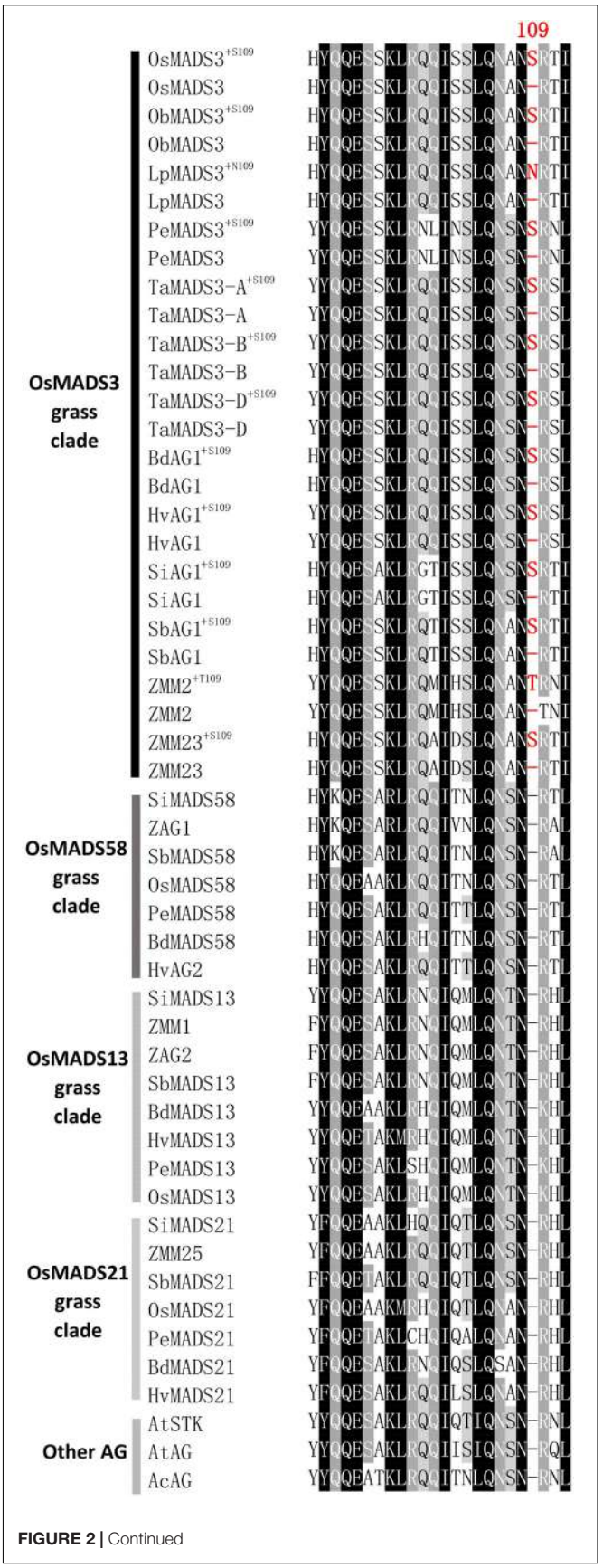

FIGURE 2 | Continued

FIGURE 2 | Alignment of the region forming the first α-helix of AGAMOUS subfamily proteins from different grasses, pineapple and Arabidopsis: Os, *Oryza sativa;* Pe, *Phyllostachys edulis;* Lp, *Leersia perrieri;* ZM, *Zea Mays;* Si, *Setaria Italica;* Sb, *Sorghum bicolor;* Ta, wheat (*Triticum aestivum*); Hv, *Hordeum vulgare;* Bd, *Brachypodium distachyon;* At, *Arabidopsis thaliana*; Ac, *Ananas comosus.* For each OsMADS3-like protein, both the isoforms with or without the additional amino acid residue 109 are shown. The protein sequences of AtSTK and AtAG from *A. thaliana* are included in the alignment as representatives of the dicotyledons.

splicing event corresponds to the one recently described for the *OsMADS3* homolog of *Aegilops tauschii* Coss (Wei, 2016), which is the D-genome donor of bread wheat (*Triticum aestivum* L.). The author interpreted the alternative splicing as involving an AGT instead of a TAG sequence, probably due to ambiguity in aligning the last two nucleotides 'AG' of the fourth exon in the short variant. However, only one of the two variants is annotated in other available grass genomes and in maize *ZMM23*. When we analyzed the genomic loci of various *OsMADS3* orthologs, we noticed that the TAGTAG duplication in the 3′ splice acceptor site of intron four, is conserved throughout the whole grass family, and only changes into CAGTAG in *Brachypodium* and barley (a selection of species is shown in **Figure 3**). This duplication is not observed in any of the three other clades of the *AGAMOUS* subfamily in grasses, i.e., *OsMADS13, OsMADS21* and *OsMADS58*. Therefore, we reasoned that the alternative splicing might occur ubiquitously in *OsMADS3* genes of grasses, without being fully represented in current databases. To verify this hypothesis, we extended our analysis of published mRNA-Seq reads to other species representative of the main grass evolutionary clades: *Streptochaeta angustifolia* Soderstr. (from the basal most subfamily Anomochlooideae), *Phyllostachys edulis* (Carrière) J. Houz. (Bambusoideae), *Leersia perrieri* (A.Camus) Launert (another species from Oryzoideae), *Brachypodium* and barley (Pooideae), *Sorghum bicolor* (L.) and maize (Panicoideae). Stunningly, the analysis revealed that the S109 alternative splicing is indeed conserved across grasses. Male, female and seed specific samples were available for *Brachypodium*, *Sorghum* and maize which indicated that, like in rice, the two transcript variants do not have any obvious tissue or stage specificity. The isoform lacking S109 was predominant only in *Streptochaeta*, *Leersia*, *Sorghum* and in maize *ZMM23*, on the contrary to maize *ZMM2* (**Table 1**).

Next, we traced the origin of this alternative splicing along the evolution of monocots. Outside the Poaceae family, the TAGTAG duplication allowing the alternative splicing doesn't seem to exist. This is the case for other commelinids like *Musa acuminata* Colla*, Elaeis guineensis* Jacq. and *Ananas comosus* (L.) Merr., as well as any of the other angiosperms and gymnosperms that we analyzed (**Figure 3**). Within the order Poales, *Ananas comosus* (pineapple) is an excellent sister group to study the evolution of grass genomes, due to the availability of a high quality whole genome sequence (Ming et al., 2015), and because it diverged before the whole genome duplication (WGD) event which shaped all grass genomes (Paterson et al., 2004). In the only pineapple *AG* lineage gene, *AcAG*, there is no TAGTAG duplication in the fourth intron 3′ splicing acceptor site (**Figure 3**) and, accordingly, all its transcripts miss S109 (**Table 1**). Despite that no genomic data are yet publicly available from Poales other than grasses and pineapple, a limited amount of mRNA-Seq experiments allowed us to test the presence of the alternative splicing in most lineages. For example, nearly 2000 reads from *Luzula elegans* (Juncaceae) support only the conserved splicing typical of the *AGAMOUS* subfamily genes, like in pineapple (**Table 1**). The same result was obtained from all the main clades of Poales. Within Poales, the so called graminid clade includes grasses and three tiny sister families of just 11 species in total (**Supplementary Figure 2**). For two of these families, we did not find enough data to draw a conclusion, however, in Ecdeiocoleaceae we have found clear evidence of S109 alternative splicing (**Table 1**). Sister to the graminid clade is the family Restionacee (**Supplementary Figure 2**), where the S109 extra residue clearly exists in the genus *Elegia* (**Table 1**). Surprisingly, in the genera *Centrolepis* and *Aphelia*, a similar alternative splicing event removes the conserved R109 residue, rather than adding a S residue, generating protein isoforms lacking one amino acid when compared to typical AGAMOUS subfamily proteins (data not shown). Therefore, the alternative splicing of *AG* intron 4 possibly arose just before the most common ancestor of grasses and their sister families and Restionaceae (**Supplementary Figure 2**).

In most grasses, the additional amino acidic residue 109 is a serine, though some species show other polar neutral amino acids. For instance, in maize ZMM2 and in *Leersia* LpMADS3, the serine is replaced by threonine and asparagine, respectively (T109 and N109). This suggests that this residue is important not only for its position, but also for it physical/chemical properties.

In almost all the species that we considered, the presence or absence of the codon for S109 does not alter the translation of the surrounding codons, which usually encode an asparagine (upstream) and an arginine (downstream). In *Leersia perrieri*, a species very close to the *Oryza* subgroup, not only S109 is replaced by N109 in the long splicing variant, but in the short variant missing N109, the downstream arginine (R) is replaced by a lysine (K) (**Figure 2**), which is an amino acid with similar properties. An exception is maize ZMM2 where, in the short variant, splicing out the codon for T109 generates another codon for T, rather than for the highly conserved basic residue. Notably, based on RNA-Seq data, the short variant of ZMM2 has a much lower abundance. The opposite holds for the paralog ZMM23 for which the short variant keeps the basic conserved residue, and is much higher expressed (**Table 1**). This suggests that in maize the presence of two *OsMADS3*-like genes is favoring their subfunctionalization.

OsMADS3 Isoforms Have Different Abilities to Induce Homeotic Changes in Arabidopsis Flowers

In order to compare the functionality of the two isoforms, $OsMADS3^{+S109}$ and *OsMADS3* were expressed in Arabidopsis as an heterologous test system, along with *OsMADS58* and Arabidopsis *AtAG* as controls. The coding sequences were

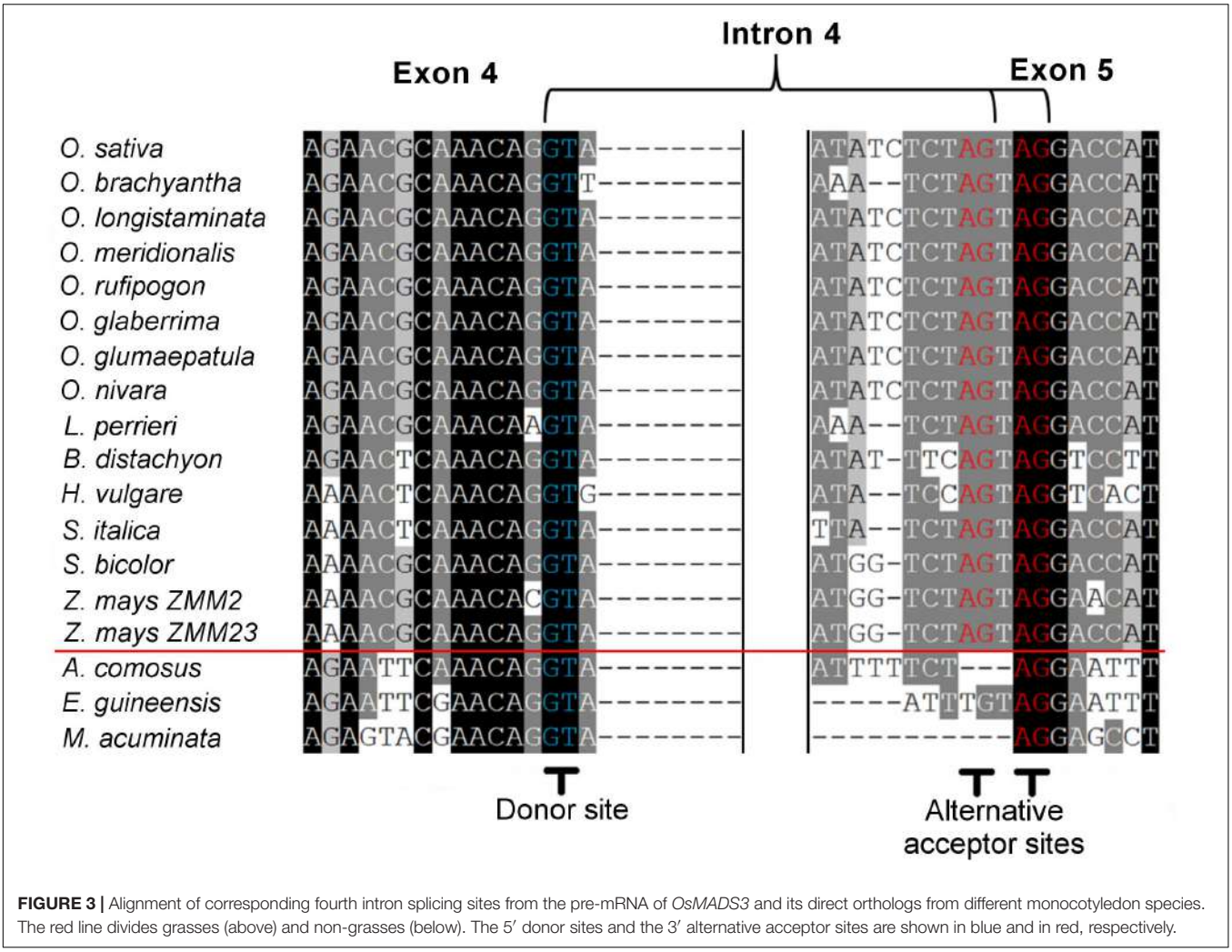

FIGURE 3 | Alignment of corresponding fourth intron splicing sites from the pre-mRNA of *OsMADS3* and its direct orthologs from different monocotyledon species. The red line divides grasses (above) and non-grasses (below). The 5′ donor sites and the 3′ alternative acceptor sites are shown in blue and in red, respectively.

cloned downstream of the CaMV 35S promoter and these constructs were used to transform Arabidopsis plants which were heterozygous for the *ag-3* mutation (Bowman et al., 1991). In many previous publications, the effects of ectopic heterologous C-class gene expression have been evaluated in a WT background (Martin et al., 2006; Airoldi et al., 2010). In this study we used the progeny of a T_1 generation segregating for the *ag-3* allele, because we were interested to observe the ability of rice proteins to complement the lack of *AtAG* activity in Arabidopsis.

By different rounds of transformation and BASTA selection, from 31 to 64 transgenic plants for each construct were selected. Of the selected transgenic plants 39% showed dwarfism, curled rosette leaves and were early flowering, except those expressing *OsMADS58* (**Supplementary Table 2** and **Supplementary Figure 3**). These are typical phenotypes for plants ectopically expressing *AG*-like genes. Many of these plants also showed floral phenotypes with homeotic changes of floral organs, except those expressing *OsMADS58* which developed normally, as explained in a following paragraph.

For each construct, a selection of T_1 plants heterozygous for the *ag-3/ +* mutation were chosen for further analysis in the T_2 generation, so that we could observe the effect of the constructs in the WT and *ag-3* mutant backgrounds compared to untransformed controls (**Figures 4A,F**, **5A**). We have also evaluated the expression level in two or more independent lines for each transgene (**Supplementary Figure 4**).

Probably due to the use of the heterologous 35S promoter lacking the correct spatial and temporal regulation of the endogenous promoter, *35S:AtAG* was not able to completely rescue the *ag* mutant phenotype.

In the WT and *ag-3/ +* backgrounds, we could observe carpelloid sepals and a mild to strong conversion of second whorl petals into stamens or staminoid-like structures (**Figures 4B**, **5C,E**). SEM images of anther-like petals in *35S:AtAG* plants showed that the lower part of the organs look very similar to anther filaments while the upper part of the organ resembles the shape of an anther, but the surface cells look spherical and resemble those of the petal surface (**Figures 5B,C,E**). Also, the shape of the upper part of the chimeric organ in the second whorl looks like a small petal (**Figures 4B**, **5E**).

In the *ag-3* mutant background, *AtAG* expression from the 35S promoter resulted in petals that acquired a yellowish appearance

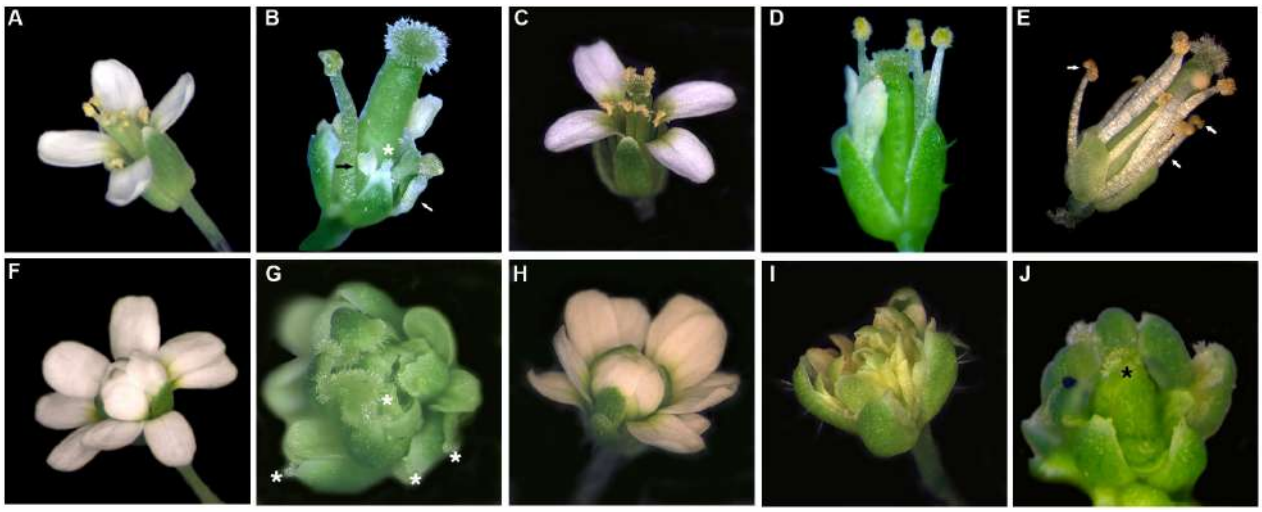

FIGURE 4 | Flowers of plants expressing: **(B,G)** *35S:AtAG,* **(C, H)** *35S:OsMADS58,* **(D, I)** *35S:OsMADS3*$^{+S109}$ and **(E, J)** *35S:OsMADS3* in WT **(B–E)** and *ag-3* **(G–J)** backgrounds, compared to WT **(A)** and *ag-3* mutant **(F)**. Ectopic stigmas on sepals (white asterisks), petal-to-stamen conversion (white arrows) and meristem determinacy recovery with formation of carpel-like organs (black asterisk) are highlighted.

and stigmatic tissues appeared on the sepals (**Figure 4G**). In addition, 30% of the plants recovered FMD almost completely. In these plants, the meristem terminated with a carpelloid organ arising from the fourth whorl, closed by stigmatic tissue at the tip (**Figures 4G**, **5F**). None of the *35S:AtAG* lines in the *ag-3* background were able to produce seeds. Petals of *35S:AtAG ag-3* plants showed a mild conversion to anthers when observed by SEM (**Figure 5H**). The cell shape mostly recalled that of a normal petal except some group of cells which acquired a lobate shape typical of anther cells. Moreover the overall shape of the terminal part of these organs look like stamens. Another detail to notice is that, in the first whorl, the nature of the cells surrounding the ectopic stigmas in *35S:AtAG* lines in the *ag-3* mutant background varied from irregular sepal cells to smoother and longer cells which mostly recalled those of the style (**Figures 5D,G**). In some plants, ectopic ovules were visible near the stigmatic tissue on sepals (**Figure 5G**).

Plants transformed with the *35S:OsMADS58* construct never showed any change in phenotype, neither in WT nor in the *ag-3* background, regardless of the transgene expression level (**Figures 4C,H**). It is worth mentioning that the OsMADS58 protein lacks a conserved *C*-terminal AG II motif (Kramer et al., 2004; Dreni et al., 2013), which might affect its functionality in Arabidopsis.

In Arabidopsis plants expressing *35S:OsMADS3*$^{+S109}$ in a WT background, the main phenotype was a strong reduction in sepal and petal length; as a result, reproductive organs were uncovered much earlier than usual, around stage 6–7 of flower development, while in WT flowers the bud opens around stage 13 (**Figure 4D**; stages indicated according to Smyth et al., 1990).

As mentioned before, the *ag-3* mutant flower is composed of a repetition of sepals – petals – petals – new flower, without any reproductive organ. *35S:OsMADS3*$^{+S109}$ expression in the *ag-3* mutant background caused some petals to acquire a yellowish appearance (**Figure 4I**). SEM images show that the overall identity of these organs is that of a petal, even if some cells acquired a lobate shape typical of an anther-like cell (**Figures 5C,I**). Notably none of the plants were able to recover the FMD.

Interestingly, the plants that expressed *OsMADS3* from the 35S promoter had a floral phenotype that resembled the *35S:AtAG* plants. In the WT background they showed a strong petal-to-stamen conversion with cells having a lobate shape typical of anther-like cells (**Figures 4E**, **5B,C,J**). In the *ag-3* background, stigmatic tissue was observed on outer sepals and about 60% of the plants also show FMD recovery and formation of carpel-like organs in the fourth whorl (**Figures 4J**, **5K,L**). SEM images revealed that also in the *ag-3* background all petals were converted to stamens in an even more pronounced way than in plants expressing *35S:AtAG* (**Figure 5K**).

For each transgene, a representative line with the described phenotypes was chosen in order to test the expression of organ identity marker genes in the *ag-3* background, as a confirmation of the microscopical observations (**Figure 6**). Therefore, we performed qRT-PCR experiments to check the expression of three genes: *SPOROCYTELESS (SPL)* (Liu et al., 2009) and *REPRODUCTIVE MERISTEM 22 (REM22)* (Romanel et al., 2011), as markers for stamen identity, and *SHATTERPROOF1 (SHP1)*(Liljegren et al., 2000), as marker for carpel identity. These genes have been described as direct targets of *AtAG* (Gómez-Mena et al., 2005; Ó'Maoiléidigh et al., 2013) and they all appear strongly down-regulated in the inflorescence of *ag-3* (**Figure 6**).

In agreement with the observed phenotypes, transgenic plants containing *35S:AtAG* in the *ag-3* background, showed an upregulation of all marker genes (**Figure 6**). This suggests that, even if the mutant phenotype was not fully complemented, the

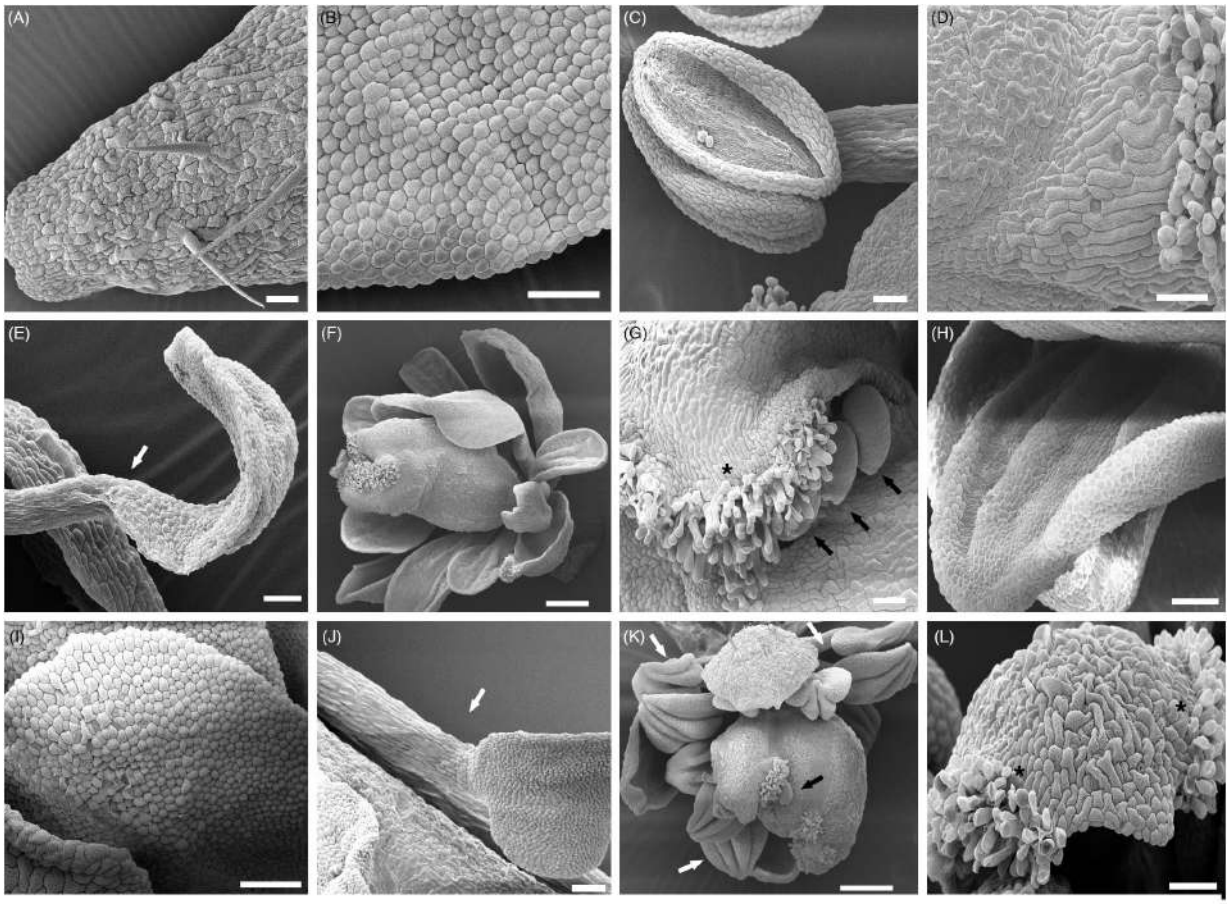

FIGURE 5 | SEM analyses of ectopic organs. **(A)** WT sepal; **(B)** WT petal; **(C)** WT stamen; **(D)** WT carpel; **(E)** Staminoid-petal in *35S:AtAG* (WT background); **(F)** Meristem determinacy recovery in *ag-3 35S:AtAG*; **(G)** Ectopic stigmas and ovules on sepals in *ag-3 35S:AtAG*; **(H)** Mild petal-to-stamen conversion in *ag-3 35S:AtAG*, cells shape are more lobate than those in WT petals **(B)** resembling the shape of anther cells **(C)**; the organ acquires the typical folds of the anther; **(I)** Mild petal-to-stamen conversion in *ag-3 35S:OsMADS3*$^{+S109}$, cells shape are more lobate than those in WT petals **(B)** resembling the shape of anther cells shown in **(C)**; **(J)** Petal-to-stamen conversion in *35S:OsMADS3;* **(K)** Staminoid-petals and meristem determinacy recovery in *ag-3 35S:OsMADS3;* an ectopic ovule is also visible; **(L)** Ectopic stigmas on sepals in *ag-3 35S:OsMADS3.* Ectopic stigmas on sepals (black asterisks), petal-to-stamen conversion (white arrows) and ectopic ovules (black arrows) are highlighted.

floral program to produce stamens an carpels was activated, as shown by the microscopic analysis (**Figure 5H**).

The expression levels of marker genes in *ag-3* plants expressing *35S:OsMADS58* remained unaltered compared to the untransformed *ag-3* mutant (**Figure 6**) which perfectly correlates with the fact that no alteration in the flower morphology was observed in these lines.

In the *ag-3* plants expressing *35S:OsMADS3*$^{+S109}$, qRT-PCR analysis showed upregulation of *REM22* and *SPL,* markers of stamen identity, despite that only a very mild homeotic transformation to stamens was observed in these plants (**Figures 5C,I**). The carpel identity marker *SHP1* remained unaltered compared to *ag-3*, and this is in line with the observed lack of carpel development, as confirmed by SEM analysis (**Figure 5I**).

The *ag-3* plants expressing *35S:OsMADS3*, as explained above, showed a phenotype that was very similar to those expressing *35S:AtAG*. This similarity is confirmed by the qRT-PCR analyses: not only the markers for stamen identity appeared upregulated, but also *SHP1* was upregulated in the *ag-3* background and this could account for the formation of carpel tissues which is not observed in plants expressing *35S:OsMADS3*$^{+S109}$ (**Figure 6**).

Comparative Interaction Studies of OsMADS3^{+S109} and OsMADS3 With SEP Proteins

The activity of AG proteins depends on the interaction with members of the SEP family. Since the difference between the two OsMADS3 isoforms is one amino acid in the first α-helix of the K region, which is known to function as the core dimerization interface between MADS-domain factors, we hypothesized that different interaction abilities may account for the difference in capacity to complement the *ag-3* mutant.

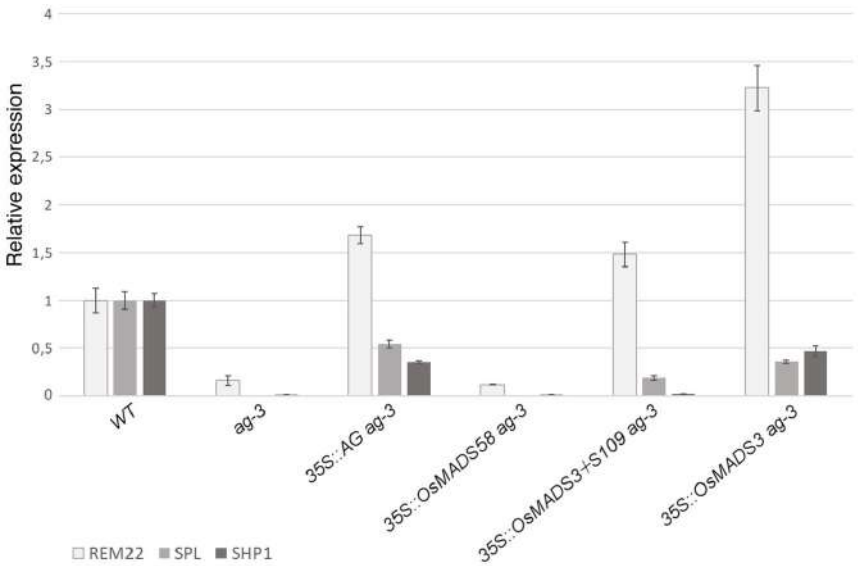

FIGURE 6 | Expression of *REM22, SPL,* and *SHP1* in transgenic plants in the *ag-3* background. For each experiment, three biological replicates were used and for each of these three technical replicates were done. The expression levels have been normalized against the WT. SEM is indicated.

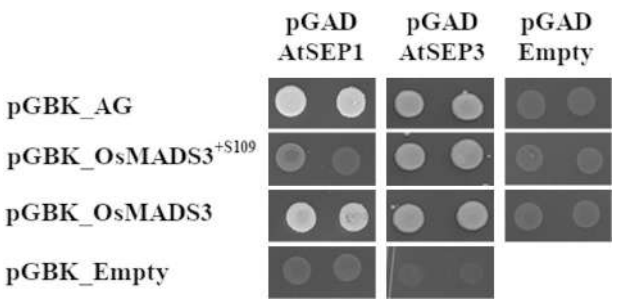

FIGURE 7 | Yeast-2-hybrid interaction assay for AtAG, OsMADS3^{+S109}, OsMADS3, AtSEP1 and AtSEP3, interactions on -W-L-H + 5 mM 3AT are shown. AtAG and OsMADS3 are able to interact with both AtSEP1 and AtSEP3, while OsMADS3^{+S109} can interact only with AtSEP3. As a positive control, the already published AtAG-AtSEP3 interaction was tested and, as a negative control, the vectors of interest were co-transformed with the empty pGAD or pGBK vectors.

We therefore tested the interaction of AtAG, OsMADS3^{+S109} and OsMADS3 with Arabidopsis AtSEP1, AtSEP2 and AtSEP3 proteins using the yeast-2-hybrid assay (**Table 2** and **Figure 7**). The result was that AtAG (as expected), OsMADS3^{+S109} and OsMADS3 were all able to interact strongly with AtSEP3. However, OsMADS3^{+S109} was not able to interact with either AtSEP1 or AtSEP2, whereas OsMADS3 showed interaction with AtSEP1 but not with AtSEP2. The interaction between OsMADS3 and AtSEP1 had the same strength as the interaction observed for AtAG. These results suggest that the differences between OsMADS3^{+S109} and OsMADS3 in their ability to complement the *ag* phenotype, might be explained, at least in part, by their different capability to interact with AtSEP1.

DISCUSSION

All the proteins in the AGAMOUS subfamily, from both ancestral and evolved seed plant families, lack S, or any other additional residue, in the considered position 109 (**Supplementary Figure 2**), indicating that the insertion has occurred later during evolution. In particular, we provide strong evidence that it occurred after the differentiation of the monocot order Poales, but before the ρ WGD event which occurred in grasses (**Supplementary Figure 1**). Indeed we found evidence of the alternative splicing of *AG*-lineage intron 4 also in sister families of grasses in the graminid clade, whereas the grass ρ WGD has been dated after the separation of grasses from them (**Supplementary Figure 1**; McKain et al., 2016). Since this grass WGD caused the duplication of the *AG*-lineage into the *OsMADS3* and *OsMADS58* clades, we reason that the conserved alternative splicing arose in the pre-grass *AG*-lineage, but later in grasses it remained conserved only in the *OsMADS3* clade, and was lost in the *OsMADS58* clade. However, there are not yet sequenced genomes for the sister families of grasses, which would allow to better study the S109 evolution and to confirm that grasses do not share their ρ WGD and the *OsMADS3/OsMADS58* duplication with any sister family.

It looks like S109 has acquired an active and fundamental role in the functionality of OsMADS3-like proteins during evolution, since selective pressure seems to keep in place both isoforms. Despite the majority of *OsMADS3*-like genes are annotated only for one of the two isoforms, we showed that alternative splicing occurs widely in grasses. In most cases, the additional amino acidic residue is a serine, or another amino acid with a polar uncharged side chain. Therefore, the physical/chemical properties of this residue are likely to be important.

The TAG duplication that we report in grasses, is similar to the CAG duplication of a splice acceptor site in the snapdragon *FAR* gene, which results in an additional glutamine (Q173) in the last α-helix of the K-box (Airoldi et al., 2010). However, there is an important difference between the two cases: S109 is not present in all the OsMADS3 peptides because both the (T)AG sequences can work as splice acceptor sites whereas, based on current analysis, in *FAR* only the 'new' (C)AG repetition seems to be recognized as splice acceptor site (Airoldi et al., 2010).

It is widely accepted that the evolution and diversification of the flower went through the evolution of MADS tetrameric complexes and extensive gene duplications followed by sub- and neo-functionalization, which increased greatly the number of possible tetrameric combinations. A recent report on eudicot MADS-box genes revealed that in this evolutionary process the contribution of alternative splicing isoforms should not be ignored (Severing et al., 2012). However, the previously reported cases represent species-specific alternative splicing isoforms, with no or limited conservation within related species. To our knowledge, the alternative splicing that we reveal here is the first case, within the MADS-box family, of an alternative splicing which is highly conserved in a whole plant family, despite the fact that it causes a difference of just one amino acidic residue in the derived polypeptide. Its position in the first α-helix is also unusual, as previous cases involved the *C*-terminal part of the K-box or the C-terminus of the protein. Through a preliminary screen of grass genome databases, we found evidence of alternative splice isoforms in other MADS-box families, but none of them seemed to be conserved among species nor affected the first α-helix (LD, unpublished data). Therefore, we might have discovered a unique case within plant floral homeotic MADS-domain proteins or, on the contrary, similar events might be more common but simply passed unnoticed so far. With the massive and continuing increase in high-throughput plant genome and transcriptome data, large scale analysis across angiosperms are nowadays possible and may clarify the frequency by which this phenomenon occurs.

The level of conservation of this alternative splice event in grasses, suggests that both OsMADS3^{+S109} and OsMADS3 have specific functions. However, mRNA-seq data showed that the two alternative transcripts share similar expression profiles, thus apparently excluding tissue- or stage-specific functions for them, although our experiments can't exclude cell specific functions for these two isoforms. Interestingly, also the results obtained from the expression and complementation experiments with the two rice *OsMADS3* isoforms revealed a clear difference in activity of these two proteins. The analysis of numerous Arabidopsis transformants revealed that *OsMADS3* complemented the *ag* mutant in a way that was comparable to the endogenous *AtAG* gene, whereas the *OsMADS3*$^{+S109}$ encoded isoform lacked greatly this ability. Since both AtAG and OsMADS3 lack the serine residue at position 109, this result indicates that the absence of S109 facilitated the *ag* mutant complementation capability of these two proteins in Arabidopsis. Since S109 is located in the first α-helix of the K-box, a domain that is important for MADS-domain protein dimerization (Puranik et al., 2014), these results suggest that S109 influences the ability to interact with SEP-like proteins, because the interaction with these proteins has shown to be fundamental for AtAG to determine stamen and carpel identity in Arabidopsis (Pelaz et al., 2000).

The yeast 2-hybrid assays showed a role for residue S109 in the ability of the OsMADS3 isoforms to interact with Arabidopsis AtSEPs, since OsMADS3, OsMADS3^{+S109} and AtAG all interacted equally well with AtSEP3, but the two OsMADS3 isoforms had a different capability to interact with Arabidopsis AtSEP1. While OsMADS3 and AtAG were able to interact with this protein, no interaction was detected between OsMADS3^{+S109} and AtSEP1.

As observed by Puranik and co-workers (Puranik et al., 2014), the K-domains establish large dimerization interfaces, where the helix 1 and the neighboring loop are involved in such interactions. The insertion of a residue in position 109 is not likely to alter the overall dimer architecture, however, a local reorganization of the loop is needed to adjust the extra residue and this likely triggers a limited reorientation/rotation of helix 2 with respect to helix 1. This implies that MADS-box proteins devoid S109 may have distinct dimerization interfaces compared to the ones with S109. Based on these observations we propose that by slightly modifying the tetramer architecture, the presence/absence of S109 may modify the functional interactions of the OsMADS3 isoforms with their cellular partners in keeping with the Yeast 2-hybrid experiments with AtSEP1 and AtSEP3.

In conclusion, in their native background, OsMADS3^{+S109} and OsMADS3 could have diverse affinity to form different tetrameric complexes. Further studies in rice will be interesting to investigate the role of OsMADS3^{+S109} and OsMADS3, including the analysis of their crystal structures. Notably is that the evolutionary conservation of these splice variants in the grass family suggests that subtle changes in a MADS-domain transcription factor may lead to a divergence in function of these important regulators of carpel and stamen development.

DATA AVAILABILITY STATEMENT

All datasets generated and analyzed for this study are cited in the article/**Supplementary Material**.

AUTHOR CONTRIBUTIONS

LD discovered the alternative splicing and conceived the project and wrote the manuscript with contributions from all the authors. LD and AR performed the research. NG-S did expression analysis. FC and VG performed yeast interaction and SEM studies. SJ and GS helped in cloning and plant transformation. SR and RR did biochemical and structural analysis. MK supervised the whole project.

FUNDING

Funding was received from these sources. Marie Curie International Research Staff exchange Scheme (2010–2014): PROPOSAL N. 247587 "Evolutionary Conservation of Regulatory Network Controlling Flower Development. FIRB-MIUR ERA-PG: "Semi per la crescita". AR, SJ, and FC were supported with Ph.D. fellowships from the doctorate school in Molecular and Cellular Biology of the University of Milan.

ACKNOWLEDGMENTS

We thank Anne Dievart for helpful suggestions for some of the experiments and Elisabetta Caporali for SEM images. We are grateful to all those research groups and institutes who have made public their RNA-seq experiments through Genebank, enabling us to study the conservation of the alternative splicing of *OsMADS3*-like genes. AR, SJ, and FC Ph.D. fellowships were funded by the doctorate school in Molecular and Cellular Biology, University of Milan.

SUPPLEMENTARY MATERIAL

The Supplementary Material for this article can be found online at: https://www.frontiersin.org/articles/10.3389/fpls.2020.00637/full#supplementary-material

REFERENCES

Airoldi, C. A., Bergonzi, S., and Davies, B. (2010). Single amino acid change alters the ability to specify male or female organ identity. *Proc. Natl. Acad. Sci. U. S. A.* 107, 18898–18902. doi: 10.1073/pnas.1009050107

Bowman, J. L. (1997). Evolutionary conservation of angiosperm flower development at the molecular and genetic levels. *J. Biosci.* 22, 515–527. doi: 10.1007/BF02703197

Bowman, J. L., Smyth, D. R., and Meyerowitz, E. M. (1989). Genes directing flower development in *Arabidopsis*. *Plant Cell* 1, 37–52. doi: 10.2307/3869060

Bowman, J. L., Smyth, D. R., and Meyerowitz, E. M. (1991). Genetic interactions among floral homeotic genes of *Arabidopsis*. *Development* 112, 1–20.

Brambilla, V., Battaglia, R., Colombo, M., Masiero, S., Bencivenga, S., Kater, M. M., et al. (2007). Genetic and molecular interactions between BELL1 and MADS box factors support ovule development in arabidopsis. *Plant Cell* 19, 2544–2556. doi: 10.1105/tpc.107.051797

Causier, B., Castillo, R., Zhou, J., Ingram, R., Xue, Y., Schwarz-Sommer, Z., et al. (2005). Evolution in action: following function in duplicated floral homeotic genes. *Curr. Biol.* 15, 1508–1512. doi: 10.1016/j.cub.2005.07.063

Chen, X., Long, H., Gao, P., Deng, G., Pan, Z., Liang, J., et al. (2014). Transcriptome assembly and analysis of Tibetan Hulless Barley (Hordeum vulgare L. var. nudum) developing grains, with emphasis on quality properties. *PLoS One* 9:e98144. doi: 10.1371/journal.pone.0098144

Clough, S. J., and Bent, A. F. (1998). Floral dip: A simplified method for Agrobacterium-mediated transformation of Arabidopsis thaliana. *Plant J.* 16, 735–743. doi: 10.1046/j.1365-313X.1998.00343.x

Cooper, B., Clarke, J. D., Budworth, P., Kreps, J., Hutchison, D., Park, S., et al. (2003). A network of rice genes associated with stress response and seed development. *Proc. Natl. Acad. Sci. U. S. A.* 100, 4945–4950. doi: 10.1073/pnas.0737574100

Davidson, R. M., Gowda, M., Moghe, G., Lin, H., Vaillancourt, B., Shiu, S.-H., et al. (2012). Comparative transcriptomics of three Poaceae species reveals patterns of gene expression evolution. *Plant J.* 71, 492–502. doi: 10.1111/j.1365-313X.2012.05005.x

Davies, B., Motte, P., Keck, E., Saedler, H., Sommer, H., and Schwarz-Sommer, Z. (1999). PLENA and FARINELLI: Redundancy and regulatory interactions between two Antirrhinum MADS-box factors controlling flower development. *EMBO J.* 18, 4023–4034. doi: 10.1093/emboj/18.14.4023

Dreni, L., and Kater, M. M. (2014). MADS reloaded: evolution of the AGAMOUS subfamily genes. *New Phytol.* 201, 717–732. doi: 10.1111/nph.12555

Dreni, L., Osnato, M., and Kater, M. M. (2013). The ins and outs of the rice AGAMOUS subfamily. *Mol. Plant* 6, 650–664. doi: 10.1093/mp/sst019

Dreni, L., Pilatone, A., Yun, D., Erreni, S., Pajoro, A., Caporali, E., et al. (2011). Functional analysis of all AGAMOUS subfamily members in rice reveals their roles in reproductive organ identity determination and meristem determinacy. *Plant Cell* 23, 2850–2863. doi: 10.1105/tpc.111.087007

Emsley, P., and Cowtan, K. (2004). Coot: Model-building tools for molecular graphics. *Acta Crystallogr. Sect. D Biol. Crystallogr.* 60, 2126–2132. doi: 10.1107/S0907444904019158

Favaro, R., Immink, R. G. H., Ferioli, V., Bernasconi, B., Byzova, M., Angenent, G. C., et al. (2002). Ovule-specific MADS-box proteins have conserved protein-protein interactions in monocot and dicot plants. *Mol. Genet. Genomics* 268, 152–159. doi: 10.1007/s00438-002-0746-6

Gómez-Mena, C., de Folter, S., Costa, M. M. R., Angenent, G. C., and Sablowski, R. (2005). Transcriptional program controlled by the floral homeotic gene AGAMOUS during early organogenesis. *Development* 132, 429–438. doi: 10.1242/dev.01600

Gregis, V., Sessa, A., Colombo, L., and Kater, M. M. (2008). AGAMOUS-LIKE24 and SHORT VEGETATIVE PHASE determine floral meristem identity in *Arabidopsis*. *Plant J.* 56, 891–902. doi: 10.1111/j.1365-313X.2008.03648.x

Hands, P., Vosnakis, N., Betts, D., Irish, V. F., and Drea, S. (2011). Alternate transcripts of a floral developmental regulator have both distinct and redundant functions in opium poppy. *Ann. Bot.* 107, 1557–1566. doi: 10.1093/aob/mcr045

Heijmans, K., Ament, K., Rijpkema, A. S., Zethof, J., Wolters-Arts, M., Gerats, T., et al. (2012). Redefining C and D in the petunia ABC. *Plant Cell* 24, 2305–2317. doi: 10.1105/tpc.112.097030

Hu, L., Liang, W., Yin, C., Cui, X., Zong, J., Wang, X., et al. (2011). Rice MADS3 regulates ROS homeostasis during late anther development. *Plant Cell* 23, 515–533. doi: 10.1105/tpc.110.074369

Hu, Y., Liang, W., Yin, C., Yang, X., Ping, B., Li, A., et al. (2015). Interactions of OsMADS1 with floral homeotic genes in rice flower development. *Mol. Plant* 8, 1366–1384. doi: 10.1016/j.molp.2015.04.009

Johansen, B., Pedersen, L. B., Skipper, M., and Frederiksen, S. (2002). MADS-box gene evolution - Structure and transcription patterns. *Mol. Phylogenet. Evol.* 23, 458–480. doi: 10.1016/S1055-7903(02)00032-5

Kaufmann, K., Melzer, R., and Theißen, G. (2005). MIKC-type MADS-domain proteins: Structural modularity, protein interactions and network evolution in land plants. *Gene* 347, 183–198. doi: 10.1016/j.gene.2004.12.014

Kitahara, K., and Matsumoto, S. (2000). Rose MADS-box genes "MASAKO C1 and D1" homologous to class C floral identity genes. *Plant Sci.* 151, 121–134. doi: 10.1016/S0168-9452(99)00206-X

Kramer, E. M., Jaramillo, M. A., and Di Stilio, V. S. (2004). Patterns of gene duplication and functional evolution during the diversification of the AGAMOUS subfamily of MADS box genes in angiosperms. *Genetics* 166, 1011–1023. doi: 10.1534/genetics.166.2.1011

Lightfoot, D. J., Malone, K. M., Timmis, J. N., and Orford, S. J. (2008). Evidence for alternative splicing of MADS-box transcripts in developing cotton fibre cells. *Mol. Genet. Genomics* 279, 75–85. doi: 10.1007/s00438-007-0297-y

Liljegren, S. J., Ditta, G. S., Eshed, Y., Savidge, B., Bowmant, J. L., and Yanofsky, M. F. (2000). SHATTERPROOF MADS-box genes control dispersal in *Arabidopsis*. *Nature* 404, 766–770. doi: 10.1038/35008089

Liu, X., Huang, J., Parameswaran, S., Ito, T., Seubert, B., Auer, M., et al. (2009). The SPOROCYTELESS/NOZZLE gene is involved in controlling stamen identity in *Arabidopsis*. *Plant Physiol.* 151, 1401–1411. doi: 10.1104/pp.109.145896

Liu, Z., Zhang, D., Liu, D., Li, F., and Lu, H. (2013). Exon skipping of AGAMOUS homolog PrseAG in developing double flowers of Prunus lannesiana (Rosaceae). *Plant Cell Rep.* 32, 227–237. doi: 10.1007/s00299-012-1357-2

Lombardo, F., and Yoshida, H. (2015). Interpreting lemma and palea homologies: a point of view from rice floral mutants. *Front. Plant Sci.* 6:61. doi: 10.3389/fpls.2015.00061

Magallon, S., Gomez-Acevedo, S., Sanchez-Reyes, L. L., and Hernandez-Hernandez, T. (2015). A metacalibrated time-tree documents the early rise of flowering plant phylogenetic diversity. *New Phytol.* 207, 437–453. doi: 10.1111/nph.13264

Martin, T., Hu, M., Labbé, H., McHugh, S., Svircev, A., and Miki, B. (2006). PpAG1, a homolog of AGAMOUS, expressed in developing peach flowers and fruit. *Can. J. Bot.* 84, 767–776. doi: 10.1139/B06-031

McKain, M. R., Tang, H., McNeal, J. R., Ayyampalayam, S., Davis, J. I., dePamphilis, C. W., et al. (2016). A phylogenomic assessment of ancient polyploidy and genome evolution across the poales. *Genome Biol. Evol.* 8, 1150–1164. doi: 10.1093/gbe/evw060

McNicholas, S., Potterton, E., Wilson, K. S., and Noble, M. E. M. (2011). Presenting your structures: The CCP4mg molecular-graphics software. *Acta Crystallogr. Sect. D Biol. Crystallogr.* 67, 386–394. doi: 10.1107/S0907444911007281

Ming, R., VanBuren, R., Wai, C. M., Tang, H., Schatz, M. C., Bowers, J. E., et al. (2015). The pineapple genome and the evolution of CAM photosynthesis. *Nat. Genet.* 47, 1435–1442. doi: 10.1038/ng.3435

Mizukami, Y., and Ma, H. (1992). Ectopic expression of the floral homeotic gene AGAMOUS in transgenic Arabidopsis plants alters floral organ identity. *Cell* 71, 119–131. doi: 10.1016/0092-8674(92)90271-D

Ó'Maoiléidigh, D. S., Wuest, S. E., Rae, L., Raganelli, A., Ryan, P. T., Kwaśniewska, K., et al. (2013). Control of reproductive floral organ identity specification in arabidopsis by the C function regulator AGAMOUS. *Plant Cell* 25, 2482–2503. doi: 10.1105/tpc.113.113209

Paterson, A. H., Bowers, J. E., and Chapman, B. A. (2004). Ancient polyploidization predating divergence of the cereals, and its consequences for comparative genomics. *Proc. Natl. Acad. Sci. U. S. A.* 101, 9903–9908. doi: 10.1073/pnas.0307901101

Pelaz, S., Ditta, G. S., Baumann, E., Wisman, E., and Yanofsky, M. F. (2000). B and C floral organ identity functions require SEPALLATTA MADS-box genes. *Nature* 405, 200–203. doi: 10.1038/35012103

Pinyopich, A., Ditta, G. S., Savidge, B., Liljegren, S. J., Baumann, E., Wisman, E., et al. (2003). Assessing the redundancy of MADS-box genes during carpel and ovule development. *Nature* 424, 85–88. doi: 10.1038/nature01741

Puranik, S., Acajjaoui, S., Conn, S., Costa, L., Conn, V., Vial, A., et al. (2014). Structural basis for the oligomerization of the MADS domain transcription factor SEPALLATA3 in *Arabidopsis*. *Plant Cell* 26, 3603–3615. doi: 10.1105/tpc.114.127910

Riechmann, J. L., Ito, T., and Meyerowitz, E. M. (1999). Non-AUG initiation of AGAMOUS mRNA translation in *Arabidopsis thaliana*. *Mol. Cell. Biol.* 19, 8505–8512. doi: 10.1128/mcb.19.12.8505

Romanel, E., Das, P., Amasino, R. M., Traas, J., Meyerowitz, E., and Alves-Ferreira, M. (2011). Reproductive Meristem22 is a unique marker for the early stages of stamen development. *Int. J. Dev. Biol.* 55, 657–664. doi: 10.1387/ijdb.113340er

Rutledge, R., Regan, S., Nicolas, O., Fobert, P., Côté, C., Bosnich, W., et al. (1998). Characterization of an AGAMOUS homologue from the conifer black spruce (Picea mariana) that produces floral homeotic conversions when expressed in Arabidopsis. *Plant J.* 15, 625–634. doi: 10.1046/j.1365-313X.1998.00250.x

Severing, E. I., van Dijk, A. D. J., Morabito, G., Busscher-Lange, J., Immink, R. G. H., and van Ham, R. C. H. J. (2012). Predicting the impact of alternative splicing on plant MADS domain protein function. *PLoS One* 7:e30524. doi: 10.1371/journal.pone.0030524

Smyth, D. R., Bowman, J. L., and Meyerowitz, E. M. (1990). Early flower development in *Arabidopsis*. *Plant Cell* 2, 755–767.

Theissen, G. (2001). Development of floral organ identity: stories from the MADS house. *Curr. Opin. Plant Biol* 4, 75–85. doi: 10.1016/s1369-5266(00)00139-4

Theissen, G., and Saedler, H. (2001). Plant biology. Floral quartets. *Nature* 409, 469–471. doi: 10.1038/35054172

Tsaftaris, A. S., Pasentsis, K., and Polidoros, A. N. (2005). Isolation of a differentially spliced C-type flower specific AG-like MADS-box gene from Crocus sativus and characterization of its expression. *Biol. Plant.* 49, 499–504. doi: 10.1007/s10535-005-0041-6

Wang, T., Wang, H., Cai, D., Gao, Y., Zhang, H., Wang, Y., et al. (2017). Comprehensive profiling of rhizome-associated alternative splicing and alternative polyadenylation in moso bamboo (Phyllostachys edulis). *Plant J.* 91, 684–699. doi: 10.1111/tpj.13597

Wei, S. (2016). Molecular cloning, characterization and expression of WAG-2 alternative splicing transcripts in developing spikes of Aegilops tauschii. *J. Genet.* 95, 581–585. doi: 10.1007/s12041-016-0668-4

Wu, D., Liang, W., Zhu, W., Chen, M., Ferrándiz, C., Burton, R. A., et al. (2018). Loss of LOFSEP transcription factor function converts spikelet to leaf-like structures in rice. *Plant Physiol.* 176, 1646–1664. doi: 10.1104/pp.17.00704

Yamaguchi, T., Lee, D. Y., Miyao, A., Hirochika, H., An, G., and Hirano, H. Y. (2006). Functional diversification of the two C-class MADS box genes OSMADS3 and OSMADS58 in Oryza sativa. *Plant Cell* 18, 15–28. doi: 10.1105/tpc.105.037200

Yanofsky, M. F., Ma, H., Bowman, J. L., Drews, G. N., Feldmann, K. A., and Meyerowitz, E. M. (1990). The protein encoded by the Arabidopsis homeotic gene agamous resembles transcription factors. *Nature* 346, 35–39. doi: 10.1038/346035a0

Yoshida, H., and Nagato, Y. (2011). Flower development in rice. *J. Exp. Bot.* 62, 4719–4730. doi: 10.1093/jxb/err272

Zahn, L. M., Leebens-Mack, J. H., Arrington, J. M., Hu, Y., Landherr, L. L., DePamphilis, C. W., et al. (2006). Conservation and divergence in the AGAMOUS subfamily of MADS-box genes: Evidence of independent sub- and neofunctionalization events. *Evol. Dev.* 8, 30–45. doi: 10.1111/j.1525-142X.2006.05073.x

Zhang, B., Liu, Z. X., Ma, J., Song, Y., and Chen, F. J. (2015). Alternative splicing of the AGAMOUS orthologous gene in double flower of Magnolia stellata (Magnoliaceae). *Plant Sci.* 241, 277–285. doi: 10.1016/j.plantsci.2015.10.017

Zhang, P., Tan, H. T. W., Pwee, K. H., and Kumar, P. P. (2004). Conservation of class C function of floral organ development during 300 million years of evolution from gymnosperms to angiosperms. *Plant J.* 37, 566–577. doi: 10.1046/j.1365-313X.2003.01983.x

Conflict of Interest: The authors declare that the research was conducted in the absence of any commercial or financial relationships that could be construed as a potential conflict of interest.

Citation: Dreni L, Ravasio A, Gonzalez-Schain N, Jacchia S, da Silva GJ, Ricagno S, Russo R, Caselli F, Gregis V and Kater MM (2020) Functionally Divergent Splicing Variants of the Rice AGAMOUS Ortholog OsMADS3 Are Evolutionary Conserved in Grasses. Front. Plant Sci. 11:637. doi: 10.3389/fpls.2020.00637